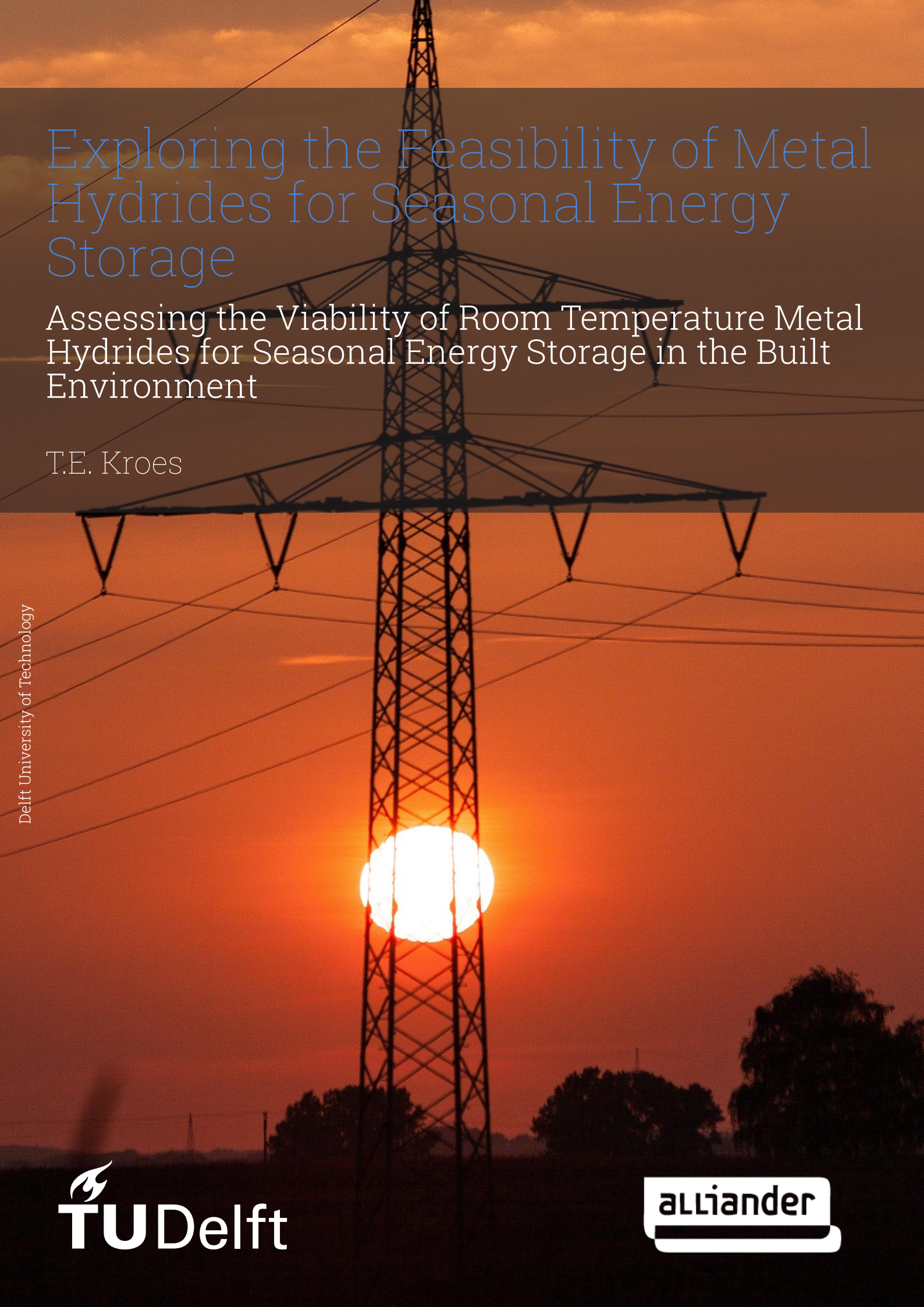

Exploring the Feasibility of Metal Hydrides for Seasonal Energy Storage

Assessing the Viability of Room Temperature Metal Hydrides for Seasonal Energy Storage in the Built Environment

T.E. Kroes

Delft University of Technology

TU Delft

alliander

Exploring the Feasibility of Metal Hydrides for Seasonal Energy Storage

Assessing the Viability of Room Temperature Metal Hydrides for Seasonal Energy Storage in the Built Environment

by

T.E. Kroes

Master Thesis

In partial fulfilment of the requirements for the degree of

Master of Science
In Mechanical Engineering
at the Delft University of Technology,

at the Department Maritime and Transport Technology of the Faculty Mechanical Engineering

to be defended publicly on Tuesday July 15, 2025 at 13:30 PM.

Thesis committee:	Dr.ir. H. Polinder,	TU Delft, chair
	Ir. E. van Rheenen,	TU Delft, supervisor
	Dr. ir. Mahinder Ramdin,	TU Delft, committee member
	Ir. M. Houkema	Company supervisor
Place:	Faculty of Mechanical Engineering, Delft	
Report number:	2025.MME.9078	
Date:	July 7, 2025	

TU Delft

alliander

Preface

Since I was eight years old, I have dreamed of studying Mechanical Engineering at the TU Delft. From that moment on, I started working towards this moment. Now, 16 years later, this thesis marks the end of my study time at the Multi-Machine Engineering master's program of the Mechanical Engineering faculty at the TU Delft. But even more importantly, I fulfilled my dream. Over the years, I have developed a strong interest in the integration of systems as well as the energy transition. This thesis allowed me to deepen both of these interests.

During this process, I found myself seeking physical challenges alongside the academic ones to maintain a good balance. I'm equally proud of completing a marathon and a half triathlon during this time.

I want to express my sincere gratitude to those who supported me throughout the process of my thesis. First and foremost, I would like to thank my supervisors, Erin, Henk, and Michiel. Thank you, Erin, for being very approachable. You made me feel at ease and provided me with invaluable input throughout the process. Henk, thank you for the critical mindset and thought-provoking questions, which helped me to elevate the impact of my work. Michiel, thank you for your curious mindset, enthusiasm, and guidance, which helped me countless times throughout the process. Your support encouraged me to take a step back and critically reflect on the situation.

Lastly, I would like to thank my friends and family for their support throughout this journey. A special thanks to my loving and encouraging girlfriend, Milou, who saw every late night and did everything she could to support me through the process.

T.E. Kroes
Delft, July 2025

Abstract

Renewable energy introduces (seasonal) imbalances between the supply and demand, contributing to net congestion on the electric grid. Seasonal energy storage offers a potential solution by shifting excess renewable generation to periods of shortage. This research investigates the feasibility of using room temperature metal hydrides for seasonal energy storage in the built environment, the pilot: Urban Energy Island project of the housing corporation deltaWonen as a case study. 40 apartments will be part of an innovative energy system to become 80% autarkic while being limited to 40 kW of available grid capacity. To evaluate this concept, a system-level model predictive control (MPC) strategy was developed to coordinate the energy supply and demand across a daily battery, the electric grid capacity, a PEM electrolyser, and a PEM fuel cell, interconnected via a TiFe metal hydride storage system. Waste heat from the different components is also recovered and utilised. After calibrating with ten-year average data and verifying using verification tests, the model was tested for the years 2013 and 2015, including extreme cases. Beyond technical performance, the research also asses safety, cost, reliability, environmental impact and spatial feasibility. The results show that while the current size of the metal hydrate storage is insufficient to cover the seasonal energy demand, it is effective in supporting shorter-term shortages, such as during a dunkelflaute. The system also shows potential for modular scaling. Future research should explore integrating dynamic energy grid prices into the MPC formulation and implementing a higher-level control layer for strategic long-term energy planning.

Contents

1

Introduction

The goal of the European Union is to become the world's first climate-neutral continent by 2050 (European Union, 2020). In 2022, the energy supply was the largest polluting sector, accounting for 27,4% of the EU's greenhouse gas emissions (European Parliament, 2024a). To tackle this, the EU plans to significantly reduce emissions from the energy sector by increasing the renewable energy supply. In 2023, 24.5% of Europe's total energy consumption came from renewable sources (Eurostat, 2023). Yet, the target is to increase this share of renewable energy to 42,5% by 2030. Additionally, renewable hydrogen is attracting the attention of the European Union. They estimate that by 2050, renewable hydrogen will be able to meet 20–50% of the transportation sector's overall energy needs and 5-20% of the industry's overall energy needs (European Parliament, 2024b).

However, the solution is not just to install more renewable power plants, because the electricity grid is already facing problems with congestion. For example, primary school Zilverackers in Veldhoven can not be connected to the grid, even though the school is built with the "zero on the meter" principle, the building generates as much energy as it consumes. Despite that, the school needs a high-capacity grid connection, which is currently unavailable as the grid is full. It could take 5 to 10 years until there is grid capacity available (Triki & Son, 2023). Furthermore, network operators, such as Liander, struggle to connect all requests for solar parks to the grid, especially in rural areas where power cables are the least robust (Alliander, 2019). The mismatch between high solar energy supply during the day and peak demand during the evening, as can be seen in Figure 1.1, is driven by simultaneously charging electric cars, heat pumps, and induction cooktops, exacerbating the grid congestion.

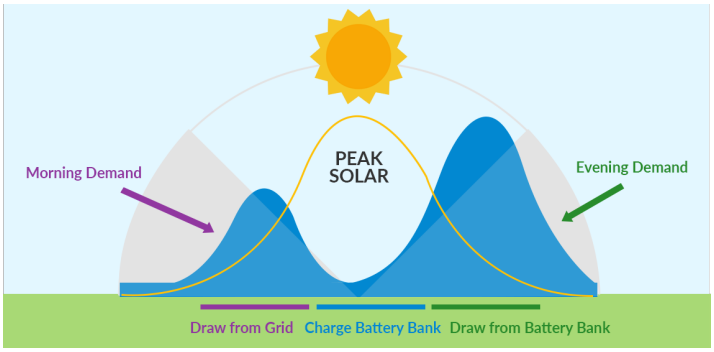

Figure 1.1: Electricity supply and demand for a solar system (LetsGoSolar, 2018)

One of the possible solutions is to use batteries as daily storage to balance the supply and demand and reduce grid congestion. This is a viable option for daily storage. However, another gap needs to be bridged: the mismatch between high solar renewable energy production in the summer and higher electricity demand in the winter (National Energy Dashboard, 2024), as is illustrated in Figure 1.2.

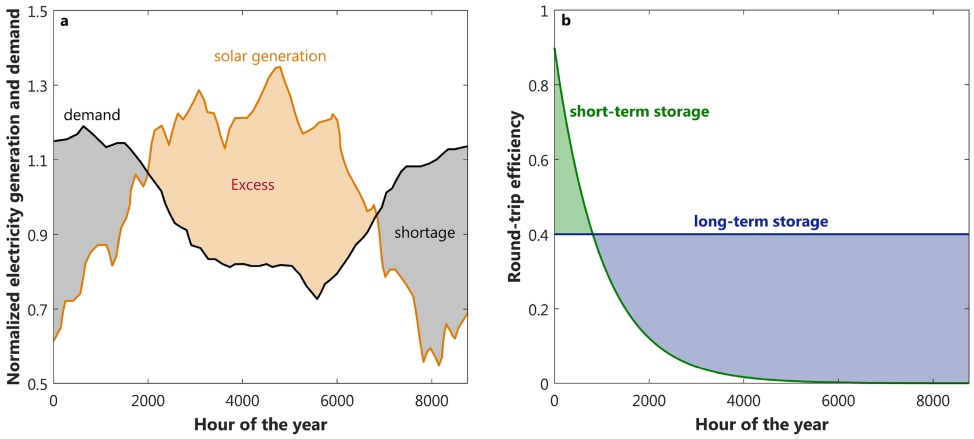

Figure 1.2: a) Seasonal correlation of electricity demand (black line) and solar generation (orange line) for Europe. b) Schematic round-trip efficiency for a short-term (e.g. battery, green line) and long-term (e.g. H2, blue line) storage technology (Gabrielli et al., 2020)

In 2024, energy suppliers in the Netherlands lost 2.5% of the annual electricity demand because wind and solar farms had to be temporarily shut down due to an excess of green energy on the grid (van der Gurp, 2024). For seasonal energy storage, batteries are not possible due to their low round-trip efficiency when used for long-term storage. This is because of their relatively low energy density and the self-discharge rate (de Wit, 2022).

Another challenge that needs to be overcome is periods with barely any wind or sunlight, also known as dunkelflaute. Recently, on the 12th of December 2024, a period of dunkelflaute occurred in the Netherlands. Between five and six PM, the energy prices reached an all-time high, 122 cents per kWh (including taxes), while the energy price is usually around 30 cents per kWh (de Vries, 2024).

The implementation of seasonal energy storage solutions could address these challenges. This was the motivation for the housing corporation deltaWonen to start a pilot. The pilot's goal is to solve the bottlenecks in the energy demand of residential areas. The technology to take residential areas off the gas network is available. Still, as for the electricity grid, the outlined prospect is that security of supply for 2030 is not guaranteed within the current frameworks. A possible solution for long-term storage is metal hydrides. These metals store hydrogen and can do so more safely and compactly than storing hydrogen under high pressure or at extremely low temperatures. There are many types of metal hydrides. The goal of this research is to explore whether they can be useful for applications in the built environment.
deltaWonen is conducting a pilot using metal hydrides for seasonal hydrogen storage, which sparked interest from network operator Alliander to further explore this technology.

1.1. Objective

Seasonal energy storage of hydrogen could be a solution to lowering the required peak capacity of the electricity grid throughout the year, as well as minimising the curtailment of green energy. This research serves to understand and learn more about the feasibility of the seasonal energy storage of hydrogen. The following main research question and subquestions will be investigated.

Main Research Question

What is the feasibility of room temperature metal hydrides for seasonal energy storage solutions in the built environment?

The research question primarily addresses the technical feasibility. Additional aspects within the scope of the research question are economic feasibility, safety requirements, spatial requirements, and system reliability.

Sub Research Questions

- How can a system-level model be developed to evaluate the performance of metal hydride as a seasonal energy storage solution?
- What is the potential for heat recovery and effective utilisation during the metal hydride storage process?
- What is the round-trip efficiency of a metal hydride storage when applied for seasonal energy storage?
- Beyond technical feasibility, what are the safety risks, economic costs, reliability challenges, spatial requirements, and environmental impact that affect the overall feasibility of implementing metal hydride seasonal energy storage?
- To what extent does integrating a seasonal metal hydride energy storage system reduce the required peak capacity of the electrical grid?
- At what scale can a seasonal metal hydride energy storage system be integrated most effectively within renewable energy systems?

1.2. Readers Guide

To answer the research question and corresponding subquestions, a room temperature metal hydride energy storage model has been built with a PEM electrolyser and PEM fuel cell. First, chapter 2 presents the relevant background literature. In chapter 3, the system description, model description, controller selection and verification are presented. In chapter 4, the results of the year model and the extreme cases are shown. This is followed by chapter 5, which assesses the non-technical feasibility aspects: the economic, reliability, maintenance, spatial requirements and environmental impact. An integrated discussion of all chapters is provided in chapter 6, and lastly, in chapter 7, the conclusion is given where the research questions will be answered, followed by recommendations for future research.

2

Literature Review

2.1. Hydrogen

Hydrogen is a potential energy carrier with a relatively low volumetric energy density and a high energy density per kilogram. That is why it is typically stored in compressed form, as a liquid, or by binding it to another element. Hydrogen is considered a clean energy carrier because its use does not lead to carbon dioxide emissions (Zohuri, 2019). This makes hydrogen energy storage potentially one of the most important means of storing available energy. When more electricity is produced than required, it can be stored as hydrogen until the electricity demand is higher than the supply. In Figure 2.1, hydrogen ranks among the best in terms of storage capacity, when the required storage space is not taken into account.

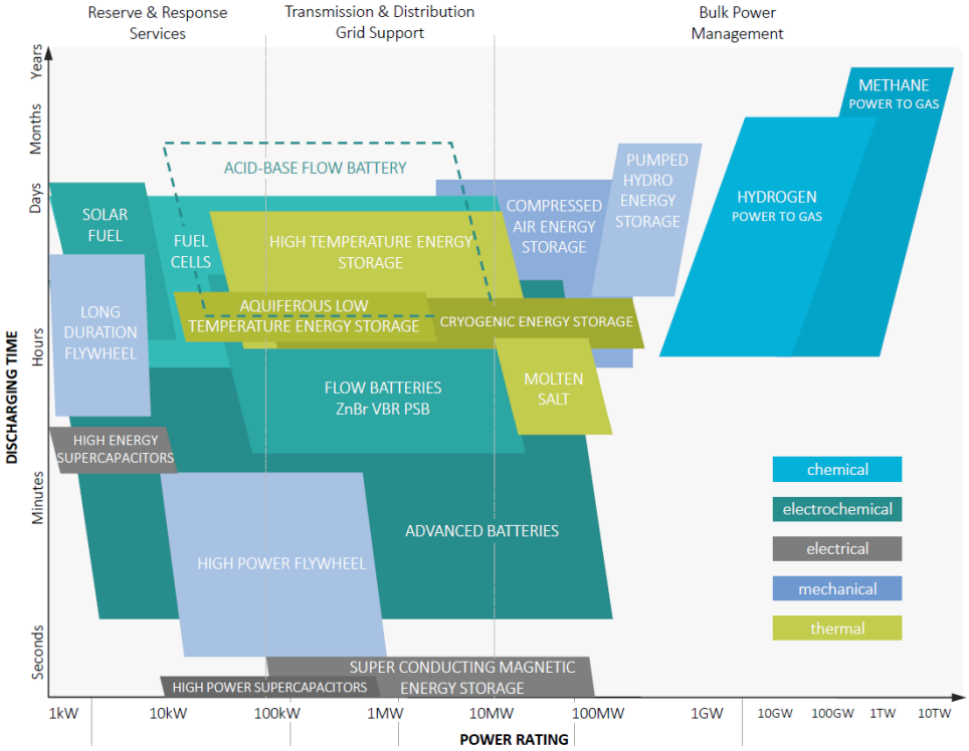

Figure 2.1: Overview energy storage systems (Pärnamäe et al., 2020)

2.1.1. How to Store Hydrogen

Hydrogen can be stored in multiple ways. It can be stored in a pure elemental form and chemically bonded to a material. The storage technologies compared in this literature review are shown in bold in Figure 2.2. Methane is not included as a hydrogen storage technology, because it is, due to the carbon, not considered a clean energy carrier.

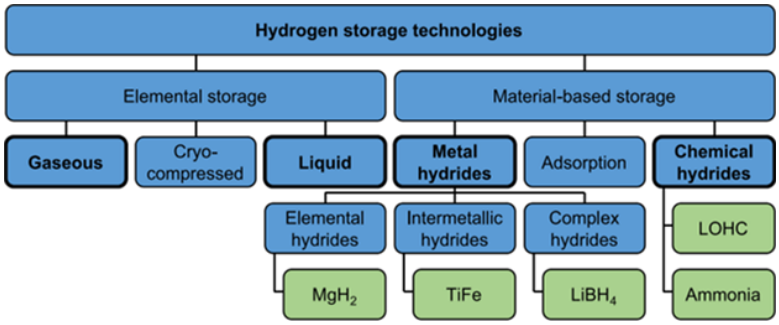

Figure 2.2: Overview of hydrogen storage technologies (Drawer et al., 2024)

2.1.2. Compressed Hydrogen Storage

Compressing the hydrogen gas is the most common way to achieve higher hydrogen storage densities. Hydrogen can be stored in tanks up to 700 bar at ambient temperatures. However, at 700 bar, the volumetric energy density is still relatively low compared to other hydrogen storage technologies in Figure 2.3. Additionally, high-pressure tanks come with high investment costs and significant safety risks and regulations (Reuß et al., 2017).
Another way to store gaseous hydrogen under pressure is in underground caves (Elberry et al., 2021).

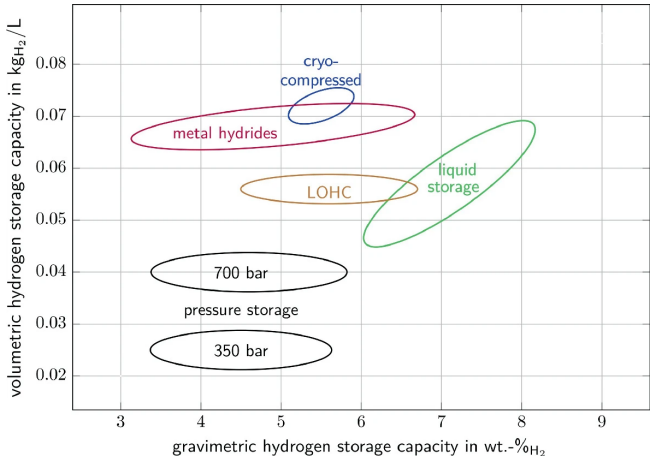

Figure 2.3: Comparison of different hydrogen storage technologies (Baetcke, 2024)

2.1.3. Liquid Hydrogen Storage

When hydrogen is cooled to -252.15°C, it becomes a liquid. Increasing the volumetric energy density up to 71 kg/m^3 (Reuß et al., 2017). This requires a high energy demand of 20% up to 50% of hydrogen's lower heating value. During storage, a part of the liquid hydrogen evaporates into gas. These boil-off losses can amount to as much as 3% per day for small tanks and 1% per day for larger tanks (Drawer et al., 2024).
Cryo-compressed hydrogen is a storage method that combines liquid hydrogen and compressed hydrogen gas. This technology will not be considered independently, as it presents the same challenges as liquid hydrogen for seasonal energy storage (Reuß et al., 2017).

2.1.4. Liquid Organic Hydrogen Carrier

Liquid organic hydrogen carriers (LOHC) allow hydrogen storage in liquid form in ambient conditions, enabling transportation similar to conventional liquid hydrocarbon-based fuels. LOHC systems consist of hydrogen-rich and hydrogen-lean organic compounds that store hydrogen through repeated catalytic hydrogenation cycles. Hydrogen is separated from the carrier for discharging using a catalyst and thermal energy at temperatures between 150 and 310°C (Drawer et al., 2024). While the process is theoretically reversible, reusing the heat released during hydrogenation to drive dehydrogenation remains technically challenging due to temperature and process mismatches. After separation, the hydrogen is used, and the carrier molecule must be stored for reloading (Reuß et al., 2017).

2.1.5. Ammonia

Chemical storage of energy can be accomplished by bonding hydrogen to another atom. Hydrogen can bond to nitrogen to form ammonia (NH_3). Ammonia has been identified as a sustainable fuel for remote and mobile applications if obtained from renewable energy sources. An advantage of ammonia is that it is a liquid when it is compressed to 8 bar at room temperature or cooled below -33°C at ambient pressure. This makes it relatively easy to transport when compared to liquid hydrogen. At the same time, the energy density of ammonia (15,6 MJ/L) is 70% more than liquid hydrogen (9.1 MJ/L) and almost three times more than 700 bar compressed hydrogen (5.6 MJ/L). However, a major drawback is that temperatures between 400 °C and 650 °C are required to separate the hydrogen from the nitrogen. Subsequently, an additional downstream cleaning step is necessary to eliminate unwanted impurities (Drawer et al., 2024). Additionally, ammonia is also considered toxic, with human exposure limits ranging from 25 to 50 ppm. Exposure to concentrations above 5000 ppm can have deadly consequences (Valera-Medina et al., 2018).

2.1.6. Metal Hydrides

There is a way to store hydrogen as a solid by bonding it to metal. A metal hydride is a metal that can bond with hydrogen atoms through a chemical process. This technology provides high volumetric energy density, making metal hydride promising for compact hydride storage. This is important as not the weight but the

system's footprint poses the limitations for a stationary system (M. V. Lototskyy et al., 2017). The reaction is reversible without loss of storage capacity throughout storage and is controlled by temperature and pressure (Bellosta von Colbe et al., 2019). The pressure and temperature required for hydrogen absorption and desorption depend on the metal hydride type. There are various types of metal hydrides, all with unique properties and challenges. For stationary applications, metal hydrides with hydrogen uptake and release near room temperature are promising candidates (Møller et al., 2017). Low-temperature metal hydrides are especially attractive because they have a lower reaction enthalpy and can operate at (near) ambient conditions (Nguyen & Shabani, 2021).

There are three types of metal hydrides: elemental hydrides, intermetallic hydrides, and complex hydrides. Elemental hydrides are chemically the simplest form of metal hydrides, as they store hydrogen through simple ionic bonding to one element. Intermetallic hydrides are formed by alloys containing two or more metal elements, often classified into AB, AB_2 and AB_5 types. Where the A bond is strongly to hydrogen, and the B elements bond weakly to hydrogen. Hydrogen can diffuse into the metal lattice, forming the hydride phase. That is why the operation temperatures are generally lower when compared to elemental hydrides. The last type are complex hydrides, salt-like materials in which hydrogen is covalently bound to the central atoms, forming a crystal structure. They have the highest hydrogen storage capacities among all hydride types, but often require temperatures above 300°C for hydrogen release and suffer from limited reversibility (Drawer et al., 2024).

Preferred Material Properties

Various metals can store hydrogen by direct dissociative chemisorption (absorption process that involves a chemical bond formation between a modifier molecule and the surface (Atif et al., 2022)) of hydrogen gas, as described in (2.1) (Nguyen & Shabani, 2021). The arrow points in two directions, indicating that the reaction is reversible.

$$M + \frac{x}{2}\mathrm{H_2} \leftrightarrow \mathrm{MH}_x + Q \tag{2.1}$$

Where M is a metal or intermetallic alloy; x is hydrogen concentration to metal; Q is the heat of reaction.

The thermolysis release reaction is endothermic; thus, Q is always positive. The heat released during the absorption process raises the temperature of the system. This rise in temperature significantly increases the pressure required for the incoming hydrogen gas. If there is no effective thermal management system, this temperature increase can lead to self-inhibition of the reaction, prolonging the filling time. Similarly, adequate heat must be supplied at a high enough temperature during desorption to sustain the equilibrium pressure necessary to release the hydrogen. The amount of heat can be determined by (2.2) (Nguyen & Shabani, 2021).

$$\dot{Q} = \frac{\dot{m}_{\mathrm{H_2}} \Delta H_{\mathrm{MH}}}{M_{\mathrm{H_2}}} = \dot{n}_{H2} * \Delta H_{MH} \tag{2.2}$$

Where $\dot{Q}$ (W) is heat released or required during the absorption and desorption process; $\dot{m}_{\mathrm{H_2}}$ is the mass flow rate of hydrogen (kg/s); $\Delta \mathrm{H}_{MH}$ is the enthalpy change (J/mol); $\mathrm{M_{H_2}}$ is the molecular weight of hydrogen (g/mol); $\dot{n_{h2}}$ is the amount of mol H_2 per second (mol/s).

To determine the operating pressure and temperature of different metal hydrides, pressure-composition-isotherms (PCIs) are typically used in conjunction with the van 't Hoff diagram, as seen in Figure 2.4.

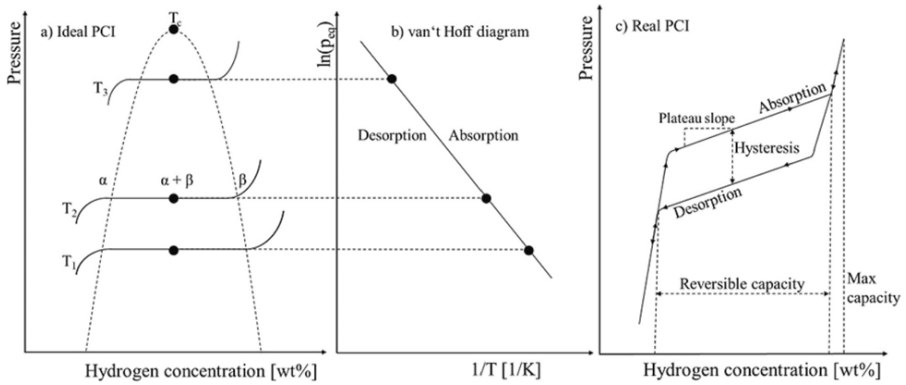

Figure 2.4: a) Ideal PCI at different temperatures, accompanied by b) van 't Hoff diagram and c) real PCI exhibiting hysteresis and plateau pressure (Klopčič et al., 2023)

The slope in the van't Hoff diagram is determined by the reaction enthalpy; this value varies significantly between low-temperature and high-temperature metal hydrides. Low-temperature metal hydrides have a lower reaction enthalpy and can operate at (near) ambient conditions. Therefore, reducing the reaction enthalpy by, for example, adding or substituting elements is beneficial (Nguyen & Shabani, 2021).

Elemental Hydrides
Elemental hydrides are the simplest form of metal hydrides. Hydrogen chemically bonds to only one element. Magnesium hydride (MgH_2) is the most prominent representative of the elemental hydride group. It has a volumetric storage capacity of 3.67 kWh/dm^3 and a gravimetric storage capacity of 7.6 wt% (Klopčič et al., 2023). It is cheap and readily available. However, the ionic bond between hydrogen and magnesium is very strong, resulting in poor reversibility. As a result, a lot of energy is needed to split the hydrogen from the magnesium, requiring temperatures above 320 °C to desorb the hydrogen from the magnesium (Bolarin et al., 2024). A disadvantage of magnesium is that when in contact with oxygen, an oxidation layer is formed at the surface, significantly inhibiting the hydrogen absorption rate. To remove the oxygen layer, an activation process is required (Drawer et al., 2024).

Intermetallic Hydrides
Intermetallic hydrides consist of at least two types of metal. The alloy scheme corresponds to $A_xB_yH_z$, where the A element bonds strongly to hydrogen and the B element bonds weakly to hydrogen. Hydrogen can diffuse into the metal lattice, forming the hydride phase. Therefore, operation temperatures are generally lower than those of elemental hydrides (M. V. Lototskyy et al., 2017). The intermetallic hydrides can be divided into three main ratios: AB, AB_2 and AB_5. Each will be discussed in the following paragraphs.

AB
A well-known low-cost AB alloy is TiFe, a combination of titanium and iron, with a volumetric storage capacity of 4.03 kWh/dm^3 and a gravimetric storage capacity of 1.86 wt% (Klopčič et al., 2023). The advantage, over some other metal hydrides, is that it can absorb and desorb near room temperatures under near-atmospheric pressures. A drawback of TiFe is the activation process, which is required before TiFe can hydrogenate. This requires high pressures (65 bar) and high temperatures (400-450°C) to remove the oxidation layer. TiFe is extremely sensitive to water vapour oxidation, possibly due to the formation of a Ti oxide layer at the surface. This oxide layer reduces the hydrogen absorption kinetics as well as the storage capacity.
However, the exact reason why the activation process works is still unsolved. Many efforts have been made to reduce this disadvantage to improve the activation process. The action process of TiFe can be significantly improved by adjusting the Ti/Fe ratios, adding a third element or adjusting the mechanical process (for example, ball milling) (H. Liu et al., 2023).

AB_2
$TiMn_2$ combines titanium and manganese, which has a volumetric storage capacity of 4.09 kWh/dm^3 and a gravimetric storage capacity of 1.86 wt%. It is a low-cost metal hydride with good kinetics and easy activation. $TiMn_2$ can achieve relatively high hydrogen absorption rates at room temperature without activation. Its properties can be further enhanced by ball milling or annealing. Mn has a high oxygen affinity, so it must be stored without contact with oxygen. The disadvantages are the relatively high plateau pressures and high hysteresis between the absorption and desorption. The best way to improve these properties is partial substitution of other elements (Klopčič et al., 2023).

AB_5
$LaNi_5$, a combination of lanthanum and nickel, is a well-investigated metal hydride. It has a volumetric storage capacity of 4.12 kWh/dm^3 and a gravimetric storage capacity of 1.49 wt%. The activation process is relatively fast and straightforward, requiring cycling below 100°C and below 100 bar of pressure. However, the material cost is higher than TiFe (Marinelli & Santarelli, 2020). In contrast to TiFe and $TiMn_2$, where mechanical treatment improves the activation process and kinetic properties, a decrease in storage capacity for $LaNi_5$ is reported after 1-3 minutes of ball milling, compared to the cast sample. Due to the good resistance to impurities, oxygen exposure is less of a problem when compared to most other metal hydrides. Enhancements can be made by partly substituting Ni with small amounts of Al, Co and Mn, decreasing the plateau pressure. While the partial substitution of La by Ce, Pr or Nd leads to better cyclability, it also increases the plateau pressure (Klopčič et al., 2023).

Complex Hydrides
Complex hydrides work differently compared to elemental and intermetallic hydrides. They are salt-like materials in which hydrogen is covalently bound to the central atoms, forming a crystal structure. Complex hydrides can store relatively large amounts of hydrogen compared to other metal hydrides, making them potentially interesting storage materials. When first discovered, complex hydrides were not considered for reversible hydrogen storage because of the high-temperature requirement for the desorption process. This changed when it was found that the kinetic barrier of the desorption process can be lowered by adding Ti as a catalyst, resulting in close to acceptable technical conditions (Hirscher & Hirose, 2010). Two common types of complex hydrides are complex borohydrides ($LiBH_4$ and $NaBH_4$) and complex aluminium hydrides ($NaAlH_4$); they will be addressed in the following two subsections.

Complex Borohydrides
Complex borohydrides are promising for hydrogen storage due to their high hydrogen content. However, the high thermal stability makes the hydrogen release process difficult, and they generally exhibit poor reversibility under moderate technical conditions (Hirscher & Hirose, 2010). This is because, unlike conventional metal hydrides where hydrogen is reversibly bonded to metal atoms, complex borohydrides store hydrogen in borohydride (BH_4) groups. Hydrogen release involves multi-step decomposition reactions, often requiring high temperatures and producing stable by-products with limited reversibility (Au & Walters, 2010). Two commonly studied complex borohydrides are $NaBH_4$ and $LiBH_4$.
The reaction of $NaBH_4$ differs from all the other metal hydrides discussed in this literature review. The hydrogen is released from the $NaBH_4$ when in contact with water. The process is called hydrolysis. This approach differs from all the other metal hydrides presented in this research, as they use heat (thermolysis) for the desorption process and endothermic reactions. The desorption process of hydrolysis is realised by adding water to $NaBH_4$, and the desorption reaction is exothermic. The advantages of the hydrolysis reaction are the fast kinetics at room temperature, the possibility of a cold start, and straightforward control. The increase in temperature, due to the exothermic reaction, also increases the reaction speed. This is why water management and cooling are important to keep the reaction safe (Andersson & Grönkvist, 2019). The reaction is described in (2.3) (Demirci et al., 2010).

$$NaBH_4 + 2H_2O \rightarrow NaBO_2 + 4H_2 + Q \tag{2.3}$$

$NaBH_4$ has a volumetric storage capacity of 3.20 kWh/dm^3 and a gravimetric storage capacity of 10.8 wt%. The $NaBH_4$ stores half of the hydrogen, and H_2O provides the other half of the hydrogen. However, the reaction is irreversible, and the regeneration of $NaBO_2$ is not yet practical. The most common industrial method for the production of $NaBH_4$ is the brown-Schelsinger process, which uses trimethyl borate ($B(OCH_3)_3$) and sodium hydride (NaH) (Dragan, 2022).
Therefore, refuelling with $NaBH_4$ remains the best solution until regeneration becomes feasible (Demirci et al., 2010). This is the reason why $NaBH_4$ will not be taken into further consideration in this literature review.

The second complex borohydride is $LiBH_4$, which is preferred to use with thermolysis for high hydrogen storage capacity. It has a volumetric storage capacity of 4.08 kWh/dm^3 and a gravimetric storage capacity of 18.5 wt%. Its high hydrogen storage capacities could make it an interesting material for hydrogen storage. However, the hydrogen desorption process occurs in four sequential endothermic peaks, increasing in temperature. The third peak, with the largest desorption (9 wt%), occurs between 400-680°C.
The harsh operating conditions and slow reaction kinetics represent the most significant challenges that must be addressed or substantially mitigated. Several strategies are available to enhance these properties; use of catalysts, partial substitution of alloy or reducing the particle size (Klopčič et al., 2023).

Complex Aluminium Hydrides
Complex aluminium hydrides offer several advantages, including low cost and low density. However, their high kinetic barriers prevented them from being considered viable hydrogen carriers for many years (Hirscher & Hirose, 2010). A well-studied complex aluminium hydride is $NaAlH_4$.
It has a volumetric storage capacity of 3.20 kWh/dm^3 and a gravimetric storage capacity of 7.5 wt%. The significant disadvantage of $NaAlH_4$ is that its kinetics are slow, and reversibility is poor. High temperatures (200-400°C) and pressures (100-400 bar) are required for absorption. To use $NaAlH_4$ in practical conditions, enhancing the properties is required. This can be achieved by using a doping agent (adding small amounts of foreign elements into an alloy to modify its properties), which is typically mixed under an inert atmosphere and then subjected to milling.

Selecting Metal Hydride for Seasonal Hydrogen Storage
Among the reviewed metal hydrides, intermetallic hydrides offer the overall best performance. Regarding volumetric energy density, the intermetallic hydrides generally perform the best. They also show favourable thermodynamic properties, allowing for hydrogen absorption and desorption at relatively low temperatures and pressures. Furthermore, considering the lifetime and cyclability, intermetallic hydrides meet the required stability for stationary applications (over 10.000 cycles with less than 30% capacity loss (Modi & Aguey-Zinsou, 2021)), whereas elemental and complex hydrides suffer from slow kinetics and poor reversibility.

Based on these advantages, only the intermetallic hydrides are considered in this research. More specifically, the focus will be on TiFe, as this material is used in the case study that is used during this research. More information about the case study is given in subsection 3.1.1.

2.2. Sodium-ion Batteries

The increasing demand for sustainable and cost-effective battery storage has driven research beyond the conventional lithium-ion battery. Sodium-ion batteries (SIBs) are a potential alternative to lithium-ion batteries (LIBs) as they use the abundant sodium reserves of the earth instead of the scarce lithium, nickel, cobalt and graphite. However, the energy density is lower than that of lithium-ion. Both batteries' components and electrochemical reaction mechanisms are identical, except for the charge carrier, which is Na^+ instead of Li^+. Furthermore, the material synthesis methods and routes can be easily borrowed and adapted from the LIBs.

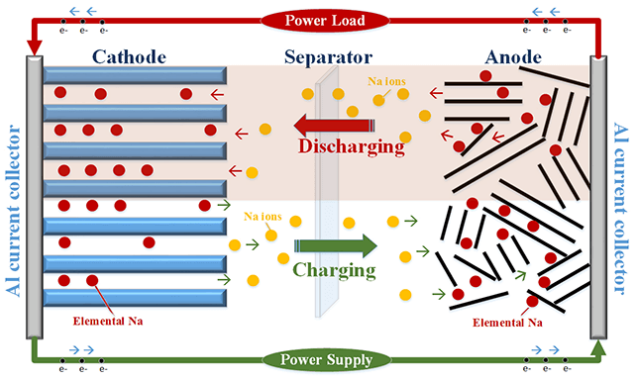

Figure 2.5: Working principle of Sodium-ion Battery (ecolithiumbattery, 2022)

The four main components in a sodium-ion battery are: a cathode material (Na^+), an anode material (hard carbon), an electrolyte (liquid sodium salt), and a separator.
The charging and discharging process is illustrated in Figure 2.5. During the charging process, sodium ions are extracted from the cathodes and inserted into the anodes, while the current travels via an external circuit in the opposite direction. When discharging, the sodium ions leave the anode and return to the cathode. The sodium-ion battery can be fully discharged without damaging the battery (Zhao et al., 2023).

2.3. PEM Electrolyser

Water electrolysis is a process that splits water into hydrogen and oxygen using electrical energy. In an electrochemical cell, an external voltage drives the redox reaction, converting electrical energy into chemical energy stored in hydrogen (Chisholm et al., 2022).

The PEM electrolyser has been selected as the electrolyser type because it has a fast response, a low startup time, compact size, and high hydrogen purity up to 99.999% (Nasser et al., 2022).
PEM electrolysis is an electrochemical process that uses a solid polymer membrane to produce hydrogen and oxygen from deionised water. High-purity deionised water is pumped into the anode, where it is oxidised to produce oxygen, protons and electrons. Only the protons can move through the membrane to the cathode, while the electrons will reach the cathode via an external circuit. At the cathode side, the electrons and protons combine again to produce hydrogen. The new generation of PEM electrolysers has a stack efficiency of 77-80% and a system efficiency of 74-79% (van der Roest et al., 2023).

The first benefit of a PEM electrolyser is that it can operate at higher current densities. The ohmic losses limit the current density. A thin membrane with good proton conductivity can improve the current density. The second benefit is a low cross-over rate over the membrane, resulting in high-purity hydrogen 5.0 quality (Shiva Kumar & Himabindu, 2019). Lastly, a solid electrolyte allows for a strong and compact system, enabling the electrolyser to operate at higher output pressures of 30-40 bar (Hancke et al., 2024). As a result, less energy is required to compress the hydrogen further, potentially removing the need for an external compressor to store the hydrogen in the metal hydride.
A disadvantage of PEM electrolysers is that the use of materials is limited. The materials must be resistant to harsh corrosive low pH conditions (pH 2) and sustain the high voltage (2 V) applied. This will demand the use of expensive, scarce materials for the catalyst and membrane (Carmo et al., 2013).

Heat Flow Electrolyser
The heat production in the electrolyser stack is due to the chemical reaction's irreversibility and the cell's ohmic resistance. At the thermoneutral voltage, the electrolysis reaction can occur without consuming or producing heat. However, the reaction rate is so slow at this potential that there is almost no hydrogen production. Therefore, an overpotential solution is applied to the electrochemical cell. This increases the reaction rate but also makes the reaction exothermic, and thus, heat is produced.

The research (Tiktak, 2019) showed that, by modelling a medium to large scale PEM electrolysis, 92% of the heat produced by the stack was extracted by the cooling circuit. The other 8% is mostly used to evaporate the water

in the stack and convection losses to the environment, reaching a stack efficiency of 98.4%.
The research of (van der Roest et al., 2023) shows in Figure 2.6 that about 5-8% of the usable heat is used to preheat the deionised water stream before it enters the stack. Additionally, 80% of the waste heat can be used for another application. In this case, the heat is locally consumed by an industrial heat consumer. This results in a total system efficiency of 90%.

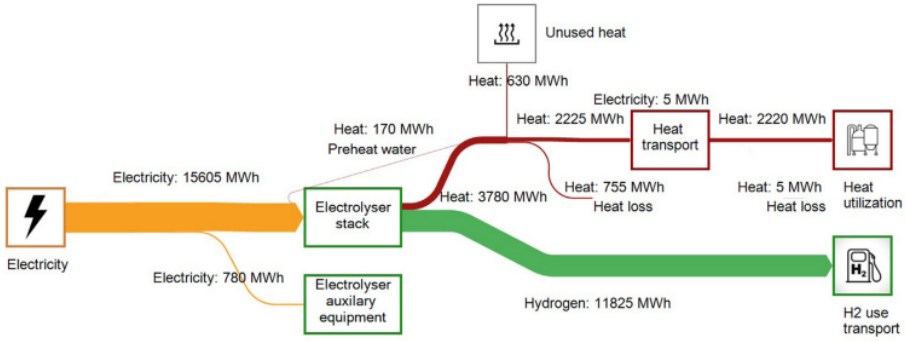

Figure 2.6: Energy flow diagram for a PEM electrolyser (van der Roest et al., 2023)

2.4. PEM Fuel Cell

A fuel cell is a device that converts chemical energy from a fuel, hydrogen, directly into electrical energy plus heat through the electrochemical reaction of hydrogen and oxygen into water. The process is that of electrolysis in reverse (Cook, 2002).

The PEM fuel cell has been selected as the fuel cell type. Among the various types of fuel cells, PEM fuel cells represent the most advanced technology and have been widely adopted in numerous systems. This is due to their ability to achieve higher power density, greater efficiency, lightweight design, compact size, lower cost, low operating temperatures, and faster start-up compared to other fuel cell types (Bvumbe et al., 2016).
The operation principle of a PEM fuel cell is as follows. First, hydrogen and oxygen are supplied to the anode and cathode, respectively, through flow channels. This leads to a generation of protons at the anode and electron transport through the external circuit. At the anode, hydrogen is oxidised, splitting into protons and electrons. The protons pass through the proton exchange membrane (PEM), while the electrons flow through the electrically conductive electrodes, the current collectors and the external electrical circuit. At this point, work is conducted before returning to the cathode. The protons and electrons combined with oxygen at the cathode produce water and heat. The overall result of this reaction is a flow of electrons through an external circuit, generating direct current. The efficiency of the stack falls within the ranges of 40% to 50% under standard operation conditions (Bvumbe et al., 2016). The operational temperature of a PEM fuel cell is between 60 °C and 85°C (Tawalbeh et al., 2022).

Heat Flow PEM Fuel Cell
Figure 2.7 gives an overview of the energy flow in the fuel cell. In this overview, the efficiency of the fuel cell is assumed to be 50%. The unreacted hydrogen (5%) can be recirculated, vented, burned or used in a secondary production step. In modern fuel cells, the hydrogen is often recirculated. However, the use case of the unreacted hydrogen is assumed to be out of scope for this research. The heat generation is 45% of the total energy put into the fuel cell, and 9% of this heat is used internally or lost due to natural convection, which leaves 36% of the heat to be reused.

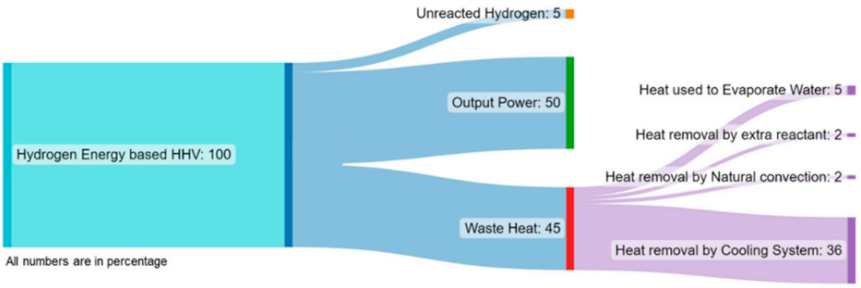

Figure 2.7: Energy flow diagram in a PEMFC (Cetinkaya et al., 2023)

A part of this heat can be internally used to preheat the hydrogen and air to improve the fuel cell performance (Nguyen & Shabani, 2020). Another application for the heat is to use it for the desorption process of the hydrogen out of the metal hydride, while the remainder of the heat can be used for other purposes. The waste heat greatly increases the hydrogen flow rate during the desorption process, reducing the discharge time of the

metal hydride. As well as reducing the capacity of metal hydride needed to fulfil the flowrate requirement of the fuel cell (Omrani et al., 2019).

The simulation in the research of Tong (Tong et al., 2023) showed that 21% of the heat produced by the PEM fuel cell is enough to heat the metal hydride reactor under ideal conditions. This shows that most of the heat produced by the PEM fuel cell remains unused. The remainder of the waste heat can be used for other purposes to increase the system's efficiency.
The remaining waste heat can be used for three applications: power generation, heating, or cooling. An organic Rankine cycle or a thermoelectric generator can be used to improve the system's electrical efficiency for power generation. The heat can also be directly used for residential applications, heating rooms, or heating domestic water. The last application of the heat can be to drive absorption and desorption chillers to cool in residential applications (Baroutaji et al., 2021; Nguyen & Shabani, 2020; Wilberforce et al., 2024).

2.5. Existing Models and Limitations

A lot of information about the technical details of the different components of the system is already available, especially about the PEM fuel cell and the possible applications for the waste heat. On the other hand, little research has been done on integrating the different components (PEM electrolyser, low temperature metal hydride system and PEM fuel cell). The most promising research is that of (Bhogilla et al., 2024). The research integrated a metal hydride hydrogen storage system with a reversible PEM membrane fuel cell, working in dual mode, as an electrolyser and a fuel cell. Part of the heat produced by the fuel cell is used for the desorption process of the metal hydride, while the remainder of the heat of the fuel cell and the heat of the electrolyser are used to drive a vapour absorption refrigeration system (VARS) for cooling applications. The research focuses on finding the maximum system efficiency and optimising the combined cooling and power efficiency. The system achieves a maximum energy efficiency of 94.1% in electrolyser mode and 73.3% in fuel cell mode. This useful and interesting research provides the initial formulas that can be used as the foundation to integrate heat utilisation into a model. However, the research does not mention the integration with the electricity grid.
A reversible PEM fuel cell has lower efficiencies than a separate electrolyser and fuel cell (Banasiak & Kienberger, 2024). Therefore, to maximise the efficiency of the seasonal energy storage system, this research will focus on a separate PEM electrolyser and fuel cell.
Additionally, in the scope of this research, the fuel cell is used during the winter. During the winter, the cooling application is not as interesting. However, during the summer, it could be a useful use of he electrolyser's waste heat during summer operation. To follow up, the research of (Chen et al., 2015) uses waste heat for cooling in the summer and heating in the winter. The maximum efficiencies are 70.1% and 82%, respectively. This shows that using the fuel cell in the winter has greater potential.

The main point of interest for stationary metal hydride systems in the literature has been to supply power to off-the-grid remote locations. Gray (Gray et al., 2011) explores using an off-the-grid power supply to remote locations that need a storage system for intermittent renewable energy sources. The system consists of: PV solar panels, a PEM electrolyser, metal hydride storage, and a PEM fuel cell. Only the surplus of energy is used for hydrogen production. It explains how to match the PV array and the electrolyser and the requirements for the metal hydride storage reactor.
The option to use the metal hydride storage system integrated with the electricity grid has been investigated less. The most extensive research available on the topic is the research of Chauhan & Ranjan (Chauhan & Ranjan, 2024). This research shows the opportunities and challenges of integrating an electrolyser fuel cell system in the electricity grid (the hydrogen storage technology is not specified). The opportunities are enhanced flexibility of the grid, balancing of the demand and decarbonising industrial processes. However, challenges remain in hydrogen storage, efficient energy conversion, and grid compatibility. Policymakers are expected to take charge of accelerating the system's adoption by establishing regulations and encouraging investments.
Frankowska (Frankowska et al., 2022) made a model, optimised from the point of view of the operator of the energy distribution system. Stored hydrogen, kept in pressurised gas tanks, can be deployed to balance fluctuations in the power grid. The results state several benefits to enhance the flexibility of the electricity grid. However, the study does not determine the impact on the effectiveness and efficiency of the electricity grid.
The only real large-scale hydrogen storage system that uses an electrolyser-fuel cell system, which can be integrated with the electricity grid, is the Fukushima Hydrogen Energy Research field (FH2R). After the hydrogen is produced, it is temporarily stored in high-pressure tanks. It uses renewable energy and the grid to power the electrolyser. The produced hydrogen can then be used to power the mobility sector and the industry or transformed back into electricity to balance the grid when there is a high electricity demand. (Toshiba, 2020). Theoretically, it is possible, and the FH2R project has shown that the system works without storage in metal hydrides. This opens up an interesting gap in the literature. How much does the integration of a metal hydride energy storage system, which is connected to the grid, increase the grid's flexibility by reducing the required connection capacity demand?

3

Methodology

This chapter is intended to describe the model and methodology used for answering the research questions. It starts with a description of the system architecture, followed by the development of the model. The control strategy is then introduced, and finally, the model verification process is discussed to ensure the accuracy and reliability of the implemented approach.

3.1. System Description

This section presents the deltaWonen case study, which forms the foundation of this research. After explaining the simplification of the case study, the background behind the input data of the supply and demand is presented.

3.1.1. Case Study deltaWonen

deltaWonen is a housing corporation that takes responsibility for its social community role as the starter of the energy transition in the residential areas. Their goal is to optimise the energy transition in their area of operation. Therefore, they are actively seeking ways to progress in the energy transition. A key step in this is to make the residential buildings independent from the gas network while not relying on the long waiting list to reinforce the electricity grid. In 2025, they plan on starting a new project in Kampen, the Urban Energy Island (UEI). This will be a pilot of 40 apartments that will be part of an innovative energy system to become 80% autarkic. This will be done with the help of daily and seasonal energy storage of self-generated renewable solar energy. The results from the project will be shared so that they can be used as a blueprint for making other neighbourhoods in the Netherlands more sustainable. The mismatch between the energy supply and demand needs to be addressed to achieve this. Most of the energy is consumed in the evening, while renewable solar energy has its peak production in the middle of the day.
The UEI project contributes to solving the challenge concerning energy supply and disconnection from the gas network in three different ways (deltaWonen, 2024):

1. Sustainability: aim to use 100% renewable and locally generated energy within the UEI concept.
2. Grid congestion: further electrification of buildings within the existing electricity grid's capabilities without grid reinforcement.
3. End user: predictable and constant living costs for residents in energy-efficient and future-proof homes.

Project Description

The Urban Energy Island (UEI) project will be demonstrated with 40 apartments in Kampen and four complexes of ten apartments. The project will be realised in six development steps (deltaWonen, 2024).

1. Each of the apartments will be made energy efficient, minimising the heat demand of each apartment. The insulation of the apartments will realise this. In addition, ventilation measures will also be implemented whereby, through heat recovery, heat from ventilation air will be reused.
2. Each apartment complex will be equipped with a heat pump and hot water booster. A hot water booster uses the heated water from the heat pump, which is used for heating the apartments, to increase the temperature further so that it can be used for domestic hot water applications. Additionally, each house will get an individual hot water buffer, ensuring efficient provision of heating, cooling and hot tap water. This system uses only electricity and will be free of natural gas.
3. On top of each of the four complexes (of ten apartments each), 75 PV panels will be installed. They will be oriented towards the south to generate as much energy as possible. The residents will be stimulated to use as much renewable energy directly as possible and match their demand to the supply. Here, the smart control of the heat pump and hot water buffer optimises direct consumption.
4. For daily energy storage, collective batteries of 95 kWh will be installed for each complex of 10 apartments.
5. One collective seasonal energy storage will be implemented for the 40 apartments in the form of hydrogen stored in the intermetallic hydride TiFe. This system includes a 40 kW PEM electrolyser, a 25 kW PEM fuel cell, and a hydrogen storage capacity of 4.8 MWh.
   The stored hydrogen can be used in periods, mainly in the winter, when too little solar energy is generated.

The fuel cell is used to generate electricity, and the waste heat will be, where possible, used directly or stored in the underground heat storage.

6. In the project's final step, a smart controller is integrated into the energy concept so that the various subsystems can be interconnected and control the use of the electricity grid. In addition to regulating potential energy surpluses, electricity will be drawn from the grid when rates are at their lowest. The interaction with the electricity grid is based on dynamic hourly rates.

Simplifications of the Case Study

Certain simplifications have been made to be able to analyse the case study:

- Step six of the project description, the integration of dynamic energy prices, is not implemented. This results in missing the opportunity to charge the metal hydride when the electricity rates are the lowest and discharge the metal hydride (and sell the electricity) when the electricity rates are the highest. This step is left out to reduce the complexity of the problem.
- The case study includes a collective ground source heat storage system, which allows heat to be stored for later use. This will not be implemented in the analysis; instead, all the required heat must be produced and consumed within the same time step of one hour. This results in an increase in the peak load compared to the real case, as in reality, the heat storage allows for heat generation during the day, while using it during the evening. This decision has been made as the size of the heat storage solutions is not known, and this problem is mitigated by using the average heat requirement of a household instead of the heat demand of a specific household. This already evens out the heat demand over the day.
- in the case study, the hot water booster uses heated water from the heat pump, which is used for heating the apartments, to increase the temperature further to use it for domestic hot water applications. In order to simplify the situation, these two heat demands are split. The available waste heat is first used to reduce the demand of the heat pump; if any remaining heat is left, it is then used to reduce the heat demand. In reality, apart from the advantages of the heat storage mentioned previously, this implementation doesn't make a difference to the case study, as the electrical energy required for each heat demand is given separately. For both, the heat demand is known independently. This decision has been made to reduce the complexity of the problem.
- In the case study, four small daily batteries are used (95 kW); this will be simplified to one daily battery of 380 kW. In reality, the use of four batteries, one at every block of apartments, allows for greater redundancy and increased flexibility during maintenance. Additionally, it lowers the peaks power delivered or required from each of the batteries, as also the PV production and demand is split equally over the four batteries. Nevertheless, using one large battery is a reasonable simplification for the analysis.
- in the case study, the energy that can be directly used to fulfil the demand does this without going through the daily battery. In the analysis, all the energy passes through the daily battery. This simplification does not affect the results, as the battery is assumed to operate without efficiency losses or degradation. This assumption is made because the goal of the analysis is to show the feasibility of seasonal energy storage; the focus is not on the daily battery. However, in reality, this does make a difference, as the battery has efficiency losses and degradation losses.

Input Data of Supply and Demand

Besides the total annual supply or demand, presented in Table 3.1, no additional profile of the energy use throughout the year has been provided by deltaWonen. However, to simulate the behaviour throughout the year, usage profiles for all the supplies and demands, with a time step of one hour between the data points for an entire year, are required to determine the expected behaviour of the model.
All usage profiles have been normalised so their values fall within a comparable range. This is necessary in order to use the shape of the usage profile rather than the total magnitude, which is already provided by deltaWonen. This is accomplished by scaling the dataset so that the sum equals one. The resulting profiles represent the relative distribution of supply or demand over the year. The normalised inputs can then be multiplied by the total annual value to find the value per hour.

Table 3.1: Total energy annual

Dataset	Value	Unit
Maximum grid capacity	40	kW_{el}
PV Production	138000	kWh_{el}
Electricity demand	72000	kWh_{el}
Heat demand	16400	kWh_{el}
Domestic hot Water demand	23160	kWh_{el}

It is decided to use ten years of data to create a dataset of one year, which is the average of the ten years. Starting from the most recent available year, 2023, up to 2013 is used; 2014 is not used as not all the data was available for 2014. Using a ten-year average as input for the analysis has the advantage that the analysis is not optimised for a single year, which could have extreme cases that do not represent a typical year of system usage. In chapter 4, a single year's data will be used to test how well the trained model works. The years 2013 and 2015 will be used, as these are the two years for which the complete input data is available.

The model starts the year on 1 October, with a full metal hydride storage. This is right before the net energy generation becomes negative, allowing for the most realistic situation, where the metal hydride storage is full at the end of the summer.

PV Generation
The data for PV generation is found using the photovoltaic geographical information system of the European Commission (Euopean Commission, 2024). This website estimates the output of a PV system in every location in Europe for up to an hour, considering solar radiation, temperature and wind speed. As described by deltaWonen, the case study will take place in the Flevowijk in Kampen. However, the exact location is unknown. Therefore, an apartment block with a flat roof in the Flevowijk is chosen for the location. The PV panels are placed towards the south to maximise solar radiation.

Ambient Tempeature
The data for the ambient temperature is supplied in the same dataset as the PV generation.
The ambient temperature determines how much of the heat generated by the system can be effectively reused to fulfil the heat and domestic hot water demand.

Electricity Demand
The data for the electrical demand is provided by deltaWonen. The E1A data is used; E1A contains the standard grid capacity size data equal to or lower than 3 x 25A. The data is provided every 15 minutes; as the model works per hour, the four data points are added together to get the value per hour. However, the data from the corresponding ten years was unavailable; only the data from 2010-2015 were available. Although a ten-year average from the corresponding years would have been preferred, it is not a limiting factor. Because electricity usage excludes the use of heating systems, it is not expected to vary a lot over the years.

Space Heat and Domestic Hot Water Demand
Both the space heat and domestic hot water demand are found on the same website of TNO (TNO, 2024). The neighbourhood of the case study, Flevowijk, can be selected on the website. For climate information, De Bilt is used as the location. The result of the dataset is the estimated space heat and domestic hot water demand per hour.

3.2. Model Description

This section explains the need for the model and outlines its development. To be able to understand the development of the model, an overview of the model is given first. Afterwards, the assumptions and input of the model are presented. Finally, the factors considered for each component are described in detail.

3.2.1. Motivation for Development of a Model

A structured and quantitative approach is required to analyse the feasibility of metal hydride as a seasonal energy storage solution, a complex interdependent system. Rather than relying on an analysis of the components or empirical testing, a model on a system level provides an integrated framework that allows the evaluation of the energy flows between the different components as well as insight into the operational strategies of the system.

The decision to build a model is based on the following motivations:

- **System complexity:** The interaction between the multiple modes of energy (electricity, hydrogen and heat) and operational constraints requires a structured approach to understand the system behaviour.
- **Performance metrics:** Through simulation, key performance indicators such as the system efficiency, (dis)charging of the daily battery and waste heat recovery can be assessed and optimised.
- **Design guidance:** The model allows easy change of the size and specifications of the components. This provides insight into the component sizing and the logic of the control of the system.
- **Exploration of different scenarios:** A model allows for evaluating various scenarios and extreme cases, without extensive prototyping.

3.2.2. Overview Model

In Figure 3.1, an overview of the energy flows between all the different components and external supply and demand in the model is shown.

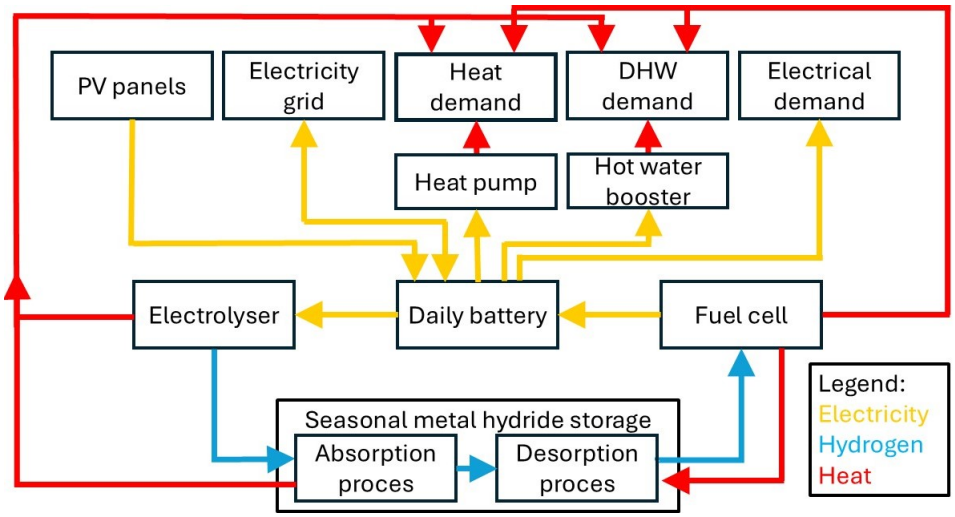

Figure 3.1: Overview of the energy flow between components

The components in the model, shown in Figure 3.1, are treated as black boxes. Their inputs and corresponding outputs are known, but not all internal details are explicitly modelled. For example, internal heat losses that can't be reused to reduce the heat demand are known. However, while these losses depend on various factors within the component, in reality, they are simplified as a constant in the model.

All the streams of supply and demand are connected to the daily battery, which works as the storage of electricity in the short term. During each time step, all the streams of supply and demand are combined into one net energy production; the storage level of the daily battery is updated every time step in the model.

The model works in discrete time, with timesteps of one hour. During that hour, the processes in the components are in a steady state. The time step of one hour is found to be sufficient, as the daily battery can manage fluctuations within the hour. The most significant peak within the hour is expected when going from no PV generation to full PV generation. In this case, the 300 PV panels with 400 W_p generate 120 kW of power. This is within the daily sodium-ion battery's power range limit of 1C (1C = 380 kW).

The control system is responsible for making optimal use of the daily battery, as well as determining when to provide electricity to the electrolyser to produce hydrogen that is used to charge the metal hydride storage, or when the fuel cell must be turned on to turn the hydrogen back into electricity. The demands that need to be fulfilled are the electrical, heat and domestic hot water demand. There are two possible external input streams of electricity: PV panels and the electricity grid. The production of the PV panels is intermittent as it depends on the solar irradiance. The second source of electricity comes from the electricity grid, which can be used to import electricity to the daily battery or export it back to the grid. The only dependency is that the maximum grid capacity is 40 kW.

Besides electricity and hydrogen, there is also an energy stream of heat within the system. Heat is generated by the electrolyser, the absorption process and the fuel cell. Part of the heat of the fuel cell is used to provide the desorption process with the required heat. This heat can be reused to first lower the heat demand, and, if there is any heat left, to reduce the domestic hot water (DHW) demand.

3.2.3. Uncertainty on the Prediction Horizon

In real-world applications, future input data is inherently unknown. However, it is possible to forecast what is expected to happen in the future. Although it is not certain that the expectation will come true, there is uncertainty in the forecast.
In the model, it would be possible to know what will happen in the future, as historical data is used in this simulation. However, to mimic the uncertainty of the forecast, a band of uncertainty is added to the input data within the prediction horizon. More information about the prediction horizon will be explained in the section about the controller in section 3.3. Each of the data points within the prediction horizon is randomly changed into a value that falls within the uncertainty band, which is uniform over the prediction horizon; the uncertainty does not increase when looking further into the prediction horizon. The boundaries of the uncertainty are different for the PV supply, electrical demand and heat demand bands, which have been based on the mean absolute percentage error (MAPE) found in other research.

Except for the first hour, the mean absolute error percentage is added as the uncertainty to all hours within the prediction horizon. The uncertainty is recalculated for the selected values within the new prediction horizon at the next time step.

Uncertainty PV Supply Forecast
The study of Theocharides (Theocharides et al., 2024) used two years' worth of data, which were measured at the test facility at the University of Cyprus. The testbench consisted of five poly-crystalline silicon PV modules, rated at 235 W_p each. The PV panels were oriented towards the south to optimise the annual energy yield. The first year of data was used to train the model, and the second year was used to test the model. The resulting mean absolute percentage error of the testing data for the PV power forecasting is 6.91%.

Uncertainty Electrical Demand Forecast
The study of Yan (Yan et al., 2015) demonstrates that the load measurements from the previous 48 hours and the predicted temperatures for the next 24 hours can be used to predict the day-ahead electrical demand. The research was based on an analysis of French power consumption and temperature data from 2010. After the training, the network is tested with a separate dataset, which was not used before in training. The resulting mean absolute percentage error of the testing data of the load demand forecasting is 3.84%.

Uncertainty Heat Demand Forecast
The study of Golmohamadi (Golmohamadi, 2022) did research into the increasing intermittency of the supply side for the heat service providers due to the increase in renewable energy. Forecasting the heat demand is required to mitigate the intermittency of renewable energy. To train the system, three months of historical data is used. The historical data contains weather information and building variables used to compute building heat demand. After training, the model is tested to predict the heat demand for the day ahead by using the 24-hour weather forecast in combination with the training data. The heat demand includes space heating and the domestic hot water demand. The resulting mean absolute percentage error of the testing data is 8.95%.

3.2.4. Assumptions Model

The list of assumptions used to create the model is listed below:

- **No integration of dynamic energy prices:** The model does not optimise grid consumption based on the fluctuations in the energy prices. For reasoning, see item 3.1.1.
- **Battery degradation and efficiency losses not considered:** The degradation and losses of the daily battery over time are not modelled. This implies that the battery will operate at nominal performance and without losses throughout the simulation. For reasoning, see item 3.1.1.
- **Neglect AC/DC conversion losses:** Electrical losses that occur during the conversion between AC and DC when using the electricity grid are not included. This simplification is made to keep the model in order to focus on the other key aspects first.
- **Uniform uncertainty distribution:** Random uncertainty, such as forecast error or demand variation, is assumed to be uniformly distributed over the entire prediction horizon. The only exception is that there is no uncertainty in the first hour, the hour within the control horizon, because the uncertainty in the first hour is deemed small enough not to take the uncertainty into account.
- **Electrolyser and fuel cell can not operate simultaneously:** The electrolyser and fuel cell can not operate within the same hour. This assumption reflects the design constraint that the metal hydride can not be charged and discharged simultaneously. This assumption aligns with the use case, as there is never an energy surplus and shortage at the same hour.
- **Hydrogen pressures neglected:** The hydrogen pressures required throughout the system are assumed to be achievable without additional external compressors. All pressure requirements are met internally within the system design. Therefore, the model does not consider the pressure of the hydrogen between different components.
- **Heat recovery constrained to current hour:** The waste heat produced by the components can only be reused within the current hour. There is no thermal energy storage, which can store the heat for a future hour. For reasoning, see item 3.1.1.
- **Sufficient power capacity of space heating heat pump and hot water booster:** The space heating heat pump and the hot water booster are assumed to have sufficient power capacity to meet the heating demand required at each time step. This assumption reflects that a hot water reservoir is implemented in the case study. Without this reservoir, the needed power is higher than in the case study, increasing the system's peak load in relation to the real situation.
- **Constant COP for space heating heat pump and hot water booster:** The coefficient of performance (COP) is assumed to be constant over the year. As a liquid-to-liquid space heat pump and hot water booster are used, the variations due to temperature are minor throughout the year. But this excludes the small effect

of the temperature variations or the effect of the part-load setpoint. As a result, the performance of the components is either overestimated or underestimated throughout the year. It is assumed, nevertheless, that these variations will balance out throughout the year, leading to an acceptable overall approximation over the year.

- **Perfect heat exchangers:** The model assumes no thermal losses between components. This assumption reduces the complexity of the problem. In reality, thermal losses will occur between components and during transport, lowering the system's overall efficiency.
- **Steady-state assumption per time step:** At each discrete time step, the system is assumed to be in steady state. Transient dynamics within each time step are not captured, simplifying the system behaviour's representation. In reality, however, the system is unlikely to remain in steady state throughout each hour, as it may need to respond to unexpected variations multiple times per hour.

3.2.5. Input model

The parameters that are required to construct the model are presented in Table 3.2. The input parameters are obtained from literature sources and information provided by deltaWonen. Subsequently, the efficiency curves of the electrolyser and fuel cell are introduced.

Table 3.2: System input parameters

Parameter	Value	Unit	Source
General			
COP space heating	4	-	(deltaWonen, 2024)
COP DHW	2.5	-	(deltaWonen, 2024)
LHV H2	241.92	kJ/mol	(T. Zhang et al., 2023)
prediction horizon	24	hour	-
Daily Salt Battery			
daily battery max charge speed	1.0	C	(Gao et al., 2021)
daily battery max discharge speed	1.0	C	(Gao et al., 2021)
daily battery min storage capacity	0	kWh	-
daily battery max storage capacity	380	kWh	(deltaWonen, 2024)
PEM electrolyser			
electrolyser min operational temp	50	°C	(Bhandari et al., 2014)
electrolyser max operational temp	80	°C	(Bhandari et al., 2014)
electrolyser useful waste heat	0.92	fraction	(Tiktak, 2019)
electrolyser preheat deionised water	0.07	fraction	(Tiktak, 2019)
electrolyser startup	30	second	(Clean Hydrogen Joint Undertaking, 2021)
electrolyser degradation rate	0.00019	%/h	(Clean Hydrogen Joint Undertaking, 2021)
electrolyser min power input	4	kW	(van der Roest et al., 2023)
electrolyser max power input	40	kW	(deltaWonen, 2024)
Metal hydride Seasonal Storage			
metal hydride min storage capacity	0	kWh	-
metal hydride max storage capacity	4800	kWh	(deltaWonen, 2024)
metal hydride degradation rate	0.017	%/cycle	(Hou et al., 2025)
metal hydride ΔH absorption	24.3	kJ/mol	(Dematteis et al., 2021)
metal hydride operational temp absorption	20	°C	(GKN Hydrogen, n.d.-a)
metal hydride ΔH desorption	27.4	kJ/mol	(Dematteis et al., 2021)
metal hydride operational temp desorption	60	°C	(GKN Hydrogen, n.d.-a)
PEM fuel cell			
fuel cell min operational temp	60	°C	(Tawalbeh et al., 2022)
fuel cell max operational temp	85	°C	(Tawalbeh et al., 2022)
fuel cell usable heat	0.8	fraction	(Cetinkaya et al., 2023)
fuel cell unreacted hydrogen	0.05	fraction	(Cetinkaya et al., 2023)
fuel cell startup	60	second	(Clean Hydrogen Joint Undertaking, 2021)
fuel cell degradation rate	0.0004	%/h	(Clean Hydrogen Joint Undertaking, 2021)
fuel cell min power output	2.5	kW	(van der Roest et al., 2023)
fuel cell max power output	25	kW	(deltaWonen, 2024)

Efficiency Curve Electrolyser and Fuel Cell

The efficiency curves of both the electrolyser and the fuel cell used in the model are shown in Figure 3.2 (Virah-Sawmy et al., 2024) and Figure 3.3 (Sammes, 2006), respectively. The minimum nominal power input

setpoint for both PEM devices is set to 10%. Although the electrolyser and fuel cell could run below a setpoint of 10%, the efficiency of both sharply decreases below 10%. Therefore, it has been decided to use the setpoint from 10% to 100%.
The curve of the electrolyser is an approximated curve of (Virah-Sawmy et al., 2024) created by fitting a cubic polynomial to the nonlinear efficiency curve, resulting in a smooth nonlinear function that closely matches the original data points.
The curve of the fuel cell is presented by a piecewise linear approximation with three segments of the original curve found in (Sammes, 2006), capturing the efficiency behaviour across the operating range.
These methods retain the essential nonlinear characteristics in the model without being more computationally efficient than using raw data or a fully nonlinear solver, while preserving the nonlinear characteristics of the curve.

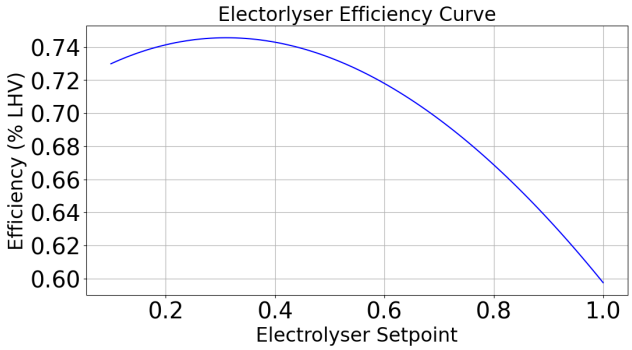

Figure 3.2: Efficiency curve of electrolyser (Virah-Sawmy et al., 2024)

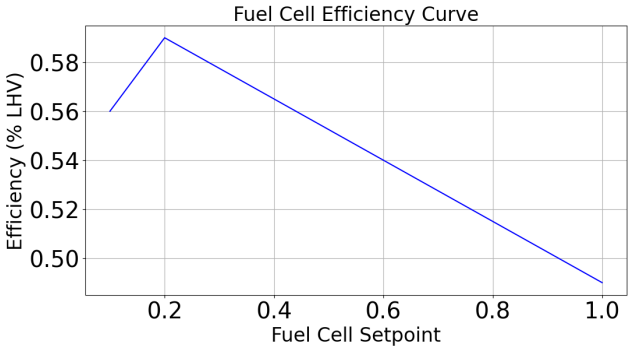

Figure 3.3: Efficiency curve of fuel cell (Sammes, 2006)

3.2.6. PEM Electrolyser

Various factors, including efficiency, startup and degradation, influence the performance of the PEM electrolyser in the model.
An electrolyser produces two main energy-related outputs: hydrogen and waste heat. The ratio of hydrogen compared to waste heat depends on the efficiency of the electrolyser. Additionally, not all the waste heat can be reused as 8% of the waste heat is used to evaporate the water in the stack as well as convection losses to the environment (van der Roest et al., 2023). Another 7% of the remaining waste heat is internally used to heat the incoming water (Tiktak, 2019). Allowing 86% of the waste heat to be reused.

The operational temperature of the electrolyser is between 50 °C and 80 °C (Bhandari et al., 2014). The waste heat is the same as the operational temperature in the model. Additionally, there is a linear correlation between the setpoint of the electrolyser and the operational temperature. At a setpoint of 10%, the operational temperature is 50°C, while at a setpoint of 100%, the operational temperature is 80°C.

Efficiency Within the Model Predictive Control Framework
First, within the Model Predictive Control (MPC) framework, the electrolyser's efficiency is approximated by four breakpoints, as seen in Figure 3.4. More information about the MPC framework is given in section 3.3. Linear interpolation is used between the determined breakpoints to determine the efficiency connected to the selected setpoint. This way, the computational power required within the MPC is minimised without compromising too much on the accuracy of the efficiency.

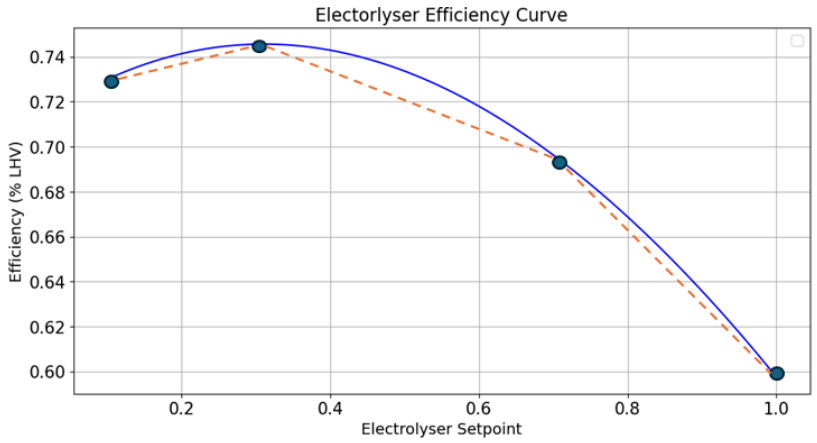

Figure 3.4: Use of breakpoints to determine efficiency MPC while using low computational power

Efficiency outside of the Model Predictive Control Framework
After the MPC has decided on a setpoint for the electrolyser, the exact efficiency corresponding to the setpoint is calculated using the efficiency curve of the electrolyser. The efficiency curve is shown in Figure 3.2. This has the advantage that the most accurate efficiency is used. However, it can cause a slight difference in electrolyser power, which may overwrite the results for daily battery and metal hydride storage outputs that ideally should remain unaffected. However, this is deemed acceptable as it greatly reduces the computational power required for the run.

Startup
It is impossible to turn the electrolyser on immediately with full power when it is cold. Therefore, the electrolyser's startup is included in the code. The startup is only implemented when the electrolyser is turned on in the first hour it is turned on. The startup time is not applied for the consecutive hours the electrolyser is turned on.
The startup of the electrolyser is implemented in the code as a linear increase of power from a zero setpoint to the desired setpoint over the time required for the setpoint. As the model works in one-hour intervals, and the startup time for the electrolyser is only 30 seconds (Clean Hydrogen Joint Undertaking, 2021), the effective hydrogen production is halved during the startup. For the remainder of the hour, the hydrogen production is equal to the setpoint of that hour.

Degradation
The electrolyser experiences degradation per hour of usage. When the degradation increases, less hydrogen is produced for the same amount of electrical energy given as input to the electrolyser. For every hour using the electrolyser, the electrolyser degrades by 0.00019% (Clean Hydrogen Joint Undertaking, 2021).
This is modelled as a linear process; the degradation over time is the same, independent of the current degradation status of the electrolyser.
Once the electrolyser reaches 10% of degradation, it is considered to be at the end of its life (U.S. Department of Energy, 2023).

3.2.7. Metal Hydride
The seasonal metal hydride storage stores the hydrogen produced by the electrolyser until the fuel cell uses the hydrogen.

Maximum Hydrogen Flow Rate
The maximum hydrogen absorption and desorption rate could constrain the flow rate of the hydrogen. The maximum loading/deloading mass flow offered by the metal hydride provider GKN Hydrogen is 105 kg H_2 per hour (GKN hydrogen, n.d.). However, the flow rate does not restrict the system's performance under the current operating conditions. In the most extreme case, the electrolyser and fuel cell operate within a range where the metal hydride storage absorbs and desorbs the hydrogen fast enough to meet the demand.

To be able to reach the flow rate that is required, it is important to take the generation of heat during the absorption process and the heat requirement of the desorption process into account.
During the absorption reaction, 10.0% of the Lower heating value of hydrogen (kJ/mol) is released at a temperature of 20°C. To sustain the desorption reaction, 11.3% of hydrogen's lower heating value is required at 60°C (GKN Hydrogen, n.d.-a). The usable heat of the fuel cell is used to fulfil the heat requirement of the desorption process. As the minimal operational temperature is also 60°C, and the heat usable heat generation is at least 29%, the fuel cell can always cover the desorption process's heat requirement.

Degradation
The degradation per cycle of pure TiFe metal hydride storage is not found in the literature. However, the degradation of the multi-element substituted variant Ti1.05Y0.02Zr0.03Fe0.8Mn0.2 has been found in literature. The highest degradation has been measured during the first 100 cycles. During the first 100 cycles, an average degradation per cycle of 0.017% is measured (Hou et al., 2025). When the degradation increases, the maximum storage capacity is lowered. The degradation is modelled as a linear process; the degradation over time is the same, independent of the current degradation status of the metal hydride storage.
Once the metal hydride reaches 20% of degradation, it is considered to be at the end of its life (L. Zhang, 1998). However, one complete cycle does not occur within a one-hour interval at which the model operates. To account for this, the hourly generation or consumption of hydrogen is divided by the entire storage capacity, and the result is then multiplied by the degradation factor. This approach objectively evaluates degradation per hour, even when the system operates in partial cycles. To account for this, the hydrogen production or demand per hour is divided by the total storage capacity and multiplied by the degradation factor per cycle. This approach estimates degradation over time, even when the system operates in partial cycles.

3.2.8. PEM Fuel Cell

Various factors, including efficiency, startup and degradation, influence the performance of the fuel cell in the model.
Three energy streams come from the fuel cell: electrical power, waste heat and unreacted hydrogen. 5% of the hydrogen put into the fuel cell does not react within the fuel cell and is assumed to be a loss of energy in this model (Tiktak, 2019). The ratio of electrical power compared to waste heat depends on the efficiency of the fuel cell. Additionally, not all the waste heat can be reused as 20% of the waste heat is lost internally or due to natural convection (Cetinkaya et al., 2023). A part of the remaining useful waste heat is used to sustain the desorption reaction in the metal hydride.

The operational temperature of the fuel cell can be between 60°C and 85°C (Tawalbeh et al., 2022). The waste heat is the same as the operational temperature in the model. Additionally, there is a linear correlation between the setpoint of the fuel cell and the operational temperature. At a setpoint of 10%, the operational temperature is 60°C, while at a setpoint of 100%, the operational temperature is 85°C (Tawalbeh et al., 2022).

Efficiency Within the Model Predictive Control Framework
First, within the MPC framework, the fuel cell's efficiency is approximated by three breakpoints. Linear interpolation is used between the determined breakpoints to determine the efficiency connected to the selected setpoint. This way, the computational power required within the MPC is minimised while not compromising too much on the accuracy of the efficiency.

Efficiency outside of the Model Predictive Control Framework
After the MPC has decided on a setpoint for the fuel cell, the exact efficiency corresponding to the setpoint is calculated using the efficiency curve of the fuel cell. The efficiency curve is shown in Figure 3.3. This has the advantage that the most accurate efficiency is used. However, it can cause a small difference in electrolyser power, which may overwrite the results for daily battery and metal hydride storage outputs that ideally should remain unaffected. However, this is deemed acceptable as it greatly reduces the computational power required for the run.

Startup
It is impossible to immediately turn the fuel cell on with full power when it is cold. Therefore, the startup of the fuel cell is included in the model. The startup is only implemented when the fuel cell is turned on in the first hour. The startup time is not applied for the consecutive hours the fuel cell is turned on.
The fuel cell startup is implemented in the model as a linear increase of power from a zero setpoint to the desired setpoint over the time required for the setpoint. As the simulation works in one-hour intervals, and the startup time for the fuel cell is only 60 seconds, the effective hydrogen production is halved during the startup (Clean Hydrogen Joint Undertaking, 2021). For the remainder of the hour, the hydrogen production is equal to the setpoint of that hour.

Degradation
The fuel cell experiences degradation per hour of usage. When the degradation increases, more hydrogen is required to produce the required electrical power output. For every hour using the fuel cell, the fuel cell degrades by 0.0004% (Clean Hydrogen Joint Undertaking, 2021).
This is modelled as a linear process; the degradation over time is the same, independent of the current degradation status of the fuel cell.
Once the electrolyser reaches 10% of degradation, it is considered to be at the end of its life (Wu et al., 2008).

3.2.9. Heat Recovery

Heat can be stored and reused in the same hour that it is produced. However, heat can not be stored for more than an hour, and any remaining waste heat after that is discarded.
The heat generated in the system carries exergy, which quantifies the fraction of thermal energy that is available for useful work. This conversion depends on the temperature of the heat and the ambient temperature. The greater the temperature difference between the heat source and the environment, the higher the exergy content of the heat, increasing its potential for useful work. This exergy can be calculated using the Carnot efficiency, as demonstrated in (3.1) (Hassanzadeh & Mansouri, 2005).

$$\text{Exergy} = Q\left(1 - \frac{T_{\text{ambient}}}{T_{\text{source}}}\right) \tag{3.1}$$

Where Q is the amount of heat (kWh); $T_{ambient}$ is the ambient temperature (K); T_{source} is the temperature of the heat source (K).

As the heat in the case study is provided by a water-to-water heat pump and a water-to-water domestic hot water heat pump, the heat demand is given in electric energy. First, the recovered heat is used to fulfil the

demand for space heating. If any recovered heat is left, it is used to (partly) fulfil the domestic hot water heat demand. To compare the thermal exergy value of the heat to the electric heat demand, the recovered heat is divided by the COP of the water-to-water space heat pump or the water-to-water domestic hot water heat pump. In the model, the COP is a constant value of 4 for the space heat pump and 2,5 for the domestic hot water heat pump, (deltaWonen, 2024). The domestic hot water heat pump further heats the water from the space heat pump. However, the COP of both heat pumps are, in reality, not constant over the year but depends on the temperature of the water. However, as the ground level temperature, where the space heat pump is connected to in the real-world situation, has been relatively stable over the year (Sakata et al., 2023), the constant COP values are deemed acceptable.

3.3. Controller Selection

This section explains why model predictive control (MPC) is chosen as the control strategy for the system. The system integrates various components such as PV panels, a PEM electrolyser, a PEM fuel cell, a daily battery, a metal hydride storage, and devices covering heat and electricity demands. Coordinating all the different subsystems while accounting for the time-dependent supply and demand, and component constraints requires a control strategy that can handle multi-energy flows, decision logic and a forecast horizon. MPC is well suited for this purpose, enabling optimisation over a prediction horizon while incorporating the system dynamics. To implement this control strategy, Mixed-Integer Linear Programming (MILP) represents both the continuous energy flows and the discrete decisions of turning components on and off.

3.3.1. Model Predictive Control

Model predictive control is used to model a process optimally while ensuring the constraints are satisfied. The controller makes the optimal decision within the finite horizon; there is the receding prediction horizon and the control horizon. The prediction horizon is the finite number of time steps that the controller can look into the future. It uses the current inputs and the expected outputs to calculate the optimal control action for every step within the prediction horizon. However, it can only take actions within the finite control horizon. For this model, a receding horizon is used. This means that once a time step has been completed, the control action is taken, and both the horizons shift ahead to the next time step to calculate the best control action for every time step within the new prediction horizon, while only taking the control action within the control horizon. Figure 3.5 shows the functionality of the MPC and the prediction horizon principle (Li Dai et al., 2012).

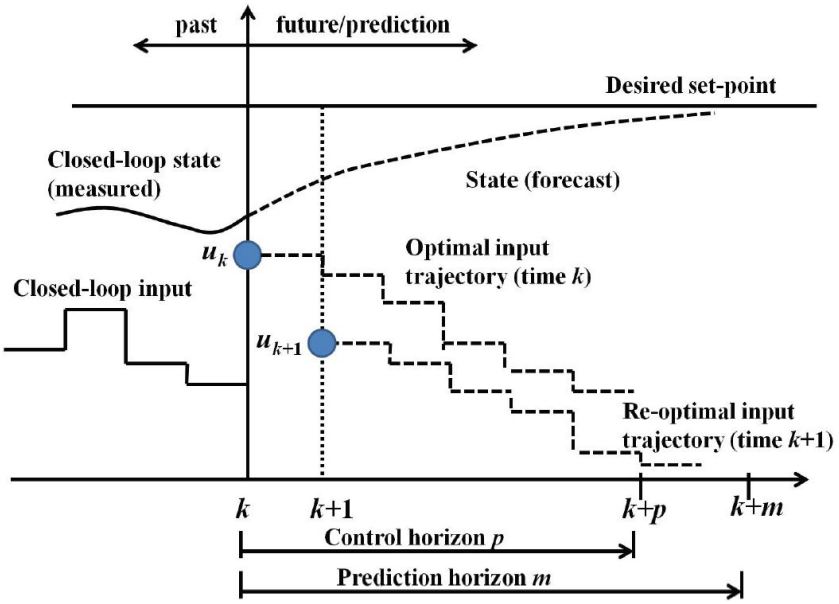

Figure 3.5: MPC receding horizon principle (Li Dai et al., 2012)

The receding prediction horizon is set to be 24 hours, corresponding to the day-ahead price of the dynamic electricity rate. While the dynamic electricity rate aspect is not included in the model, adding the dynamic energy prices in future research makes sense. Therefore, a prediction horizon of 24 hours appears to be the most logical. The effect of the 24-hour prediction horizon is best shown in one of the implementation checks in the Appendix B. In this check, the prediction horizon is set to 1 hour; by doing so, the model is not able to look into the future beyond the control horizon. The control horizon is set to be 1 hour; only the control action planned for the next hour can be taken.

Reasons why MPC, a control strategy-based model, is the best type of controller to use for this model (Banasiak & Kienberger, 2024):

- **Multi-variable Optimalisation:** The system has many interacting components with different constraints and dynamics. MPC is designed for multi-variable systems.
- **Prediction of Future Demand and Generation:** MPC uses a precision horizon, which is perfect for a system when:
  - A forecast for the supply and demand of the system is known.
  - Anticipating on future supply and demand is required.
  - Optimising over time. This is perfect with a system that needs to plan when to charge/discharge the daily battery and the metal-hydride storage.
- **Flexibility and Extensibility:** MPC frameworks scale well and allow to:
  - Add more constraints and states
  - Modify the objective function
  - Test different control strategies or scenarios.

MPC is ideal for a hybrid energy system because it can anticipate future conditions, handle complex constraints and interactions, and optimise performance across multiple time steps and objectives.

3.3.2. Mixed-Integer Linear Programming

To perform the optimisation at each step, the mathematical problem must be formulated in a solvable way. This is where mixed-integer linear programming (MILP) comes in. It provides a structured optimisation framework that can handle both continuous variables (energy flows and storage levels) and discrete or binary decisions (like turning on or off the electrolyser or fuel cell, or selecting between a low and a high setpoint) (Floudas & Lin, 2005).

The formulation of this optimisation problem influences the quality of the results and the computational power required to solve it. MILP was selected as the optimisation technique because of its suitability for this type of problem, in particular due to the following advantages (Floudas & Lin, 2005):

- **Ability to model discrete operational decisions:** MILP can include binary variables to represent the on/off states of components and switch from setpoint, which are essential to capture the system behaviour.
- **Efficient handling of linear constraints:** The operational constraints of most components, such as minimum and maximum power or storage capacities, can be expressed as linear inequalities. MILP can efficiently solve these combinations of linear constraints.
- **Deterministic and globally optimal solutions:** MILP solvers are reliable and have robust control actions because they ensure that a globally optimal solution will be found within a specified optimality gap.
- **Scalability to complex systems:** MILP solvers, can handle large-scale problems involving many constraints, time steps and variables. This makes it suitable to use in combination with an MPC with a 24-hour receding prediction horizon. In the model, Gurubi is used as the solver.

3.3.3. Assumptions controller

The list of assumptions used to create the controller is listed below:

- **24-hour prediction horizon:** The prediction horizon is set to be 24 hours, which aligns with the day-ahead electricity pricing data of the dynamic energy market. While the dynamic electricity rate aspect is not included in the model, adding the dynamic energy prices in future research makes sense. Therefore, a prediction horizon of 24 hours appears to be the most logical.
- **One hour control horizon:** The control horizon is limited to one hour, meaning that only the control action determined for the next hour is implemented at each step.
- **Simplified efficient modelling within the MPC:** Within the MPC, the operation efficiencies of the electrolyser and the fuel cell are approximated using linear interpolation between predefined breakpoints, as can be seen in Figure 3.4. Outside of the MPC, the exact efficiency corresponding to the efficiency curves represents a more detailed behaviour. This allows for minimisation of the computational power required for the model, while preserving the accurate efficiency of the model.

3.3.4. Flow Diagram Controller

A flow diagram of the controller is presented in Figure 3.6 to provide a clear understanding of the system's architecture. Part of the process within the controller happens inside the MPC, while some processes happen afterwards, outside the MPC. This is a trade-off between computing power and accuracy.

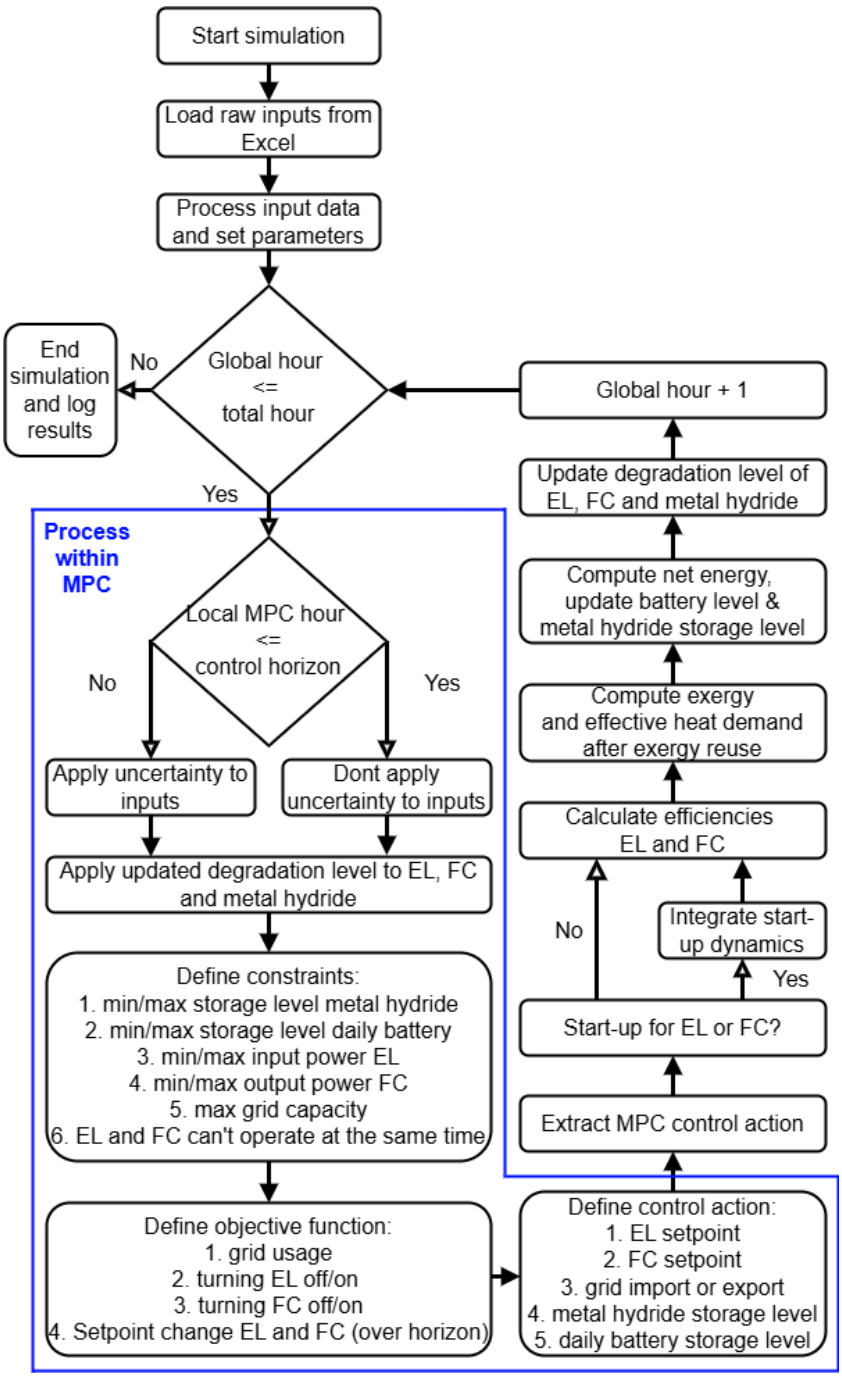

Figure 3.6: Flow diagram controller

3.3.5. MPC Formulation

The goal of the MPC is to choose the lowest objective function possible. Therefore, selecting the right constraints to the objective function that constrain the MPC where required is important, while leaving enough freedom for the model to reach the best control action possible.

MPC Constraints

Constraints are added to ensure that the MPC does not break physical boundaries while trying to solve the objective function with the lowest score possible. The following constraints have been added within the MPC:

- The storage level of both the daily battery and the metal hydride storage is constrained between the minimum and maximum storage capacity.
- The electrolyser's input power and the fuel cell's output power are constrained between the minimum and maximum power.
- The electrolyser and fuel cell can not be turned on simultaneously.
- The grid usage is limited to the maximum available grid capacity.

MPC Objective Function

The objective function is a combination of several terms. Each term will be explained individually before being combined as one objective function. The goal of the MPC is to minimise the objective function, and every term of the objective function could be interpreted as a punishment for the MPC.

Grid Usage

The grid usage objective is calculated by multiplying the grid usage (in kW) during that hour by the weight factor λ_{grid}. The penalty increases when more grid power is used. The same penalty applies to importing and exporting electricity from and towards the grid. The equation is shown in (3.2).

$$J_{\text{grid}} = \lambda_{grid} * |u_g| \tag{3.2}$$

Where J_{grid} (kW) is the grid-related objective, λ_{grid} is the weight factor, and u_g (kW) is the amount of grid usage per hour.

Switching the Electrolyser and the Fuel Cell On and Off

The binary variable for both components is calculated by checking if the previous setpoint was smaller than ϵ, set to be 1%. For example, the model checks if the last electrolyser setpoint was off and if the electrolyser turns on in the current hour, the binary deviation variable is set to 1. The equation can be found in (3.3). The objective is to minimise the number of times the electrolyser or fuel cell is turned on or off within the prediction horizon. The penalty is the same for turning on or off the component. The electrolyser and fuel cell have a separate objective function in the model, which work similarly. The combined objective function can be found in (3.4).

$$\begin{aligned} a[t] &:= \begin{cases} 1 & \text{if } s[t] > \varepsilon \\ 0 & \text{otherwise} \end{cases} \\ \delta[t] &\geq a[t] - a[t-1] \quad \forall t \in \{0, \ldots, T-1\} \\ \delta[t] &\geq a[t-1] - a[t] \quad \forall t \in \{0, \ldots, T-1\} \end{aligned} \tag{3.3}$$

where a[t] ϵ{0,1} is the active state of the component, s[t] ϵ[0,1] is the setpoint of the electrolyser or fuel cell, ε is the small threshold value, $\delta[t]$ ϵ{0,1} is the on/off transition indicator respectively $\delta_{\text{el}}[t]$ for the electrolyser and $\delta_{\text{fc}}[t]$ for the fuel cell, λ_{el} and λ_{fc} are the associated weight factors.

$$J_{\text{on\_off}} = \lambda_{\text{el}} \cdot \sum_{t=0}^{T-1} \delta_{el}[t] + \lambda_{\text{fc}} \cdot \sum_{t=0}^{T-1} \delta_{fc}[t] \tag{3.4}$$

Where $J_{\text{on\_off}}$ is the on/off transition-related objective, λ_{el} and λ_{fc} are the weight factors for the electrolyser and fuel cell, and $\delta_{\text{el}}[t]$ and $\delta_{\text{fc}}[t]$ are the corresponding on/off transition indicators at time step t.

Changing the Setpoint of the Electrolyser and Fuel Cell

The objective is to regulate the change in setpoint between hours for both the electrolyser and the fuel cell across the prediction horizon. It minimises the cumulative absolute change in setpoint values between consecutive time steps, including the transition from the previous time step (before the horizon) to the first time step within the horizon. This is designed to reduce the total change in setpoint over the entire horizon. The equations are shown in (3.5) and the objective function is shown in (3.6).

$$\begin{aligned} \Delta_s[t] &\geq s[t] - s[t-1] \quad \forall t \in \{0, \ldots, T-1\} \\ \Delta_s[t] &\geq s[t-1] - s[t] \quad \forall t \in \{0, \ldots, T-1\} \end{aligned} \tag{3.5}$$

Where s[t] ϵ[0,1] is the setpoint of the electrolyser or fuel cell, and Δ_s the magnitude of the setpoint change of the electrolyser or fuel cell.

$$J_{\Delta_s} = \lambda_{\Delta_s} \cdot \sum_{t=0}^{T-1} \Delta_s[t] \tag{3.6}$$

Where J_{Δ_s} is the change in setpoint-related objective, λ_{Δ_s} is the weight factor for change in setpoint for both the electrolyser and the fuel cell, and Δ_s the magnitude of the setpoint change of the electrolyser or fuel cell.

Total Objective Function

The final objective function can be found in (3.7), which is the addition of all the individual objective functions.

$$J_{\text{total}} = J_{\text{grid}} + J_{\text{on\_off}} + J_{\Delta_s} \tag{3.7}$$

3.3.6. Calibration of Weight Factors

To make the controller behave as desired, it is important to calibrate the weight factors of every term in the objective function. The weight factors have been calibrated by hand using trial and error. During this process, the following criteria have been taken into account:

- The electrolyser and fuel cell have, in reality, a relatively high degradation when turning them on and off. Therefore, the electrolyser and fuel cell are preferred to run for longer periods at a lower setpoint, instead of operating at full power for a short period(Lu et al., 2023).
- The electrolyser and fuel cell have, in reality, a higher degradation when having great changes from setpoints. Therefore, it is preferred to have the electrolyser and fuel cell running with relatively little change in setpoint between subsequent hours. Nevertheless, the degradation is less than turning on and off the electrolyser and fuel cell (Lu et al., 2023).
- The electrolyser and fuel cell tend to turn on when the metal hydride storage is full. As this occurs, the system 'wastes' energy while not being punished (enough) for using the grid to export the power surplus. This occurs when exporting to the grid is penalised more heavily than using the electrolyte and fuel cell. To avoid this, it is essential to choose an appropriate weight factor for using the grid.

Following calibration, the final weighting factors applied are as follows: $\lambda_{\text{grid}} = 20$, $\lambda_{\text{on\_off\_el}} = 130$, $\lambda_{\text{on\_off\_fc}} = 190$, and $\lambda_{\Delta_s} = 74$

3.3.7. MPC Control Actions

The control actions are the output of the MPC and the input for the next time step of the model. This is the overview of the control action that the MPC has:

- Electrolyser setpoint
- Fuel cell setpoint
- Electricity grid import/ export

3.4. Verification Model

Verifying a model aims to find and fix modelling errors (Carson, 2002). First, an overview of the different verification tests is presented in this chapter. The complete list of the verification checks can be found in Appendix B.

Overview of verification checks:

- **Data check:** All the used datasets are checked for irregularities and errors.
- **Data modelling check:** All the datasets implemented from Excel into the model are checked to see if the data conversion is done correctly. It also checks whether the uncertainty is correctly applied to the data.
- **Boundary constraint check:** Each component is checked if the boundaries are respected. This is done by exceeding the boundaries in the input to see if the boundaries hold, and looking into the results to see if any boundary is exceeded.
- **Implementation checks of:** Efficiency within and outside of MPC, startup, degradation, added uncertainty, MPC objective function, prediction horizon and exergy heat. The expected workings of each of the implementation checks are explained. Afterwards, the results are checked to see if they align with the expected working method.
- **Energy balance check:** The inputs should be the same as the outputs and losses. However, many components are involved in the system, which could result in losses due to modelling errors. An additional goal of this check is to see whether a hand calculation corresponds to the model's output.

In conclusion, all the verification tests have been verified.

3.5. Discussion

This section reflects on the assumptions and limitations of the current model.

Reflection on the Assumptions:

- **No integration of dynamic energy prices:** The assumption has the effect that was assumed beforehand. The reduction in complexity was deemed useful, while the performance of the metal hydride can be determined by the model. In future research, including the dynamic energy prices would be useful to be able to include the economic aspect into the model.
- **Battery degradation and efficiency losses not considered:** The assumption has the effect that was assumed beforehand. The reduction of the complexity was deemed useful. However, to make this simplification, to

use the daily battery as an energy storage where all the energy streams come together, it was required not to consider the efficiency losses. If the development of the model continues in the future, it would be useful to directly use the possible energy and the daily battery to process the remaining energy. This would allow for the implementation of efficiency and degradation of the daily battery. While it lowers the overall efficiency of the model, it leads to a more accurate outcome.

- **Neglect AC/DC conversion losses:** This assumption only applies to the electricity from and towards the grid. In retrospect, it would have been possible to implement the AC/DC losses, but it was chosen not to implement the losses to keep the model simpler and focus on the other key aspects first. It is suggested to include these losses in future work. Implementing it would increase the import of electricity from the grid and decrease the amount of electricity exported to the grid.
- **Uniform uncertainty distribution:** The assumption has the effect that was assumed beforehand. However, there are some disadvantages to this approach. The uncertainty is, in reality, not always between these bounds, as the mean absolute error is used as input. Moreover, uncertainty typically increases with time, rather than remaining constant across the production horizon. In retrospect, it would have been better to use an uncertainty band that increases over the horizon, reaching the mean absolute error at the end of the horizon.
- **Electrolyser and fuel cell can not operate simultaneously:** The assumption has the positive effect that was assumed beforehand. It reflects the design constraint that the metal hydride can not be charged and discharged simultaneously.
- **Hydrogen pressures neglected:** The assumption has the effect that was assumed beforehand. However, it relies on the assumption that the electrolyser can reach the required pressures within the startup and that the pressure during the desorption process is instantly high enough to provide the necessary pressure to the PEM fuel cell. This assumption could neglect some delays during the operation of the system. Therefore, it is suggested as future work.
- **Heat recovery constrained to current hour:** The assumption has the effect that was assumed beforehand. Excluding the heat storage limits the system's ability to heat the boiler when PV generation peaks or when a high heat demand is forecasted within the prediction horizon. Including the heat storage would enhance flexibility, especially in maximising the consumption of the PV generation. However, the current domestic hot water demand profile is already the average demand of a group of households, rather than a single household profile, which is already flattening the peak demand occurrences and reducing the impact of this limitation. To further reduce the grid capacity required for export, it is suggested that this be included in future work.
- **Sufficient power capacity of heat pump and hot water booster:** The assumption has the positive effect that was assumed beforehand; it simplifies the model by avoiding sizing for peak power demand at every timestep.
- **Constant COP for heat pump and hot water booster:** The assumption has the positive effect that was assumed beforehand; both the liquid-to-liquid heat pump and hot water booster experience minor temperature differences throughout the year. Therefore, it is justified to assume that the COPs are constant.
- **Perfect heat exchangers:** Although the assumption has the expected effect, the assumption is, in reality, incorrect. In future research, including losses at the heat exchangers would be useful. This would lower the amount of heat that can be recovered, but it will lead to a more accurate outcome.
- **Steady-state assumption per time step:** The assumption has the effect that was assumed beforehand. Although in reality, the system is unlikely to remain in a steady state throughout each hour due to intermittent PV production and unexpected events, it is necessary to reduce the complexity of the model.
- **24-hour prediction horizon:** The assumption has the positive effect that was assumed beforehand. The 24-hour horizon is justified as it corresponds with the day-head. One of the verification checks, which can be found in Appendix B, shows the positive effect that using the prediction has on the results.
- **One hour control horizon:** The assumption corresponds to the reality; it is not possible to do actions in the future. Therefore, a control horizon of one hour is justified.
- **Simplified efficient modelling within the MPC:** The assumption to use breakpoints instead of the full efficiency curve within the MPC has the effect assumed beforehand, significantly lowering the time required to run the model. However, because the efficiency is calculated again outside of the MPC, using the more detailed efficiency curve, it could result in a slight power difference, overwriting the storage value of the daily battery and metal-hydride storage determined by the MPC. Ideally, these outputs are not overwritten. Therefore, it is worth exploring whether only using the less accurate efficiency within the MPC is sufficient. If deemed sufficient, it is possible to explore in future research if the process that now occurs after the MPC can also be calculated inside the MPC. During this process, the trade-off with calculating time should be considered.

Limitations of the Model and Controller:

- **Potential improvements on start date:** By choosing 1 October as the starting date, right before the net energy generation becomes negative, the positive surplus of energy of the first few days is not stored in the metal hydride storage, because that is full from the start of the year. Starting on October 15th avoids this issue by beginning during a negative net energy generation period, preventing the waste of an early surplus of net energy. However, this approach overlooks the initial days when net energy generation starts to become negative, potentially giving an overly optimistic impression. Therefore, the starting date presents a trade-off between accurately representing the storage availability and avoiding energy losses.
- **Improvements for space heat demand profile:** The space heat demand profile that is used is for an average household, not a highly insulated household. A highly insulated household would have a shorter period in which space heat is required. As a result, this would increase the required space heat in the winter, as now the same total annual demand is split over fewer hours.
- **Variability in domestic hot water demand:** The model uses a domestic hot water demand, which is repeated for the same day for the entire year. In reality, the usage varies significantly due to seasonal trends. As a result, this would increase the required domestic hot water demand in the winter and reduce the domestic hot water demand in the summer.
- **Linear degradation process:** The degradation process is, in reality, not linear. For example, the degradation of TiFe metal hydride is higher at the start of its lifetime. This results in an overestimation at the beginning and an underestimation at the end of its lifetime (Hou et al., 2025).
- **Different parameters within total objective function:** The objective function that is used uses different parameters that do not have the same unit; therefore, it is impossible to compare one value directly to another. That is why another method has been explored to address this limitation. This method only used the degradation of the electrolyser and fuelcell for the objective function, where degradation was applied for having a low or high setpoint, the amount of change of the setpoint between the hours and the amount of degradation when turning the component on or off. As they all use degradation, it was possible to directly compare them in the objective function. However, this resulted in the electrolyser and fuel cell never being used, as the daily battery and grid capacity are sufficiently large, and there is only a punishment and no stimulation in the objective function.
  That is why the original approach is still valid to use. Even though the parameters in the objective function have different units and cannot be directly compared, they represent different priorities in the system. By assigning appropriate weight factors, a trade-off can be made between these aspects. This makes it possible to guide the optimisation meaningfully, even if the terms are not physically comparable.

3.6. Conclusion

In this chapter, a systematic framework has been presented to create a model and optimise the control of the seasonal energy balance system, consisting of a daily sodium-ion battery, a PEM electrolyser, a TiFe metal hydride, a PEM fuel cell and an exergy-based heat recovery. The components are modelled as a black box, incorporating characteristics such as efficiency, startup, maximum flow rate, and degradation effects.
Model predictive control has been selected as the control strategy of the model because of its ability to handle multi-variable optimisation problems, make use of the prediction horizon to anticipate future supply and demand, and the MPC framework is flexible. The MPC framework can be extended to include additional constraints, states, or alternative strategies.
The objective function minimises the usage of the grid, penalises switching on and off the electrolyser and fuel cell, and changing the setpoint of the electrolyser or fuel cell. Weight factors have been applied to each term, allowing calibration of the model to reflect the system's priorities.

While several simplifications were made to reduce the complexity of the model, including the steady state assumption, excluding the dynamic energy prices, and excluding the heat storage. The model remains effective for evaluating the performance of the seasonal metal hydride storage. The impact of these assumptions is assessed in the discussion, and various opportunities for future improvement have been identified.

This approach provides a structured foundation for evaluating the results of the metal hydride seasonal energy storage solution.

4

Results

This chapter will present the results of the developed model. First, the yearly results of the 10-year average dataset and the test dataset will be presented and discussed in section 4.1. This is followed by the result of the Extreme cases in section 4.2.

4.1. Results Year Model

First, the results obtained using the training dataset are presented. This training data represents the average values over ten years. Subsequently, the model is evaluated using data from two individual years: 2013 and 2015. These years were selected because complete individual data sets are available for both.

4.1.1. Results Average Ten Year Dataset

The average dataset has been used to calibrate the weight factors that are used in the objective function.

Net Energy Usage

Figure 4.1 shows the daily energy balance. The blue line represents the PV panel supply, the green line represents the total heat demand, and the orange line represents the electricity demand. The black line is the total sum of the energy supply and demand, the daily net energy. The horizontal axis represents time, and the vertical axis represents energy usage (kWh). It includes both positive and negative values, with the zero line located about one-quarter from the bottom of the graph.

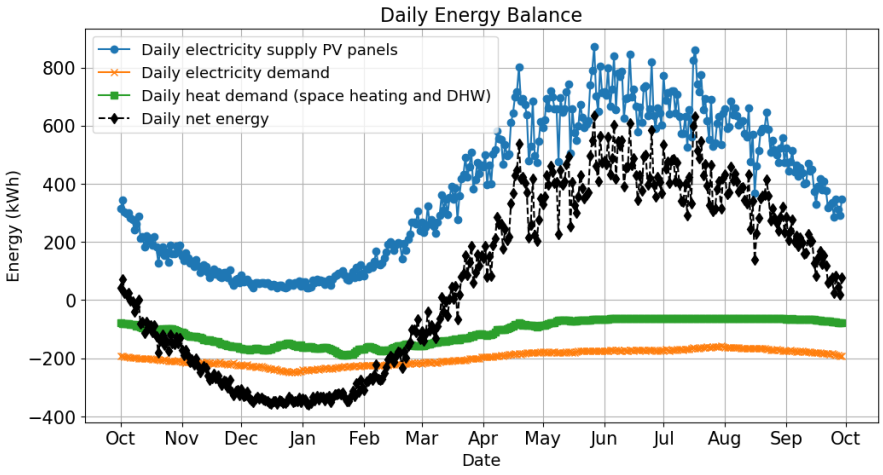

Figure 4.1: Daily energy balance average ten-year dataset

The net energy becomes negative in October, reaching its lowest values in December and January. It turns positive again in March, after which the daily net energy gradually increases, peaking around June. From August onwards, a decline in net energy is observed.

It is important to note that the area under the daily net energy curve with negative values represents the amount of energy that must be supplied by the metal hydride storage system, assuming the storage capacity is sufficient to meet the entire demand. On the other hand, the area where the daily net energy is positive corresponds to the amount of energy that can be stored in the metal hydride system. However, a significant amount of energy is still lost due to the conversion of electricity to hydrogen and vice versa. Therefore, a positive daily net energy area should be substantially greater than the negative area to compensate for these conversion losses.

Hydrogen Storage Level in Metal Hydride

In Figure 4.2, it can be seen that from the moment at which the net energy (in Figure 4.1) becomes negative, the seasonal metal hydride storage starts to be used. The metal hydride storage is empty after 22 days, around the start of November. Please note that the most energy-demanding months (December and January) are still ahead of that moment in time.

In March, the net energy becomes positive again, allowing the metal hydride storage to recharge. After 32 days, the metal hydride storage is full. From that moment on, the energy surplus must be exported back to the grid.

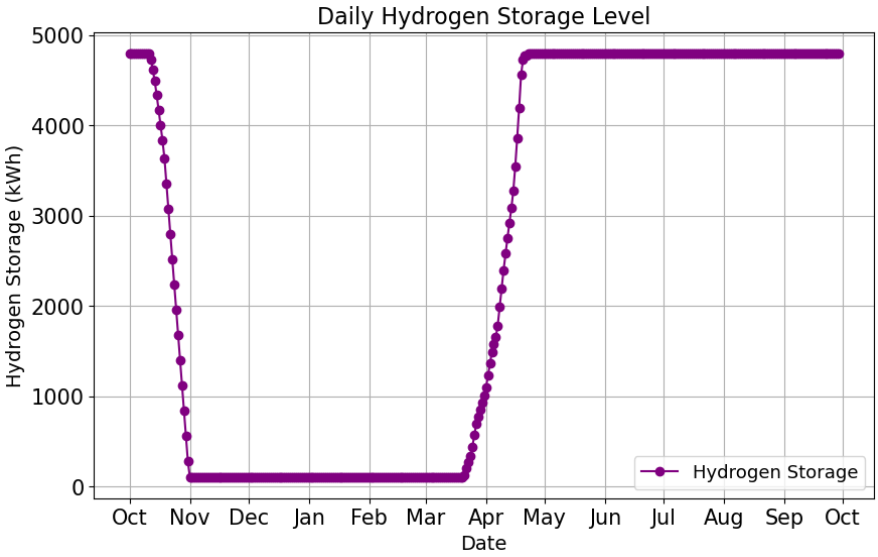

Figure 4.2: Daily metal hydride storage level average ten-year dataset

Electrolyser Input and Fuel Cell Output Power

Figure 4.3 correlates with Figure 4.2, illustrating the relationship between the metal hydride storage and the use of the electrolyser and fuel cell. The fuel cell was used for 500 hours until the metal hydride storage was fully discharged, and the electrolyser operated for 727 hours to recharge the metal hydride.

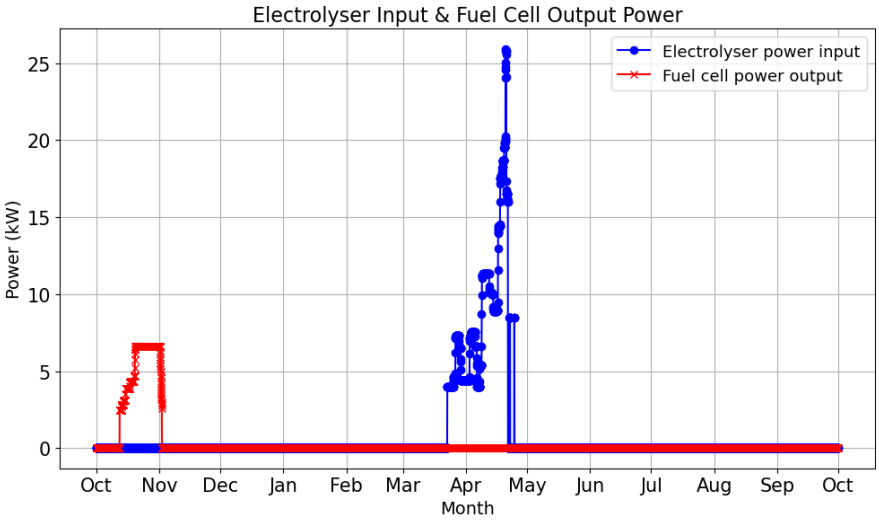

Figure 4.3: Hourly electrolyser input and fuel cell output average ten-year dataset

As the hydrogen storage was full at the start and finish of the year, it is possible to compare the average efficiency of the seasonal energy storage system. The electrical energy put into the electrolyser was 6.4 MWh, and the total energy in the form of hydrogen produced was 4.7 MWh, resulting in an average efficiency of 73,9% for the electrolyser. The total amount of hydrogen the fuel cell used was 4.7 MWh, and the total amount of electrical energy produced was 2.7 MWh, resulting in an average efficiency of 57.9% for the fuel cell. Additionally, 235 kWh of hydrogen did not react in the fuel cell. The total combined average efficiency of the seasonal energy storage system was 48.7% (excluding use of recovered heat).

Heat Recovery

In total, the electrolyser, fuel cell and absorption process produce 3.4 MWh of usable waste heat (already excluding internal losses). However, when this heat is converted to its exergy equivalent and the heat required for the desorption process is subtracted, only 381 kWh is available to reduce the heat demand.

The fuel cell produced 223 kWh of exergy, 77 kWh of which was used to provide the required heat to the desorption process. All of the 381 kWh of thermal exergy produced through heat recovery could be reused. In total, 381 kWh was used to reduce the space heating demand. Only 0.5 kWh of exergy remained, spread over five moments during the year, which could contribute to reducing the domestic hot water demand. This

occurred in mid-April when the electrolyser's power output was at its peak.
When taking into account the heat recovery, the average efficiency of the seasonal energy storage system is increased to 48.7%.

Degradation of components
The electrolyser, metal hydride and fuel cell experienced degradation when in operation. In total, the electrolyser degraded for 0.1%, the metal hydride for 0.04% and the fuel cell for 0.2%.

Electricity Import and Export From the Grid
In Figure 4.4, it can be seen that in October and half of March to half of April, the metal hydride storage is used. All the remaining electricity needs to be delivered by the grid from November to mid-March, with a peak electricity import of 15.1 kW and a total grid import of 35.2 MWh. Similarly, the electricity surplus needs to be exported to the grid from mid-April till the end of the year in October, with a peak electricity export of 31.0 kW and a total export of 58.0 MWh. Both are staying under the maximum grid capacity of 40 kW.

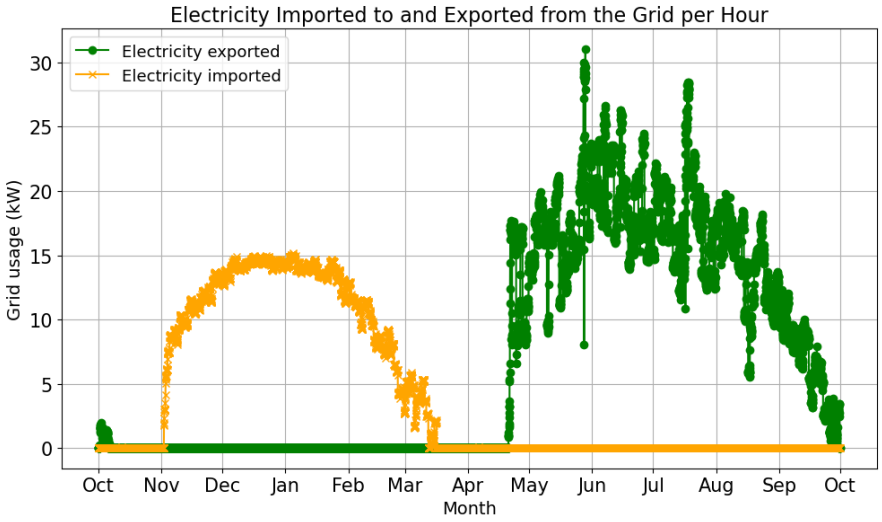

Figure 4.4: Hourly import and export of the grid average ten-year dataset

4.1.2. Results Test Data Set 2013

Net Energy Usage 2013
Figure 4.5 shows the daily energy balance. The blue line represents the PV panel supply, the green line represents the total heat demand, and the orange line represents the electricity demand. The black line is the total sum of the energy supply and demand, the daily net energy. The horizontal axis represents time, and the vertical axis represents energy usage (kWh). It includes both positive and negative values, with the zero line located about one-quarter from the bottom of the graph.

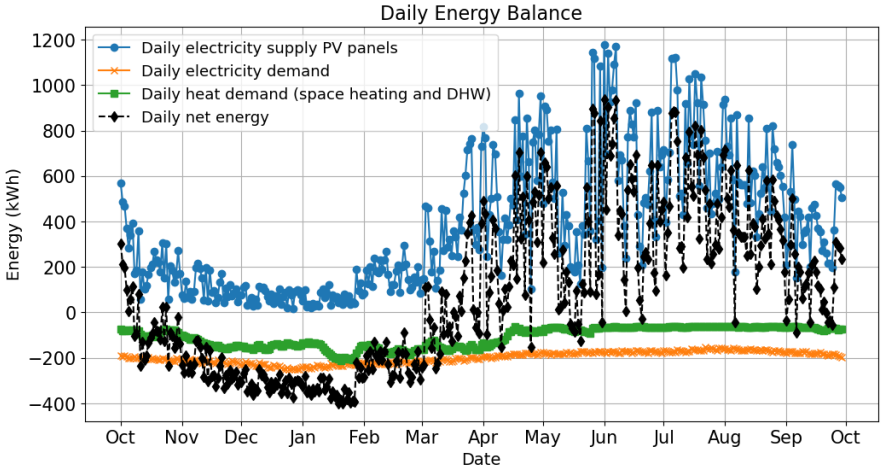

Figure 4.5: Daily net energy usage 2013

The net energy becomes negative in October, reaching its lowest values in December and January. It turns positive again in March, after which the daily net energy gradually increases, peaking around June. From July onwards, a decline in net energy is observed.

The difference between 2013 and the average ten-year dataset is that there are more spikes and jumps throughout the year, mainly due to the electricity supply from PV panels. This is logical as this is the data of one individual year instead of an average of ten years of data. This creates greater differences in the daily net energy generation and even dips into the negative a few times during the year, with the most significant dip around mid-May.

Hydrogen Storage Level in Metal Hydride 2013
In Figure 4.6, it can be seen that from the moment at which the net energy (in Figure 4.5) becomes negative, the seasonal metal hydride storage starts to be used. During the peak of the net energy at the end of October, it can be seen that the use of the metal hydride storage is temporarily paused. The metal hydride storage is empty after 25 days. In March, the net energy becomes positive again, allowing the metal hydride storage to recharge. After 34 days, the metal hydride storage is full. From that moment on, the energy surplus needs to be exported back to the grid. During the charging of the metal hydride, there are a few moments when hydrogen is used to power the fuel cell, when the net energy dips below zero.

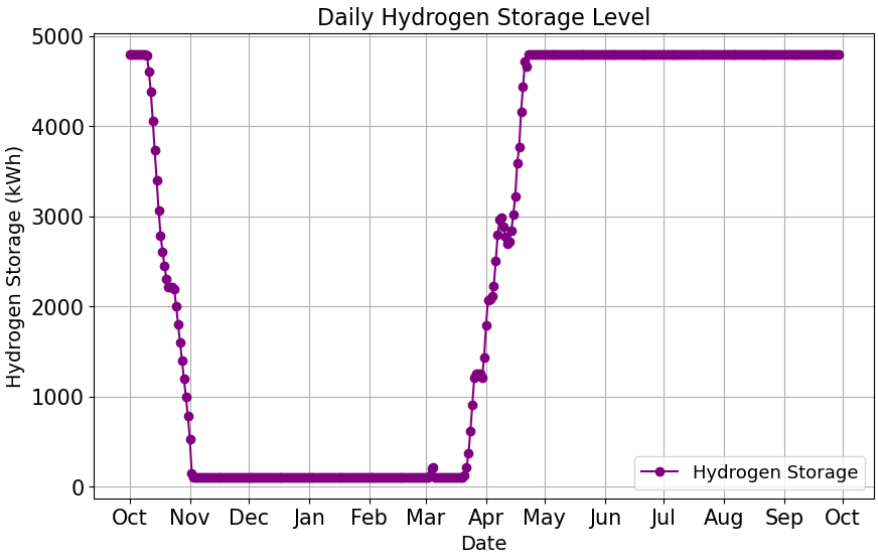

Figure 4.6: Daily metal hydride storage level 2013

Electrolyser Input and Fuel Cell Output Power 2013
The fuel cell was used for 594 hours until the metal hydride storage was fully discharged, and the electrolyser operated for 598 hours to recharge the metal hydride.
The electrolyser usage is especially intermittent when compared to the ten-year average data, with relatively higher setpoints. This makes sense as it relates to the PV panel supply, which is more intermittent in a year.

In March and April, there are four moments when the fuel cell is used. The use of the fuel cell at these moments is justified as they correspond to moments when the net energy dipped below zero, as seen in subsection 4.1.2.

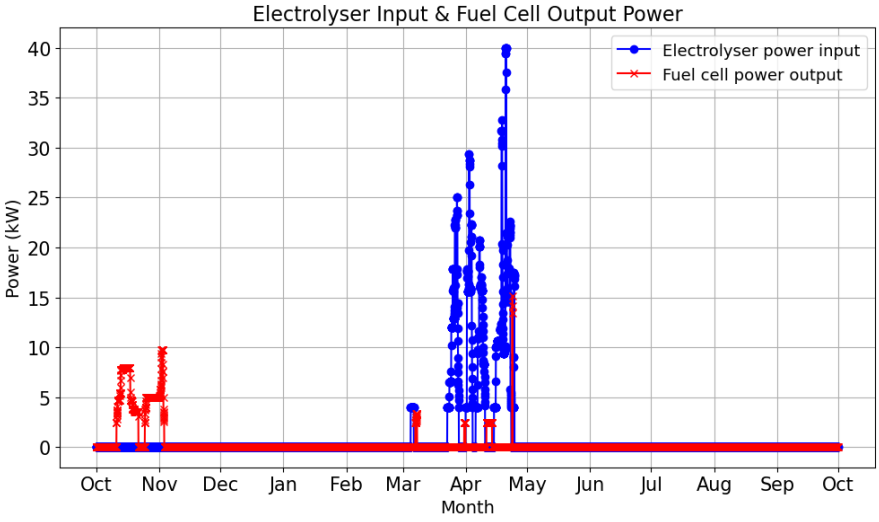

Figure 4.7: Hourly electrolyser input and fuel cell output power 2013

The electrical energy put into the electrolyser was 7.2 MWh, and the total energy in the form of hydrogen

produced was 5.2 MWh. Resulting in an average efficiency of 72,7% for the electrolyser. The total amount of hydrogen that the fuel cell used was 5.2 MWh, and the total amount of electrical energy produced was 3.0 MWh, resulting in an average efficiency of 57.7% for the fuel cell. Additionally, 275 kWh of hydrogen did not react in the fuel cell. The total combined average efficiency of the seasonal energy storage system was 42,0% (excluding use of recovered heat).

Heat recovery
In total, the electrolyser, fuel cell and absorption process produce 3.8 MWh of usable waste heat (already excluding internal losses). However, when this heat is converted to its exergy equivalent and the heat required for the desorption process is subtracted, only 482 kWh is available to reduce the heat demand.
The fuel cell produced 256 kWh of exergy, 88 kWh of which was used to provide the required heat to the desorption process. All of the 482 kWh of thermal exergy produced through heat recovery could be reused. In total, 458 kWh was used to reduce the space heating demand, and 24 kWh was used to reduce the domestic hot water demand.
When taking into account the heat recovery, the average efficiency of the seasonal energy storage system is increased to 48.6%, 0.1% lower compared to the ten-year average dataset.

Degradation of Components
The electrolyser, metal hydride and fuel cell experienced degradation when in operation. The electrolyser degraded for 0.1%, the metal hydride for 0.04%, and the fuel cell for 0.2%.

Electricity Import and Export From the Grid 2013
In Figure 4.8, it can be seen that the metal hydride storage is used in October and from mid-March to mid-April. All the remaining electricity needs to be delivered by the grid from November to mid-March. With a peak electricity import of 16.8 kW, with a total grid import of 35.2 MWh. Similarly, the electricity surplus needs to be exported to the grid from mid-April till the end of the year in October, with a peak electricity export of 55.3 kW and a total export of 57.4 MWh. This does not meet the requirement to stay below 40 kW of network capacity. However, it is technically feasible to turn off part of the PV panels when exceeding the 40 kW limit of the grid capacity. Nevertheless, 1.7 MWh, 1.3% of the total annual PV production, is curtailed this way.

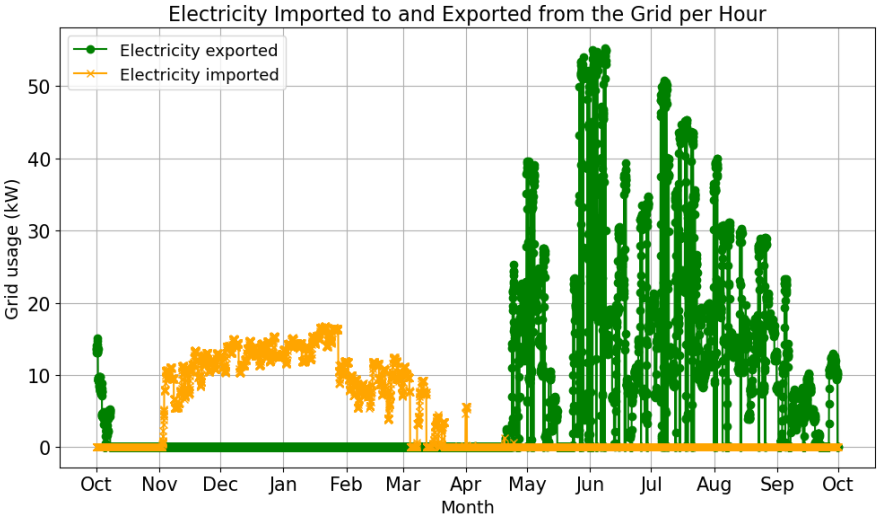

Figure 4.8: Hourly import and export of the grid 2013

4.1.3. Results Test Data Set 2015

Net Energy Usage 2015
Figure 4.9 shows the daily energy balance. The blue line represents the PV panel supply, the green line represents the total heat demand, and the orange line represents the electricity demand. The black line is the total sum of the energy supply and demand, the daily net energy. The horizontal axis represents time, and the vertical axis represents energy usage (kWh). It includes both positive and negative values, with the zero line located about one-quarter from the bottom of the graph.

In October, the net energy becomes negative, gradually lowering until reaching its lowest value at the end of January. It turns positive again in March, after which the daily net energy gradually increases, peaking around June. From June onwards, a decline in net energy is observed.
As with the results of 2013, there are more spikes and jumps throughout the year compared to the test data. This creates greater differences in the daily net energy generation and even dips into the negative a few times during the year, with the most significant dip around mid-May.

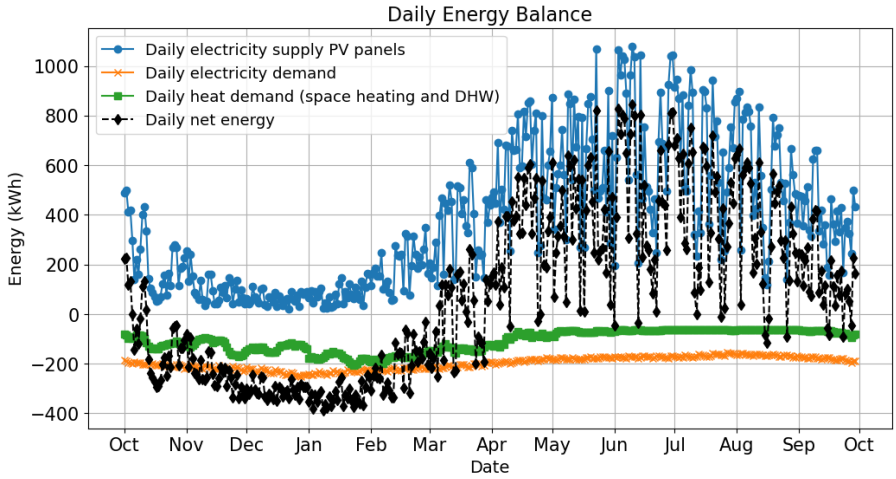

Figure 4.9: Daily net energy usage 2015

Hydrogen Storage Level in Metal Hydride 2015
In Figure 4.10, it can be seen that from the moment at which the net energy (in Figure 4.9) becomes negative, the seasonal metal hydride storage starts to be used. The metal hydride storage is empty after 17 days. In March, the net energy becomes positive again, beginning to recharge the metal hydride storage until the net energy has two dips and discharges the metal hydride again. Afterwards, from April onwards, it takes 22 days to recharge the metal hydride storage fully. From that moment on, the energy surplus needs to be exported back to the grid.

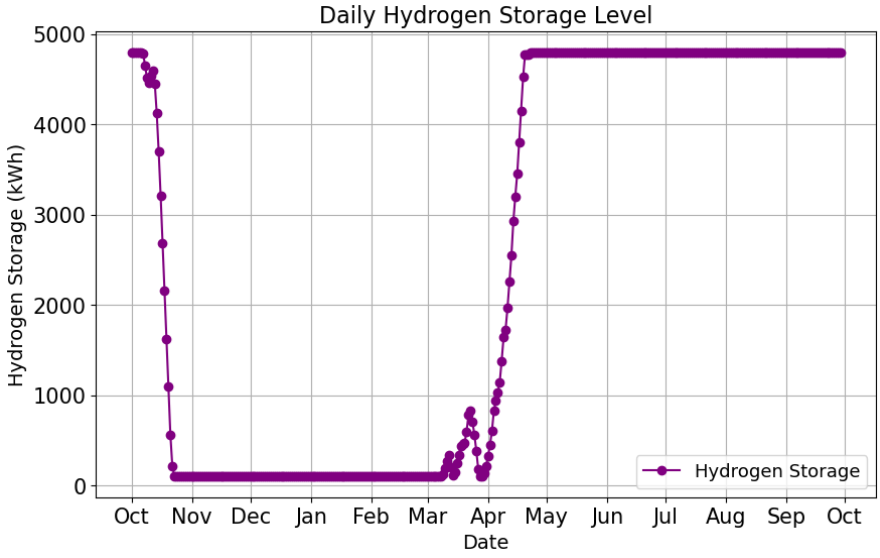

Figure 4.10: Daily metal hydride storage level 2015

Electrolyser Input and Fuel Cell Output Power 2015
The fuel cell, see Figure 4.11, was used for a total of 468 hours until the metal hydride storage was fully discharged, and the electrolyser operated for 790 hours to recharge the metal hydride.
The electrolyser usage is especially intermittent compared to the training data, with relatively higher setpoints than the test data. This makes sense as it relates to PV panel supply, which is more intermittent in a single year.

In March, there were two moments when the fuel cell was used. The use of the fuel cell at these moments is justified as they correspond to moments when the net energy dipped below zero, as seen in subsection 4.1.3.

The electrical energy put into the electrolyser was 8.0 MWh, and the total energy in the form of hydrogen that the electrolyser produced was 5.8 MWh, resulting in an average efficiency of 73.2% for the electrolyser. The total amount of hydrogen the fuel cell used was 5.8 MWh, and the total amount of electrical energy produced was 3.2 MWh, resulting in an average efficiency of 56.2% for the fuel cell. Additionally, 291 kWh of hydrogen did not react in the fuel cell. The total combined average efficiency of the seasonal energy storage system was 41.1% (excluding the use of exergy heat).

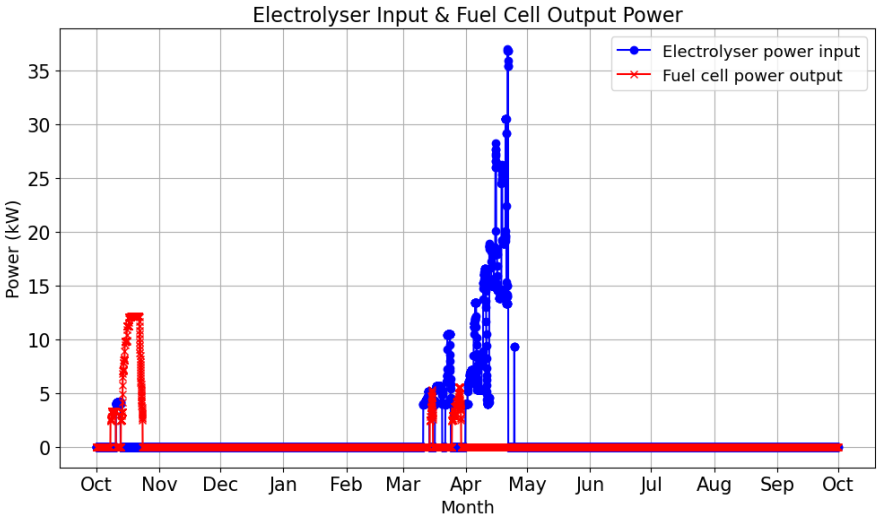

Figure 4.11: Hourly electrolyser input and fuel cell output power 2015

Exergy Reuse

In total, the electrolyser, fuel cell and absorption process produce 4.2 MWh of usable waste heat (already excluding internal losses). However, when this heat is converted to its exergy equivalent and the heat required for the desorption process is subtracted, only 531 kWh is available to reduce the heat demand.

The fuel cell produced 322 kWh of exergy, 103 kWh of which was used to provide the required heat to the desorption process. All of the 531 kWh of thermal exergy produced through heat recovery could be reused. In total, 512 kWh was used to reduce the space heating demand, and 19 kWh was used to reduce the domestic hot water demand.

When taking into account the heat recovery, the average efficiency of the seasonal energy storage system is increased to 47.8%, 0.9% lower compared to the ten-year average dataset.

Degradation of Components

The electrolyser, metal hydride and fuel cell experienced degradation when in operation. In total, the electrolyser degraded for 0.2%, the metal hydride for 0.05% and the fuel cell for 0.2%.

Electricity Import and Export From the Grid 2015

In Figure 4.12, it can be seen that during the majority of October and from March to April, the metal hydride storage is used. All the remaining electricity needs to be delivered by the grid from November to March. With a peak electricity import of 15.9 kW, with a total grid import of 35.2 MWh. Similarly, the electricity surplus needs to be exported to the grid from the end of April till the end of the year in October, with a peak electricity export of 46.9 kW and a total export of 57.0 MWh. This does not meet the requirement to stay below 40 kW of network capacity. However, it is technically feasible to turn off part of the PV panels when exceeding the 40 kW limit of the grid capacity. Nevertheless, 426 kWh, 0.3% of the total annual PV production, is curtailed this way.

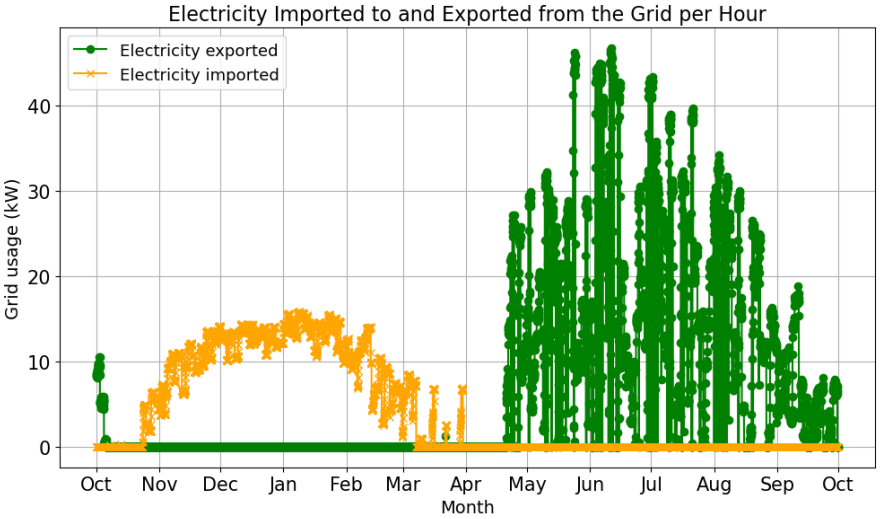

Figure 4.12: Hourly import and export of the grid 2015

4.1.4. Discussion Year Result

This section will discuss the model's results for the year.

- The current metal hydride seasonal energy storage system is not large enough to meet the full energy demand during winter. However, its capacity makes it well suited to be used as a buffer, for example, during a dunkelflaute. The current model starts using the metal hydride storage once the net energy generation becomes negative. This way, the metal hydride storage can provide a minimum of 17 days in October until it is empty, and 22 days to recharge it in April.
- When comparing the positive daily netto energy area to the negative daily netto energy area, while taking the efficiency losses from the electrolyser and fuel cell into account, it can be seen that the PV production is too little to recover all the energy the system has used.
- Due to the storage capacity of 380 kW, the daily battery is the component that proves to be beneficial. Its storage capacity is big enough to act as an energy buffer all year round, even if the seasonal energy storage is not included. However, it would be interesting to see what the minimum size of the daily battery can be.
- Both the test datasets pass the criteria set for calibrating the weight factors in subsection 3.3.6. Hence, it can be concluded that the calibration of the weight factor by hand has been done correctly.
- Although the ten-year average training dataset has different normalised input data than the individual year test data, the total annual supply or demand, given by deltaWonen, is the same for all three. In reality, the annual supply and demand are not the same for every year and are related to the input data. However, as only normalised input data is available, this is not possible to implement.
- The degradation of the metal hydride is low, as it is effectively only used for two complete cycles during each year. In future research, it is worth exploring other types of metal hydride that have higher degradation while also offering a higher volumetric energy density. This could lower the spatial requirement of the metal hydride while maintaining the required level of reliability.
- A way of lowering the required grid capacity beyond the limit of 40 kW is by reducing the number of PV panels. This reduces the peak production of the PV panels during the summer, while the relatively small change in the PV panel production in the winter can be compensated for by an increase in the relatively low grid demand in the winter. Reducing the number of PV panels from 300 to 250 in the years 2013 and 2015 lowers the required grid capacity to 38.3 kW and 30.3 kW, respectively. For 2013, this reduction is illustrated in Figure 4.13. However, this increases the reliance on the external energy from the electrical grid. This would result in the case study not reaching its goal of being 80% autarkic.

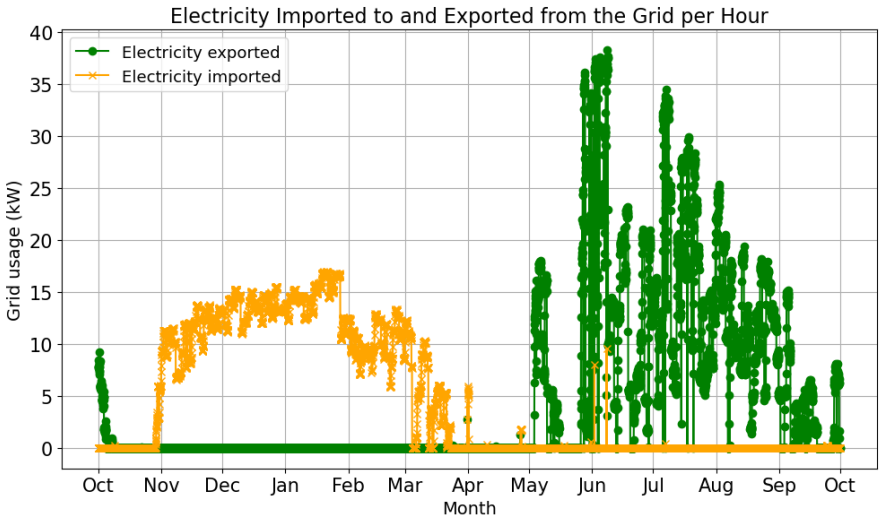

Figure 4.13: Hourly import and export of the grid (250 PV panels) 2013

4.1.5. Conclusion Year Result

The model results have been evaluated using the ten-year average dataset and two individual years (2013 and 2015). Overall, the results show that the metal hydride storage falls short as a seasonal energy storage, as the storage is empty around roughly two to three weeks after the net energy becomes negative. On the other hand, it still proves a robust buffer during dunkelflaute. Across all cases, the electrolyser achieves an average efficiency between 72% and 74% and the fuel cell at between roughly 56% and 58% efficiency. Together, the round-trip efficiency of the metal hydride storage is around 41% to 43%, rising to 47.5% to 48.3% when including the use of heat recovery.

The result of the training data never exceeded the maximum grid capacity of 40 kW. In case of the test data, the electricity exported to the grid occasionally surpassed 40 kW. This issue can be solved by turning off some PV panels during those hours. But due to this, about 0.3% to 1.3% of the annual PV production is curtailed. Most importantly, the demand for grid imports never exceeded 40 kW. Another way of not exceeding the grid capacity is by reducing the number of PV panels.

Due to the reasonably small amount of operation hours, the component degradation proved to be minor, with the electrolyser losing about 0.3% to 0.4% of capacity, the metal hydride around 0.04% to 0.05%, and the fuel cell about 1.4% to 1.8% over the year. This supports the longevity of the system.

4.2. Results Extreme Cases

In this section, the results of extreme cases are presented and discussed. The results of one year of data might not cover the possible extreme cases that the model needs to be able to handle. That is why, in this section, multiple possible extreme cases are put to the test. The most important extreme cases are presented in this chapter. The complete list of extreme cases can be found in Appendix C.

Overview of types of extreme cases:

1. Maximum and minimum PV generation
2. Maximum and minimum net energy
3. Degradation of components
4. Removing components (only daily battery, metal hydride system or grid)
5. Off-grid system
6. Grid power outage

For all extreme cases, the data of 2013 is used, because this year presented the relatively most extreme differences throughout the year. Additionally, for all the extreme cases the the most extreme day of the year is selected and is repeated for 14 days in a row. This has been determined by the number of days without sun in the Netherlands, which is 14 days, measured in 1959 (NU.nl, 2024).

2. Maximum and minimum demand

Case 5: Maximum net energy surplus in the summer, starting with empty metal hydride

The day with the maximum sum of net energy surplus was measured on the 2nd of June. As can be seen in Figure 4.14, it takes 230 hours to charge the metal hydride storage. In Figure 4.15, it can be seen that from the moment the metal hydride storage is full, the surplus of electricity is exported to the grid. This results in a required grid capacity of 54.2 kW.

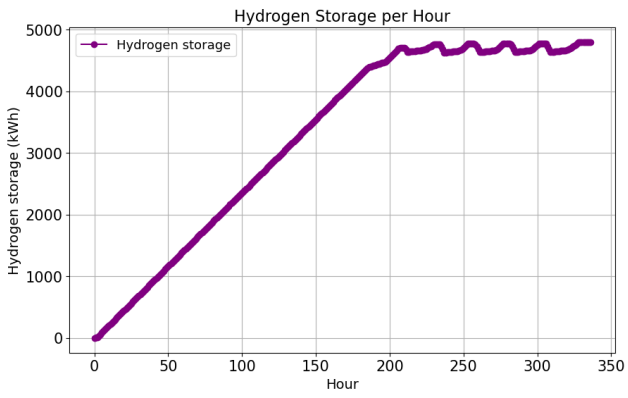

Figure 4.14: Extreme case 5: Maximum net energy surplus in the summer - Hydrogen storage per hour

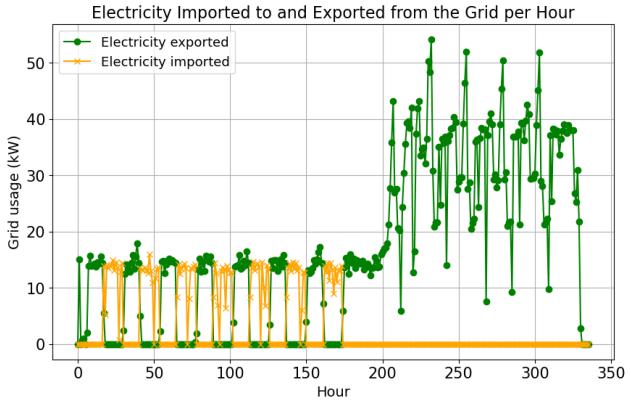

Figure 4.15: Extreme case 5: Maximum net energy surplus in the summer - Grid usage per hour

Case 7: Minimum net energy demand in the winter, starting with full metal hydride

The day of the year with the minimum net energy demand in the winter is the 19th of January; in total, there was a shortage of 399 kWh of net energy.

As can be seen in Figure 4.16, it takes 185 hours to discharge the metal hydride storage. However, about 0.1 MWh of hydrogen is stored until hour 312, which is the hour when the prediction horizon has the last 24 values within the horizon. From the moment the metal hydride storage is empty, the grid starts to be used again, resulting in a required grid capacity of 16.9 kW.

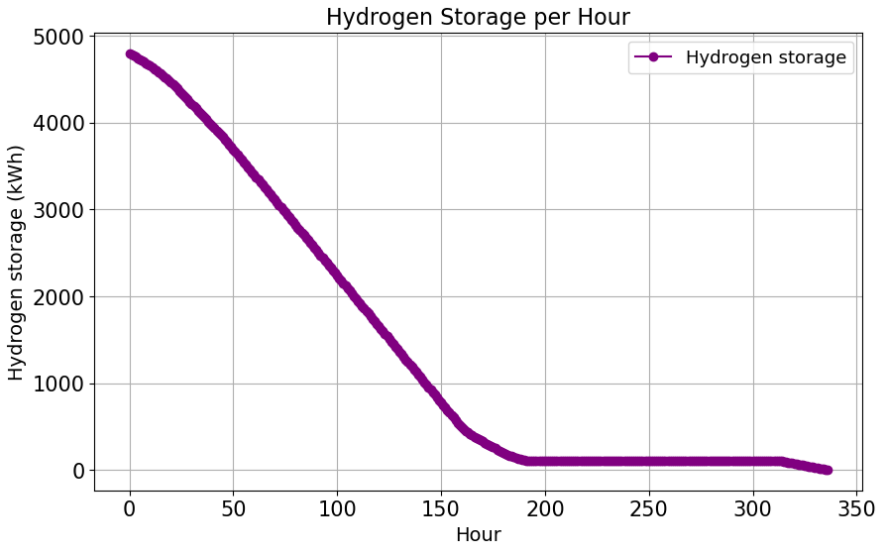

Figure 4.16: Extreme case 7: Minimum net energy demand in the winter - Hydrogen storage per hour

3. Degradation of components
Case 8: Degradation of components
The lifetime of the PEM electrolyser, metal hydride, and PEM fuel cell is finite in the model due to degradation. However, the moment that each component reaches its end of life is different.
The end of life for the PEM electrolyser is reached when degraded by 10% (U.S. Department of Energy, 2023). It takes 52631 hours of operation until the electrolyser reaches the end of its life.
The end of life for the PEM fuel cell is reached when degraded by 10% (Wu et al., 2008). It takes 25000 hours of operation until the fuel cell reaches the end of its life.

The higher the degradation, the lower the efficiency of the electrolyser and the fuelcell. Therefore, more energy is required as input to reach the same output. To make a better estimation of the operational hours when the system is at the end of its life, a run will be done with the degraded starting values for all the components (using the average ten-year data). The average number of operational hours of the first and last years of operation will be taken to determine the average number of operational hours per year. The results can be seen in Table 4.1

	Operation hours: no degradation	Operational hours: max degradation	Average hours
Electrolyser	500	699	600
Fuel cell	727	385	556

Table 4.1: Operational hours without degradation and with full degradation

This results in a lifetime of 87 years for the electrolyser and 44 years for the fuel cell before the components are degraded past their end of life.

The end of life for the TiFe metal hydride is reached when degraded by 20% (L. Zhang, 1998). It takes 1176 cycles until the metal hydride reaches the end of its life. It experiences two full cycles in a year, taking 588 years of use until the metal hydride is fully degraded.

This lifetime expectancy is very long. However, the effect values for degradation are determined by the use of a system that runs for more hours during the year. When running this little hour during the year, calendar time degradation becomes more important, and it involves aspects such as corrosion and membrane drying.

4. Removing components
Case 9: Available component: grid
The metal hydride storage is set to 0 kWh capacity and the daily battery to 0.001 kW capacity, because setting it to 0 causes decision by zero errors in the model.

In Figure 4.17, it can be seen that the peak of the electricity import is 36.6 kW, with a total grid import of 68.6 MWh. The peak export to the grid is 122.1 kW, with a total export of 95.1 MWh.

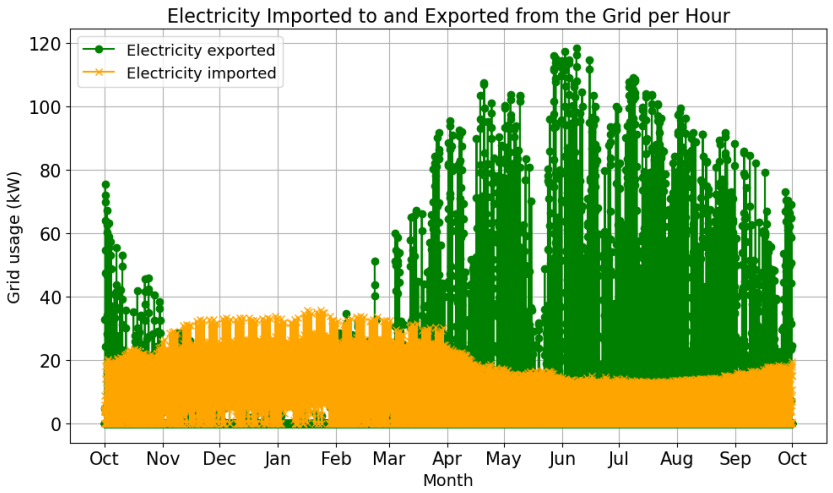

Figure 4.17: Extreme case 9: Available component: grid - Grid level per hour

Case 10: Available component: daily battery
The year starts with a full daily battery; to be able to do so, the year needs to start on the 15th of October (instead of the 1th of October), as there is a surplus of net energy at the start of October, that can't be stored in the metal hydride or sent to the grid. For the system to sustain over the years of using the system, the daily battery should be fully charged at the end of the year.

Remember that a minimalistic version of the daily battery was used in the model, as there are no efficiency losses. Additionally, the self-discharge losses are not taken into account. Therefore, the outputs of this extreme case do not correspond to a real case, but show the extreme case of the model.

As a result, 239 PV panels are required instead of 300, and a 41.9 MWh capacity for the daily battery. In Figure 4.18, the daily battery level over the year is shown.

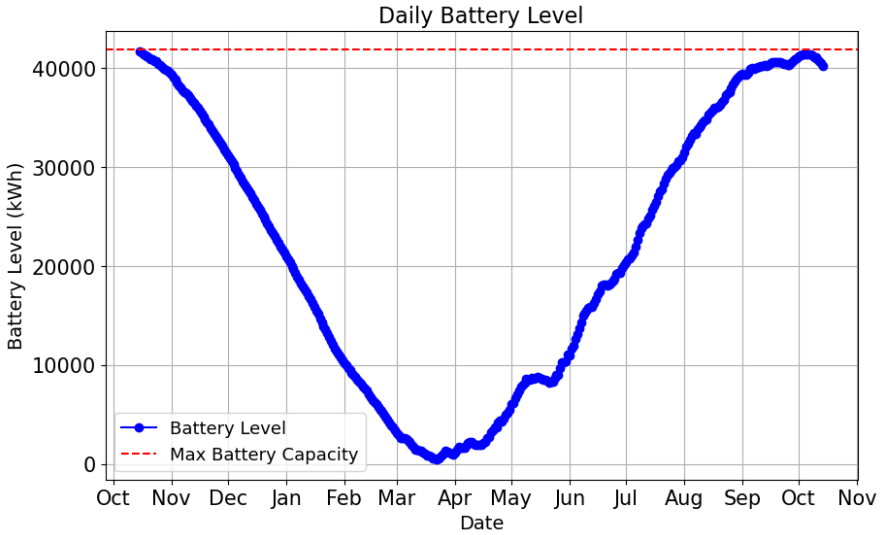

Figure 4.18: Extreme case 10: Only using the daily battery - Battery storage per day

Case 11: Available component: metal hydride
The year starts with a full metal hydride; to be able to do so, the year needs to start on the 15th of October, as there is a surplus of net energy at the start of October that can't be stored in the metal hydride or sent to the grid. For the system to sustain over the years of using the system, the metal hydride storage should be full at the end of the year.
It is not possible in the model to set the daily battery capacity to 0 kWh; 20 kWh is the minimum battery capacity that is required for the model to not result in an error in this extreme case.
As the grid is unavailable, the electrolyser power should be increased to 167 kW to match the maximum net energy generation. The fuel cell power should be increased to 26 KW to match the most negative net energy value.

As a result, a 63.0 MWh metal hydride storage is required. In total, 8.3 20-ft containers are required for the storage of the metal hydride. In Figure 4.19, the daily metal hydride storage level over the year is shown.

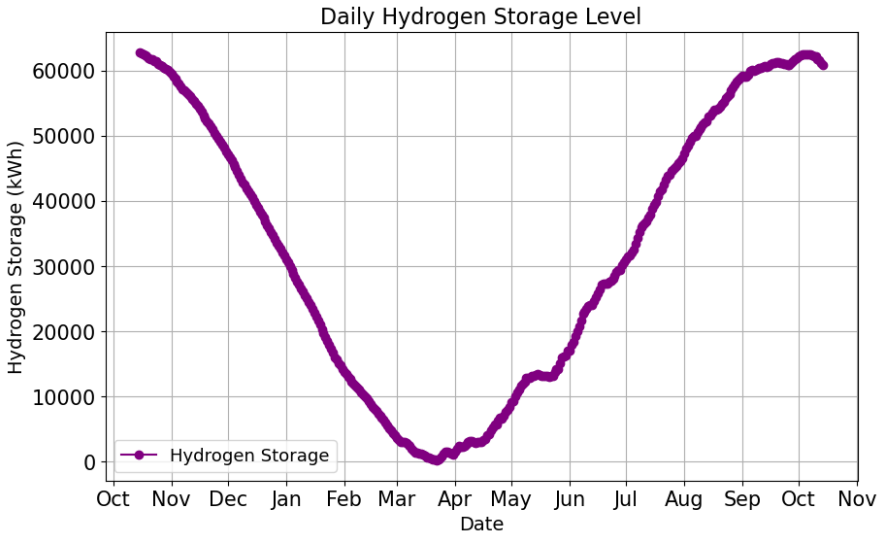

Figure 4.19: Extreme case 11: Available component - Metal hydride per day

5. Off-grid system
Case 12: Off-grid system
The year starts with a full metal hydride; to be able to do so, the year needs to start on the 15th of October, as there is a surplus of net energy at the start of October that can't be compensated for by the grid.
In case there is no grid available, the metal hydride storage should be large enough to cover the entire net energy demand with the metal hydride storage and be able to recharge the metal hydride storage back to full again, to be ready for next year. This is calculated by changing the metal hydride's size and the number of PV panels, as the original number of PV panels is insufficient to charge the metal hydride storage to full again. This is required for the system to sustain over the years of using the system.

This results in an increase of the size of the metal hydride storage from 4.8 MWh to 60.8 MWh, as can be seen in Figure 4.20. In total, 8.1 20-ft containers are required for the storage of the metal hydride. Additionally, an increase of PV panels from 300 to 346 is required to fill the metal hydride storage back up to full again at the end of the year. The electrolyser power must also increase from 40 kW to 74 kW to handle peaks in the solar power and prevent the daily battery from exceeding its upper limit.

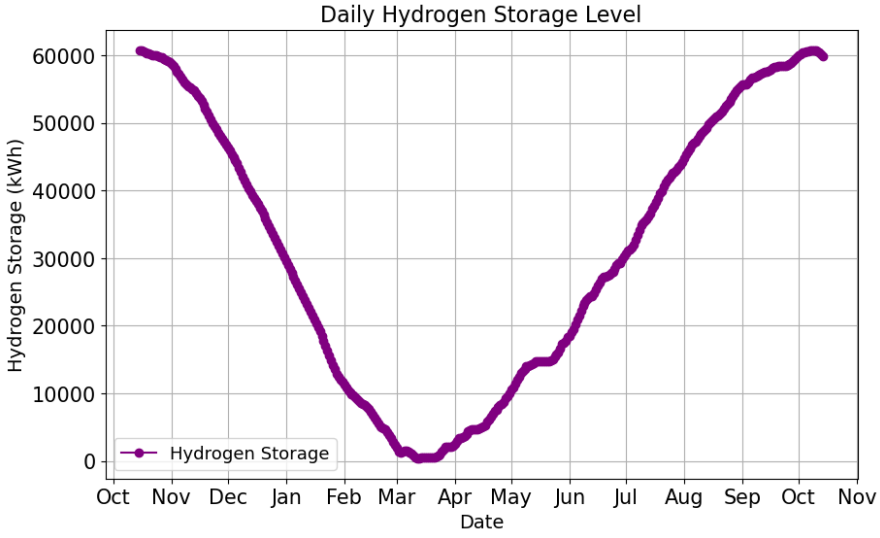

Figure 4.20: Extreme case 12: Off-grid system - Metal hydride storage per day

4.2.1. Discussion Extreme Cases

This section will discuss the results of the extreme cases.

- The calibration is not always sufficient when testing the extreme cases. For example, in extreme case 5, the electrolyser is not turned off during the run; instead, the controller imports electricity at night to keep the electrolyser running, as can be seen in Figure 4.15. However, in an optimal situation, the electrolyser would shut down in the evening. This shows that in some extreme cases, the calibration of the model is

not optimal.

- The current metal hydride seasonal energy storage system is not large enough to meet the full energy demand during winter. However, in extreme case 7, it is concluded that the metal hydride storage provides a sufficient backup for up to a week (185 hours) in the winter with the lowest net energy generation. However, this is different to the way that the model is implemented. In the current version of the model, the metal hydride storage starts to be used when the net energy generation becomes negative.
- In extreme case 7, the metal hydride is completely used. However, the last 0.1 MWh of the metal hydride is saved and only used as the last 24 hours of the run are within the prediction horizon. This indicates that the model predictive control conserves energy to satisfy the final 24 hours of its prediction horizon, rather than using all available storage earlier when it might be more beneficial.
- In extreme case 8, it was found out that due to little use of the components over the year, the expected time before the components fully degrade and reach their end of life is not an accurate representation of the real situation. Because degradation is not solely driven by operational use, calendar time ageing also plays a role. This involves aspects such as corrosion and membrane drying.
- In extreme case 9, it was found out that when only using the grid in the model, a grid capacity of 112.1 kW is required. However, what should be kept in mind is that the model adds all the supply and demand up to one net energy per hour, which already balances out the peaks that occur within the hour. In normal operation, this effect is handled by the daily battery, as it can absorb the fluctuations. However, this effect does not occur in reality when relying solely on the grid. Therefore, the model may underestimate the actual peak of the grid.

4.2.2. Conclusion Extreme Cases

This chapter has explored a range of extreme scenarios to test the limits of the model system.
The key findings are:

- In extreme case 7, where the minimum net energy demand in the winter is tested, it takes 185 hours (a bit less than 8 days) to discharge the metal hydride fully.
- Extreme case 8: The operation degradation of the components does not fully cover the total degradation of the component, as its total use over the year is limited and constrained to a particular part of the year. To better match reality, calendar time degradation should be taken into consideration.
- When only using one of the three components, in extreme cases 9, 10 and 11, the size of the components drastically increases.
  - Extreme case 9: When only using the grid, the grid capacity should be increased to 122.1 kW.
  - Extreme case 10: The capacity should be increased to 41.9 MWh when only using the daily battery. Remember that a minimalistic version of the daily battery was used in the model, as there are no efficiency losses. Additionally, the self-discharge losses are not taken into account. Therefore, the outputs of this extreme case do not correspond to a real case but show the extreme case of the model.
  - Extreme case 11: When only using the metal hydride, the capacity should be increased to 63.0 MWh, requiring a volume corresponding to the equivalent of 8.3 20-ft containers. Additionally, the number of PV panels should be increased from 300 to 426.
- In case of an off-grid application in extreme case 12, the grid can not be used. This results in a required metal hydride storage of 60.8 MWh, corresponding to the equivalent of 8.1 20-ft containers.

5

Feasibility

Besides the performance of metal hydride as a seasonal energy storage solution, it is also essential to consider other factors. These include safety, economic viability, reliability, spatial, and environmental feasibility, all of which contribute to determining the overall feasibility of the system.

5.1. Safety Feasibility

Safety is always crucial to take into account, especially in the built environment. Each component presents unique challenges to ensure the safety of the total system. Therefore, the following sections will explore the safety hazards of the different components.
This section compares the safety hazards of the system with those of other hydrogen storage technologies. The safest alternative would be to install electrical cables capable of handling the system's full supply and demand. However, this is not directly possible in most cases. In such cases, hydrogen presents an attractive alternative because it is a clean energy carrier that ranks among the best regarding seasonal energy storage capacity.

Hydrogen is highly flammable and has a flammability range in the air between 4 and 75%, and a detonation range of 18% to 59% (Dagdougui et al., 2018). Furthermore, detecting a hydrogen flame without a special sensor is hard, as hydrogen flames are invisible and odourless. Lastly, hydrogen is the lightest element, allowing it to rise and disperse quickly in open air. This can be beneficial outdoors, but problematic in non-ventilated confined spaces. This makes the storage of hydrogen one of the biggest challenges in working with hydrogen, as hazards in storage related to leaking and ventilation may result in a hydrogen-air mixture that could ignite (Najjar, 2013). Hydrogen leak sensors and ventilation are essential in mitigating safety risks. Additionally, pressure-release valves prevent the possibility of overpressurising the system.

PEM Electrolyser and Fuel Cell
The PEM electrolyser and fuel cell have the same safety concerns. The primary safety concern is gas crossover. This is the flow of the oxygen side of the membrane to the hydrogen side and vice versa, creating an extremely reactive hydrogen and oxygen gas mixture that could ignite. This can happen due to membrane thinning, the membrane's degradation, or a hole created due to faulty operation. For example, a short circuit could make a hole in the membrane. Therefore, mitigating the risk of crossover is essential to ensure the optimal function and integrity of the PEM electrolyser and fuel cell stack (Ubale et al., 2025). This can be mitigated by incorporating reinforced layers into the membranes. This enhances the durability, but at the cost of increasing the ohmic and charge-transfer resistance (Kodir et al., 2024).
Other safety concerns are (Norazahar et al., 2024):

- Small leaks of hydrogen via the stack or imperfect sealing. Even small hydrogen leaks can be hazardous due to the low ignition energy and wide flammability range.
- High voltage, electrical short circuits or discharges. PEM electrolysers and fuel cells operate at stack voltages of up to several hundred volts. Inadequate insulation can lead to a short circuit.
- Thermal hazard, improper thermal management can lead to overheating of the components and cause surfaces to heat up.

Metal Hydride
Metal hydrides are an inherently safer way of storing hydrogen than compressed gas or liquid hydrogen storage because of their low temperature and low pressure storage requirements (Srinivasan & Demirocak, 2017). The pressure is increased up to a maximum of 40 bar solely during the absorption process. During the desorption process, the temperature is increased to a maximum of 60 °C. According to (Kukkapalli et al., 2023), "Metal hydrides are generally considered a safe storage option because they do not release hydrogen gas unless subjected to specific conditions, such as high temperatures or pressures. This reduces the risk of explosions and fires." This gives safety advantages over gas and liquid storage methods. The improved safety arises from hydrogen being chemically bound and stored in its atomic form rather than its molecular state (Nguyen & Shabani, 2021).

To prevent the release of hydrogen during storage, the temperature of the metal hydride is actively controlled. The control system of the metal hydride should prevent the metal hydride from overfilling and surpassing the saturated hydrogen concentration. Therefore, the pressure in the metal hydride tank is lowered to the

equilibrium pressure after the absorption process is finished (Yang et al., 2010). The equilibrium pressure of TiFe at 25 °C is 2.7 bar (M. V. Lototskyy et al., 2014). In case the active temperature control fails, and the temperature increases, the equilibrium pressure increases. If the surrounding pressure gets below the new equilibrium pressure, the hydrogen will begin to desorb and increase the internal pressure. The desorption continues as long as the gas pressure equals the new equilibrium pressure, at which the desorption stops (Nguyen & Shabani, 2021). To ensure the safety of the system in case of an extreme situation, there are pressure release valves installed on the metal hydride tank that are designed to open if the pressure within the tank exceeds the maximum allowable pressure.

The research of Rosino Messa (Rosino Messa et al., 2024) uses a 20-ft container that contains up to a total of 40 kg of hydrogen stored in TiFe metal hydride at less than 50 bar and less than 100 °C. The metal hydride storage in the case study of Deltawonen stores up to 145 kg of hydrogen. Unfortunately, information on the size of the case study is not provided.
The research started with identifying the scenarios of potential risk in a TiFe metal hydride storage tank, after which a risk assessment was conducted, and a consequence analysis was done of the identified risks. The two worst-case scenarios with the highest safety distances are presented.
The first scenario is the explosion inside the metal hydride tank due to an air-hydrogen mixture. Due to the use of the metal hydride in the form of pellets, gaps are created. About 30% of the internal volume of the tank is free volume that can be occupied by gaseous hydrogen. An explosion of the gas mixture inside the metal hydride pellet is ruled out by having a pore size in the pellet that is smaller than the mean explosion gap limit. Only the gaseous hydrogen in the tank's internal free volume could explode (Rosino Messa et al., 2024).
The second worst-case scenario with the highest safety distance is a confined explosion in a container. The safety distances that are required between houses and humans can be found in Table 5.1.

Table 5.1: Safety distance for extreme cases (Rosino Messa et al., 2024)

Scenario Description	Windows broken (m)	Irreversible effects to human life (m)	lethal effects (m)	serious lethal effects (m)
Explosion inside metal hydride tank	48	24	11	7
Confined explosion in container	36	18	15	7.5

The explosion inside the metal hydride tanks is not related to the use of the metal hydride; an explosion could only occur if air is present inside the tank because of insufficient purging of the electrolyser after maintenance or because of air contamination. Both of these scenarios can potentially be observed in any gaseous hydrogen storage system.
In order to mitigate the risks, the following safety measures are implemented (Rosino Messa et al., 2024):

- Control of ignition sources through hazardous area classification.
- Overpressure protection to avoid a burst of the metal hydride tanks.
- Mechanical ventilation is activated when hydrogen is detected at or below 25% of the lower flammable limit.
- Fire and hydrogen detection inside the container trigger the system's emergency shutdown.
- Cables attached to the doors and ground to limit the movement of the doors in case of a hydrogen explosion inside the container.

Sodium-ion Battery
Sodium-ion batteries are generally considered safer than lithium-ion batteries (Gorman, 2023). However, the primary safety concern of sodium-ion batteries is that they can overheat and catch fire due to misuse. For example, overcharging the battery can cause the formation of sodium dendrites to grow, which increases the chance of an internal short circuit.
A safety advantage of sodium-ion batteries over lithium-ion batteries is that they can be transported at zero charge. In contrast, lithium-ion batteries require to be transported under a specific state of charge, typically about 30% (Zhao et al., 2023).
An important component of the battery is the electrolyte. It plays a crucial role in transporting ions between the cathode and the anode. However, the electrolyte is inherently unstable, flammable, highly electrochemically reactive, and prone to corrosion. These properties make the electrolyte highly related to the battery safety issues. The flammability due to thermal runaway of the electrolytes is the most serious safety hazard in applying the sodium-ion battery. It was found that with a fully charged battery, thermal runaway occurred at a surrounding temperature of between 133 °C and 165 °C with air. In comparison, the normal operational temperature of the sodium-ion battery is between -20°C and 60 °C. No thermal runaway was found when the battery was charged below 50%. To solve this flammability issue, various nonflammable electrolytes have been developed. However,

until now, no nonflammable electrolyser can fully replace the traditional organic electrolyser due to the lower electrochemical performance and increased cost (Wang et al., 2024).

5.2. Economic Feasibility

It is essential to assess the economic feasibility of the seasonal energy storage system, as costs are the primary driver of implementing a potential solution in a real-life situation. Nevertheless, the exact costs are deemed confidential information by deltaWonen. That is why it is not possible to do an extensive economic analysis. The case study would not have been possible at this pilot scale as the system is too small to be economically viable. However, with the grant of 854 thousand euros from the Rijksdienst voor Ondernemend Nederland, the project can be realised. The fact that the pilot is not economically viable is not a dealbreaker, as the goal of the pilot is to share the results as open source so that they can serve as a blueprint for the sustainability of other neighbourhoods in the Netherlands (Rijksdienst voor Ondernemend Nederland, 2025).

Economic Scaling Potential

There is great potential in scaling the seasonal energy storage solution to a greater scale. As the size of the electrolyser, fuel cell, and metal hydride increases, the cost per kWh decreases. At a certain scale, the seasonal energy storage price can start competing with the dynamic energy market prices.
From that moment on, the seasonal energy storage potential of the metal hydride storage increases as it creates opportunities to participate in the energy market, buy and store electricity at low prices, and supply it during high-demand intervals. This economic incentive could accelerate the adoption of the system.

5.3. Reliability Feasibility

Reliability is critical to ensure safe production, storage, and usage of hydrogen and safe storage and use of electricity. Due to the seasonal energy storage, the reliability of the components needs to be especially ensured during specific seasons of the year. In the spring, the metal hydride storage, which is empty after the winter, is charged by the electrolyser until the metal hydride storage is full at some point in the summer. Once net energy generation becomes negative in the autumn, the metal hydride storage will be discharged by the fuel cell, until the metal hydride is empty at some point in the summer.
Therefore, the reliability of the electrolyser is most important in the spring and summer, while for the fuel cell, it is most important in the autumn and winter. The metal hydride storage needs to be ensured throughout the year, except when it is empty between winter and spring. The daily battery is used the whole year, making the reliability of the daily battery essential.

This highlights the best moment to conduct maintenance on the different components in the system. Regular maintenance is essential to monitor degradation and ensure the reliability of the long-term operation of the system. The end of winter is the best time of year to do the planned maintenance for the metal hydride because the storage will have the highest probability of being empty by then. Meanwhile, summer is the best time to maintain the fuel cell and heat pumps. The best time to maintain the electrolyser is in the winter. Although the daily sodium-ion battery is constantly in use, the risk is decreased because the daily battery, in reality, consists of four smaller units. They can be maintained separately to avoid downtime. The best time to do the maintenance would be when the battery capacity is the lowest. In Figure 5.1, it can be seen that in the months of December and January, the battery capacity is, on average, the lowest.

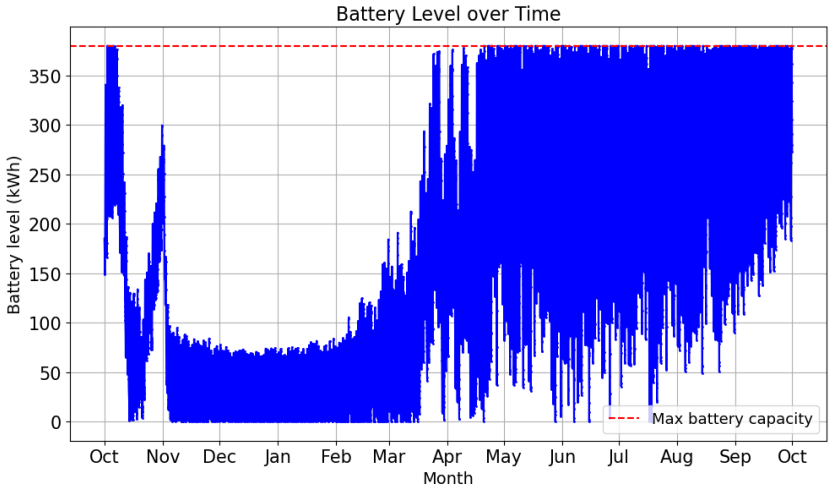

Figure 5.1: Battery level per hour using average 10-year dataset

Early problem detection can be made possible by remote monitoring, which can help to minimise the amount of

downtime and the amount of required labour.

Depending on the system, maintenance activities can include anything from cleaning to replacement of parts. Some of the most critical reliability concerns per component are presented.

Sodium-ion Battery
Thermal and chemical stability is crucial for the reliability of sodium-ion batteries. It is essential to monitor the temperatures across the battery pack to ensure reliability, as hotspots or thermal gradients may signal local degradation or thermal management failure. The control system should prevent the battery from overcharging or over-discharging, as this allows dendrites to grow (Sirengo et al., 2023).
An advantage in the reliability of sodium-ion batteries is that they can be stored at zero charge without losing storage capacity, while the lithium-ion batteries do (Zhao et al., 2023).

PEM Electrolyzer and Fuel Cell
The most important thing to consider to ensure reliability is whether all the parts within the component and the auxiliary equipment work as expected, as the failure of a single part within the electrolyser or fuel cell can cause the failure of the component itself.
For example, for the electrolyser, a malfunctioning water purification system can result in contaminated water entering the stack, which could poison the catalyst. Besides this, the main failure mechanisms of the PEM electrolyser mainly apply to the degradation of the membrane, which could result in gas crossover (Norazahar et al., 2024).
An example of the fuel cell is that a failure of the cooling subsystem may create high temperatures, which increase the rate of catalyst and membrane degradation and the formation of local hotspots. On the other hand, low temperature facilitates conditions for liquid water to accumulate in the gas supply channels and the stack, which leads to flooding, causing a drop in voltage output (Vasilyev et al., 2021).

Other main failure mechanisms for both apply to the degradation of the membrane, which could result in gas crossover. This can mainly be caused by:

- A failure of thermal management, resulting in a hotspot in the membrane or accelerating corrosion of the corrosive electrolyte (Norazahar et al., 2024).
- Mechanical degradation of the membrane, including thinning, creaking or pinhole formation (Norazahar et al., 2024).
- Flooding or drying out of the membrane (Dotelli et al., 2014).
- Electrolyser specific: The water quality and quantity at the anode could impact the local drying of the membrane (Norazahar et al., 2024).
- Fuel cell-specific: The air quality and impurities in the air could poison the membrane (Mehrabadi et al., 2016).
- Fuel cell-specific: The hydrogen quality needs to be over 99.995 vol.% to limit the nitrogen feeding into the anode (Steinberger et al., 2018). This is not a limitation in this system as the electrolyser produces quality 5.0 hydrogen (99.999 vol.%) (Shiva Kumar & Himabindu, 2019) and the metal hydride storage works as a hydrogen purifier as it selectively only stores hydrogen (Miura et al., 2012).

Metal Hydride
To maintain a reliable operation with high cycling stability, high-purity hydrogen must be used. Fortunately, the PEM electrolyser produces high-quality hydrogen (Shiva Kumar & Himabindu, 2019). This minimises the degradation of the metal hydride, as TiFe is highly reactive with oxygen (Davids & Lototskyy, 2012). However, due to a possible failure, the electrolyser could supply hydrogen with increased oxygen impurities. Contact with oxygen passivates the outer layer of the metal hydride, reducing the storage capacity. Fortunately, the oxidation layer forms a protective layer that prevents further oxidation, which is crucial to avoiding thermal runaway. When nitrogen comes into contact with the metal hydride, the nitrogen has no safety risks but deactivates the metal hydride. That is why argon is used for flushing instead of nitrogen (Rosino Messa et al., 2024).
Furthermore, it is essential to take thermal management into account. During storage, it is important to prevent hydrogen from being released from the metal hydride. At the same time, during the absorption process, heat removal is required to avoid the buildup of thermal energy. During the desorption process, heat should be supplied to the metal hydride to allow the hydrogen to be released from the metal hydride.

5.4. Spatial Feasibility

When evaluating the feasibility of seasonal metal hydride storage systems, the spatial requirement of the system plays a crucial role, as space is limited in the built environment. This section explores the spatial requirements, focusing on modularity, scalability and potential improvements. A comparison is also made with a conventional battery-only system to compare the space requirements of both systems.

Spatial Requirement
The storage capacity of the metal hydride in the case study is 4.8 MWh. Given by the manufacturer, GKN Hydrogen, 2 MWh of hydrogen can be stored in the first 20-ft container, as the remaining part of the container is filled up by the electrolyser and fuel cell (GKN hydrogen, n.d.). The storage capacity of the metal hydride can be increased by 8.3 MWh for every additional 20-ft container because any additional container can only contain metal hydride (GKN Hydrogen, n.d.-b). In total, the required volume to store all the metal hydride, including the electrolyser and fuel cell, corresponds to the equivalent of 1.3 20-ft containers.

Modularity and Scalability
The modular design in 20-ft containers provides the advantage that the solution can be scaled up relatively easily. Another benefit is that the containers can be stacked on top of each other, reducing the required spatial area.

The highest volumetric hydrogen density currently is 150 kg/m^3 in Mg_2FeH_6 (Züttel, 2003). TiFe, by comparison, has a density of 105 kg/m^3 (H. Liu et al., 2023). This is an increase of 42.9%, which could reduce the amount of 20-ft containers to 5.9. When stacking two containers on top of each other, an area of 41.6 m^2 would be required. However, Mg_2FeH_6 is a complex high-temperature metal hydride. The addition of Fe to the elemental metal hydride MgH_2 increases the volumetric energy density but also increases the absorption and desorption enthalpy (Khan et al., 2020). The higher operational temperature between 410 and 450 °C (Poupin et al., 2021) and the poor cyclability (Thiangviriya et al., 2021) make Mg_2FeH_6 not a suitable replacement for this moment in time to TiFe.

There is a lot of ongoing research into metal hydride alloy, which shows the potential for future metal hydride to reduce the spatial requirement of metal hydride storage.

Spatial Requirement of an Only Battery System
Extreme case 10 from section 4.2 is used for this comparison. During this extreme case, only the daily battery could be used. As a result, a 41.9 MWh capacity is required for the daily battery, and 239 PV panels are required instead of 300. Remember that a minimalistic version of the daily battery was used in the model, as there are no efficiency losses. Additionally, the self-discharge losses are not taken into account. Therefore, the outputs of this extreme case do not correspond to a real case but show the extreme case of the model.

An approximate estimate of the efficiency and self-discharge losses for both sodium-ion and lithium-ion batteries is provided. These parameters, summarised in Table 5.2, are evaluated over a six-month self-discharge period.

Table 5.2: Performance and capacity values for sodium-ion and lithium-ion batteries

Parameter	Sodium-ion	Lithium-ion
Efficiency	80% (Yu et al., 2023)	90% (Yu et al., 2023)
Self-discharge rate	3%/month (Delongtop, 2024)	3.5%/month (Babu, 2024)
Storage capacity (per 20-ft container)	2.3 MWh (Murray, 2024)	5.0 MWh (Murray, 2024)

This results in a required daily battery capacity of 62.9 MWh for the sodium-ion battery, requiring a volume corresponding to the equivalent of 27.3 20-ft containers. A total battery capacity of 57.7 MWh is required for the lithium-ion battery, which requires a volume corresponding to the equivalent of 11.5 20-ft containers.
This approximation shows that the sodium-ion battery requires many more containers than the TiFe metal hydride storage. The lithium-ion battery storage requires 3.4 20-ft containers more than the TiFe metal hydride storage.
This shows the importance of implementing seasonal metal hydride energy storage to minimise spatial requirements in an urban environment where space is scarce.

5.5. Environmental Feasibility

There are multiple ways to assess the environmental impact of metal hydrides. The first benefit of metal hydrides is that they have no energy losses over time and a long lifetime. However, small hydrogen leaks due to imperfect sealing occur during production, storage and transport. Although the leakage is small, the total leakage adds up over the years of using the system. Therefore, it is important to carefully take the leakage of hydrogen into account, as well as making sure that the 5% of unreacted hydrogen in the PEM fuel cell, which is assumed to be a loss in this research, is in reality reused in the PEM fuel cell.
The main environmental impact comes from processing the material. The selection of the hydrogen storage material considerably impacts the environmental feasibility. Using a pressurised compressed gas tank can obtain the lowest emissions. However, the cylinder gas tank has a low volumetric energy density and requires pressurising of hydrogen at 300-700 bars. Using metal hydrides can lower the storage volume and enhance safety (L. Liu & Johnson, 2025).
The material impact of TiFe mainly comes from titanium, as it is labelled as a critical raw material by the EU. It as a CO_2 footprint of 8.1 $kgCO_{2,eq}$/kg whereas iron has a CO_2 footprint of 1.5 $kgCO_{2,eq}$/kg. Recently, it has been found that TiFe produced from recycled industrial iron and titanium scraps can achieve a storage capacity of

1.5-1.6 wt%, which is close to the storage capacity of 1.86 wt% of that of high-purity TiFe. This could help to reduce the production costs of TiFe greatly. However, the production of TiFe has an increased energy demand (and thus higher CO_2-footprint) due to the requirement of an extensive activation step (Klopčič et al., 2023). The alloy TiFe0.85Mn0.05 requires a far less extensive activation step while minimising the loss of storage capacity and is therefore the more common alloy to use, which only has a CO_2 footprint of about 0.03 $kgCO_{2,eq}/kg$ (Alves et al., 2025).
After reaching the end-of-life, the recovery of materials of the metal hydride installation, including the metal hydride, reduces the environmental impact of resource use by 60%.

Comparing the Life cycle assessment (LCA) of the TiFe0.85Mn0.05 metal hydride (excluding the PEM electrolyser and fuel cell) to a simple reference system, which stores the same amount of hydrogen (46 kg) at the same pressure as the metal hydride storage (30 bar) over a period of 50 years. The total LCA score (including ranked on influence: climate change, fossil resource use, minerals and metals resource use, particulate matter, freshwater eutrophication, acidification, photochemical ozone formation, freshwater ecotoxicity) of the reference system is 24.5 points, and for the metal hydride system is 19 points. One point is equivalent to the annual environmental load of a European person (Alves et al., 2025).
The metal hydride storage in the case study of deltaWonen stores up to 145 kg of hydrogen. This results in an annual environmental load of 60 European persons.

5.6. Discussion

All the different feasibility aspects of the system, consisting of interrelated components, have been considered to provide a feasible system. All the feasibility aspects are related to each other and represent trade-offs. For example, it is possible to increase the system's safety by selecting a nonflammable electrolyte for the sodium-ion battery, but this lowers the economic feasibility as well as the total efficiency of the system. Another example is selecting another type of metal hydride with a higher volumetric density, which would lower the amount of 20-ft containers required for the storage, but would potentially decrease the feasibility of the reliability and maintenance.

The metal hydride is, in most cases, involved in the worst-case scenarios of the system. The worst-case scenario, safety-wise, is an explosion inside the metal hydride tank. If there were an explosion inside the metal hydride tank, a distance of 48 meters is required to prevent the windows from breaking, and a distance of 7.5 meters is required to prevent serious, lethal effects. However, this scenario is highly unlikely as the electrolyser should be either insufficiently purged after maintenance, or air contamination should occur, and there should be a source of ignition. It is worth noting that the hydrogen quantity in the case study is larger than considered in the research. As a result, the safety distance may be greater in practice.
The worst-case scenario for the system's reliability would be if maintenance is required for the internals of the metal hydride at the end of the summer due to a failure. This would require discharging (part of) the metal hydride storage. After maintenance, this would leave a not (fully) charged seasonal energy storage at the start of the winter.
These worst cases can be mitigated using an extensive control system with sensors that shut down the system when malfunctioning and allow for predictive maintenance.

5.7. Conclusion

The feasibility assessment shows a number of safety, economic, reliability, spatial and environmental challenges. Nevertheless, with the right design choices, control strategies and smart maintenance, these can be successfully managed. Each component presents unique risks but shows promising safety advantages over other hydrogen storage technologies. The scalability and long-term potential of the system offer an economical perspective to compete with the market dynamics in future larger-scale projects. Nevertheless, more research into the exact economic costs is required to determine the competitive scale of the system. The system's reliability varies seasonally, as different components become critical at different times of the year. This seasonal variation requires a clear maintenance window to be identified in order to ensure year-round performance in combination with a control system that includes predictive maintenance. The life cycle assessment shows a 20% lower total impact than the conventional compressed gas reference, even though the critical raw material, titanium, is used for the metal hydride system. On top of that, the spatial requirement of the metal hydride system is lower than that of the compressed hydrogen reference system because of its higher volumetric energy density.
Overall, the feasibility assessment demonstrates that, when carefully implemented, the system establishes the foundation for a future hydrogen storage that is scalable and sustainable. Future work should focus on detailed economic analysis, pilot-scale demonstration and continued R&D work aimed at developing metal hydrides which have a higher volumetric energy density at a lower cost.

6

Discussion

This chapter reflects on the outcomes of the system-level model and evaluates the performance of the proposed energy system and control strategy. Currently, the MPC controller does not use the seasonal energy storage when it is most needed, in mid-winter when the storage is already empty, and in mid-summer when it is already full, thereby limiting the seasonal potential. In this section, the limitations of the current system related to the size of the metal hydride and the current control behaviour are discussed, and possible improvements are explored.

6.1. Storage Capacity Limitations Metal Hydride

The first way to improve the performance of the metal hydride as a seasonal energy storage is to significantly increase the size of the metal hydride storage to fully cover the net energy demand over a year, while also allowing it to reach full capacity by the end of the year.

Using extreme case 12 from section 4.2 as a reference, the storage volume must increase from 3.8 MWh to 60.8 MWh. The required volume corresponds to the equivalent of 8.1 20-foot containers. Additionally, an increase of 300 to 346 PV panels is necessary to fill the metal hydride storage backup until it is complete at its peak. The electrolyser power must also increase from 40 kW to 74 kW to handle peaks in solar power and prevent the daily battery from exceeding its upper limit.

An offline multi-objective optimisation is proposed to more effectively determine the optimal size of the components for a viable seasonal energy storage solution that covers the entire demand in the winter. This model aims to identify the minimum required component sizes to meet the annual net energy demand and ensure that the storage is fully recharged by the end of the year (Kim et al., 2025).

Such a scale-up has spatial and financial consequences. Although technically possible, the large physical footprint of the metal hydride containers and the high cost associated with the metal hydrides raise questions about the practicality of this configuration. The current system is better suited for the use of peak shaving or as a buffer in extreme situations, rather than full seasonal energy storage. Unless it is implemented on a larger, collective scale, where economies of scale can be leveraged.

6.2. Improving Control Strategy for Limited Storage Metal Hydride

The current MPC implementation does not prioritise hydrogen use during critical periods, such as mid-winter or during a dunkelflaute. This is because the MPC controller operates on a 24-hour horizon. Since the MPC only considers the upcoming 24 hours, it lacks foresight into broader seasonal patterns, making it difficult to enforce the strategic use of the storage system. At the same time, it is inherently impossible to predict precisely when seasonal energy storage will be most needed; any model will ultimately rely on estimations rather than precise predictions.

The current limitation of the MPC raises an important question: What is the optimal operational strategy for utilising the metal hydride storage when it is not large enough to cover the entire net energy demand? The remainder of this section explores several strategies to use the limited hydrogen storage capacity more effectively.

Strategy 1: Use dynamic energy prices:
Optimise the system based on the dynamic electricity grid prices. During periods of high grid prices, the system will prioritise using stored energy from the metal hydride storage over the use of the grid import.
A limitation of this approach is the high cost of the energy stored in the metal hydride storage, especially at the scale considered in the case study. Given the grid's lower cost and sufficient capacity, the system would likely use the grid year-round, thereby limiting the use of seasonal storage in the metal hydride size of the model.
By scaling the number of apartments, the relative cost of the metal hydride storage per kW is expected to decrease while the dynamic energy prices stay fixed. Further research is required to determine the optimal number of apartments for which the implementation of the seasonal storage system becomes both technically and economically favourable.

Strategy 2: Threshold-based control:
A heuristic strategy could trigger the hydrogen discharge once a predetermined threshold is reached. This threshold value can be precalculated to determine when the seasonal energy storage system can be utilised. Specifically, the system may begin discharging the metal hydride storage once the cumulative negative net energy drops below this threshold. This threshold is derived from the average net energy generation over a year. As a result, the strategy is expected to perform effectively under average yearly conditions and in extreme scenarios, such as during a Dunkelflaute.
Another option is to calculate a threshold value for the grid usage using the seasonal energy storage. The system can charge or discharge the metal hydride storage when the import or export to the grid surpasses the threshold. As a result, the system can be used for peak shaving. The strategy is expected to perform effectively under average yearly conditions and in extreme scenarios, such as during a Dunkelflaute.

Strategy 3: Seasonal objective function terms:
A more integrated solution involves modifying the MPC objective function to include seasonal incentives. For example, penalty terms could enforce a minimum hydrogen state-of-charge in the winter months. The severity of the penalty increases as the year progresses toward the peak winter demand. For example, a larger penalty is applied in December than in October. While this approach would work for the typical variations of net energy generation, it would not work well if a dunkelflaute occurs outside of the winter season.

Implementing these possible strategies would require significant modifications to the current model. Currently, no constraint or objective function term covers this long-term interest. Therefore, in future research, it is suggested that other modelling options are explored. When trying to minimise the changes to the current model, it would be interesting to explore a higher second level of control. This separates long-term strategic planning from short-term operational control. This additional, long-term strategic planning could be either an offline optimisation or another MPC (Gupta et al., 2023). An offline optimisation is the most logical approach, given the high uncertainty in long-term forecasts over weeks or months. This level of uncertainty makes it impractical for a second, long-horizon MPC to reliably guide seasonal energy storage decisions. A key advantage of offline optimisation is that it can be integrated relatively easily into the existing short-term MPC structure, for example by using the 10-year average dataset. However, a drawback is that it is less adaptive to real-time deviations from the offline scenario, potentially leading to suboptimal behaviour under unexpected conditions.

7

Conclusion and Recommendations

7.1. Conclusion

This research explored how hydrogen can be stored in a room temperature metal hydride and used for seasonal energy storage, in combination with solar energy, a PEM electrolyser, a PEM fuel cell and a reduced connection to the electrical grid.
To conclude this research, the sub-research questions will be answered first, followed by an answer to the main research question.

Sub-research questions:
How can a system-level model be developed to evaluate the performance of metal hydride as a seasonal energy storage solution?
A system-level model that captures the interactions between the different components needs to be developed to evaluate the performance of a metal hydride seasonal energy storage system. To evaluate the performance over the full year, where in reality only limited information is known beforehand, model predictive control with a receding horizon of 24 hours is selected as the controller for the model.
The first step in developing the model is to define the system setup, which components should be included, and how they are related. The next step is to determine the assumptions and input parameters of the model. Afterwards, model predictive control can be formulated. The constraints, objective function, and control actions of the model predictive control should be defined. Ideally, the objective function consists of different terms that can be directly added together; if not, weight factors should be added and calibrated. The last step is to verify the model, aiming to find and solve the potential modelling errors.

What is the potential for heat recovery and effective utilisation during the metal hydride storage process?
In the test data, it is found that from 3.8 MWh to 4.2 MWh of heat is generated, only 482 kWh to 531 kWh is effectively reused to lower the heat demand of the households. On average, 12.7% of the heat can be recovered and utilised effectively.

What is the round-trip efficiency of a metal hydride storage when applied for seasonal energy storage?
The round-trip efficiency of the test data of the metal hydride system is found to be 41.1% to 42.0% when the heat recovery is excluded. Including the recovery of heat, the round-trip efficiency can be increased up to 47.8% to 48.6%. Resulting in an average round-trip efficiency of 48.2%.

Beyond technical feasibility, what are the safety risks, economic costs, reliability challenges, spatial requirements, and environmental impact that affect the overall feasibility of implementing metal hydride seasonal energy storage?
Beyond the performance of the system, implementing a metal hydride seasonal energy storage in the built environment depends on safety, economic, reliability, spatial and environmental feasibility of the system. Safety-wise, the metal hydride offers a relatively safe alternative to other types of hydrogen storage technologies due to the low pressure and low temperature storage. However, one should be cautious of hydrogen leaks and hydrogen explosions. Economically, the high costs challenge the affordability of the solution. For an economically feasible solution, the seasonal energy storage should be scaled up to the point that it could compete with the dynamic energy prices of the grid. Reliability hinges on the seasonal demands. The electrolyser must perform in the spring and summer, and the fuel cell must be in the autumn and winter. The metal hydride storage is operating when either the electrolyser or the fuel cell is operating. The daily battery operates throughout the entire year. Smart maintenance scheduling and remote monitoring help to minimise downtime. The spatial feasibility depends on the scarcity of space. The modular design allows for an easy scale-up of the capacity if required. Nevertheless, in residential areas, the required safety distance due to a worst-case explosion inside the metal hydride storage tank must be carefully considered during the design process. Finally, the environmental feasibility assessment indicates that the metal hydride has a lower impact than the gaseous hydrogen reference system. This is possible due to the reuse of materials after the metal hydride has reached its end-of-life.

To what extent does integrating a seasonal metal hydride energy storage system reduce the required peak capacity of the electrical grid?
In a normal situation, each of the 40 apartments would have gotten a 1x35A grid connection, resulting in a total of 320 kW required grid capacity. In extreme case 9, where only the grid was available, discussed in more

detail in section 4.2, a maximum grid capacity of 122.1 kW was required to export to the grid. This is already significantly lower than the original connection. What should be kept in mind is that the model adds all the supply and demand up to one net energy per hour, which already balances out the peaks. The peak balancing effect occurs when using a battery, since it can absorb fluctuations. However, this effect does not occur in reality when relying solely on the grid. Therefore, the model may underestimate the actual peak of the grid.
With the daily battery and metal hydride system, discussed in more detail in subsection 4.1.3, a maximum of 16.8 kW is required for electricity import from the grid, and up to 55.7 kW is required for electricity export, based on the 2013 test data. While this is significantly lower than 320 kW, it would still surpass the 40 KW grid capacity allocated to the project. A solution to this would be to turn off part of the solar panels for a few moments during the year when the export to the grid exceeds 40 KW. This would, in the year 2013, result in a curtailment of 1.3% of the annual PV production. Another option would be to reduce the number of PV panels. This reduces the peak production of the PV panels during the summer, while the relatively small change in the PV panel production in the winter can be compensated for by the grid.

At what scale can a seasonal metal hydride energy storage system be integrated most effectively within renewable energy systems?
The most effective scale of the metal hydride energy storage system depends on many factors.
In an off-the-grid scenario, a large-scale storage system must match the seasonal demand. For example, in the extreme case 12 analysed in section 4.2, a 60.8 MWh metal hydride is sufficient to fulfil the yearly demand of the 40 apartments in the case study of deltaWonen. At this scale, the system achieves seasonal autonomy, though it comes with a high capital investment that is only used for two full cycles per year. Additionally, the required volume to store all the metal hydride corresponds to the equivalent of 8.1 20-ft containers.

However, in most realistic scenarios, some grid capacity will be available. The amount of grid capacity that is available and the type of demand have a significant influence on the most effective size of the metal hydride storage capacity. In a grid-connected scenario, the effectiveness of the metal hydride storage system shifts from autonomy to economic viability. The optimal storage scale then depends on the ability of the system to:

- Reduce the dependency of the grid on periods with severe grid congestion and/or high dynamic energy prices.
- Shift renewable overproduction to periods with high demands.
- Economically compete with the dynamic energy prices.

In these cases, the effective integration is achieved at a scale large enough to benefit economically, but small enough to maintain good storage utilisation.
Although during this research, an extensive economic analysis of the seasonal metal hydride system at this relatively small scale was not possible. The system is expected to be best implemented at a community scale. On that scale, it is big enough to become economically viable, but not too large to start losing its cost-competitive edge, for example, by storing hydrogen in a salt cavern. A transformer substation that supplies electricity to a neighbourhood might represent a suitable unit size for such an installation. Its scale aligns well with the energy demand of up to a few hundred households, making it a promising scale for decentralised seasonal storage.

Main-research question:
What is the feasibility of room temperature metal hydrides for seasonal energy storage solutions in the built environment?
Room temperature metal hydrides offer promising characteristics for hydrogen-based, seasonal energy storage in the built environment, but their feasibility depends on different factors. This research mainly addresses technical feasibility, but the safety, economic, reliability, maintenance, spatial, and environmental feasibility have also been touched upon.

Room temperature metal hydride systems absorb and desorb hydrogen at moderate pressures and near ambient temperatures, which aligns well with the safety and integrational requirements in the built environment.
Additionally, metal hydride can achieve higher volumetric hydrogen storage densities than compressed gas or liquid hydrogen, making them attractive when planning on using hydrogen in the built environment, where space is limited.
The results show that the metal hydride can effectively store hydrogen produced during the summer and convert it back into electricity during the winter when the energy demand is higher. This is enabled by the lack of self-discharge during storage. However, sufficient storage capacity is required to maintain year-round functionality. The current size of the metal hydride only allows for a 1 to 3 week backup when the demand is high in relation to the PV production, or in case of a dunkelflaute.
The round trip efficiency of the metal hyride system is, when recovering the waste heat, on average 47.7%.
While the technology is technically feasible, economic factors remain a barrier to large-scale adoption. The current high cost of the metal hydride system, including PEM electrolyser and fuel cell, prevents scaling to a size where it becomes competitive with dynamic energy prices. While any system would eventually become

competitive if scaled up enough, the required scale for the metal hydride to become a seasonal energy storage is too large to be implemented for the case study. Therefore, cost reductions or performance improvements in system components are essential before scale-up becomes viable.
Scale-up of the metal hydride storage could, on the other hand, lead to issues with the spatial feasibility, as the required volume corresponds to the equivalent of 8.1 20-foot containers. Additionally, as the amount of gaseous hydrogen increases, so should the safety distance between the metal hydride storage and the buildings.

Room temperature metal hydrides are a technically feasible solution for seasonal energy storage in the built environment, particularly when recovering part of the waste heat. While their moderate efficiency, high capital cost, and spatial area currently limit the adoption of the solution, their unique potential to enable renewable energy shifting makes them a compelling candidate for community-scale systems. With smart control strategies and heat recovery, metal hydrides could help to bridge the gap between daily fluctuations and long-term seasonal energy needs in the energy transition.

7.2. Recommendations

Some simplifications have been made during this research, and some aspects of the problem have not been thoroughly researched. First, the final recommendation for the model will be given. The second part consists of research-related recommendations.

7.2.1. Recommendation Model

- Heat storage is not implemented in the current model, although this does not affect the recovery of the waste heat in the model, it does influence the peak heat demand. By incorporating heat storage, the peak of PV production can be flattened by generating heat, while in winter, the peak in heat demand can be flattened by preheating the heat storage before heat demand is needed.
- Currently, weight factors are required to add up the different terms within the objective function. For future research, it is recommended that all the objective terms be transformed into a cost function. This, combined with the dynamic energy pricing, can help find the optimal size for the metal hydride storage system. Suppose it is not possible to add up the different terms in the objective function directly. In that case, it is recommended to use an optimiser to calibrate the weight factors instead of optimising it by hand, as this could result in a more efficient operating system.
- Look into implementing a second, long-term level within the MPC controller. Allowing for short-term optimisation, while keeping the long-term goals a part of the optimisation.
- The efficiency losses and degradation of the daily sodium-ion battery are not included. This had a greater influence on the results than was anticipated beforehand. Therefore, adding these aspects to the model in future research is recommended.
- The AC/DC conversion losses associated with grid usage are not included in the current model. While the implementation would increase the import of electricity from the grid, which is not a problem, as it is far below the maximum grid capacity. It would decrease the export to the grid, which would positively affect the year results, reducing the amount of grid export that currently exceeds the maximum grid capacity.
- A practical extension to the model would be to curtail the PV production that exceeds the maximum grid capacity. This would, while only curtailing a small share of energy, allow the system to respect the maximum grid capacity.

7.2.2. Recommendation Research-Related

- Future research should further explore the aspects introduced in the feasibility chapter, including safety, economic viability, system reliability, spatial requirements, and environmental impact.
- This research focused on room temperature metal hydrides. While room temperature metal hydrides have advantages in the built environment, it is worth exploring the potential of other types of metal hydrides with an increased volumetric energy density. In this search for an increased volumetric energy density, it is suggested that the degradation of the metal hydride be re-evaluated. Currently, it is expected that only two full cycles are required per year. Therefore, exploring a metal hydride with a volumetric energy density and a higher degradation rate could be interesting.
- This research was limited to the application of a metal hydride storage in the built environment, excluding the potential feasibility for an industrial area. In industrial settings, energy demand and PV production peak during daytime hours, resulting in a stronger alignment between supply and demand. This improved match could enhance the effectiveness of local energy storage solutions. Additionally, there could be a demand for higher temperature heat in the industrial area. It is recommended to look into high-temperature metal hydrides and other types of electrolysers and fuel cells, which could further utilise this demand for higher temperatures.

References

Alliander. (2019, June). Zonneparken alleen daar waar het nog kan. https://www.alliander.com/nl/nieuws/zonneparken-alleen-daar-waar-het-nog-kan/

Alves, E., Costamagna, M., von Colbe, J. B., Barale, J., Dematteis, E., Stühff, H., Stühff, T., Ante, M., Bellahcene, R., Nouvelot, Q., Luetto, C., Baricco, M., & Rizzi, P. (2025). Life cycle assessment for the determination of the environmental impacts of an advanced large-scale hydrogen storage system from HyCARE EU project. *Journal of Cleaner Production*, *515*, 145836. https://doi.org/10.1016/j.jclepro.2025.145836

Andersson, J., & Grönkvist, S. (2019). Large-scale storage of hydrogen. *International Journal of Hydrogen Energy*, *44*(23), 11901–11919. https://doi.org/10.1016/j.ijhydene.2019.03.063

Atif, M., Haider, H. Z., Bongiovanni, R., Fayyaz, M., Razzaq, T., & Gul, S. (2022). Physisorption and chemisorption trends in surface modification of carbon black. *Surfaces and Interfaces*, *31*. https://doi.org/10.1016/j.surfin.2022.102080

Au, M., & Walters, R. T. (2010). Reversibility aspect of lithium borohydrides. *International Journal of Hydrogen Energy*, *35*(19), 10311–10316. https://doi.org/10.1016/j.ijhydene.2010.07.130

Babu, B. (2024). Self-discharge in rechargeable electrochemical energy storage devices. *Energy Storage Materials*, *67*, 103261. https://doi.org/10.1016/j.ensm.2024.103261

Baetcke, L. (2024, December). Hydrogen Transport and Storage Options. In *Powerfuels status and prospects* (pp. 281–297). Springer. https://doi.org/10.1007/978-3-031-62411-7{_}11

Banasiak, D., & Kienberger, T. (2024). A comparative analysis of the economic feasibility of reversible hydrogen systems based on time-resolved operation optimisation. *Applied Energy*, *371*, 123639. https://doi.org/10.1016/j.apenergy.2024.123639

Baroutaji, A., Arjunan, A., Ramadan, M., Robinson, J., Alaswad, A., Abdelkareem, M. A., & Olabi, A. G. (2021). Advancements and prospects of thermal management and waste heat recovery of PEMFC. *International Journal of Thermofluids*, *9*. https://doi.org/10.1016/j.ijft.2021.100064

Bellosta von Colbe, J., Ares, J. R., Barale, J., Baricco, M., Buckley, C., Capurso, G., Gallandat, N., Grant, D. M., Guzik, M. N., Jacob, I., Jensen, E. H., Jensen, T., Jepsen, J., Klassen, T., Lototskyy, M. V., Manickam, K., Montone, A., Puszkiel, J., Sartori, S., . . . Dornheim, M. (2019). Application of hydrides in hydrogen storage and compression: Achievements, outlook and perspectives. *International Journal of Hydrogen Energy*, *44*(15), 7780–7808. https://doi.org/10.1016/j.ijhydene.2019.01.104

Bhandari, R., Trudewind, C. A., & Zapp, P. (2014). Life cycle assessment of hydrogen production via electrolysis - A review. *Journal of Cleaner Production*, *85*, 151–163. https://doi.org/10.1016/j.jclepro.2013.07.048

Bhogilla, S., Pandoh, A., & Singh, U. R. (2024). Cogeneration system combining reversible PEM fuel cell, and metal hydride hydrogen storage enabling renewable energy storage: Thermodynamic performance assessment. *International Journal of Hydrogen Energy*, *52*, 1147–1155. https://doi.org/10.1016/j.ijhydene.2023.08.028

Bolarin, J. A., Zou, R., Li, Z., Munyentwali, A., Zhang, Z., & Cao, H. (2024). Recent path to ultrafine Mg/MgH2 synthesis for sustainable hydrogen storage. *International Journal of Hydrogen Energy*, *52*, 251–274. https://doi.org/10.1016/j.ijhydene.2023.04.234

Bvumbe, T. J., Bujlo, P., Tolj, I., Mouton, K., Swart, G., Pasupathi, S., & Pollet, B. G. (2016). Review on management, mechanisms and modelling of thermal processes in PEMFC. *Hydrogen and Fuel Cells*, *1*(1), 1–20. https://doi.org/10.1515/hfc-2016-0001

Carmo, M., Fritz, D. L., Mergel, J., & Stolten, D. (2013). A comprehensive review on PEM water electrolysis. *International Journal of Hydrogen Energy*, *38*(12), 4901–4934. https://doi.org/10.1016/j.ijhydene.2013.01.151

Carson, J. (2002). Model verification and validation. *Proceedings of the Winter Simulation Conference*, 52–58. https://doi.org/10.1109/WSC.2002.1172868

Cetinkaya, S. A., Disli, T., Soyturk, G., Kizilkan, O., & Colpan, C. O. (2023). A Review on Thermal Coupling of Metal Hydride Storage Tanks with Fuel Cells and Electrolyzers. *Energies*, *16*(1). https://doi.org/10.3390/en16010341

Chauhan, S., & Ranjan, R. (2024). Opportunities and Challenges in Power Grid Integration of Hydrogen Electrolyzers and Fuel Cells. Springer. https://doi.org/10.1007/978-981-97-1339-4{_}21

Chen, X., Gong, G., Wan, Z., Luo, L., & Wan, J. (2015). Performance analysis of 5 kW PEMFC-based residential micro-CCHP with absorption chiller. *International Journal of Hydrogen Energy*, *40*(33), 10647–10657. https://doi.org/10.1016/j.ijhydene.2015.06.139

Chisholm, G., Zhao, T., & Cronin, L. (2022). Hydrogen from water electrolysis. In *Storing energy* (pp. 559–591). Elsevier. https://doi.org/10.1016/B978-0-12-824510-1.00015-5

Clean Hydrogen Joint Undertaking. (2021, November). Clean Hydrogen JU SRIA – Key Performance Indicators (KPIs). https://www.clean-hydrogen.europa.eu/knowledge-management/strategy-map-and-key-performance-indicators/fch-2-ju-mawp-key-performance-indicators-kpis_en

Cook, B. (2002). Introduction to fuel cells and hydrogen technology. *Engineering Science & Education Journal*, *11*(6), 205–216. https://doi.org/10.1049/esej:20020601

Dagdougui, H., Sacile, R., Bersani, C., & Ouammi, A. (2018). Hydrogen Logistics: Safety and Risks Issues. In *Hydrogen infrastructure for energy applications* (pp. 127–148). Elsevier. https://doi.org/10.1016/B978-0-12-812036-1.00007-X

Davids, M. W., & Lototskyy, M. (2012). Influence of oxygen introduced in TiFe-based hydride forming alloy on its morphology, structural and hydrogen sorption properties. *International Journal of Hydrogen Energy*, *37*(23), 18155–18162. https://doi.org/10.1016/j.ijhydene.2012.09.106

de Vries, M. (2024, December). Torenhoge stroomprijzen door dunkelflaute: waarom we vandaag zuinig moeten zijn. https://www.rtl.nl/nieuws/binnenland/artikel/5484822/energie-elektriciteit-dunkelflaute-zuinig-goedkoop-rekening-wind

de Wit, S. (2022, March). Innovations in energy storage. https://www.tno.nl/en/sustainable/energy-built-environment/energy-storage/

Delongtop. (2024, March). Which Is Better? | Sodium Ion Battery VS. Lead Acid Battery.

deltaWonen. (2024, August). *Urban Energy Island Kampen* (tech. rep.). deltaWonen. Kampen.

Dematteis, E. M., Dreistadt, D. M., Capurso, G., Jepsen, J., Cuevas, F., & Latroche, M. (2021). Fundamental hydrogen storage properties of TiFe-alloy with partial substitution of Fe by Ti and Mn. *Journal of Alloys and Compounds*, *874*, 17–17. https://doi.org/10.1016/j.jallcom.2021.159925

Demirci, U. B., Akdim, O., Andrieux, J., Hannauer, J., Chamoun, R., & Miele, P. (2010). Sodium Borohydride Hydrolysis as Hydrogen Generator: Issues, State of the Art and Applicability Upstream from a Fuel Cell. *Fuel Cells*, *10*(3), 335–350. https://doi.org/10.1002/fuce.200800171

Dotelli, G., Ferrero, R., Stampino, P. G., Latorrata, S., & Toscani, S. (2014). Diagnosis of PEM Fuel Cell Drying and Flooding Based on Power Converter Ripple. *IEEE Transactions on Instrumentation and Measurement*, *63*(10), 2341–2348. https://doi.org/10.1109/TIM.2014.2318371

Dragan, M. (2022). Hydrogen Storage in Complex Metal Hydrides NaBH4: Hydrolysis Reaction and Experimental Strategies. *Catalysts*, *12*(4), 356. https://doi.org/10.3390/catal12040356

Drawer, C., Lange, J., & Kaltschmitt, M. (2024). Metal hydrides for hydrogen storage – Identification and evaluation of stationary and transportation applications. *Journal of Energy Storage*, *77*. https://doi.org/10.1016/j.est.2023.109988

ecolithiumbattery. (2022, August). Sodium Ion Battery: The Definitive Guide. https://www.ecolithiumbattery.com/sodium-ion-battery/

Elberry, A. M., Thakur, J., Santasalo-Aarnio, A., & Larmi, M. (2021). Large-scale compressed hydrogen storage as part of renewable electricity storage systems. *International Journal of Hydrogen Energy*, *46*(29), 15671–15690. https://doi.org/10.1016/j.ijhydene.2021.02.080

Euopean Commission. (2024, December). PHOTOVOLTAIC GEOGRAPHICAL INFORMATION SYSTEM. https://re.jrc.ec.europa.eu/pvg_tools/en/

European Parliament. (2024a, December). Greenhouse gas emissions by country and sector (infographic). https://www.europarl.europa.eu/topics/en/article/20180301STO98928/greenhouse-gas-emissions-by-country-and-sector-infographic

European Parliament. (2024b, June). How the EU is boosting renewable energy. https://www.europarl.europa.eu/topics/en/article/20221128STO58001/how-the-eu-is-boosting-renewable-energy

European Union. (2020, March). *Submission by Croatia and the European Commission on behalf of the European Union and its Member States* (tech. rep.). European Union. Zagreb. https://unfccc.int/sites/default/files/resource/HR-03-06-2020%20EU%20Submission%20on%20Long%20term%20strategy.pdf

Eurostat. (2023). Renewable energy statistics. https://ec.europa.eu/eurostat/statistics-explained/index.php?title=Renewable_energy_statistics#Renewable_energy_produced_in_the_EU_increased_by_two_thirds_in_2006-2016

Floudas, C. A., & Lin, X. (2005). Mixed Integer Linear Programming in Process Scheduling: Modeling, Algorithms, and Applications. *Annals of Operations Research*, *139*(1), 131–162. https://doi.org/10.1007/s10479-005-3446-x

Frankowska, M., Rzeczycki, A., Sowa, M., & Drożdż, W. (2022). Functional Model of Power Grid Stabilization in the Green Hydrogen Supply Chain System—Conceptual Assumptions. *Energies*, *16*(1), 154. https://doi.org/10.3390/en16010154

Gabrielli, P., Poluzzi, A., Kramer, G. J., Spiers, C., Mazzotti, M., & Gazzani, M. (2020). Seasonal energy storage for zero-emissions multi-energy systems via underground hydrogen storage. *Renewable and Sustainable Energy Reviews*, *121*, 109629. https://doi.org/10.1016/j.rser.2019.109629

Gao, H., Grundish, N. S., Zhao, Y., Zhou, A., & Goodenough, J. B. (2021). Formation of Stable Interphase of Polymer-in-Salt Electrolyte in All-Solid-State Lithium Batteries. *Energy Material Advances*, *2021*. https://doi.org/10.34133/2021/1932952

GKN Hydrogen. (n.d.-a). *Metal Hydride | Solid H2 Storage* (tech. rep.). GKN Hydrogen. https://www.gknhydrogen.com/wp-content/uploads/2023/03/GKN-Hydrogen_Company-Brief_20230224_final.pdf

GKN Hydrogen. (n.d.-b). Modularity of Hydrogen storage 20ft unit.

GKN hydrogen. (n.d.). Hydrogen storage 20ft Unit. https://www.gknhydrogen.com/wp-content/uploads/2024/12/GKN_H2_20ft_ProductSheet-A4.pdf

Golmohamadi, H. (2022). Data-Driven Approach to Forecast Heat Consumption of Buildings with High-Priority Weather Data. *Buildings*, *12*(3), 289. https://doi.org/10.3390/buildings12030289

Gorman, S. (2023, August). 6 ways solid-state batteries are better than lithium-ion alternatives in electric vehicles. https://www.uk-cpi.com/blog/6-ways-solid-state-batteries-are-better-than-lithium-ion-alternatives-in-electric-vehicles

Gray, E. M., Webb, C. J., Andrews, J., Shabani, B., Tsai, P. J., & Chan, S. L. (2011). Hydrogen storage for off-grid power supply. *International Journal of Hydrogen Energy*, *36*(1), 654–663. https://doi.org/10.1016/j.ijhydene.2010.09.051

Gupta, S., Saini, R. S., & Ganesh, H. S. (2023). Hierarchical MPC for a dynamic process system employing parametric global optimization strategy. *Digital Chemical Engineering*, *9*, 100120. https://doi.org/10.1016/j.dche.2023.100120

Hancke, R., Bujlo, P., Holm, T., & Ulleberg, Ø. (2024). High-pressure PEM water electrolyser performance up to 180 bar differential pressure. *Journal of Power Sources*, *601*. https://doi.org/10.1016/j.jpowsour.2024.234271

Hassanzadeh, H., & Mansouri, S. H. (2005). Efficiency of ideal fuel cell and Carnot cycle from a fundamental perspective. *Proceedings of the Institution of Mechanical Engineers, Part A: Journal of Power and Energy*, *219*(4), 245–254. https://doi.org/10.1243/095765005X28571

Hirscher, M., & Hirose, K. (2010). *Handbook of Hydrogen Storage: New Materials for Future Energy Storage* (M. Hirscher, Ed.). Wiley-vch. https://doi.org/10.1002/9783527629800

Hou, Z., Guo, S., Zhang, X., Xu, L., Qi, Y., Zhang, Y., Li, P., & Zhao, D. (2025). Hydrogen storage and stability of rare earth-doped TiFe alloys under extensive cycling. *International Journal of Hydrogen Energy*, *136*, 469–476. https://doi.org/10.1016/j.ijhydene.2025.05.043

Khan, D., Panda, S., Ma, Z., Ding, W., & Zou, J. (2020). Formation and hydrogen storage behavior of nanostructured Mg2FeH6 in a compressed 2MgH2–Fe composite. *International Journal of Hydrogen Energy*, *45*(41), 21676–21686. https://doi.org/10.1016/j.ijhydene.2020.06.025

Kim, M., Gu, J., Yuan, Y., Yun, T., Liu, Z., Bengio, Y., & Chen, C. (2025). Offline Model-Based Optimization: Comprehensive Review. https://doi.org/https://doi.org/10.48550/arXiv.2503.17286

Klopčič, N., Grimmer, I., Winkler, F., Sartory, M., & Trattner, A. (2023). A review on metal hydride materials for hydrogen storage. *Journal of Energy Storage*, *72*. https://doi.org/10.1016/j.est.2023.108456

Kodir, A., Yim, S.-D., Lee, H., Shin, D., & Bae, B. (2024). Comprehensive study of hydrogen-crossover reducing agents for polymer electrolyte membranes. *Journal of Membrane Science*, *707*, 122989. https://doi.org/10.1016/j.memsci.2024.122989

Kukkapalli, V. K., Kim, S., & Thomas, S. A. (2023). Thermal Management Techniques in Metal Hydrides for Hydrogen Storage Applications: A Review. *Energies*, *16*(8). https://doi.org/10.3390/en16083444

LetsGoSolar. (2018). What is a Solar Battery. https://www.letsgosolar.com/faq/what-is-a-solar-battery/

Li Dai, Mengyin Fu, Magdi S. Mahmoud, & Yuanqing Xia. (2012). Discrete-Time Model Predictive Control. *InTech*. https://doi.org/10.5772/51122

Liu, H., Zhang, J., Sun, P., Zhou, C., Liu, Y., & Fang, Z. Z. (2023). An overview of TiFe alloys for hydrogen storage: Structure, processes, properties, and applications. *Journal of Energy Storage*, *68*. https://doi.org/10.1016/j.est.2023.107772

Liu, L., & Johnson, J. X. (2025). Technical and environmental feasibility of renewable metal hydride-based off-grid energy systems. *International Journal of Hydrogen Energy*, *130*, 595–604. https://doi.org/10.1016/j.ijhydene.2025.03.448

Lototskyy, M. V., Yartys, V. A., Pollet, B. G., & Bowman, R. C. (2014). Metal hydride hydrogen compressors: A review. *International Journal of Hydrogen Energy*, *39*(11), 5818–5851. https://doi.org/10.1016/j.ijhydene.2014.01.158

Lototskyy, M. V., Tolj, I., Pickering, L., Sita, C., Barbir, F., & Yartys, V. (2017). The use of metal hydrides in fuel cell applications. *Progress in Natural Science: Materials International*, *27*(1), 3–20. https://doi.org/10.1016/j.pnsc.2017.01.008

Lu, X., Du, B., Zhou, S., Zhu, W., Li, Y., Yang, Y., Xie, C., Zhao, B., Zhang, L., Song, J., & Deng, Z. (2023). Optimization of power allocation for wind-hydrogen system multi-stack PEM water electrolyzer considering degradation conditions. *International Journal of Hydrogen Energy*, *48*(15), 5850–5872. https://doi.org/10.1016/j.ijhydene.2022.11.092

Marinelli, M., & Santarelli, M. (2020). Hydrogen storage alloys for stationary applications. *Journal of Energy Storage*, *32*. https://doi.org/10.1016/j.est.2020.101864

Mehrabadi, B. A. T., Dinh, H. N., Bender, G., & Weidner, J. W. (2016). Effect of System Contaminants on the Performance of a Proton Exchange Membrane Fuel Cell. *Journal of The Electrochemical Society*, *163*(14), F1527–F1534. https://doi.org/10.1149/2.0761614jes

Miura, S., Fujisawa, A., & Ishida, M. (2012). A hydrogen purification and storage system using metal hydride. *International Journal of Hydrogen Energy*, *37*(3), 2794–2799. https://doi.org/10.1016/j.ijhydene.2011.03.150

Modi, P., & Aguey-Zinsou, K. F. (2021). Room Temperature Metal Hydrides for Stationary and Heat Storage Applications: A Review. *Frontiers in Energy Research*, *9*. https://doi.org/10.3389/fenrg.2021.616115

Møller, K. T., Jensen, T. R., Akiba, E., & Li, H. w. (2017). Hydrogen - A sustainable energy carrier. *Progress in Natural Science: Materials International*, *27*(1), 34–40. https://doi.org/10.1016/j.pnsc.2016.12.014

Murray, c. (2024, November). BYD launches sodium-ion grid-scale BESS product. https://www.energy-storage.news/byd-launches-sodium-ion-grid-scale-bess-product/

Najjar, Y. S. (2013). Hydrogen safety: The road toward green technology. *International Journal of Hydrogen Energy*, *38*(25), 10716–10728. https://doi.org/10.1016/j.ijhydene.2013.05.126

Nasser, M., Megahed, T. F., Ookawara, S., & Hassan, H. (2022). A review of water electrolysis–based systems for hydrogen production using hybrid/solar/wind energy systems. *Environmental Science and Pollution Research*, *29*(58), 86994–87018. https://doi.org/10.1007/s11356-022-23323-y

National Energy Dashboard. (2024, December). Totale electriciteitsproductie (National Energy Dashboard, Trans.). https://ned.nl/nl/dataportaal/energie-productie/elektriciteit/totale-elektriciteitsproductie

Nguyen, H. Q., & Shabani, B. (2020). Proton exchange membrane fuel cells heat recovery opportunities for combined heating/cooling and power applications. *Energy Conversion and Management*, *204*. https://doi.org/10.1016/j.enconman.2019.112328

Nguyen, H. Q., & Shabani, B. (2021). Review of metal hydride hydrogen storage thermal management for use in the fuel cell systems. *International Journal of Hydrogen Energy*, *46*(62), 31699–31726. https://doi.org/10.1016/j.ijhydene.2021.07.057

Norazahar, N., Khan, F., Rahmani, N., & Ahmad, A. (2024). Degradation modelling and reliability analysis of PEM electrolyzer. *International Journal of Hydrogen Energy*, *50*, 842–856. https://doi.org/10.1016/j.ijhydene.2023.07.153

NU.nl. (2024, December). Zon weer terug na langste sombere periode in 35 jaar. https://www.nu.nl/binnenland/6339777/zon-weer-terug-na-langste-sombere-periode-in-35-jaar-was-deels-toevallig.html

Omrani, R., Nguyen, H. Q., & Shabani, B. (2019). Open-cathode PEMFC heat utilisation to enhance hydrogen supply rate of metal hydride canisters. *Energy Procedia*, *160*, 542–549. https://doi.org/10.1016/j.egypro.2019.02.204

Pärnamäe, R., Gurreri, L., Post, J., van Egmond, W. J., Culcasi, A., Saakes, M., Cen, J., Goosen, E., Tamburini, A., Vermaas, D. A., & Tedesco, M. (2020). The acid–base flow battery: Sustainable energy storage via reversible water dissociation with bipolar membranes. *Membranes*, *10*(12), 1–20. https://doi.org/10.3390/membranes10120409

Poupin, L., Humphries, T. D., Paskevicius, M., & Buckley, C. E. (2021). An operational high temperature thermal energy storage system using magnesium iron hydride. *International Journal of Hydrogen Energy*, *46*(78), 38755–38767. https://doi.org/10.1016/j.ijhydene.2021.09.146

Reuß, M., Grube, T., Robinius, M., Preuster, P., Wasserscheid, P., & Stolten, D. (2017). Seasonal storage and alternative carriers: A flexible hydrogen supply chain model. *Applied Energy*, *200*, 290–302. https://doi.org/10.1016/j.apenergy.2017.05.050

Rijksdienst voor Ondernemend Nederland. (2025, March). Urban Energy Island Kampen. https://projecten.topsectorenergie.nl/projecten/urban-energy-island-kampen-39020

Rosino Messa, A., Quesnel, S., Bellosta von Colbe, J., Ante, M. J., Stühff, H. H., Luetto, C., & Baricco, M. (2024). Risk Management in a Containerized Metal Hydride Storage System. *Hydrogen Safety*, *1*(1), 33–45. https://doi.org/10.58895/hysafe.10

Sakata, Y., Akeyama, Y., Katsura, T., & Nagano, K. (2023). Evaluating Long-Term Performance of a Residential Ground-Source Heat Pump System under Climate Change in Cold and Warm Cities of Japan. *Energies*, *16*(6), 2742. https://doi.org/10.3390/en16062742

Sammes, N. (2006). *Fuel Cell Technology* (N. Sammes, Ed.). Springer Londen. https://doi.org/10.1007/1-84628-207-1

Shiva Kumar, S., & Himabindu, V. (2019). Hydrogen production by PEM water electrolysis – A review. *Materials Science for Energy Technologies*, *2*(3), 442–454. https://doi.org/10.1016/j.mset.2019.03.002

Sirengo, K., Babu, A., Brennan, B., & Pillai, S. C. (2023). Ionic liquid electrolytes for sodium-ion batteries to control thermal runaway. *Journal of Energy Chemistry*, *81*, 321–338. https://doi.org/10.1016/j.jechem.2023.02.046

Srinivasan, S. S., & Demirocak, D. E. (2017). Metal Hydrides used for Hydrogen Storage. In *Nanostructured materials for next-generation energy storage and conversion* (pp. 225–255). Springer Berlin Heidelberg. https://doi.org/10.1007/978-3-662-53514-1{_}8

Steinberger, M., Geiling, J., Oechsner, R., & Frey, L. (2018). Anode recirculation and purge strategies for PEM fuel cell operation with diluted hydrogen feed gas. *Applied Energy*, *232*, 572–582. https://doi.org/10.1016/j.apenergy.2018.10.004

Tawalbeh, M., Alarab, S., Al-Othman, A., & Javed, R. M. N. (2022). The Operating Parameters, Structural Composition, and Fuel Sustainability Aspects of PEM Fuel Cells: A Mini Review. *Fuels*, *3*(3), 449–474. https://doi.org/10.3390/fuels3030028

Theocharides, S., Makrides, G., & Georghiou, G. E. (2024). PV generation forecasting utilizing a classification-only approach. *EPJ Photovoltaics*, *15*, 12. https://doi.org/10.1051/epjpv/2024011

Thiangviriya, S., Plerdsranoy, P., Hagenah, A., Le, T. T., Kidkhunthod, P., Utke, O., Dornheim, M., Klassen, T., Pistidda, C., & Utke, R. (2021). Effects of Ni-loading contents on dehydrogenation kinetics and reversibility of Mg2FeH6. *International Journal of Hydrogen Energy*, *46*(63), 32099–32109. https://doi.org/10.1016/j.ijhydene.2021.06.206

Tiktak, W. J. (2019, October). *Heat Management of PEM Electrolysis* (tech. rep.). TU Delft. Delft. https://resolver.tudelft.nl/uuid:c046820a-72bc-4f05-b72d-e60a3ecb8c89

TNO. (2024, September). warmteprofielengenerator. https://www.warmteprofielengenerator.nl/

Tong, L., Yuan, C., Yang, T., Yuan, Y., Chahine, R., & Xiao, J. (2023). Thermal management of metal hydride hydrogen storage tank coupled with proton exchange membrane fuel cells. *Case Studies in Thermal Engineering*, *43*. https://doi.org/10.1016/j.csite.2023.102812

Toshiba. (2020, March). The world´s largest-class hydrogen production, Fukushima Hydrogen Energy Research Field (FH2R) now is completed at Namie town in Fukushima. https://www.global.toshiba/ww/news/energy/2020/03/news-20200307-01.html

Triki, F., & Son, R. (2023). Nieuwe school krijgt komende 5 tot 10 jaar geen aansluiting op stroomnet. https://www.omroepbrabant.nl/nieuws/4372869/nieuwe-school-krijgt-komende-5-tot-10-jaar-geen-aansluiting-op-stroomnet

Ubale, S., Remenyte-Prescott, R., Stuart, A., Hague, A., & Grant, D. M. (2025). Reliability Analysis of PEM Electrolyser Balance of Plant. *2025 Annual Reliability and Maintainability Symposium (RAMS)*, 1–6. https://doi.org/10.1109/RAMS48127.2025.10935111

U.S. Department of Energy. (2023, March). Technical Targets for Proton Exchange Membrane Electrolysis. https://www.energy.gov/eere/fuelcells/technical-targets-proton-exchange-membrane-electrolysis

Valera-Medina, A., Xiao, H., Owen-Jones, M., David, W. I., & Bowen, P. J. (2018). Ammonia for power. *Progress in Energy and Combustion Science*, *69*, 63–102. https://doi.org/10.1016/j.pecs.2018.07.001

van der Gurp, T. (2024, December). Dit jaar voor het eerst meer groene dan grijze stroom opgewekt. https://www.nu.nl/economie/6340719/dit-jaar-voor-het-eerst-meer-groene-dan-grijze-stroom-opgewekt.html

van der Roest, E., Bol, R., Fens, T., & van Wijk, A. (2023). Utilisation of waste heat from PEM electrolysers – Unlocking local optimisation. *International Journal of Hydrogen Energy*, *48*(72), 27872–27891. https://doi.org/10.1016/j.ijhydene.2023.03.374

Vasilyev, A., Andrews, J., Dunnett, S., & Jackson, L. (2021). Dynamic Reliability Assessment of PEM Fuel Cell Systems. *Reliability Engineering & System Safety*, *210*, 107539. https://doi.org/10.1016/j.ress.2021.107539

Virah-Sawmy, D., Beck, F. J., & Sturmberg, B. (2024). Ignore variability, overestimate hydrogen production – Quantifying the effects of electrolyzer efficiency curves on hydrogen production from renewable energy sources. *International Journal of Hydrogen Energy*, *72*, 49–59. https://doi.org/10.1016/j.ijhydene.2024.05.360

Wang, Y., Ou, R., Yang, J., Xin, Y., Singh, P., Wu, F., Qian, Y., & Gao, H. (2024). The safety aspect of sodium ion batteries for practical applications. *Journal of Energy Chemistry*, *95*, 407–427. https://doi.org/10.1016/j.jechem.2024.03.060

Wilberforce, T., Olabi, A. G., Muhammad, I., Alaswad, A., Sayed, E. T., Abo-Khalil, A. G., Maghrabie, H. M., Elsaid, K., & Abdelkareem, M. A. (2024). Recovery of waste heat from proton exchange membrane fuel cells – A review. *International Journal of Hydrogen Energy*, *52*, 933–972. https://doi.org/10.1016/j.ijhydene.2022.08.069

Wu, J., Yuan, X. Z., Martin, J. J., Wang, H., Zhang, J., Shen, J., Wu, S., & Merida, W. (2008). A review of PEM fuel cell durability: Degradation mechanisms and mitigation strategies. *Journal of Power Sources*, *184*(1), 104–119. https://doi.org/10.1016/j.jpowsour.2008.06.006

Yan, X., Francois, B., & Abbes, D. (2015). Operating power reserve quantification through PV generation uncertainty analysis of a microgrid. *2015 IEEE Eindhoven PowerTech*, 1–6. https://doi.org/10.1109/PTC.2015.7232577

Yang, F. S., Wang, G. X., Zhang, Z. X., Meng, X. Y., & Rudolph, V. (2010). Design of the metal hydride reactors - A review on the key technical issues. *International Journal of Hydrogen Energy*, *35*(8), 3832–3840. https://doi.org/10.1016/j.ijhydene.2010.01.053

Yu, T., Li, G., Duan, Y., Wu, Y., Zhang, T., Zhao, X., Luo, M., & Liu, Y. (2023). The research and industrialization progress and prospects of sodium ion battery. *Journal of Alloys and Compounds*, *958*, 170486. https://doi.org/10.1016/j.jallcom.2023.170486

Zhang, L. (1998). AC impedance studies on sealed nickel metal hydride batteries over cycle life in analog and digital operations. *Electrochimica Acta*, *43*(21-22), 3333–3342. https://doi.org/10.1016/S0013-4686(98)00056-5

Zhang, T., Uratani, J., Huang, Y., Xu, L., Griffiths, S., & Ding, Y. (2023). Hydrogen liquefaction and storage: Recent progress and perspectives. *Renewable and Sustainable Energy Reviews*, *176*, 113204. https://doi.org/10.1016/j.rser.2023.113204

Zhao, L., Zhang, T., Li, W., Li, T., Zhang, L., Zhang, X., & Wang, Z. (2023). Engineering of Sodium-Ion Batteries: Opportunities and Challenges. *Engineering*, *24*, 172–183. https://doi.org/10.1016/j.eng.2021.08.032

Zohuri, B. (2019). The Chemical Element Hydrogen. In *Hydrogen energy* (pp. 1–35). Springer International Publishing. https://doi.org/10.1007/978-3-319-93461-7{_}1

Züttel, A. (2003). Materials for hydrogen storage. *Materials Today*, *6*(9), 24–33. https://doi.org/10.1016/S1369-7021(03)00922-2

A

Appendix: Scientific Research Paper

Exploring the Technical Potential of Metal Hydrides for Seasonal Energy Storage of Hydrogen

Thijs Kroes TU Delft Mechanical Engineering

July 7, 2025

Abstract

The seasonal mismatch between solar energy generation and demand causes net congestion on the electricity grid. While PEM fuel cells and their thermal integration are well studied, less attention has been given to integrated seasonal energy storage systems combining PEM electrolysers, low-temperature metal hydride storage, and PEM fuel cells, especially in grid-connected applications. This research investigates the potential of the metal hydride TiFe for seasonal energy storage in the built environment. A system-level MPC controller was developed, integrating supplies and demands with a daily battery, TiFe metal hydride (4.8 MWh), PEM electrolyser and fuel cell. The metal hydride storage provided up to 17 days of discharge and required 22 days to recharge, but in an extreme case, it was limited to 185 hours of discharging and 230 hours of charging. Under typical operation, the system achieved a total efficiency of 47.5% with a required grid capacity of 46.5 kW to balance supply fluctuation and ensure reliable power. While the current size of the metal hydride storage is insufficient for seasonal energy storage, it is effective for shorter periods of imbalance. Future work may optimise the storage size or control strategy by integrating dynamic energy prices or integrating long-term MPC planning.

1 Introduction

In 2022, the energy supply was the largest polluting sector, accounting for 27.4% of the EU's greenhouse gas emissions [8]. To tackle this, the EU plans to significantly reduce emissions from the energy sector by increasing the renewable energy supply. In 2023, 24.5% of the total energy consumed in Europe came from renewable sources [10]. Yet, the target is to increase this share of renewable energy to 42.5% by 2030 [9].

The electricity grid is already facing problems with grid congestion. In the Netherlands, network operators such as Liander struggle to connect all requests for solar parks to the grid [1], due to a mismatch between high solar energy supply during the day and peak electricity demand in the evening. In 2024, energy suppliers in the Netherlands curtailed electricity production equivalent to 2.5% of the annual demand, as wind and solar farms had to be temporarily shut down due to an excess of green energy on the grid [14].

One of the possible solutions is to use batteries as daily storage to balance the supply and demand, in order to reduce grid congestion. This would be a viable option for daily storage, but another gap needs to be bridged. This concerns the mismatch between high solar renewable energy production in the summer and higher electricity demand in the winter [20]. For seasonal energy storage, batteries are not feasible due to their relatively low energy density and the self-discharge rate [26]. Metal hydrides are better suited for seasonal energy storage as they have no self-discharge [7]

However, despite extensive research on the individual components that are required for a metal hydride seasonal energy storage, such as PEM fuel cells and their thermal integration, limited attention has been paid to the full integration of PEM electrolysers, low-temperature metal hydride storage, and PEM fuel cells into a cohesive seasonal energy storage system. The most promising research is that of Bhogilla [3]. The study integrated a metal hydride hydrogen storage system with a reversible PEM membrane fuel cell. Part of the heat produced by the fuel cell is used for the desorption process of the metal hydride, while the remainder of the produced heat is used to drive a vapour absorption refrigeration system (VARS) for cooling applications. The integration with the electricity grid is not mentioned in the research. The only real large-scale hydrogen storage system that uses an electrolyser-fuel cell system, which can be integrated with the electricity grid, is the Fukushima Hydrogen Energy Research field (FH2R). Once the hydrogen is produced, it is temporarily stored in high-pressure tanks. Theoretically, it is possible, and the FH2R project has shown that the system works without storage in metal hydrides [25].

As for the electricity grid, the outlined prospect is that the security of supply for 2030 is not guaranteed within the current frameworks. Therefore, the housing corporation deltaWonen started a pilot with the goal of solving the bottlenecks in the energy demand of residential areas. deltaWonen is investigating the use of metal hydrides for seasonal hydrogen energy storage. Therefore, the project of deltaWonen is taken as a case study for this research, which aims to answer the following research question: *What is the technical potential of room-temperature metal hydride TiFe for seasonal energy storage solutions in the built environment?*

The paper starts with a background about hy-

drogen storage using TiFe metal hydride. Afterwards, the case study that is used for this research is outlined in the system description. Then, it describes how the system-level model is developed, including assumptions and an explanation of the components. Model predictive control is used as a controller. The formulation of the MPC will be presented. Finally, the simulation results for the year 2013 are presented and discussed.

2 Background: Hydrogen Storage

Hydrogen is a potential energy carrier with a relatively low volumetric energy density and a high energy density per kilogram. That is why it is typically stored in compressed form, as a liquid, or by binding it to another element. A metal hydride is a metal that can bond with hydrogen atoms through a chemical process, reaching higher volumetric energy densities compared to compressed or liquid hydrogen [30]. In this research, the intermetallic metal hydride TiFe will be explored.

2.1 Metal Hydride: TiFe

TiFe is a combination of titanium and iron, with a volumetric storage capacity of 4.03 kWh/dm^3 [15]. The advantage, over some other metal hydrides, is that it can absorb and desorb near room temperatures under near-atmospheric pressures. A drawback of TiFe is the activation process, which is required before TiFe can absorb hydrogen. This requires high pressures (65 bar) and high temperatures (400-450°C) to remove the oxidation layer [17]. Hydrogen is stored in the metal by direct dissociative chemisorption (absorption process that involves a chemical bond formation between a modifier molecule and the surface [2]) of hydrogen gas, as described in (1) [21]. The arrow points in two directions, indicating that the reaction is reversible.

$$M + \frac{x}{2}\mathrm{H_2} \leftrightarrow \mathrm{MH}_x + Q \tag{1}$$

Where M is a metal or intermetallic alloy; x is the hydrogen concentration to metal; Q is the heat of reaction.

The thermolysis release reaction is endothermic; thus, Q is always positive. The heat released during the absorption process raises the temperature of the system. This temperature rise significantly increases the pressure required for the incoming hydrogen gas. Without an effective thermal management system, this temperature rise can lead to self-inhibition of the reaction, prolonging the filling time. Similarly, adequate heat must be supplied at a sufficient temperature during desorption to sustain the equilibrium pressure necessary to release the hydrogen.

2.2 PEM Electrolyser and Fuel Cell operation

The electrolyser converts electrical energy from the battery into hydrogen through water electrolysis. Further modelling details can be found in [11].

The fuel cell converts the hydrogen stored in the metal hydride into electrical energy. Further details can be found in [5].

3 System Description

3.1 Case Study

This section presents the deltaWonen case study, which forms the foundation for this research. deltaWonen plans on starting a new project, the Urban Energy Island (UEI). This will be a pilot of 40 apartments that will be part of an innovative all-electric energy system where 300 PV panels, daily energy storage (380 KWh) and seasonal energy storage of hydrogen in a metal hydride (4.8 MWh) are used. The system includes a 40 kW PEM electrolyser and a 25 kW PEM fuel cell to enable the conversion between electricity and hydrogen. The system operates within a limited electrical grid capacity of 40 kW [6], which is significantly lower than the 320 kW (40*8 kW) typically required in a conventional neighbourhood setting.

3.2 Input Supply and Demand

To accurately model the energy usage of a residential area, an interval of one hour between the data points has been selected. The total annual supply or demand can be found at Table 1.

Table 1: Total energy usage models [6]

Dataset	Value	Unit
PV Production	138000	kWh_{el}
Electricity Demand	72000	kWh_{el}
Heat demand	16400	kWh_{el}
Domestic Hot Water demand	23160	kWh_{el}

Since the annual total is known, the profile per hour of the supply or demand is normalised to sum to one and then scaled accordingly. Additionally, the ambient temperature is used to calculate the exergy content of the waste heat.

4 Model Description

A system-level model was built to evaluate the potential of metal hydride for seasonal energy storage. This allows for a structured analysis of the system's energy flows and operational behaviour, which would be challenging to capture through component-level testing alone. It enables the assessment of key performance metrics such as system efficiency and reuse of heat, offers flexibility in changing component sizes, and allows for testing different scenarios without requiring prototyping.

4.1 Overview Model

In Figure 1, an overview of the energy flows between all the different components and external supply and demand in the model is shown.

The components in the model are treated as black boxes. Their inputs and corresponding outputs are known, but not all internal details are explicitly modelled. For example, internal heat losses that can't be reused to reduce the heat demand are known. However, while these losses depend on var-

ious factors within the component, in reality, they are simplified as a constant in the model.

All the streams of electricity come together in the daily battery, which works as the storage of electricity in the short term. All the streams of supply and demand are combined into one net energy production.

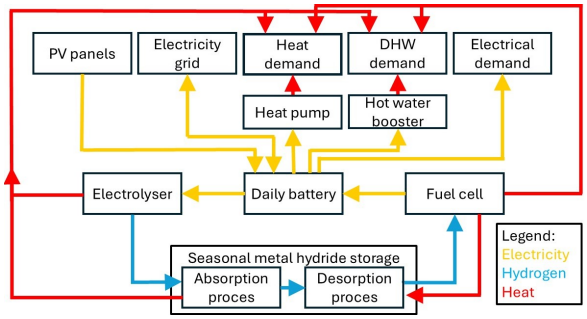

Figure 1: Overview of the energy flow between components

The control system decides when to charge or discharge the daily battery. It determines when to provide electricity to the electrolyser for hydrogen production to charge the metal hydride storage. It also determines when the fuel cell should convert hydrogen back into electricity. The demands that need to be fulfilled are the electrical, space heat and domestic hot water demand. There are two possible supply sources of electricity: PV panels and the electricity grid.

Heat is generated during the absorption process of the metal hydride as hydrogen bonds to it. Along with the heat produced by the electrolyser and the fuel cell, it is first converted into exergy to account for its useful work potential. This exergy can then be used to reduce the space heat demand and, if any is left over, to meet the domestic hot water demand. However, a portion of the heat of the fuel cell is required to fulfil the heat demand of the desorption process. Therefore, only part of the exergy heat production of the fuel cell can be used to reduce the heat demand. The remainder of the heat demand is met by the heat pump for the space heating and the hot water booster for the domestic hot water (DHW).

4.2 Assumptions

The key assumptions are:

- Hydrogen pressures are neglected in the model. The required pressures are assumed to be achievable without additional compressors. All pressure requirements are met internally within the design.
- Steady-state assumption per timestep. At each discrete timestep, the system is assumed to be in a steady state. Transient dynamics within each timestep are not captured, simplifying the system behaviour's representation. In reality, however, the system is unlikely to remain in a steady state throughout each hour, as it may need to respond to unexpected variations multiple times per hour.
- Perfect heat exchangers. The model assumes no thermal losses during heat transport between components.

4.3 Uncertainty on Prediction Horizon

In real-world applications, future input data is inherently unknown. However, it is possible to forecast what is expected to happen. Although it is not certain that the expectation will come true, there is uncertainty in the forecast. This is similar to a weather forecast, which provides the best estimate of future conditions, even though actual outcomes may differ.

In the model, it would be possible to know what will happen in the future, as historical data is used in this simulation. However, to mimic the uncertainty of the forecast, a band of uncertainty is added to the input data within the prediction horizon. Each data point in the future is randomly changed into a value that falls within the uncertainty band, which is uniform over the prediction horizon; the uncertainty does not increase when looking further into the prediction horizon. The uncertainty boundaries are different for the PV supply, electrical demand and heat demands, which have been based on the mean absolute percentage error (MAPE) and can be found in Table 2.

Table 2: Uncertainty mean absolute percentage error

Input	MAPE (%)
PV supply	6.91 [24]
Electric demand	3.84 [28]
Heat demand	8.95 [12]

4.4 Daily Battery

All the electricity supply and demand go through the daily battery. The sum of the supply and demand, the net energy, is the value added or subtracted from each timestep's daily battery storage level. The battery capacity is 380 kWh [6]. As the research goal is to show the potential of seasonal energy storage, the complexity of the daily battery is reduced by not incorporating efficiency losses, self-discharge losses and not including degradation losses.

4.5 TiFe Metal Hydride

The seasonal metal hydride storage stores the hydrogen produced by the electrolyser until the fuel cell uses the hydrogen. During the storage process, there is no self-discharge or efficiency losses [7]. The metal hydride storage operates within a defined capacity range. The maximum storage capacity is set at 4.8 MWh [6].

The degradation is 0.017% per cycle [4]. The degradation is modelled as a linear process; the degradation over time is the same, independent of the current degradation status of the metal hydride storage. When the degradation increases, the maximum storage capacity is lowered.

4.6 PEM Electrolyser and PEM Fuel Cell

The PEM electrolyser and PEM fuel cell are modelled in the same way. They both have the characteristics of an efficiency curve, start-up, and degradation.

4.6.1 Efficiency

The efficiency of the electrolyser and the fuel cell within the MPC framework is approximated using piecewise linear functions defined by selected breakpoints. A breakpoint is a chosen input value on the efficiency curve at which the efficiency is explicitly defined. Linear interpolation is applied between these breakpoints to determine the efficiency connected to the selected setpoint. This way, the computational power required within the MPC is minimised without compromising too much on the accuracy of the efficiency curve.

After the MPC has given its control outputs, the exact efficiency corresponding to the setpoint is calculated using the efficiency curve.

4.6.2 Start-up

Turning on the electrolyser and fuel cell directly at full power is impossible when they were previously turned off. Therefore, a start-up is included, which is only implemented when the electrolyser or fuel cell is turned on in the first hour; it is not applied for the consecutive hours it is turned on. During the start-up, the power is expected to increase linearly from 0 to the desired setpoint over a fixed time of 30 seconds for the electrolyser [22], and 60 seconds for the fuel cell [29].

4.6.3 Degradation

The electrolyser and fuel cell experience degradation per hour of usage. The degradation is modelled as a linear process; the degradation per hour is constant, independent of the current degradation status. Per hour, the electrolyser degrades 0.00019% [27], and the fuel cell degrades 0.004% [23].

5 Controller Selection

This section explains why model predictive control is chosen as the control strategy for the system.

5.1 Model Predictive Control

Model Predictive Control (MPC) is a control strategy where, at each time step, an optimisation problem is solved over a finite time horizon. This problem uses the system's current state as the starting point and calculates the best sequence of control actions. Only the control action for the next timestep is applied, which is repeated at the next time step. An advantage of MPC is that it can cope with hard constraints on controls and states [19]. Figure 2 shows the functionality of the MPC and the prediction horizon principle.

The model simulates an entire year with an interval of 1 hour. The receding prediction horizon is set to 24 hours, which aligns with the day-ahead electricity pricing data of the dynamic energy market. The control horizon is set to 1 hour in the model.

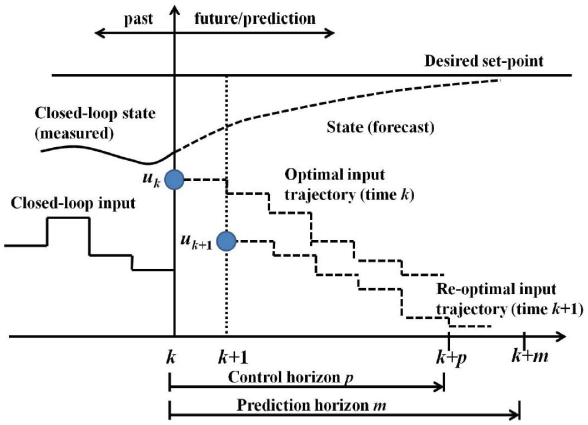

Figure 2: MPC receding horizon principle [16]

MPC was selected as the controller for the model because it allows for multi-variable optimisation, prediction of future demand and generation, flexibility to adjust and extend the MPC framework, and testing of different control strategies or scenarios.

A flowchart of the model, indicating which steps are handled within the MPC and which are computed afterwards based on its control actions, is shown in Figure 3.

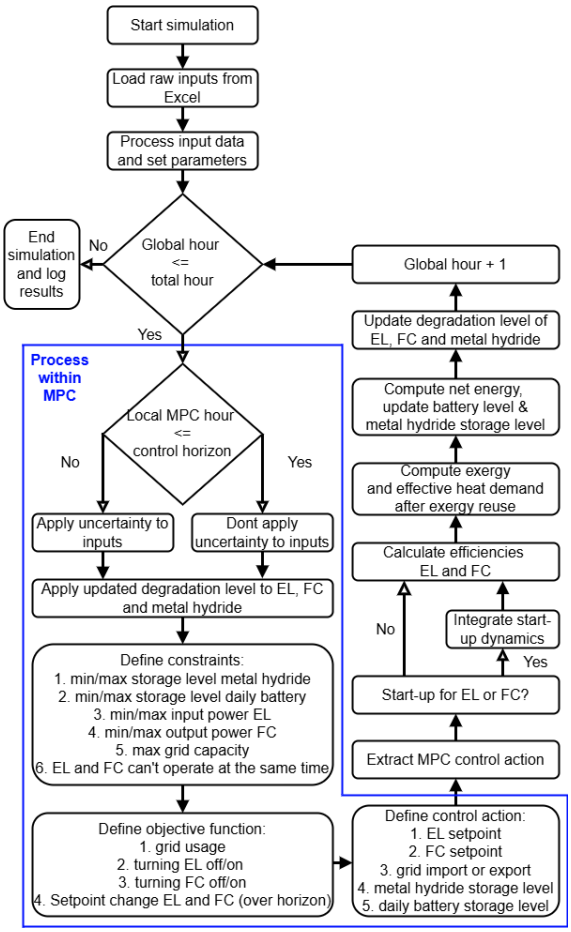

Figure 3: Flow diagram model

5.2 MPC Formulation

The goal of the MPC is to choose the lowest objective function possible. Therefore, selecting the right constraints to the objective function that constrain the MPC, where required, is essential, while leaving enough freedom for the model to reach the best control action possible.

5.3 MPC Constraints

Constraints are added to ensure that the MPC does not break physical boundaries while trying to solve the objective function with the lowest score possible. The following constraints have been added within the MPC:

- The storage level of the daily battery and the metal hydride storage is constrained between the minimum and maximum storage capacity.
- The electrolyser's input power and the fuel cell's maximum output power are constrained between the minimum and maximum power.
- The electrolyser and fuel cell can not be turned on simultaneously.
- The grid usage is limited to the maximum available grid capacity.

5.4 MPC Objective

The objective function is a combination of three terms. Each term will be explained individually before being combined in a total objective function.

5.4.1 Grid Usage

The grid usage objective is calculated by multiplying the grid usage (in kW) during that hour by the weight factor λ_{grid}. The same penalty applies to importing and exporting electricity from and towards the grid.

$$\mathrm{J_{grid}} = \lambda_{grid} * |\mathrm{u}_g| \tag{2}$$

Where J_{grid} (kW) is the grid-related objective, λ_{grid} is the (constant) weight factor, and u_g (kW) is the amount of grid usage per hour.

5.4.2 Electrolyser and Fuel Cell On-Off Control

The binary variable for both components is calculated by checking if the previous setpoint was smaller than ϵ, set to be 1%. For example, the model checks if the last electrolyser setpoint was off and if the electrolyser turns on in the current hour, the binary deviation variable is set to 1. The equation can be found in (3). The objective is to minimise the number of times the electrolyser or fuel cell is turned on or off within the prediction horizon. The penalty is the same for turning on or off the component. The electrolyser and fuel cell have a separate objective function in the model, which work in a similar way. The combined objective function can be found in (4).

$$\begin{aligned} \mathrm{a}[t] &:= \begin{cases} 1 & \text{if } \mathrm{s}[t] > \varepsilon \\ 0 & \text{otherwise} \end{cases} \\ \delta[t] &\geq \mathrm{a}[t] - \mathrm{a}[t-1] \quad \forall t \in \{0, \ldots, T{-}1\} \\ \delta[t] &\geq \mathrm{a}[t-1] - \mathrm{a}[t] \quad \forall t \in \{0, \ldots, T{-}1\} \end{aligned} \tag{3}$$

where a[t] $\epsilon\{0,1\}$ is the active state of the component, s[t] $\epsilon[0,1]$ is the setpoint of the electrolyser or fuel cell, ε is the small threshold value, $\delta[t]$ $\epsilon\{0,1\}$ is the on/off transition indicator respectively $\delta_{el}[t]$ for the electrolyser and $\delta_{fc}[t]$ for the fuel cell, λ_{el} and λ_{fc} are the associated (constant) weight factors.

$$\mathrm{J_{on\_off}} = \lambda_{\mathrm{el}} \cdot \sum_{t=0}^{T-1} \delta_{el}[t] + \lambda_{\mathrm{fc}} \cdot \sum_{t=0}^{T-1} \delta_{fc}[t] \tag{4}$$

Where $\mathrm{J_{on\_off}}$ is the on/off transition-related objective, λ_{el} and λ_{fc} are the (constant) weight factors for the electrolyser and fuel cell, and $\delta_{el}[t]$ and $\delta_{fc}[t]$ are the corresponding on/off transition indicators at timestep t.

5.4.3 Changing Setpoint Electrolyser and Fuel Cell

The objective is to minimise the change in setpoint between hours for both the electrolyser and the fuel cell across the prediction horizon. The objective is to reduce the total change in setpoint over the entire horizon. The equations are shown in (5) and the objective function is shown in (6).

$$\begin{aligned} \Delta_s[t] &\geq \mathrm{s}[t] - \mathrm{s}[t-1] \quad \forall t \in \{0, \ldots, T{-}1\} \\ \Delta_s[t] &\geq \mathrm{s}[t-1] - \mathrm{s}[t] \quad \forall t \in \{0, \ldots, T{-}1\} \end{aligned} \tag{5}$$

Where s[t] $\epsilon[0,1]$ is the setpoint of the electrolyser or fuel cell, and Δ_s is the magnitude of the setpoint change of the electrolyser or fuel cell.

$$J_{\Delta_s} = \lambda_{\Delta_s} \cdot \sum_{t=0}^{T-1} \Delta_s[t] \tag{6}$$

Where J_{Δ_s} is the change in setpoint-related objective, λ_{Δ_s} is the (constant) weight factor for change in setpoint for both the electrolyser and the fuel cell, and Δ_s the magnitude of the setpoint change of the electrolyser or fuel cell.

5.5 Calibration of Weight Factors

As the terms in the objective function do not all have the same unit, they can't be directly compared with each other. Weight factors are added to make the model behave as desired. A dataset consisting of 10 years of data is used to calibrate the model. Starting from the most recent available year, 2023, up to 2013 is used; 2014 is not used as not all the data was available for 2014. Using a ten-year average as input prevents the model from optimising for a year that may include atypical or extreme conditions, ensuring a more representative assessment of typical system usage. The

weight factors have been calibrated by hand, which could have resulted in a non-optimal solution. Future work could explore optimisation-based tuning methods to enhance the robustness and performance of the system. The following criteria have been taken into account to complete the calibration.

- The electrolyser and fuel cell have a relatively high degradation when turning them on and off. Therefore, it is preferred to have the electrolyser and fuel cell running for multiple consecutive hours [18].
- The electrolyser and fuel cell experience more degradation when changing the setpoint. Therefore, it is preferred to have the electrolyser and fuel cell running with relatively little change in setpoint between subsequent hours. [18].
- The electrolyser and fuel cell tend to turn on when the metal hydride storage is full. As they do this, they 'waste' energy while not being punished (enough) for using the grid to export the power surplus. This happens when the grid's punishment is greater than for using the electrolyser and fuel cell. It is essential to carefully select the right weight factor for using the grid to prevent this from happening.

Following calibration, the final weighting factors applied are as follows: $\lambda_{\text{grid}} = 20$, $\lambda_{\text{on\_off\_el}} = 130$ $\lambda_{\text{on\_off\_fc}} = 190$, $\lambda_{\Delta_s} = 74$

5.6 MPC Control Actions

The control actions are the output of the MPC and the input for the next timestep of the model. The control actions that the MPC has are: electrolyser setpoint, fuel cell setpoint, and electricity grid import/export.

6 Results

After calibrating the model with the ten-year average dataset, the model is verified. After successfully completing all the verification steps, the model was tested for the years 2013 and 2015. Since both show similar results, only 2013, the year with the relatively most extreme supply and demand profiles, is presented.

6.1 Model Verification

First, all datasets were checked for errors, and if they were correctly converted from Excel to Python, including the added uncertainty on the input data, was checked. Component boundaries were tested by intentionally exceeding the inputs to confirm they were enforced. Key model features such as efficiency, start-up, degradation, the MPC objective function, prediction horizon and exergy heat were individually checked to see if they behaved as expected. Lastly, an energy balance check was performed to ensure that all inputs, outputs, and losses matched. All verification checks were successfully completed.

6.2 Net Energy Usage

Figure 4 shows the daily energy balance. The blue line represents the PV panel supply, the green line represents the total heat demand, and the orange line represents the electricity demand. The black line is the total sum of the energy supply and demand, the daily net energy. The horizontal axis represents time, and the vertical axis represents energy usage (kWh). It includes both positive and negative values, with the zero line located about one-quarter from the bottom of the graph.

The model starts the year on 1 October, with a full metal hydride storage. This is right before the net energy generation becomes negative.

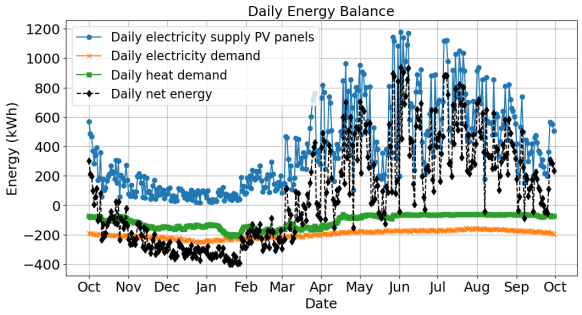

Figure 4: Daily net energy usage 2013

6.3 Metal hydride storage

From half of October, when the net energy becomes negative, the metal hydride storage starts to be used, as can be seen in Figure 5. The metal hydride storage is empty after 25 days. In March, the net energy becomes positive again, starting to recharge the metal hydride storage until the net energy has two dips and discharges the metal hydride again. It takes 34 days from April onwards to recharge the metal hydride storage. From that moment on, the energy surplus must be exported back to the grid.

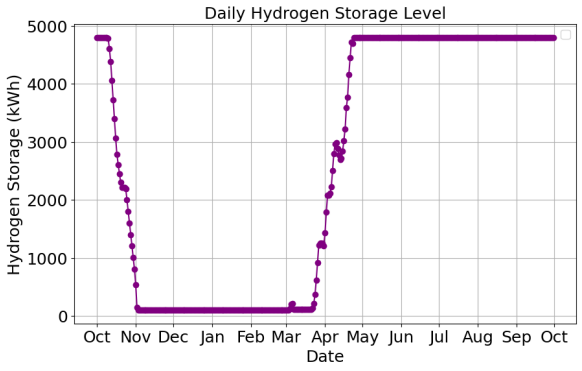

Figure 5: Daily metal hydride storage level 2013

6.4 Electrolyser Input and Fuel Cell Output Power

The fuel cell, see Figure 6, operated for a total of 594 hours until the metal hydride storage was fully discharged, and the electrolyser operated for 598 hours to recharge the metal hydride.

The electrolyser usage is especially intermittent when compared to the 10-year average dataset,

with relatively higher setpoints compared to the test data. This makes sense as it relates to PV panel supply, which is more intermittent in a single year. During the charging of the metal hydride, there are a few moments when hydrogen is used to power the fuel cell, when the net energy dips below zero, as seen in Figure 4.

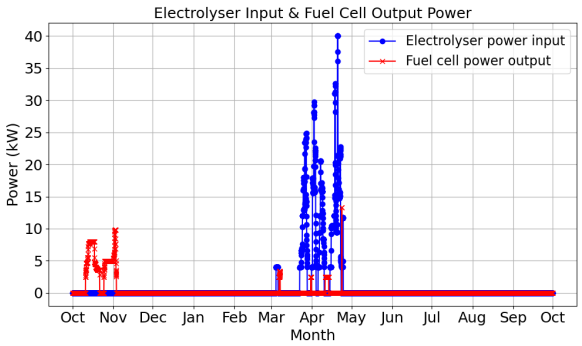

Figure 6: Hourly electrolyser input and fuel cell output power 2013

The electrical energy put into the electrolyser was 7.2 MWh, and the total hydrogen produced was 5,2 MWh. Resulting in an average efficiency of 72,7% for the electrolyser. The total amount of hydrogen the fuel cell used was 5.2 MWh, and the total amount of electrical energy produced was 3.0 MWh. Resulting in an average efficiency of 57.7% for the fuel cell. The total combined average efficiency of the seasonal energy storage system was 42.0% (excluding using exergy heat).

The electrolyser, fuel cell and absorption process produce 3.8 MWh of usable heat (excluding internal losses). However, when converting this heat to exergy and subtracting the required exergy for the desorption process, only 482 kWh of exergy is available to reduce the heat demand. In total, 458 kWh was used to reduce the space heating demand, and 24 kWh was used to reduce the domestic hot water demand.

When considering the reuse of exergy, the average efficiency of the seasonal energy storage system is increased to 48.6%, 0.1% lower compared to the ten-year average dataset.

6.5 Electricity Import and Export From the Grid

In Figure 7, it can be seen that the peak of the electricity import is 16.8 kW, with a total grid import of 35.2 MWh, as the peak export to the grid is 55.3 kW, with a total export of 57.4 MWh.

This does not meet the requirement to stay below 40 kW of grid capacity. However, it is technically feasible to turn off part of the PV panels when exceeding the 40 kW limit of grid capacity. Nevertheless, 1.7 MWh, 1.3% of the total annual PV production, is curtailed this way. Another option would be to reduce the number of PV panels. This reduces the peak production of the PV panels during the summer, while the relatively small change in the PV panel production in the winter can be compensated for by the grid.

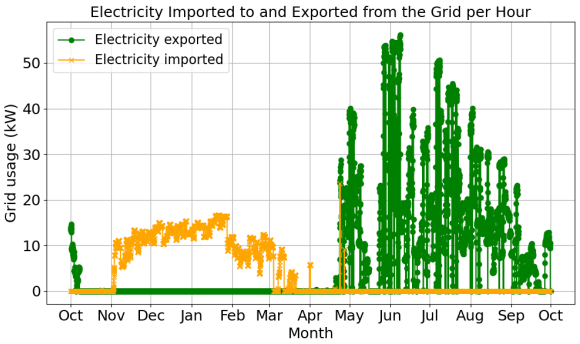

Figure 7: Hourly import and export of the grid 2013

6.6 Extreme Cases

Two extreme cases show the effective duration of the metal hydride storage. For both extreme cases, the day with either the highest or the lowest net energy is selected, and that day is repeated for several consecutive days in the model. The first one uses the day with the lowest net energy production, the 19th of January, to simulate that it takes 185 hours to fully discharge the metal hydride storage. On the other hand, on the 2nd of June, the day with the highest net energy production, it was simulated that it takes 230 hours to fully charge the metal hydride.

7 Discussion

The results show that the metal hydride storage is too small to effectively function as a seasonal energy storage. Consequently, the model does not provide the metal hydride storage during the periods when it is most needed, in mid-winter when the storage is already empty, and in mid-summer when it is already full, thereby limiting the seasonal potential. This section discusses the main limitations of the current model and possible directions for future improvements.

A key challenge comes to light from the model's 24-hour receding horizon. Since the Model Predictive Control (MPC) operates with a limited 24-hour horizon, it cannot anticipate future energy demand or supply beyond this window, which restricts its ability to manage seasonal storage strategically. This is an issue as the current metal hydride storage is insufficient to cover the entire winter season. While it is inherently difficult to predict precisely when the metal hydride storage will be most required, any model would need to rely on estimates rather than exact forecasts, underscoring the complexity of optimising seasonal energy storage in this context.

The results of the model suggest two potential directions for deeper analysis.

1. What is the required capacity of the metal hydride to fully cover the net energy demand over a year, while also being fully recharged at the end of the year?

2. What is the optimal operational strategy for the metal hydride storage when it is too small to cover the entire winter energy demand?

The first direction can be investigated by increasing the size of the metal hydride and the number of PV panels, as the original total PV generation is insufficient to charge the metal hydride storage back up to 100% again.

This increases the size of the metal hydride storage from 4.8 MWh to 60.8 MWh, as can be seen in Figure 8. In total, 8.1 20ft containers are required to store the metal hydride. Additionally, increasing the number of PV panels from 300 to 346 is required for off-grid operation. The electrolyser power must also increase from 40 kW to 74 kW to handle peaks in solar power and prevent the daily battery from exceeding its upper limit.

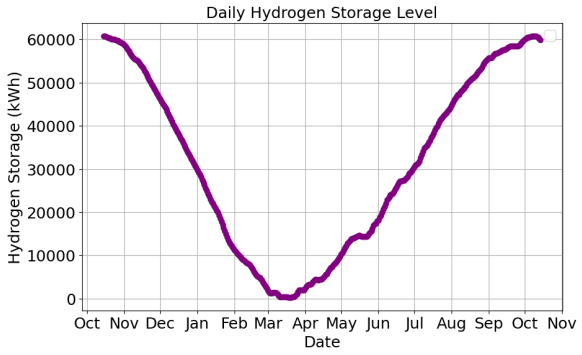

Figure 8: Metal hydride storage level when scaled up to 60.8 MWh

The second relevant consideration is to use the limited metal hydride storage capacity most effectively. This would be when the net energy demand is the lowest, in December and January, or in case of a dunkelflaute. There are multiple options to use the limited amount of energy in the metal hydride storage in the most effective way:

The first option would be to integrate the dynamic energy price into the objective function. When connecting the grid usage to the current dynamic energy price and converting the degradation for the setpoint change and on-off control into cost, the objective function can be used without adding additional weight factors. The current scale of the metal hydride storage system limits this approach. As the cost per kWh is higher than that of the grid. However, by scaling up the metal hydride size, the cost per kWh of the metal hydride system is expected to decrease while the dynamic energy prices stay fixed. Further research is required to determine the optimal size of the metal hydride storage for the number of apartments for which the storage becomes both technically and economically favourable.

The second option would be to integrate a second level of control for long-term strategic planning. This separates long-term strategic planning from short-term operational control. This additional, long-term strategic planning could be either an offline optimisation or another MPC [13]. An offline optimisation appears to be the most logical approach, given the high uncertainty in long-term forecasts over weeks or months. This level of uncertainty makes it impractical for a second, long-horizon MPC to guide seasonal energy storage decisions reliably. A key advantage of offline optimisation is that it can be integrated relatively easily into the existing short-term MPC structure, for example by using the 10-year training dataset. However, a drawback is that it is less adaptive to real-time deviations from the offline scenario, potentially leading to suboptimal behaviour under unexpected conditions.

There are several limitations to the current model:

- To respect the 40 kW limit of the grid capacity, part of the solar panels must be turned off for a few moments during the year.
- Although the heat can be reused, no heat storage is included in the model. Including a heat storage can shave off the peaks of the PV production and the peaks of the heat demand.
- The daily battery is modelled as minimalistic, as the research focuses on showing the feasibility of the metal hydride seasonal energy storage. However, the impact of the daily battery has been greater than first anticipated. Future research should include efficiency losses, degradation, and AC/DC losses in the daily battery model for more accurate results.

8 Conclusion

This research shows that room-temperature TiFe metal hydride has technical potential as a seasonal energy storage solution in the built environment. However, its current storage capacity (4.8 MWh) is insufficient to fully cover the seasonal energy demand. Nevertheless, TiFe storage proves effective for shorter periods of high demand, such as during dunkelflaute events. It can help mitigate grid congestion and seasonal renewable energy mismatches where battery-only solutions are impractical.

In the results of the year 2013, the metal hydride storage bridged the supply-demand gap between winter and summer over cycles of 25 to 34 days, achieving a combined round-trip efficiency of 45.5% by reusing exergy heat. However, in the more extreme cases, the storage was only sufficient for 185 hours of discharge and 230 hours of charging.

To improve the accuracy of matching real-world performance, the following directions for future work can be explored:

1. Integration of dynamic prices and degradation costs into the MPC objective.
2. Integrate a second-level offline level in the model that combines offline strategic planning with the short-term MPC.

References

[1] Alliander. *Zonneparken alleen daar waar het nog kan*. June 2019. URL: https://www.alliander.com/nl/nieuws/zonneparken-alleen-daar-waar-het-nog-kan/.

[2] Muhammad Atif et al. "Physisorption and chemisorption trends in surface modification of carbon black". In: *Surfaces and Interfaces* 31 (July 2022). ISSN: 24680230. DOI: 10.1016/j.surfin.2022.102080.

[3] Satyasekhar Bhogilla et al. "Cogeneration system combining reversible PEM fuel cell, and metal hydride hydrogen storage enabling renewable energy storage: Thermodynamic performance assessment". In: *International Journal of Hydrogen Energy* 52 (Jan. 2024), pp. 1147–1155. ISSN: 03603199. DOI: 10.1016/j.ijhydene.2023.08.028.

[4] Clean Hydrogen Joint Undertaking. *Clean Hydrogen JU SRIA – Key Performance Indicators (KPIs)*. Nov. 2021. URL: https://www.clean-hydrogen.europa.eu/knowledge-management/strategy-map-and-key-performance-indicators/fch-2-ju-mawp-key-performance-indicators-kpis_en.

[5] W.R.W. Daud et al. "PEM fuel cell system control: A review". In: *Renewable Energy* 113 (Dec. 2017), pp. 620–638. ISSN: 09601481. DOI: 10.1016/j.renene.2017.06.027.

[6] deltaWonen. *Urban Energy Island Kampen*. Tech. rep. Kampen: deltaWonen, Aug. 2024.

[7] A. El Kharbachi et al. "Metal Hydrides and Related Materials. Energy Carriers for Novel Hydrogen and Electrochemical Storage". In: *The Journal of Physical Chemistry C* 124.14 (Apr. 2020), pp. 7599–7607. ISSN: 1932-7447. DOI: 10.1021/acs.jpcc.0c01806.

[8] European Parliament. *Greenhouse gas emissions by country and sector (infographic)*. Dec. 2024. URL: https://www.europarl.europa.eu/topics/en/article/20180301STO98928/greenhouse-gas-emissions-by-country-and-sector-infographic.

[9] European Parliament. *How the EU is boosting renewable energy*. June 2024. URL: https://www.europarl.europa.eu/topics/en/article/20221128STO58001/how-the-eu-is-boosting-renewable-energy.

[10] Eurostat. *Renewable energy statistics*. 2023. URL: https://ec.europa.eu/eurostat/statistics-explained/index.php?title=Renewable_energy_statistics#Renewable_energy_produced_in_the_EU_increased_by_two_thirds_in_2006-2016.

[11] D.S. Falcão et al. "A review on PEM electrolyzer modelling: Guidelines for beginners". In: *Journal of Cleaner Production* 261 (July 2020), p. 121184. ISSN: 09596526. DOI: 10.1016/j.jclepro.2020.121184.

[12] Hessam Golmohamadi. "Data-Driven Approach to Forecast Heat Consumption of Buildings with High-Priority Weather Data". In: *Buildings* 12.3 (Mar. 2022), p. 289. ISSN: 2075-5309. DOI: 10.3390/buildings12030289.

[13] Subhi Gupta et al. "Hierarchical MPC for a dynamic process system employing parametric global optimization strategy". In: *Digital Chemical Engineering* 9 (Dec. 2023), p. 100120. ISSN: 27725081. DOI: 10.1016/j.dche.2023.100120.

[14] Tom van der Gurp. *Dit jaar voor het eerst meer groene dan grijze stroom opgewekt*. Dec. 2024. URL: https://www.nu.nl/economie/6340719/dit-jaar-voor-het-eerst-meer-groene-dan-grijze-stroom-opgewekt.html.

[15] Nejc Klopčič et al. "A review on metal hydride materials for hydrogen storage". In: *Journal of Energy Storage* 72 (Nov. 2023). ISSN: 2352152X. DOI: 10.1016/j.est.2023.108456.

[16] Li Dai et al. "Discrete-Time Model Predictive Control." In: *InTech* (Dec. 2012). DOI: 10.5772/51122.

[17] Huang Liu et al. "An overview of TiFe alloys for hydrogen storage: Structure, processes, properties, and applications". In: *Journal of Energy Storage* 68 (Sept. 2023). ISSN: 2352152X. DOI: 10.1016/j.est.2023.107772.

[18] Xinyu Lu et al. "Optimization of power allocation for wind-hydrogen system multi-stack PEM water electrolyzer considering degradation conditions". In: *International Journal of Hydrogen Energy* 48.15 (Feb. 2023), pp. 5850–5872. ISSN: 03603199. DOI: 10.1016/j.ijhydene.2022.11.092.

[19] D.Q. Mayne et al. "Constrained model predictive control: Stability and optimality". In: *Automatica* 36.6 (June 2000), pp. 789–814. ISSN: 00051098. DOI: 10.1016/S0005-1098(99)00214-9.

[20] National Energy Dashboard. *Totale elektriciteitsproductie*. Trans. by National Energy Dashboard. Dec. 2024. URL: https://ned.nl/nl/dataportaal/energie-productie/elektriciteit/totale-elektriciteitsproductie.

[21] Huy Quoc Nguyen et al. "Review of metal hydride hydrogen storage thermal management for use in the fuel cell systems". In: *International Journal of Hydrogen Energy* 46.62 (Sept. 2021), pp. 31699–31726. ISSN: 03603199. DOI: 10.1016/j.ijhydene.2021.07.057.

[22] John M. Stansberry et al. "Experimental dynamic dispatch of a 60 kW proton exchange membrane electrolyzer in power-to-gas application". In: *International Journal of Hydrogen Energy* 45.16 (Mar. 2020), pp. 9305–9316. ISSN: 03603199. DOI: 10.1016/j.ijhydene.2020.01.228.

[23] Rok Stropnik et al. “The influence of degradation effects in proton exchange membrane fuel cells on life cycle assessment modelling and environmental impact indicators”. In: *International Journal of Hydrogen Energy* 47.57 (July 2022), pp. 24223–24241. ISSN: 03603199. DOI: 10.1016/j.ijhydene.2022.04.011.

[24] Spyros Theocharides et al. “PV generation forecasting utilizing a classification-only approach”. In: *EPJ Photovoltaics* 15 (Apr. 2024), p. 12. ISSN: 2105-0716. DOI: 10.1051/epjpv/2024011.

[25] Toshiba. *The world´s largest-class hydrogen production, Fukushima Hydrogen Energy Research Field (FH2R) now is completed at Namie town in Fukushima.* Mar. 2020. URL: https://www.global.toshiba/ww/news/energy/2020/03/news-20200307-01.html.

[26] Sten de Wit. *Innovations in energy storage.* Mar. 2022. URL: https://www.tno.nl/en/sustainable/energy-built-environment/energy-storage/.

[27] Chengxiang Xiang et al. “Principles and implementations of electrolysis systems for water splitting”. In: *Materials Horizons* 3.3 (2016), pp. 169–173. ISSN: 2051-6347. DOI: 10.1039/C6MH00016A.

[28] Xingyu Yan et al. “Operating power reserve quantification through PV generation uncertainty analysis of a microgrid”. In: *2015 IEEE Eindhoven PowerTech*. IEEE, June 2015, pp. 1–6. ISBN: 978-1-4799-7693-5. DOI: 10.1109/PTC.2015.7232577.

[29] Shelli Zargary. *Comparing Fuel Cell Technologies.* Aug. 2018. URL: https://www.gencellenergy.com/resources/blog/comparing-fuel-cell-technologies/.

[30] Bahman Zohuri. “The Chemical Element Hydrogen”. In: *Hydrogen Energy*. Cham: Springer International Publishing, 2019, pp. 1–35. DOI: 10.1007/978-3-319-93461-7{_}1.

B

Appendix: Verification

Every verification check that has been done is presented. For every test, the training data is used. Note that the uncertainty is not taken into account during any of the verification checks. Additionally, after the verification checks have been done, some weight factors of the objective function have been changed, some input data have been altered, and the start date of the simulation has been changed. This does not influence the impact of each of the verification checks, but this could result in different values when replicating a check.

Data Check
Before doing each of the data checks, hypotheses have been drawn up. After conducting the check, a conclusion is given.

The First verification check is to see whether the raw input data does not show unexplainable irregularities or patterns. For each production or demand, a figure of the normalised input or demand over the year is provided. Additionally, a figure of one day of input or demand is presented to check if that matches the hypothesis.

It is important to remember that the data is the average of the neighbourhood, not the data of a single household.

Normalised PV Production
Hypothesis year: The PV production is the greatest in the summer and gradually lowers till reaching the lowest point in the winter, as solar irradiance is greater and there are more daylight hours. Due to changing weather conditions between days, the production varies on the day and between days.

Hypothesis day (1st of July): The production is the greatest during the day when the solar irradiance is the highest. During the morning and evening, when there is no sun, there is also no PV input.

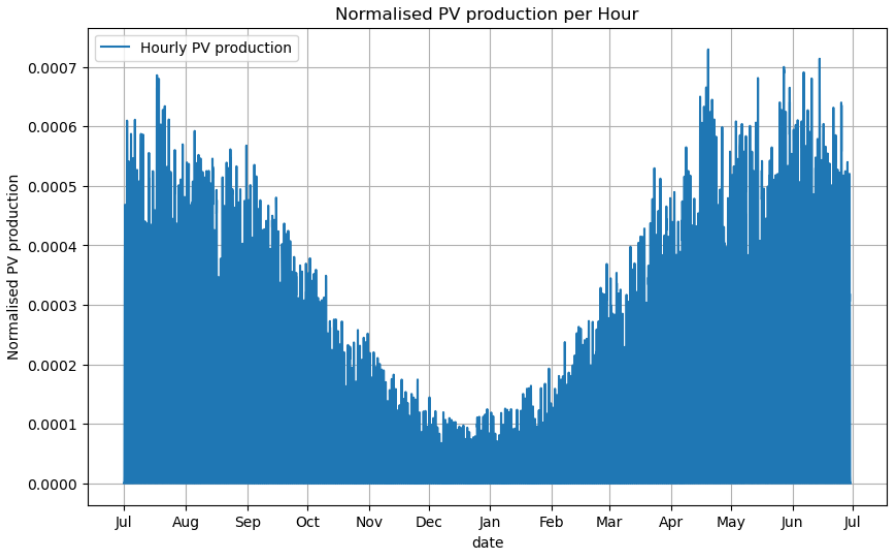

Figure B.1: Normalised PV production per hour

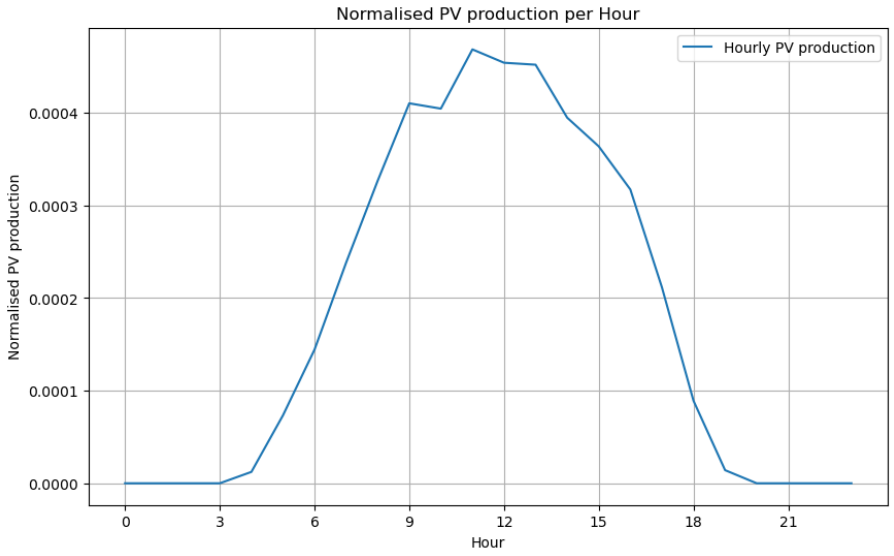

Figure B.2: Normalised PV production per hour 1th of July

Conclusion: Figure B.1 shows that the PV production shows seasonal and daily fluctuations. The production in the summer is higher than in the winter, and the production varies over the days.
Figure B.2 shows that there are a lot of hours of irradiance, as there is a production of solar energy between 4 AM and 9 PM. The production is the highest around the middle of the day, at 11 AM in this case.
No irregularities have been found in the data.

Normalised Electricity Demand
Hypothesis year: The demand for electricity is greater in the winter than in the summer because there are fewer daylight hours and people spend more time at home.
Hypothesis day (1st of July): The demand between the days shows the peaks around the same time every day. There is little electricity use during the night, with peaks in the morning and the evening.

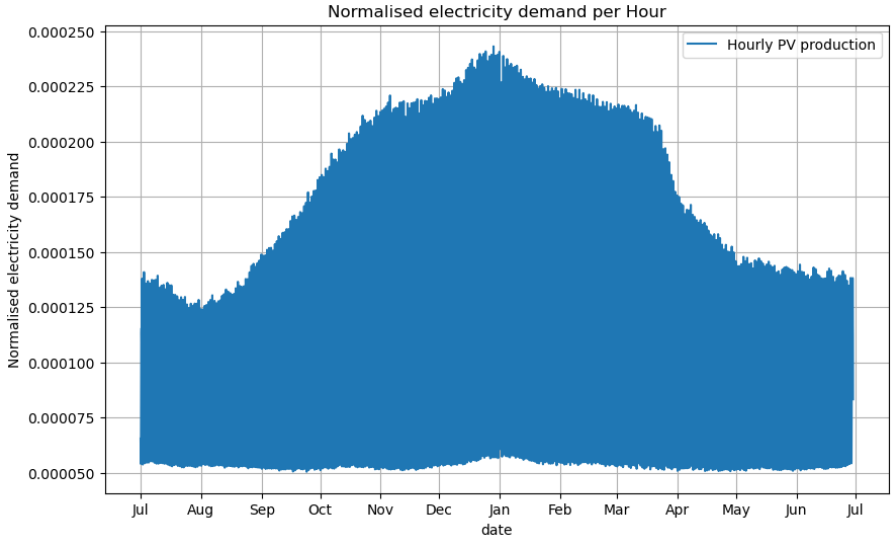

Figure B.3: Normalised electricity demand per hour

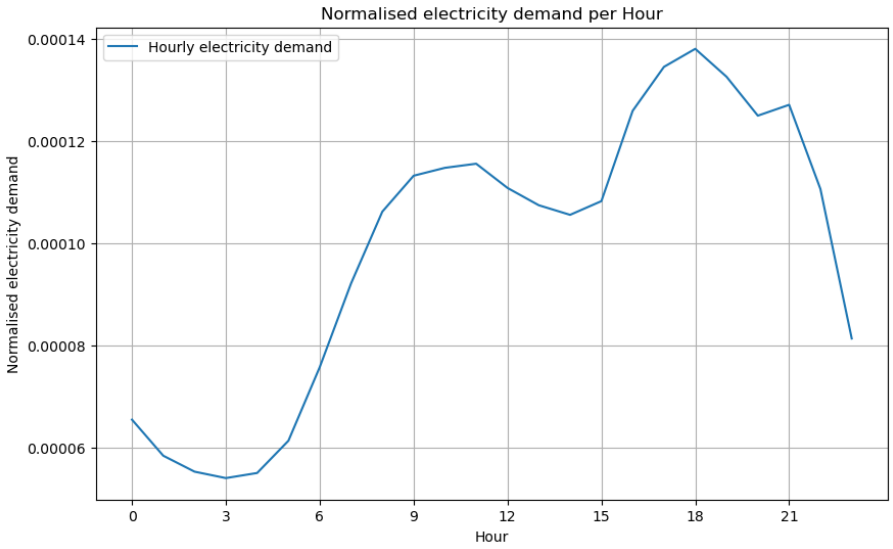

Figure B.4: Normalised electricity demand per hour 1st of July

Conclusion: Figure B.3 shows that there is greater electricity demand in the winter than in the summer. Figure B.4 shows that the highest demand is in the morning and the evening. This is when most people either go to work or return from work.
No irregularities have been found in the data.

Normalised Heat Demand
Hypothesis year: Heat demand begins in the autumn, peaks during the winter, and gradually decreases to zero as spring approaches.
Hypothesis day (1st of Jan): The heat demand is higher during the day than at night, with peaks in the morning and the evening.

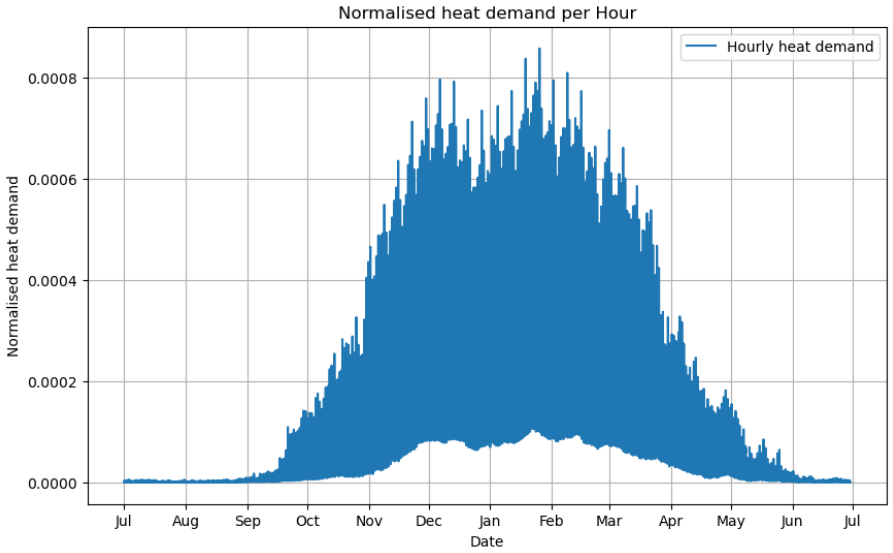

Figure B.5: Normalised heat demand per hour

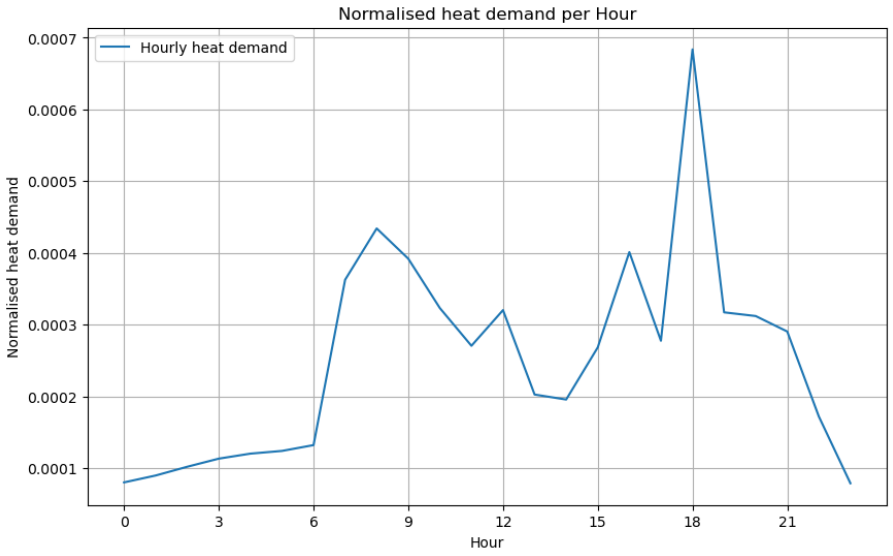

Figure B.6: Normalised heat demand per hour 1st of Jan

Conclusion: Figure B.6 shows that the heat demand is the highest in the winter and almost no heat demand during the winter.
There are relatively high peaks in the winter that show periodic behaviour. After further investigation of the data, the reason for this is that every peak reoccurs on a Sunday evening in the model. This is logical considering that this is the day of the week that most people spend their evening inside, increasing the demand for heat during that evening compared to other days of the week.
Figure B.6 shows that the heat demand peaks in the morning and the evening, as these are the times that most people are home and heat their houses.

Normalised Domestic Hot Water Demand
The normalised domestic hot water demand is the same every day because it is an estimation from the dataset of TNO (TNO, 2024). Therefore, only one day will be taken into consideration for the data check.
Hypothesis day: Domestic hot water usage follows the same trend as the hot water demand. The heat demand is higher during the day than during the night, with peaks in the morning and the evening.

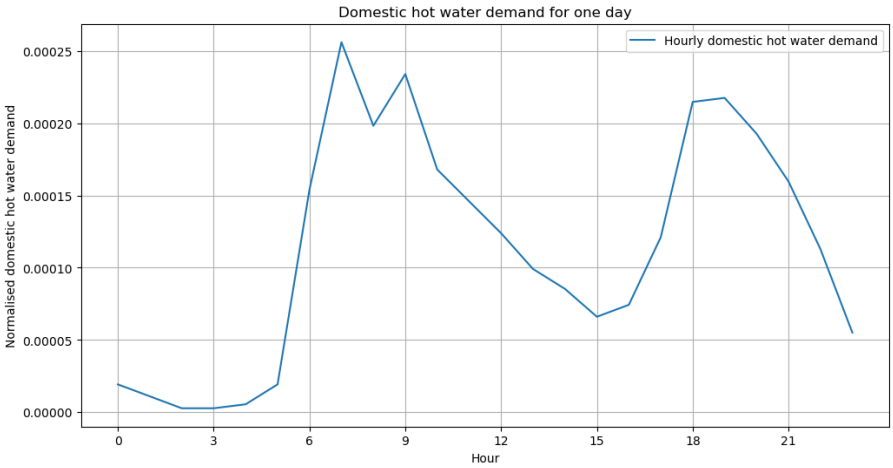

Figure B.7: Normalised domestic hot water demand per hour for one day

Conclusion: Figure B.7 shows a peak in the domestic hot water demand during the morning and evening. However, it is surprising that the morning peak is higher than the evening peak, while this is the other way around for the heat demand. A reason for this could be that more people shower around the same hour, while this is more spread out over multiple hours in the evening.

Data modelling check
The data modelling check checks if the data is correctly imported from Excel into the Python model. This is done by checking if:

1. The total sum of the normalised data is equal to one for the dataset in Excel and Python.
2. The first day (24 values) of the data in Python matches the first day of the data in Excel.
3. The last value of the data in Python matches the last value of the data in Excel.

PV production:
The sum of the PV production in both Excel and Python is equal to one. Also, the first day's data is the same for Excel and Python, and the last data point is the same. Concluding that the data is correctly converted from Excel to Python.

Electricity demand:
The sum of the normalised electricity demand in both Excel and Python is equal to one. There is a small error of 1.6E-6% between the value in Excel and the value in Python. However, this was found to be a rounding error. Also, the first day's data is the same for Excel and Python, and the last data point is the same. Concluding that the data is correctly converted from Excel to Python.

Heat demand:
The sum of the normalised heat demand in both Excel and Python is equal to one. There is a small error of 2.9E-6% between the value in Excel and the value in Python. However, this was found to be a rounding error. Also, the first day's data is the same for Excel and Python, and the last data point is the same. Concluding that the data is correctly converted from Excel to Python.

Domestic hot water demand:
The sum of the normalised domestic hot water demand in both Excel and Python is equal to one. There is a small error of 8.9E-14% between the value in Excel and the value in Python. However, this was found to be a rounding error. Also, the first day's data is the same for Excel and Python, and the last data point is the same. Concluding that the data is correctly converted from Excel to Python.

Applied Uncertainty Check
The applied uncertainty check checks if the uncertainty is applied to the right input values (PV production, electricity demand, heat demand, domestic hot water demand) and used within the selected bounds.

This is done by checking if:

1. The uncertainty is not applied to the first value, representing the current hour.
2. The uncertainty is applied to the other 23 values within the MPC horizon, and each value is verified to lie within the defined boundaries.
3. The uncertainty allows the original value to be either increased or decreased.
4. The values can't become negative after applying the uncertainty, as this would be physically impossible.

The first check is verified. The current hour in the MPC remains unchanged after applying the uncertainty.

The second check looked correct at first, as uncertainty was applied in relation to the original values. However, it was found that the uncertainty was not applied as a percentage of the original value but as an actual value. For example, the total uncertainty in the heat demand is 8.95%, with a deviation of ±4.475% from the nominal value in both directions. The implementation in the code was that the uncertainty was ±0.0475 from the original value. This resulted in a lower uncertainty than required.
After solving this issue, the uncertainty is applied correctly and verified by the second check.

The third check is verified. After the uncertainty is applied to the original value, the new values are found to possibly be increased or decreased.

The fourth check is verified. The result can never be negative since all input data is positive, and the applied uncertainty is a percentage of this positive value. Additionally, as a redundancy measure, any value that would become negative after applying uncertainty is set to zero.

Boundary Check
The boundary check checks if constrained components can't surpass the boundary values that have been set. This is done in two ways:

1. Increasing or decreasing the starting value past the maximum or minimum value.
2. If that is not possible, check whether the boundaries are not exceeded during the run.
3. If that is not possible, alter the boundary conditions to 'force' the component to reach the boundary.

Min/Max Daily Battery
This can be verified using the first check. Normally, the initial daily battery value is set to 190 kWh, half of

the battery capacity. Two tests have been done, inserting a negative value for the initial daily battery value or inserting a positive value beyond the limit of 380 kWh. Both tests result in an error with the warning: "MPC optimisation did not find an optimal solution". Concluding that the boundaries of the daily battery can't be exceeded.

Min/ Max Input Power Electrolyser
The electrolyser input power value can't be verified using the first check, as the power is determined by the MPC. The lower boundary can be tested by using the second check. This is done by checking if no value in the electorlyser_energy_usage list is negative and has a lower setpoint than 4 kW when the electorlyser is turned on. Because 4 kW is the minimum input power for the electrolyser. The list does not exceed any boundaries, concluding that the minimum boundary of the input power electrolyser can't be exceeded.
The maximum input power of 40 kW is not reached in a normal run of the electrolyser. That is why the third check is used to test this. The boundary of the max electrolyser power is lowered to 20 kW, this is lower then would be reached in a normal run (about 25 kW). The results show a maximum electrolyser setpoint of 20 kW for this run. Concluding that the boundaries of the electrolyser can't be exceeded.

Min/ Max Metal Hydride
This can be verified using the first check. Normally the initial metal hydride storage value is set to 4800 kWh. Two tests have been done, inserting a negative value for the initial metal hydride storage value or inserting a positive value beyond the limit of 4800 kWh. Both tests result in an error with the warning: "MPC optimisation did not find an optimal solution". Concluding that the boundaries of the daily battery can't be exceeded.

Min/ Max Metal hydride Speed Limit
The minimum/ maximum speed of the metal hydride is not a constraint in the model, as it was confirmed in the preliminary stages that the hydrogen. The maximum flow allowed by GKN hydrogen is 105 kg/hr (GKN hydrogen, n.d.). In comparison, in the model, only 1.11 kg/hr is reached.

The code limits the potential negative hydrogen flow, as it is directly linked to the electrolyser setpoint, which is a constraint between the positive values 0.1 and 1.0.

Min/ Max Fuel Cell
The fuel cell input power value can't be verified using the first check, as the power is determined by the MPC. The lower boundary can be tested by using the second check. This is done by checking if no value in the fuelcell_energy_usage list is negative and has a lower setpoint than 2.5 kW when the electrolyser is turned on. Because 2.5 kW is the minimum input power for the fuel cell. The list does not exceed any boundaries, concluding that the minimum boundary of the input power fuel cell can't be exceeded.
The maximum input power of 25 kW is not reached in a normal run of the fuel cell. That is why the third check is used to test this. The boundary of the max fuel cell power is lowered to 15 kW, this is lower then would be reached in a normal run (about 20 kW). The results show a maximum fuelcell setpoint of 15 kW for this run. Concluding that the boundaries of the fuel cell can't be exceeded.

Min/ Max Grid Capacity
The maximum input and output grid capacity can be checked using the second check. In a normal run the max input and output grid capacity is the allowed 40 kW. Therefore the maximum grid capacity will be set to 32 kW. The results of the run show that the maximum grid input and output was 32 kW. Concluding that the maximum boundaries can't be exceeded.

Min/ Max Battery Speed Limit
The maximum charge and discharge speed of the battery can be checked using the second check. In a normal run, the charge rate does not exceed 0.27 C, and the discharge rate does not exceed 0.08 C. Therefore, both boundaries will be set to 0.05 C. The results of the run show that the battery charge and discharge log do not exceed the 0.05 C speed for both charge and discharge. Concluding that the maximum boundaries can't be exceeded.

Implementation Check
The implementation check checks if the model implements certain features as expected. The expected way of working is explained in chapter 3.

Efficiency
The efficiency within the MPC is calculated using breakpoints, and linear interpolation is used between the breakpoints to determine the efficiency that is connected to the selected setpoint. This way, the computation power required within the MPC is minimised while allowing the MPC to know the influence that the efficiency curve has on the selection of a setpoint for the electrolyser and fuelcell.
Outside of the MPC, the determined setpoint is used to accurately calculate the efficiency of the electrolyser or

fuel cell. To see if the efficiency is calculated correctly, the efficiency that is connected to a setpoint is calculated by hand for both the electrolyser and the fuelcell.

The results for both the fuelcell and electrolyser show that the planned power corresponds with the right efficiency for every setpoint, except for the first setpoint when the electrolyser or fuel cell is turned on. This can be explained due to the start-up factor that is applied outside of the MPC. When multiplying by the start-up factor, the efficiency corresponds with the planned power.

Start-up
The startup is implemented in the same way for both the electrolyser and the fuel cell. Therefore, the same verification check can be done for both in the same run. To clearly see if the start-up works, the upper and lower boundary of the electrolyser are set to 10 kW and for the fuel cell to 5 kW. In the data can be seen that the first non-zero setpoint is 0.9583 for the electrolyser and 0.916 for the fuel cell. This corresponds with the start-up time of 300 seconds for the electrolyser and 60 seconds for the fuelcell. Both the results of the electrolyser and the fuelcell clearly show that the first setpoint is lower than the others, and all other setpoints have the same setpoint value of 1.0. Concluding that the start-up of the electrolyser and fuelcell works.

Degradation
The degradation of the electrolyser and the fuel cell is implemented in the same way. To check if the degradation works, the number of hours that a non-zero setpoint is given for the electrolyser or fuelcell can be multiplied by the degradation factor per hour. In the run, there were 709 active hours for the electrolyser and 516 for the fuelcell. These should correspond to 0.9964 and 0.9995, respectively. The degradation results are the same, concluding that the degradation of the electrolyser and the fuel cell work.

The degradation of the metal is a bit different. The degradation is given per cycle instead of per hour of operation. To check if the degradation works, the total value of the electrolyser output and the fuelcell input summed up together can be multiplied by the maximum storage capacity of the metal hydride and divided by the maximum storage capacity of the metal hydride, this value is multiplied by the degradation factor. The degradation value should correspond to 0.9995, and that aligns with the degradation output of the run. Concluding that the degradation of the metal hydride works.

Operational temperature
This check can be implemented similarly for the electrolyser and the fuel cell. The values of the component's setpoint and the output's temperature are stored. After the run is finished, three non-zero setpoints of each component will be randomly selected. Those setpoints are checked by hand if the operational temperature matches the stored value in the model.

Electrolyser: The operational temperature is 50°C at a setpoint of 0 and 80°C at a setpoint of 1.0. The three checked non-zero setpoints can be found in Table B.1

Setpoint	Temperature (K)	Correct?
1.0	353.15	yes
0.57	340.3	yes
0.2	329.15	yes

Table B.1: Operational temperature check electrolyser

Fuel cell: The operational temperature is 60°C at a setpoint of 0 and 85°C at a setpoint of 1.0. The three checked non-zero setpoints can be found in Table B.2

Setpoint	Temperature (K)	Correct?
0.44	344.1	yes
0.25	339.3	yes
0.1	335.65	yes

Table B.2: Operational temperature check fuel cell

Electrolyser and fuel cell can't be turned on at the same time
The best way to check this is to "force" this behaviour by changing the inputs of the system. This resulted in Figure B.8.

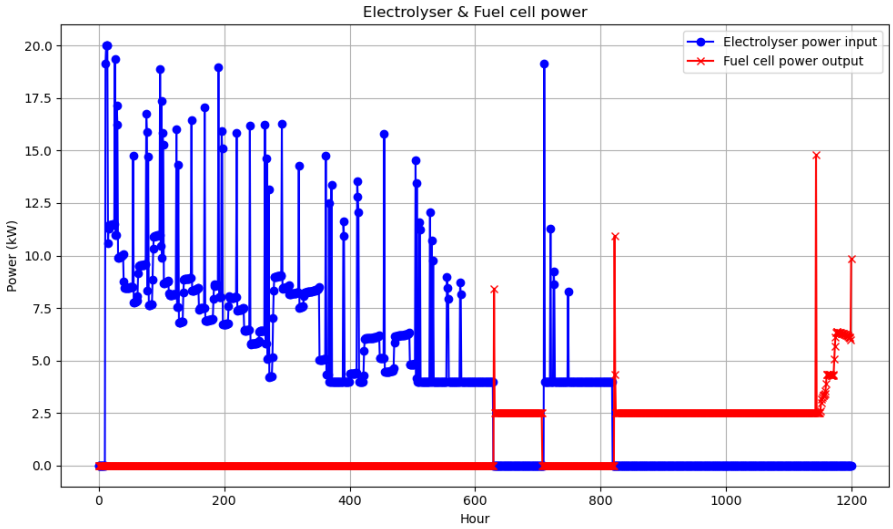

Figure B.8: Check if electrolyser and fuel cell are on at the same hour

The first point of interest is around the 700-hour mark, where the fuel cell turns off and the electrolyser turns on almost directly with a high setpoint. The list of setpoints shows that the fuelcell turns off after hour 706, while the electrolyser turns on at hour 710.
The second point of interest is around the 820-hour mark, where the electrolyser turns off, and the fuel cell turns on almost directly with a high setpoint. The list of setpoints shows that the electrolyser turns off after hour 818, while the fuel cell turns on at hour 822.
Concluding that the electrolyser and fuel cell can't operate within the same hour.

MPC objective
The MPC objective determines how to run the model in the most optimal way, as every objective term works as a punishment to the model.
There are three different terms in the objective function. In order to verify if they all work as expected, each weight factor will be individually set to zero. Effectively turning each objective function off individually.
Before conducting the verification test, a hypothesis will be given.

λ_ grid equal to zero:
Hypothesis: The grid capacity is sufficiently large to fulfil the entire energy supply and Demand. Therefore, it is expected that without a punishment for using the grid, the model won't use the grid at all.

Conclusion: Setting λ grid equal to zero results in the model not using the metal hydride storage and the daily battery as little as possible. As can be seen in Figure B.9 and Figure B.10.
Concluding that the verification test works as expected.

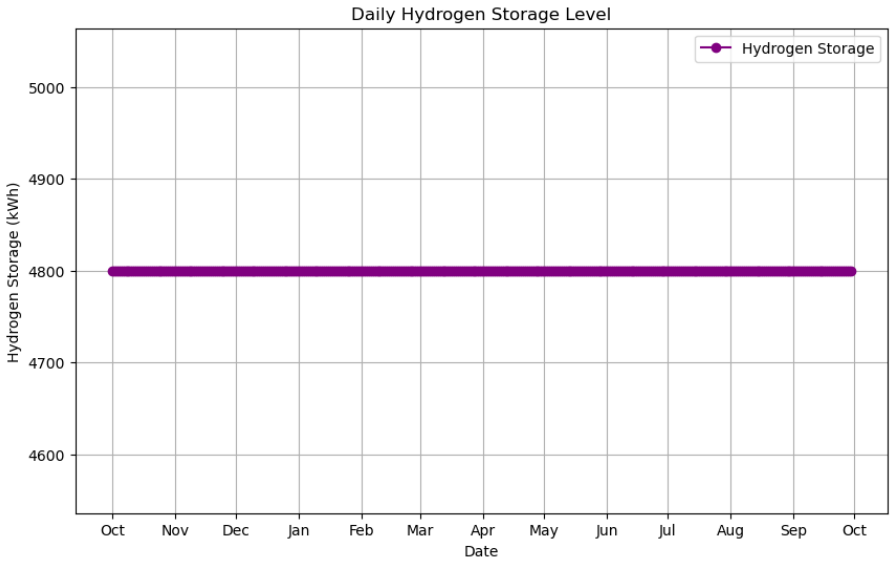

Figure B.9: Daily hydrogen storage level: lambda_grid equal to zero

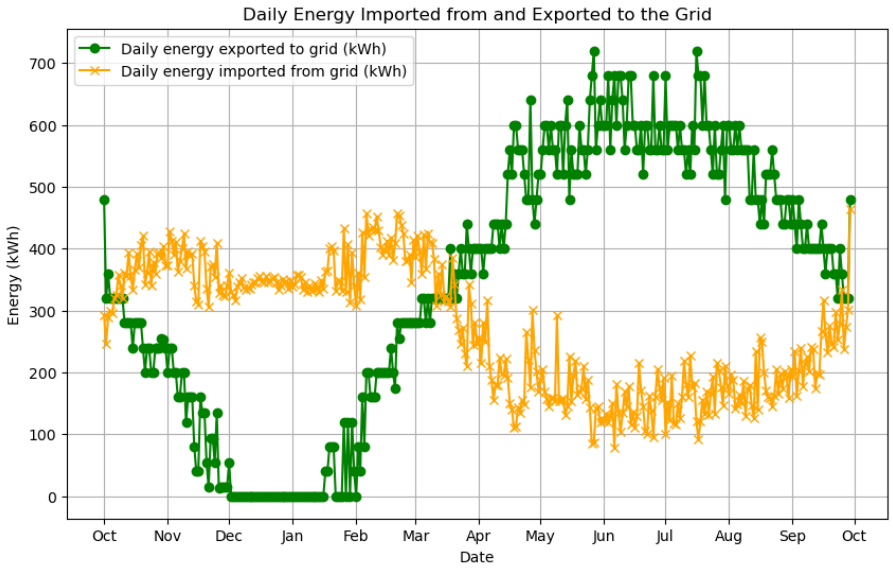

Figure B.10: Daily grid usage: lambda_grid equal to zero

λ_on_off_electrolyser equal to zero:
Hypothesis: The electrolyser will be turned on and off more often, as this is not punished by the model. It is expected that the electrolyser will have fewer total operating hours in total due to this change.

Conclusion: Setting λ_on_off_electrolyser equal to zero results in the model turning the electrolyser more frequently on and off, as can be seen in Figure B.11. This reduced the number of operational hours of the electrolyser from 724 to 605.
Concluding that the verification test works as expected.

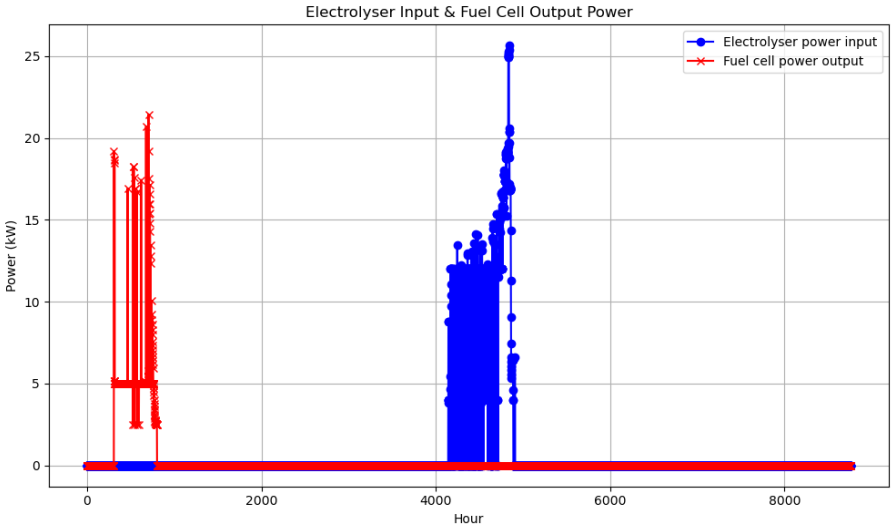

Figure B.11: Electrolyser input and fuel cell output power: lambda on/off electrolyser equal to zero

λ_on_off_fuelcell equal to zero:
Hypothesis: The fuel cell will be turned on and off more often, as this is not punished by the model. It is expected that the fuel cell will have fewer total operating hours in total due to this change.

Conclusion: First, the model gave an error that setting λ_on_off_fuelcell equal to zero results in the model turning the fuel cell more frequently on and off, as can be seen in Figure B.12.

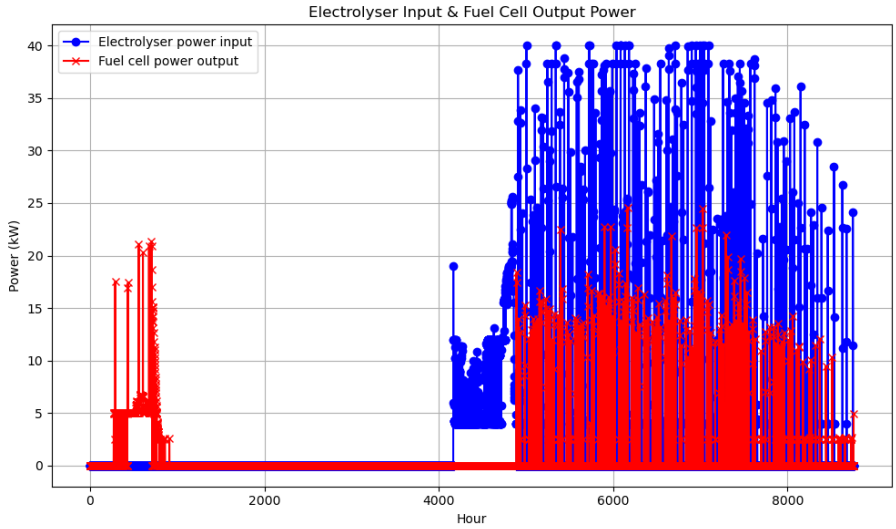

Figure B.12: Electrolyser input and fuel cell output power: lambda on/off fuel cell equal to zero

However, from the moment that the metal hydride storage is full (around 4400 hours), the fuelcell and electrolyser start to operate subsequential in order to 'waste' energy. Apparently, it is punished less for the model to do this than to use the grid more.
But this is not a verification error, it would be an issue if it occurred while calibrating the weight factors. That is why it can be concluded that the verification test works as expected.

λ_change_setpoint equal to zero:
Hypothesis: The electrolyser and fuelcell will run with a greater change in setpoint in subsequent hours. This will result in relatively higher setpoints and, therefore, fewer operational hours than normal.

Conclusion: At first, the MPC gave the error: "MPC optimisation did not find an optimal solution. This error was solved by running the model with an increased maximum grid capacity. The grid capacity was increased to 100 kW.

This solved the error, but the results were not as expected. The maximum grid capacity increased to a maximum of 55.61 kW in the period where there is a surplus of energy and the metal hydride storage is full (from April onwards). However, during this period, the electrolyser and fuel cell are not used; therefore, setting the weight factor of the setpoint change to zero should not make any difference.
The problem was: while the hydrogen storage level within the MPC was checked at the first hour, it was not within again within each step within the prediction horizon, this allowed for the MPC to turn on the electrolyser and fuel cell to 'waste' energy, without showing up in the results as there was and additional check of the hydrogen storage outside of the MPC which overwrite the electrolyser setpoint to zero when the metal hydride storage was full. This was only a problem when λ change setpoint is equal to zero, as before the punishment for changing the setpoint was great enough to prevent this behaviour from occurring.
To solve this problem Equation B.1 and Equation B.2 have been added to the constraints within the MPC.

If the hydrogen storage is full:

$$\text{If } H_{\text{storage}} \geq H_{\max} - P_{\text{el,min}} \Rightarrow \begin{cases} \text{binary\_variable}_{\text{el}}(t) = 0 \\ \text{setpoint}_{\text{el}}(t) = 0 \end{cases} \qquad \forall t \tag{B.1}$$

If the hydrogen storage is empty:

$$\text{If } H_{\text{storage}} \leq H_{\min} + P_{\text{fc,min}} \Rightarrow \begin{cases} \text{binary\_variable}_{\text{fc}}(t) = 0 \\ \text{setpoint}_{\text{fc}}(t) = 0 \end{cases} \qquad \forall t \tag{B.2}$$

While solving this problem, another problem showed, that it was found that only the first hour of the horizon (at T=0) was punished when turning on/off the electrolyser or fuelcell and not within the entire horizon. This was changed, and now turning the components on/off is punished for every step within the prediction horizon.

Now the results show the answer that is expected. First off, the maximum grid usage is the expected 29.13 kW. Secondly, Figure B.13 shows that the change in setpoints is much greater than in a normal run.

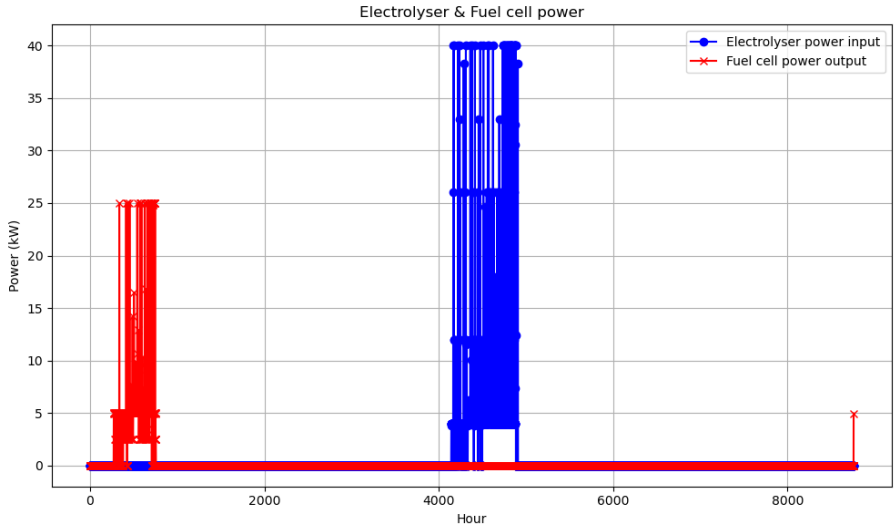

Figure B.13: Electrolyser input and fuel cell output power: lambda change setpoint equal to zero

Furthermore, the amount of operational hours of the electrolyser decreases from 724 to 651 hours, and the amount of operational hours from the fuel cell decreases from 487 to 417 hours.
Concluding that the verification test works as expected.

λ_on_off and λ_setpoint_change are equal to zero:
Hypothesis: The (maximum) grid usage will stay the same, but as the control of the electrolyser and fuel cell is turned off, it is expected that the electrolyser and fuel cell turn on/off frequently and have great changes in the setpoint.

Conclusion: the grid usage throughout the year and the maximum grid import and export are the same, as can be seen in Figure B.14.

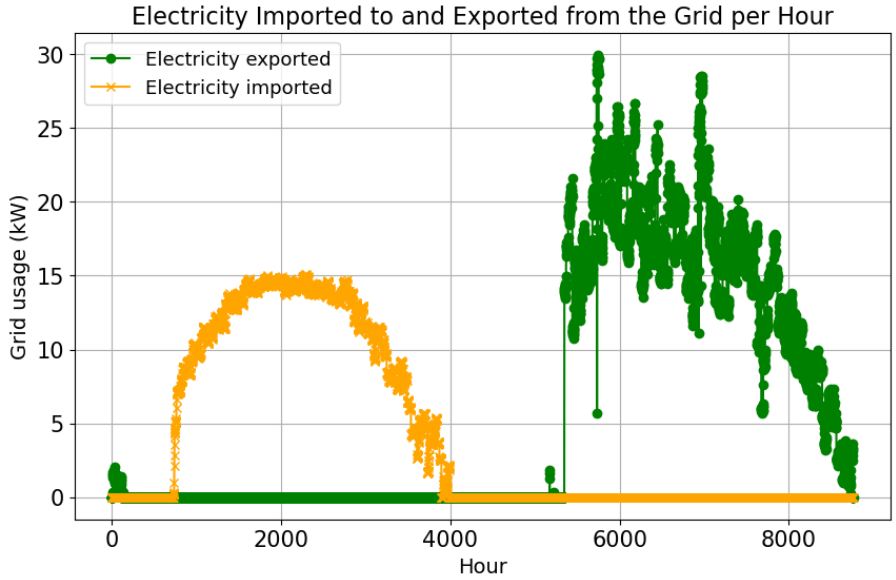

Figure B.14: Hourly grid grid import and export: lambda on/off and lambda setpoint change equal to zero

Additionally, as expected, the control of the electrolyser and fuel cell is turned off, the change between the setpoints is great, and they are frequently turned on and off, as can be seen in Figure B.15.

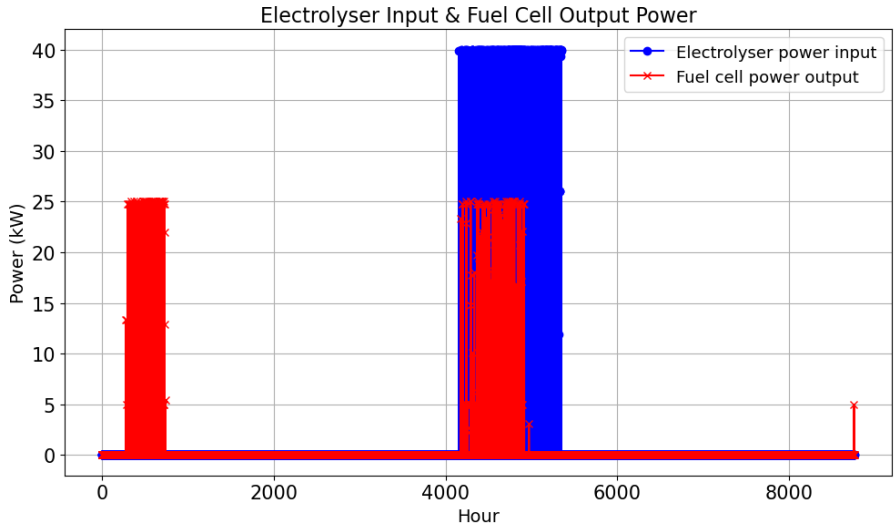

Figure B.15: Electrolyser input and fuel cell output per hour: lambda on/off and lambda setpoint change equal to zero

λ_grid and λ_setpoint_change are equal to zero:
Hypothesis: The grid usage will increase as there is no motivation for the model to minimise the grid usage. Additionally, the electrolyser and fuel cell will not turn off and on after, but will have great changes in setpoint.

Conclusion: The peak grid usage is the maximum 40 kW for both the import and the export to the grid, as there is no punishment for using the grid, and there is a punishment for using the electrolyser and fuel cell, as can be seen in Figure B.16. This results in the model not using the electrolyser and fuel cell at all.

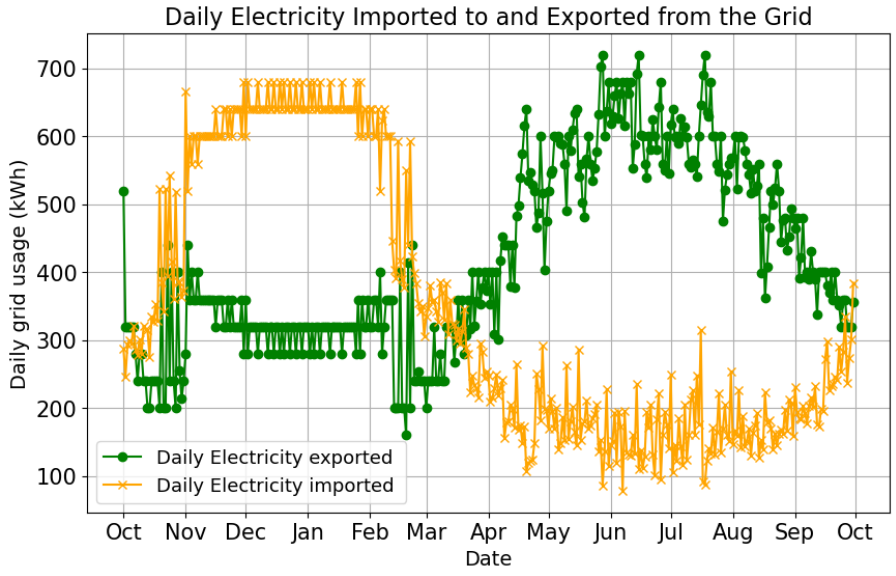

Figure B.16: Daily grid usage: lambda grid and lambda on/off equal to zero

λ_grid and λ_on_off are equal to zero:
Hypothesis: The grid usage will increase as there is no motivation for the model to minimise the grid usage. There is only a punishment for using the electrolyser and fuel cell, they will not be used.

Conclusion: The peak grid usage is the maximum 40 kW for both the import and the export to the grid, as there is no punishment for using the grid, and there is a punishment for using the electrolyser and fuel cell, as can be seen in Figure B.17. Notice that the pattern is different to that of Figure B.16.This results in the model not using the electrolyser and fuel cell at all.

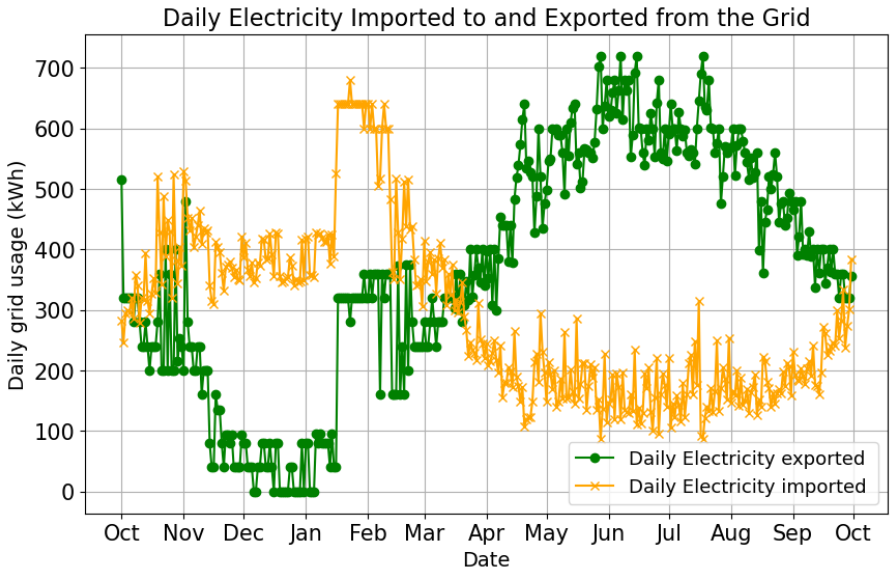

Figure B.17: Daily grid usage: lambda grid and lambda setpoint change equal to zero

Prection horizon
To check if the prediction horizon works, the prediction horizon will be set to 1 hour. Effectively removing the ability of the model predictive control to look further than the current hour in the model.

Hypothesis: As it is not possible for the model to plan ahead, it is expected that the model will use the electrolyser and fuel cell more often, as well as the grid.

Conclusion: At first, the MPC gave the error: "MPC optimisation did not find an optimal solution. This can be expected as the model should behave much less efficiently than it did before. To solve this error, the grid capacity limit was increased to 100 kW.
This solved the error. The model now uses more grid power. Increasing the max electricity exported to the grid from 30.30 kW to 86.7 kW and the max electricity imported from the grid from 15.15 kW to 35.24 kW. While the total amount imported from the grid and exported to the grid did not change a lot.
Concluding that the verification check works as expected.

Reusing (exergy) heat
To check if the exergy heat works, the exergy results of the model will be compared to a hand calculation.
The simulation will be run for only the months of September, October and November. These months are chosen because this is the transition from a positive to a negative net energy generation, and the seasonal energy storage would be empty halfway through November. This allows for testing all situations that can occur during the model (empty or full seasonal energy storage and positive or negative net energy generation). By running the model only for two months, the uncertainty and complexity of the hand calculation are reduced without reducing the added value of the verification check. At the start of the run, both the daily battery and the seasonal energy storage are half full, 90 kWh and 2400 kWh, respectively.

The useful pictures with results of the run can be seen in Figure B.18 and Figure B.19. These figures might be useful to understand the simulation run.

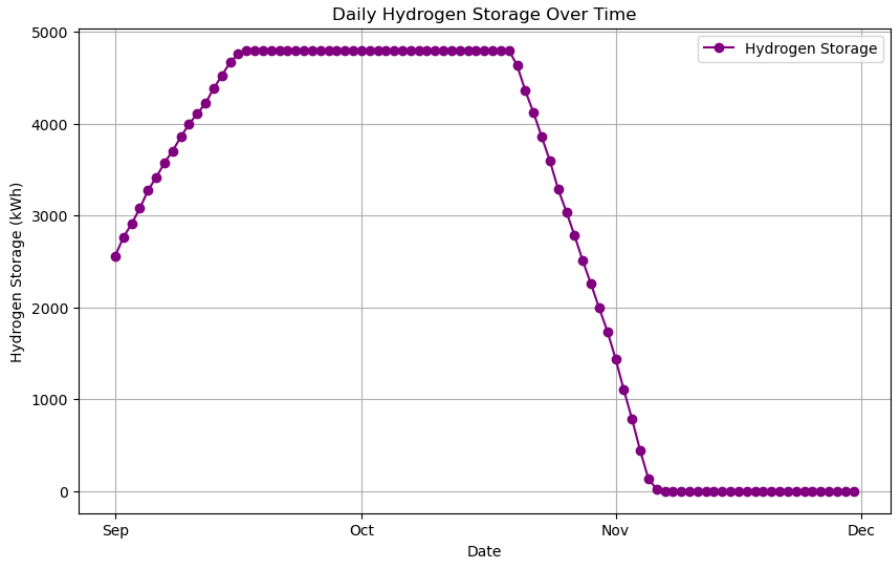

Figure B.18: hydrogen storage over time result for hand calculation

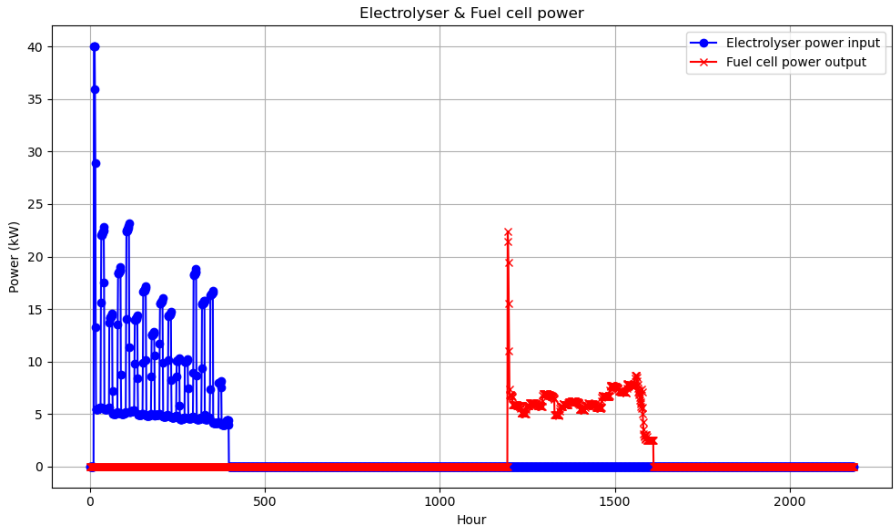

Figure B.19: Electrolyser and fuel cell power over time result for hand calculation

The inputs and results of the run that will be used for the hand calculation can be found in Table B.3.

Table B.3: Inputs for hand calculation

Parameter	Value	Unit
efficiency electrolyser	0.70	%
efficiency fuel cell	0.54	%
Non-zero setpoint electrolyser	386	hours
Non-zero setpoint fuel cell	417	hours
Average non-zero setpoint electrolyser	8.9	kW
Average non-zero setpoint fuel cell	6.2	kW
Useful waste heat electrolyser	86	%
Useful waste heat fuel cell	80	%
Unreacted hydrogen fuel cell	5	%
Average ambient temperature	284.8	°K
Average operating temperature electrolyser	330	°K
Average operating temperature fuel cell	339	°K
Temperature absorption process	293	°K
Temperature desorption process	333	°K
Absorption enthalpy	24.3	kJ/mol
Desorption enthalpy	27.4	kJ/mol
LHV H2	241.92	kJ/mol

Please note that the efficiency and operating temperatures are, during this test, forced to be constant. This simplified the hand calculation, without reducing the added value of the energy balance check. Because these variables have already been tested in previous verification checks.

Exergy calculation electrolyser:

$$\begin{aligned} \text{Heat production}_{el} &= \text{Active hours}_{el} \cdot \text{Average setpoint}_{el} \cdot (1 - \text{Efficiency}_{el}) \cdot \text{Useful heat fraction}_{el} \\ &= 886 \text{ kWh} \\ \text{Exergy heat}_{el} &= \text{Heat production} \cdot \left(1 - \frac{T_{\text{ambient}}}{T_{\text{electrolyser}}}\right) \\ &= 121 \text{ kWh} \end{aligned} \tag{B.3}$$

Exergy calculation absorption process:

$$\begin{aligned} \text{Heat production}_{abs} &= \frac{\Delta H_{\text{abs}}}{\text{LHV}} \cdot \text{Active hours}_{el} \cdot \text{Average setpoint}_{el} \cdot \text{Efficiency}_{el} \\ &= 230 \text{ kWh} \\ \text{Exergy heat}_{abs} &= \text{Heat production}_{abs} \cdot \left(1 - \frac{T_{\text{ambient}}}{T_{\text{absorption}}}\right) \\ &= 6 \text{ kWh} \end{aligned} \tag{B.4}$$

Exergy calculation desorption process:

$$\begin{aligned} \text{Heat production}_{abs} &= \frac{\Delta H_{\text{des}}}{\text{LHV}_{H_2}} \cdot \frac{\text{Active hours}_{fc} \cdot \text{Average setpoint}_{fc}}{\text{Efficiency}_{fc}} \\ &= -542 \text{ kWh} \\ \text{Exergy heat}_{des} &= \text{Heat production}_{des} \cdot \left(\frac{1 - \frac{T_{\text{amb}}}{T_{\text{des}}}}{1 - \frac{T_{\text{amb}}}{T_{\text{fc}}}}\right) \\ &= -498 \text{ kWh} \end{aligned} \tag{B.5}$$

Exergy calculation fuel cell:

$$\begin{aligned}\text{Heat production}_{fc} &= \frac{\text{Active hours}_{fc} \cdot \text{Average setpoint}_{fc}}{\text{Efficiency}_{fc}} \cdot (1 - \text{Efficiency}_{fc} - \text{Unused H2}) \cdot \text{Useful heat fraction}_{fc} \\ &= 1570 \text{ kWh} \\ \text{Exergy heat}_{fc} &= (\text{Heat production}_{fc} + \text{Heat production}_{abs}) \cdot \left(1 - \frac{T_{\text{ambient}}}{T_{\text{fuelcell}}}\right) \\ &= 169 \text{ kWh}\end{aligned} \tag{B.6}$$

Total exergy production = exergy_{el} + exergy_{abs} + exergy_{fc} = 296 kWh.

This result of the hand calculation is quite close to the result of the model: total exergy production = 293 kWh. The error between the two solutions (of 3 kWh) could be explained due to rounding errors. Concluding that the exergy heat is reused in the model, as was expected.

Energy Balance Check
This is the most important check in the verification, as the thermodynamic laws are not actively used in this model. This could create a situation where the model 'creates' energy. The energy balance check is used to check if this is happening.
The simulation will be run for only the months of September, October and November. These months are chosen because this is the transition from a positive to a negative net energy generation, and the seasonal energy storage would be empty halfway through November. This allows testing all situations that can occur during the model (empty or full seasonal energy storage and positive or negative net energy generation). At the start of the run, the daily battery and the seasonal energy storage are filled up to 190 kWh and 1500 kWh, respectively.
Additionally, the following components, which have proven to be working as expected in other verification checks, are not taken into account in the hand calculation and turned off in the model. This simplified the hand calculation, without reducing the added value of the energy balance check.

- The reuse of exergy heat
- Degradation of components
- Start-up of components
- A constant value is used for the efficiency of the electrolyser and the fuelcell, 70% and 54%, respectively.

To make this calculation, the raw input data from Excel is used to prevent any use of values calculated in Python. The sum of the net energy is the PV generation, and subtract all the demands. The total net energy is -5515 kWh and corresponds to the sum of the net_energy_history in Python.

In figure Figure B.20, it is shown that the metal hydride storage is charged until just reaching the upper boundary of 4800 kWh. Therefore, ((4800-1500)/0.7) 4714 kWh of power for the electrolyser is required, bringing the total net energy to (-5515 - 4714) -10230 kWh.

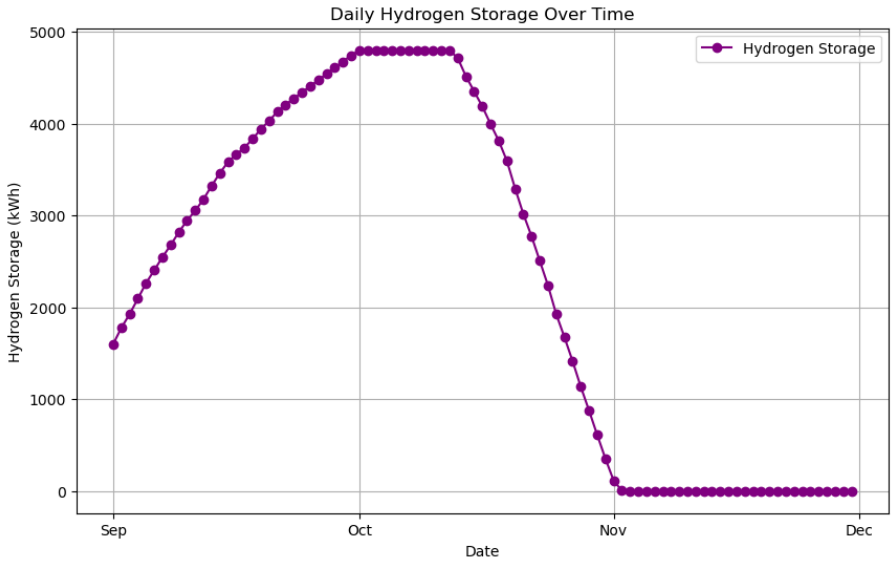

Figure B.20: Hydrogen storage over time Energy balance check

The daily battery and metal hydride storage store together (4800*0.54 + 190) 2782 kWh of electrical energy. This means that the remaining total net energy of (-10230 + 2782) -7448 kWh should come from the grid.

The results of the model export 20 kWh to the grid, and the import to the grid is 7617 kWh. In total, 7761 kWh is imported from the grid.
This leaves a difference of (-7448 -20 + 7617) 149 kWh. This energy difference could not be explained.

It was eventually found that after calculating the outputs of the MPC, the battery energy level state was updated in two separate steps within each time increment. While within the MPC, this was done in one timestep. The two steps can be seen in Equation B.7.

$$\begin{aligned} \text{net\_energy\_effective} &= \text{electricity\_input\_total[global\_hour]} - \text{electricity\_demand[global\_hour]} - \text{effective\_heat} \\ \text{battery\_energy} &\mathrel{+}= -\text{applied\_electrolyser\_power} + \text{actual\_fuelcell\_output} + (\text{grid\_input} - \text{grid\_export}) \end{aligned} \tag{B.7}$$

In the first step, the battery energy level was adjusted using the net_energy_effective based on the effective heat demand, electricity demand, and surplus or shortage from the PV panel production. Subject to the (dis)charge limits, the code then updated the battery state by either charging (if net_energy_effective >= 0) or discharging (if negative).

The second step introduced the flow of power to the electrolyser or grid, or from the fuel cell or grid. Although these two steps nominally operate on different inputs, both updates affect the same battery level state. In effect, energy flows related to the conversion processes and grid exchanges were being added twice: once through the net balance (which indirectly included these flows) and a second time directly. In the overall simulation, this redundancy resulted in an energy imbalance of about 149 kWh.

The battery level state was combined into a single step to address this problem, as can be seen in Equation B.8. The definition of the variable delta_energy allowed for adding all the flow of energy in one step. This single step ensures that each energy contribution is accounted for once, instead of twice.

$$\begin{aligned} \text{delta\_energy} = \text{electricity\_input\_total[global\_hour]} &- \text{electricity\_demand[global\_hour]} \\ &- \text{effective\_heat} - \text{applied\_electrolyser\_power} \\ &+ \text{actual\_fuelcell\_output} + (\text{grid\_input} - \text{grid\_export}) \end{aligned} \tag{B.8}$$

After implementing the changes, the check is done again. The results are the same until the model imports and exports energy from the grid. Now, the model export is 44 kWh to the grid, and the import is 7490 kWh. In total, 7446 kWh is net imported grid energy.
This leaves a difference of -2 kWh. This difference could be explained due to rounding errors. Concluding that the energy balance check has now passed the verification check.

C

Appendix: Extreme Cases

For all the extreme cases, the test data that will be checked per case, and the most extreme case of the input data, will be used.

Extreme Case PV Generation
All the extreme cases are taken for 14 days. This has been determined by the fact that the period of days without sun in the Netherlands is 14 days, measured in 1959 (NU.nl, 2024).

Maximum PV Generation During the Summer
The day of the year with the maximum sum of PV generation was measured in 2013 on the 2nd of June, in total 1179 kWh of electricity was generated. To build the extreme case, the data from this day is used for 14 days in a row, as can be seen in Figure C.1.

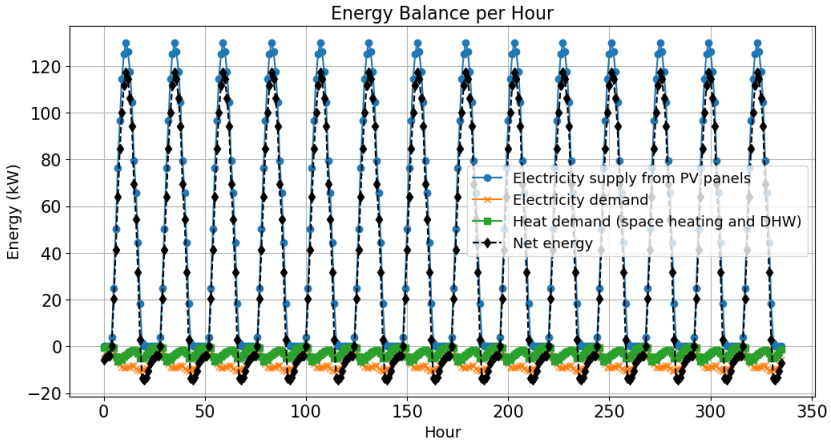

Figure C.1: Maximum PV generation during the summer: Energy balance per hour

Case 1: Normally, the metal hydride is already full in this period. What is the maximum grid capacity required in this extreme case?

As can be seen in Figure C.2, the required grid capacity is 55.6 kW.

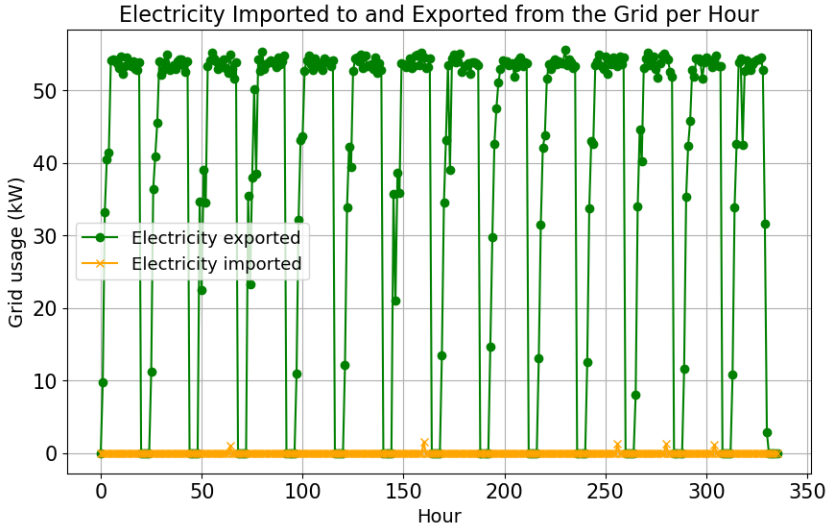

Figure C.2: Case 1: Grid usage per hour

Case 2: If starting from an empty metal hydride, with no maximum storage capacity, what would be the storage level at the end of the 14 days?

It is found that the calibration of the model is not optimal in this extreme case, as the electrolyser is not turned off and barely changes setpoint, as can be seen in Figure C.3. While in the meantime, during the hours without electricity from the PV panels, the grid is used to compensate for the required power of the electrolyser, as can be seen in Figure C.4. The final hydrogen storage level is 8.0 MWh, as can be seen in Figure C.5. It took 203 hours to reach the original capacity of the metal hydride of 4.8 MWh.

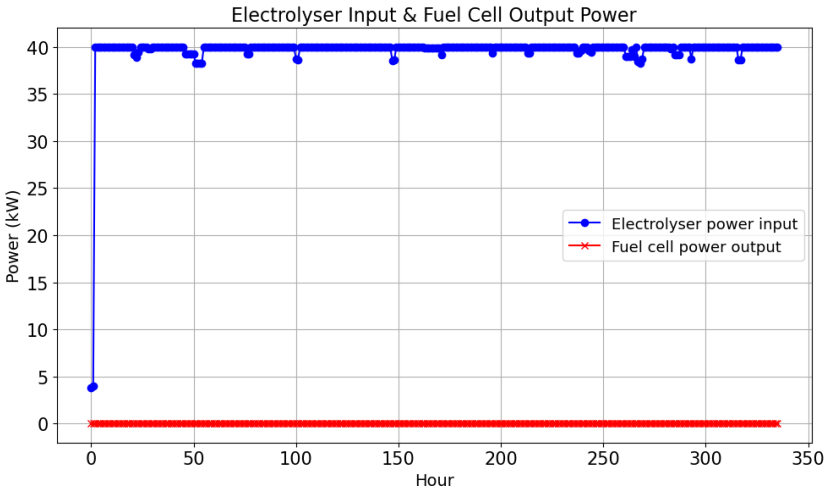

Figure C.3: Case 2: electrolyser input power

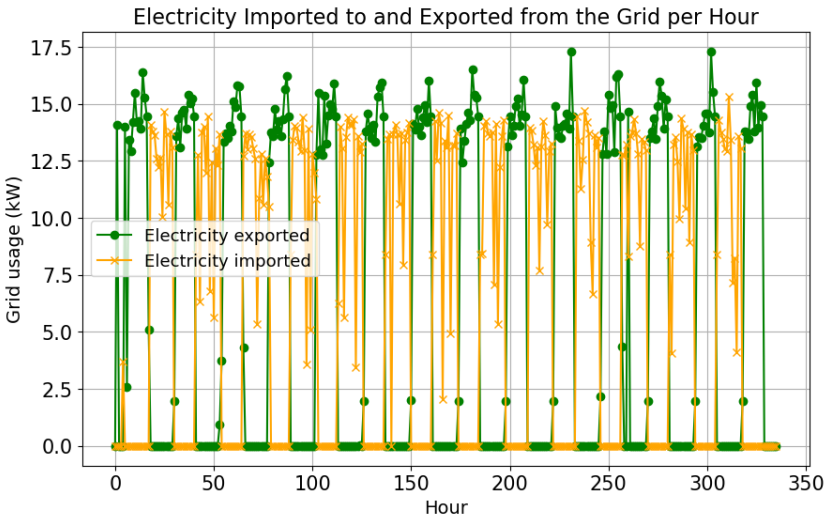

Figure C.4: Case 2: Grid usage per hour

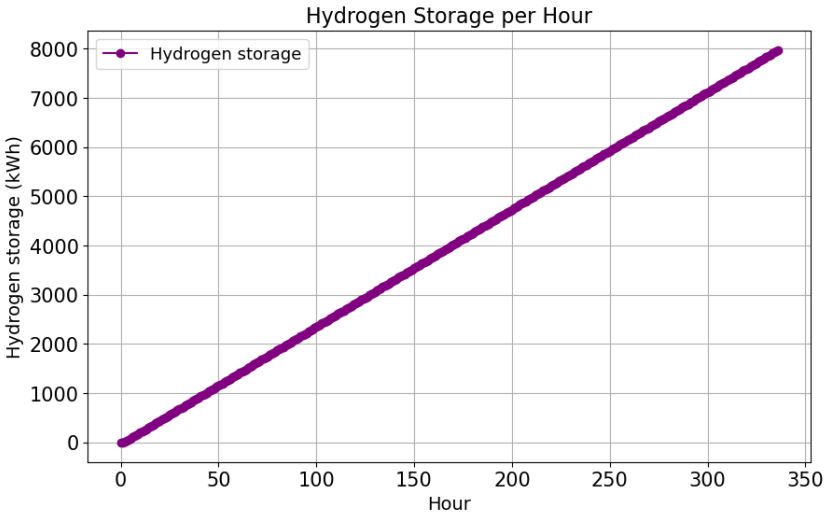

Figure C.5: Case 2: Hydrogen storage per hour

Minimum PV Generation During the Winter
The day of the year with the minimum sum of PV generation was measured in 2013 on the 27th of December; in total, 17 kWh of electricity was generated. To build the extreme case, the data from this day is used for 14 days in a row, as can be seen in Figure C.6.

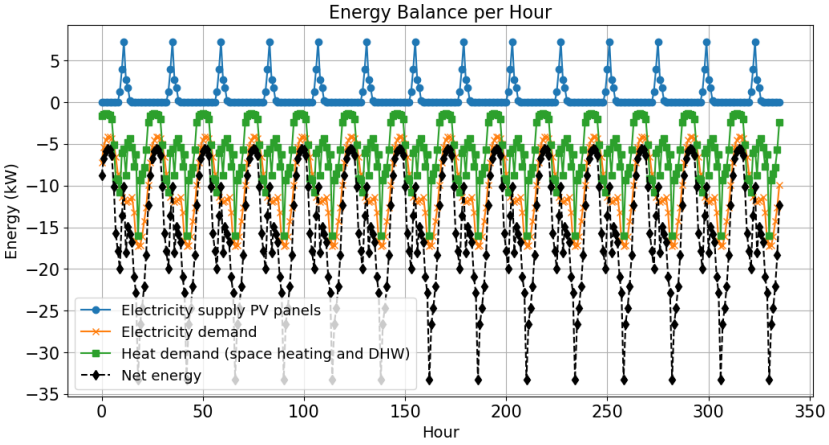

Figure C.6: Minimum PV generation during the winter: Energy balance per hour

Case 3: Normally, the metal hydride is already empty in this period. What is the maximum grid capacity required in this extreme case?

As can be seen in Figure C.7, the required grid capacity is 15.8 kW.

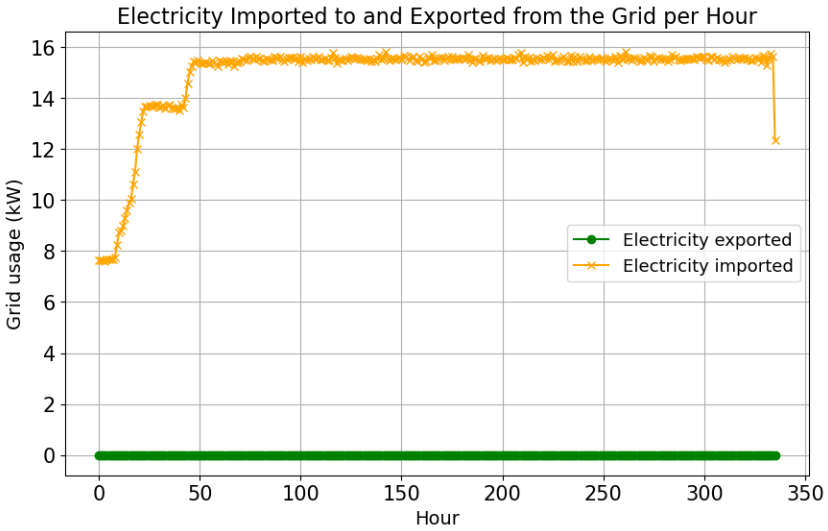

Figure C.7: Case 3: Grid usage per hour

Case 4: If starting from a full metal hydride, how many days does it take to use the entire metal hydride storage?

As can be seen in Figure C.8, it takes 195 hours to discharge the metal hydride storage. Although about 0.1 MWh of hydrogen is stored until hour 312, this is the hour when the prediction horizon has the last 24 values within the horizon.
From the moment the metal hydride storage is empty, the grid starts to be used again, resulting in the same required grid capacity of 15.8 kW.

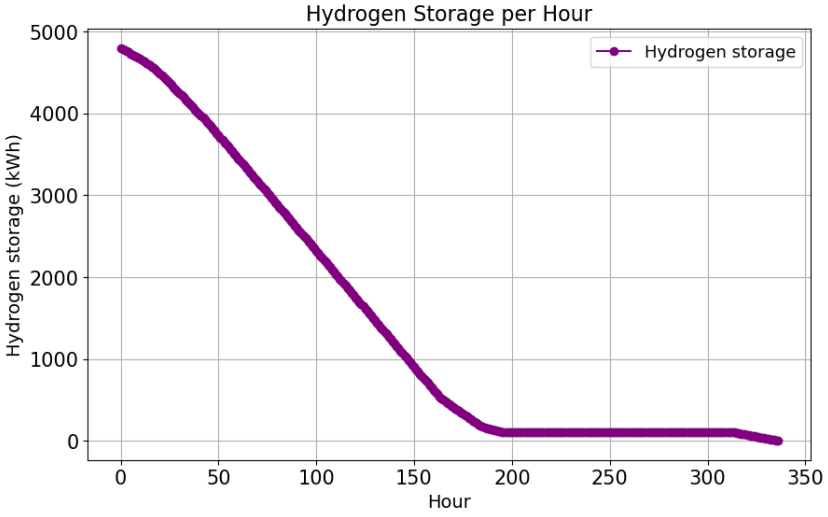

Figure C.8: Case 4: hydrogen storage per hour

Extreme Case Net Energy
All the extreme cases are taken for 14 days. This has been determined by the fact that the period of days without sun in the Netherlands is 14 days, measured in 1959 (NU.nl, 2024).

Maximum Net Energy surplus in the Summer
The day with the maximum sum of net energy surplus was measured on the 2nd of June, the same as for the maximum PV generation during the summer case. However, for this case, the metal hydride storage has its original maximum capacity of 4.8 MWh.

As can be seen in Figure C.9, it takes 230 hours to charge the metal hydride storage. From the moment the metal hydride storage is full, the grid starts to be used (as can be seen in Figure C.10), resulting in a required grid capacity of 54.2 kW

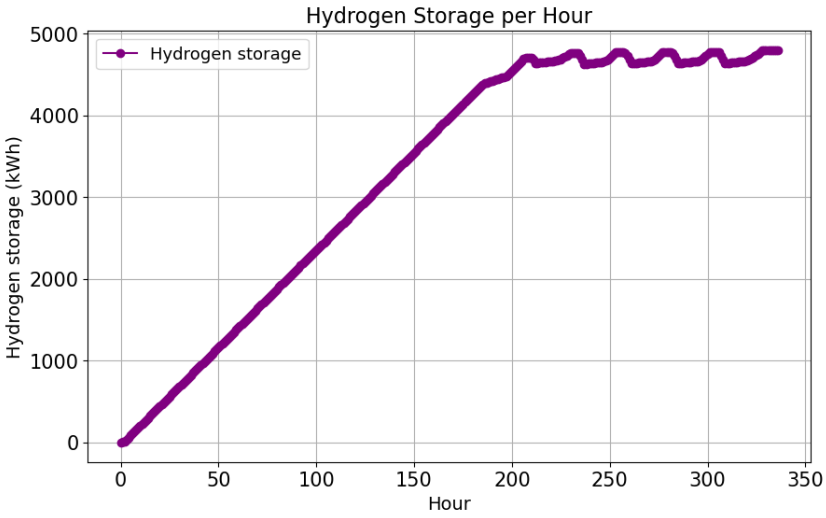

Figure C.9: Extreme case 5: Maximum net energy surplus in the summer - Hydrogen storage per hour

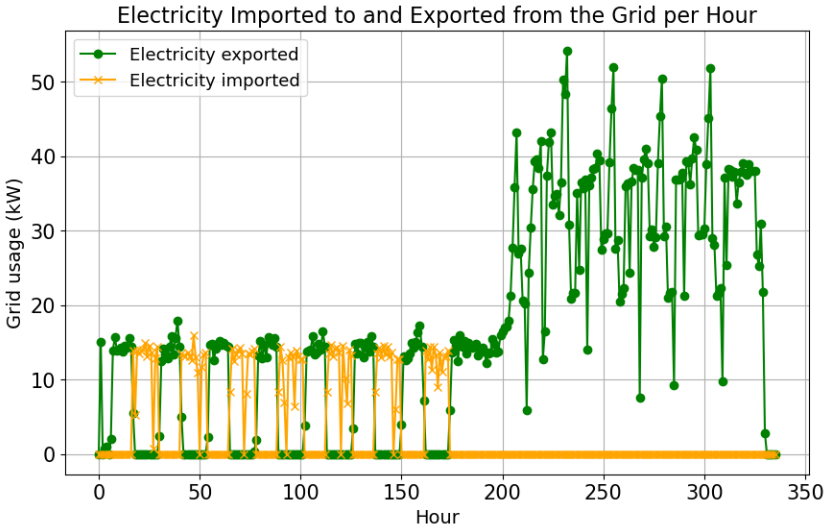

Figure C.10: Extreme case 5: Maximum net energy surplus in the summer - Grid usage per hour

Minimum Net Energy Demand in the Winter
The day of the year with the minimum net energy demand in the winter is the 19th of January; in total, there was a shortage of 399 kWh of net energy. To build the extreme case, the data from this day is used for 14 days in a row, as can be seen in Figure C.11.

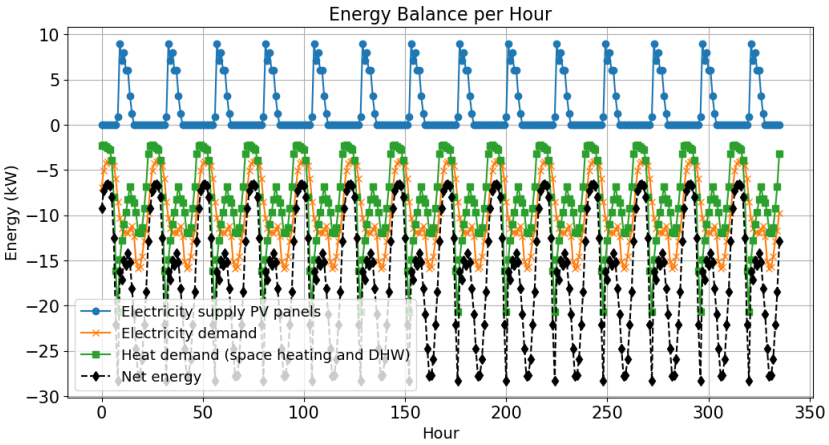

Figure C.11: Minimum net energy demand during the winter: Energy balance per hour

Case 6: Normally, the metal hydride storage is already empty in this period. What is the maximum grid capacity required in this extreme case?

As can be seen in Figure C.12, the required grid capacity is 16.9 kW.

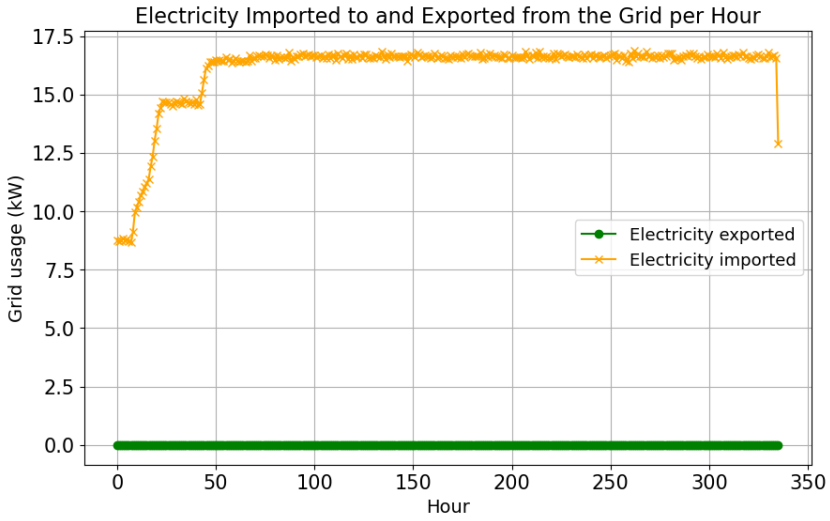

Figure C.12: Case 6: Grid usage per hour

Case 7: If starting from a full metal hydride, how many days does it take to use the entire metal hydride storage?

As can be seen in Figure C.13, it takes 185 hours to discharge the metal hydride storage. Although about 0.1 MWh of hydrogen is stored until hour 312, which is the hour when the prediction horizon has the last 24 values within the horizon. From the moment the metal hydride storage is empty, the grid starts to be used again, resulting in the same required grid capacity of 16.9 kW

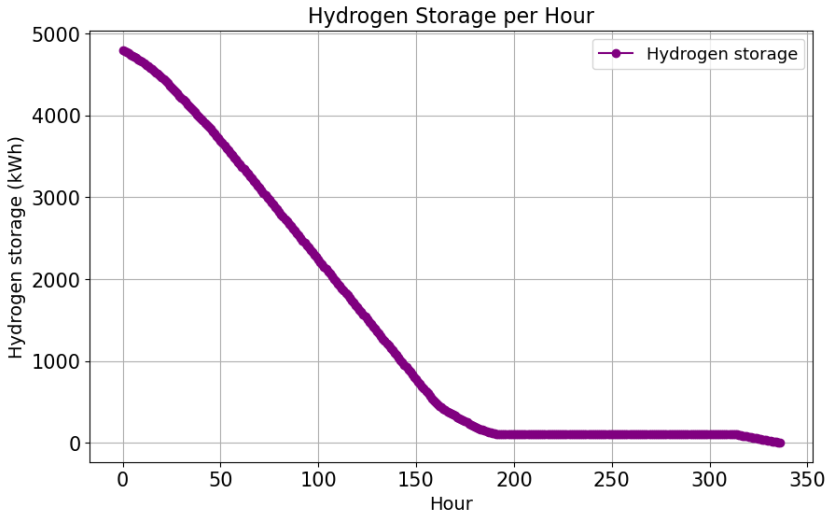

Figure C.13: Case 7: Hydrogen storage per hour

Case 8: Degradation of Components
The lifetime of the PEM electrolyser, metal hydride and PEM fuel cell is finite in the model as there is degradation. The end of life is different for each of the components.
The end of life for the PEM electrolyser is reached when degraded by 10% (U.S. Department of Energy, 2023). It takes 52631 hours of operation until the electrolyser reaches the end of its life.
The end of life for the PEM fuel cell is reached when degraded by 10% (Wu et al., 2008). It takes 25000 hours of operation until the fuel cell reaches the end of its life.

The higher the degradation, the lower the efficiency of the electrolyser and the fuelcell. Therefore, more energy is required as input to reach the same output. To make a better estimation of the operational hours when the system is at the end of its life, a run will be done with the degraded starting values for all the components (using average data of the 10 years). The average number of operational hours of the first year of operation and the last year of operation will be taken to determine the average number of operational hours per year. The results can be seen in Table C.1

	Operation hours: no degradation	Operational hours: max degradation	Average hours
Electrolyser	500	699	600
Fuel cell	727	385	556

Table C.1: Operational hours without degradation and with full degradation

This results in a lifetime of 87 years for the electrolyser and 44 years for the fuel cell.

The end of life for the TiFe Metal hydride is reached when degraded by 20% (L. Zhang, 1998). It takes 1176 cycles until the metal hydride reaches the end of its life. It experiences 2 full cycles in a year, taking 588 years of use until the metal hydride is fully degraded.

This lifetime expectancy is very long. However, the effect values for degradation are determined by the use of a system that runs for more hours during the year. When running this little hour during the year, calendar time degradation becomes more important, which involves aspects such as corrosion and membrane drying.

Remove components from the system:
The year 2013 is used, as it has the relatively worst performance of the two test years.

Case 9: Available component: grid
The metal hydride storage is set to 0 kWh capacity and the daily battery to 0.001 kWh capacity, because setting it to 0 causes decision by zero errors in the model.

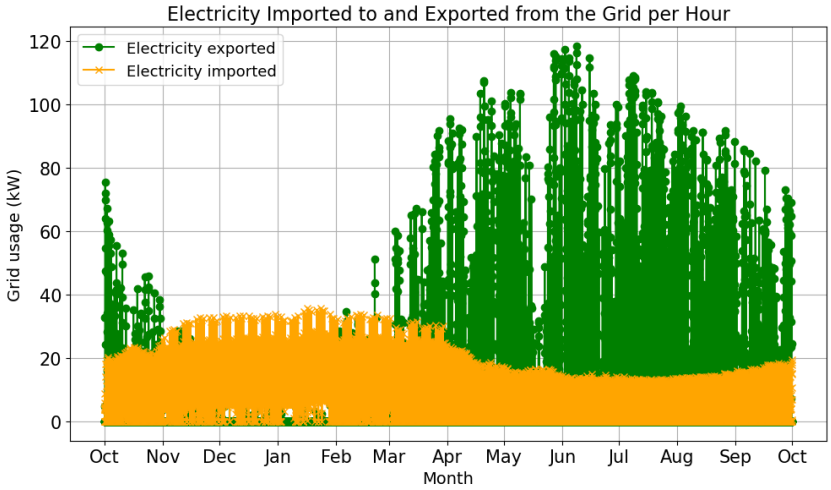

Figure C.14: Extreme case 9: Available component: grid: Grid level per hour

In Figure C.14, it can be seen that the peak of the electricity import is 36.6 kW, with a total grid import of 68.6 MWh kWh. As the peak export to the grid is 122.1 kW, with a total export of 95.1 MWh.

Case 10: Available component: Daily Battery
The year 2013 is used, as it has the relatively worst performance of the two test years.

The year starts with a full daily battery; to be able to do so, the year needs to start on the 15th of October, as the surplus of energy at the start of October, that can't be stored in the metal hydride or sent to the grid. To be able to sustain over multiple years, the required energy over the year, the daily battery should be full at the end of the year as well.
Neither the grid nor the metal hydride can be used.

Keep in mind that a minimalistic version of the daily battery was used in the model, as there are no efficiency losses. Additionally, the self-discharge losses are not taken into account. Therefore, the outputs of this extreme case do not correspond to a real case, but show the extreme case of the model.

As a result, 239 PV panels are required instead of 300, and a 41.9 MWh capacity for the daily battery. In Figure C.15, the daily battery level over the year is shown.

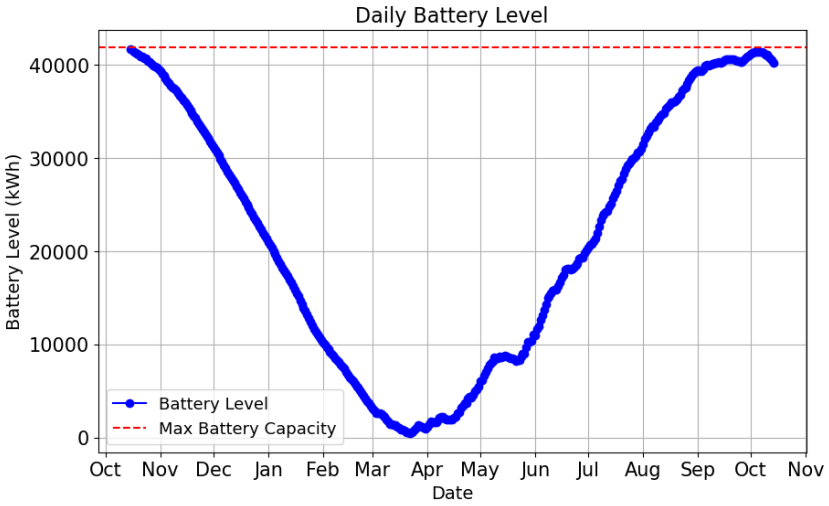

Figure C.15: Extreme case: Only using the daily battery: Battery level per day

Case 11: Available component: metal hydride
The year 2013 is used, as it has the relatively worst performance of the two test years.

The year starts with a full metal hydride; to be able to do so, the year needs to start on the 15th of October, as the surplus of energy at the start of October, that can't be stored in the metal hydride or sent to the grid. To be able to sustain over multiple years, the required energy over the year, the metal hydride should be full at the end of the year as well.
Neither the grid nor the daily battery can be used. However, it is not possible in the model to set the daily battery capacity to 0 kWh; 20 kWh is the minimum battery capacity that is required for the model to not result in an error in this extreme case.
As the grid is unavailable, the electrolyser power should be increased to 167 kW to match the maximum net energy generation. The fuel cell should be increased to 26 KW to match the lowest net energy value.
To be able to fully charge the metal hydride at the end of the year, 426 PV panels are required instead of 300.

As a result, a 63.0 MWh metal hydride storage is required. In total, 8.3 20ft containers are required for the storage of the metal hydride. In Figure C.16, the daily metal hydride storage level over the year is shown.

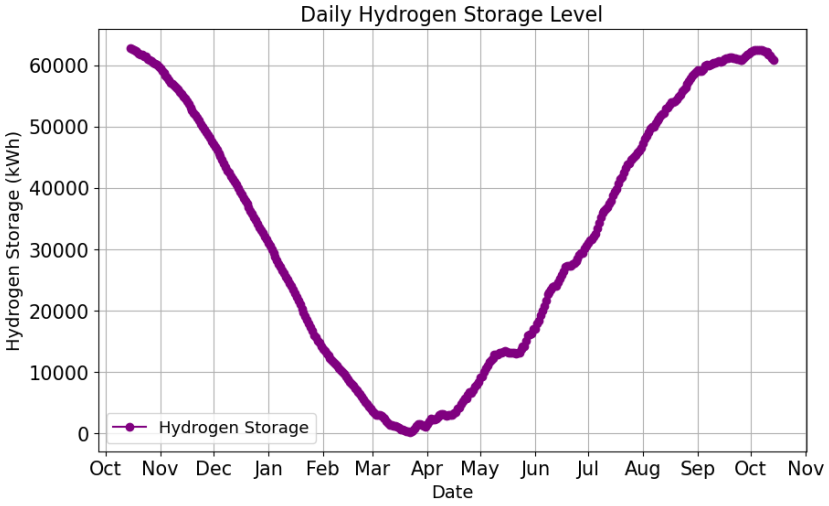

Figure C.16: Extreme case: Only using the metal hydride: Metal hydride level per day

Case 12: Off-grid system
The year 2013 is used, as it has the relatively worst performance of the two test years.

The year starts with a full metal hydride; to be able to do so, the year needs to start on the 15th of October, as the surplus of energy at the start of October, that can't be compensated for by the grid.
In case there is no grid available, the metal hydride storage should be large enough to cover the entire net energy demand with the metal hydride storage and be able to recharge the metal hydride storage back to full again, to be ready for next year. This is calculated by changing the size of the metal hydride as well as the number of PV panels. As the original total PV generation is insufficient to charge the metal hydride storage to full again.

This results in an increase of the size of the metal hydride storage from 4.8 MWh to 60.8 MWh, as can be seen in Figure C.17. In total, 8.1 20ft containers are required for the storage of the metal hydride. Additionally, an increase of PV panels from 300 to 346 is required to fill the metal hydride storage back up to full again at the end of the year.

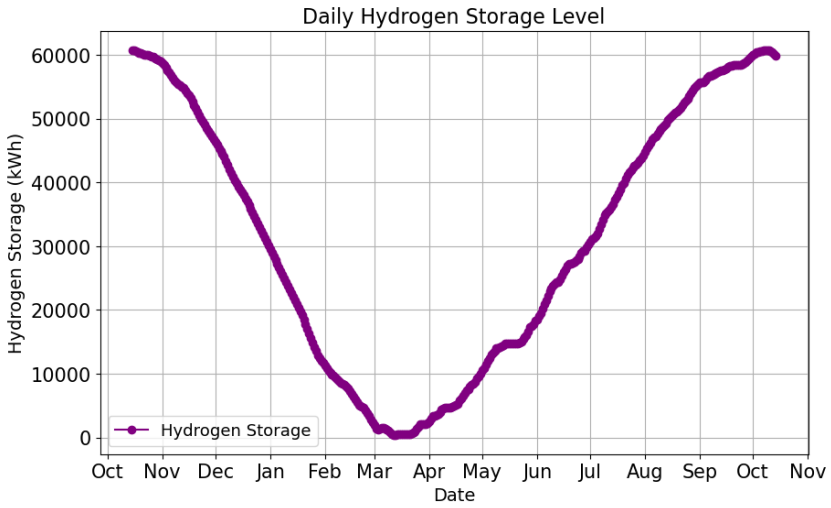

Figure C.17: Extreme case: No grid capacity available: Metal hydride storage per day

Grid Power outage

During a power outage, the grid is not available to be used. In reality, there is no export or import of electricity possible. In code, only the import of electricity will be set to 0 kW. In reality, the solar panels will be turned off to prevent the surplus of electrical energy from being exported to the grid. To imitate this in the code, the export to the grid will be unlimited. All the electricity in the model that is exported will be curtailed in reality.

The year 2013 is used, as it has the relatively worst performance of the two test years.
The extreme cases of the start of the astrometric seasons will be put to the test.

Case 13: How Long Could the System Last if There Is a Power Outage During the Summer

During the start of the summer (21st of June), the metal hydride storage is already full under normal conditions. This means that all the surplus electricity from the solar panels is curtailed in the summer. From the moment that the net energy becomes negative, the metal hydride storage needs to be used.

This results in a possible power outage of 135 days. In the first 110 days, the PV production in combination with the daily battery is sufficient to fulfil the energy demand. From day 111, as can be seen in Figure C.18, the metal hydride needs to be used; after 25 days, the metal hydride storage is empty. From that moment on, the system would need to start using the grid.

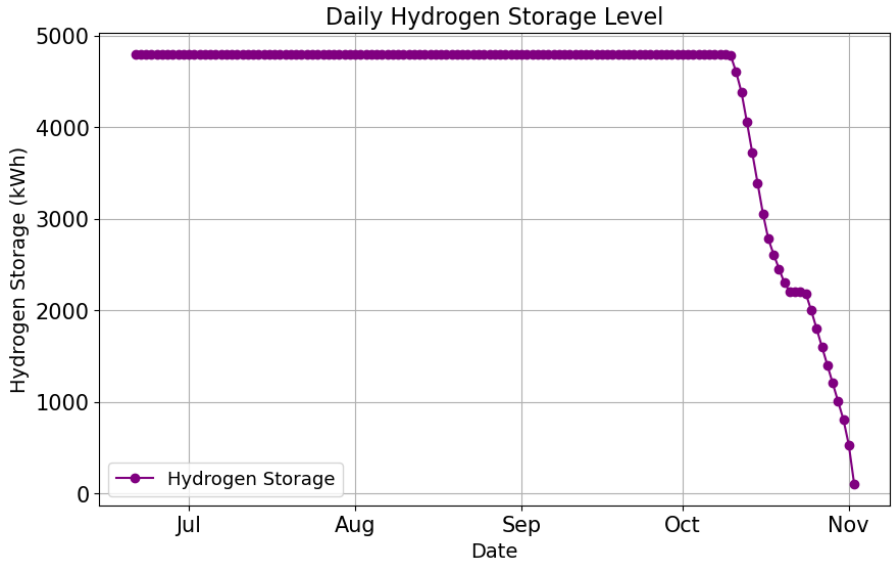

Figure C.18: Extreme case: grid outage summer: Hydrogen storage per day

In Figure C.19, it can be seen how much electricity from the PV power should be curtailed in reality per day. In total, 36 MWh of electricity from the PV panels needed to be curtailed in the summer.

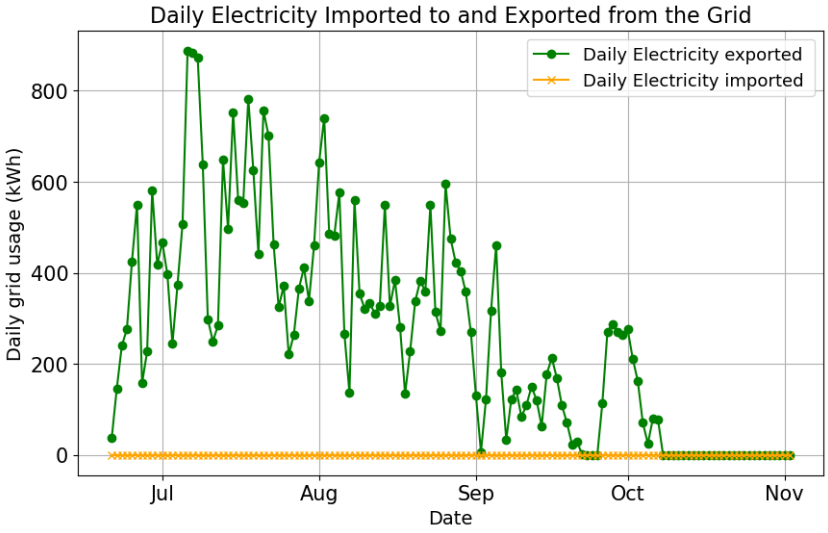

Figure C.19: Extreme case: grid outage summer: Grid export per day

Case 14: How Long Could the System Last if There Is a Power Outage During the Autumn
During the start of the autumn (22nd of September), the metal hydride storage is already full under normal conditions.

Therefore, the results are the same for the summer, but the power outage would only be able to last for 42 days, as there are fewer days with a positive net energy generation, compared to starting in the summer.

Case 15: How Long Could the System Last if There Is a Power Outage During the Winter
During the start of the winter (21st of December), the metal hydride storage is already empty under normal conditions. In that case, a full daily battery would empty after 1 day. From the second day, the system would need to start using the grid.

However, in order for this extreme case, the run will also start with a full metal hydride. This results in a possible power outage of 8 days. In Figure C.20, it can be seen that after 8 days, the metal hydride storage is empty. From that moment on, the system would need to start using the grid.

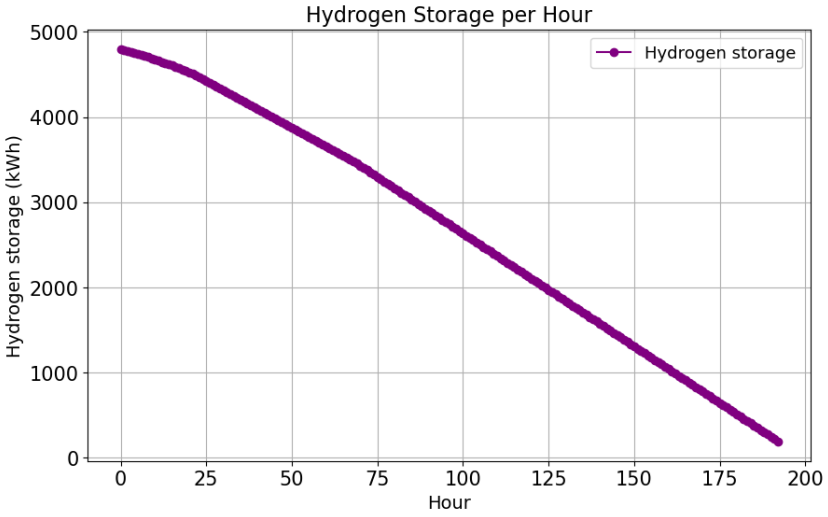

Figure C.20: Extreme case: grid outage winter: Grid export per hour

Case 16: How Long Could the System Last if There Is a Power Outage During the Spring
During the start of the spring (20th of March), the metal hydride storage is almost empty (around 800 kWh) under normal conditions. But the net energy is high enough during the not require the grid. Therefore, the results are the same as for the summer, but the power outage would be able to last for 228 days, as there are more days with a positive net energy, compared to starting in the summer. In Figure C.21, the metal hydride storage level per day can be seen.

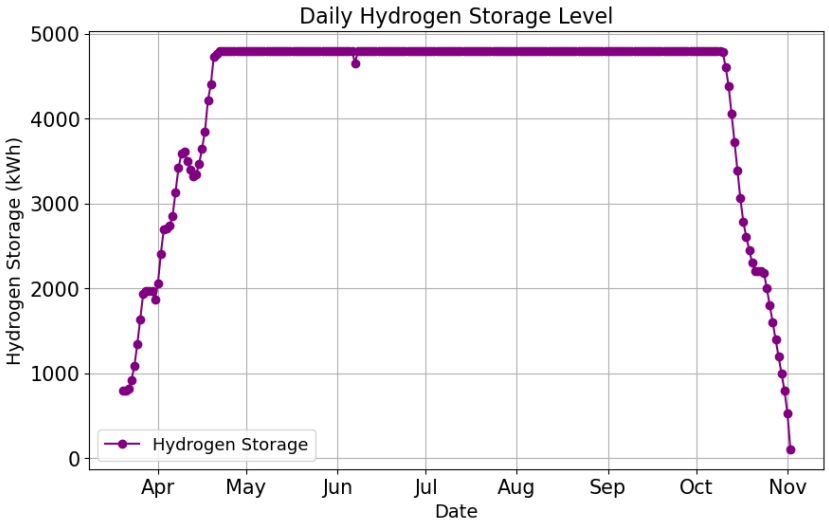

Figure C.21: Extreme case: grid outage spring: Hydrogen storage per day

In total, 58 MWh of electricity from the PV panels needed to be curtailed during the spring and summer.

D

Appendix: Python Code

```python
import numpy as np
import matplotlib.pyplot as plt
import matplotlib.dates as mdates
import pandas as pd
from datetime import date
from dateutil.rrule import rrule, DAILY
from gurobipy import Model, GRB

file_path = r"C:\Users\AL33325\OneDrive - Alliander NV\Documents\Thesis\Input python model.xlsx"
df_ipp = pd.read_excel(file_path, sheet_name="Average over 10 years", skiprows=10) #Average over 10 years , 2013, 2015

# Simulation time & season settings
startup = True                    # Components require a startup ramp when turned on
degradation = True                # Degradation multipliers will update over time
grid_capacity_limit = True        # Limit the grid capacity
use_exergy_heat = True            # The exery heat is used to (partly) fulfill the heat demand
use_efficiency_curve_MPC = True   # Use breakpoints of efficiency curve in MPC, if off a constant is used
use_uncertainty = True            # Add uncertainty to the prediction horizon

# MPC-specific parameters (switching, setpoint change, grid weight)
lambda_grid = 20                  # punish the grid input and output # onder de 10 gaat het systeem het grid niet meer gebruiken...
lambda_on_off_electrolyser = 130  # additional penalty for electrolyser on/off switching
lambda_on_off_fuelcell = 190      # additional penalty for fuel cell on/off switching
lambda_setpoint_change = 74       # punish how much the EL and FC change their setpoint

num_days = 365                    # Days
start_date = date(2013, 10, 1)    # Year/month/day # start date of simulation # in normal conditions start 1th of October
horizon_hour = 24                 # Hours

# Fixed input parameters
yearly_space_heat_demand = 16400  # kWh
yearly_domestic_hot_water = 23160 # kWh
yearly_electricty_demand = 72000  # kWh
yearly_PV_supply = 138000         # kWh
maximum_grid_capacity = 40        # kW

# Battery parameters
C_charge_battery = 1                                    # Charging rate
C_discharge_battery = 1                                 # Discharging rate
min_energy_battery = 0                                  # kWh
max_storage_capacity_battery = 380                      # kWh
initial_energy_battery = max_storage_capacity_battery/2     # kWh

# Electrolyser parameters
electrolyser_temp_min = 50                          # DegC
electrolyser_temp_max = 80                          # DegC
electrolyser_useful_waste_heat = 0.92               # Fraction
electrolyser_preheat_deionized_water = 0.07         # Fraction
electrolyser_startup = 30                           # seconds startup ramp
electrolyser_degradation_rate = 0.0000019           # fraction degradation per hour
electrolyser_max_power = 40                         # kW
electrolyser_min_power = electrolyser_max_power*0.1 # kW (minimum operating power)

# Metal hydride storage parameters
min_storage_capacity_MH = 0             # kWh
max_storage_capacity_MH = 4800          # kWh
initial_energy_MH_year =  4800          # kWh
metalhydride_degradation_rate = 0.00017  #fraction # degradation per cycle!!
MH_molarmass = 0.1037                   # kg/mol

# Absorption process (for TiFe)
```

```
deltaH_abs = 24.3   # kJ/mol
temp_abs = 20       # degC

# Desorption process (for TiFe)
deltaH_des = 27.4   # kJ/mol
temp_des = 60       # DegC

# Fuel cell parameters
fuelcell_usable_heat = 0.8                                  # Fraction of heat that is not internally used
fuelcell_unreacted_hydrogen = 0.05                          # Fraction of hydrogen that remains unreacted
fuelcell_temp_min = 60                                      # DegC
fuelcell_temp_max = 85                                      # DegC
fuelcell_startup = 60                                       # Seconds startup ramp
fuelcell_degradation_rate = 0.000004                        # Fraction degradation per hour
fuelcell_max_power_output = 25                              # kW
fuelcell_min_power_output = fuelcell_max_power_output*0.1   # kW (minimum operating power)

# Other constants
COP_space_heating = 4
COP_dhw = 2.5
LHV_H2_mol = 241.92      # kJ/mol
hours_per_day = 24       # Hour
seconds_per_hour = 3600  # Seconds

# Uncertainty parameter
if use_uncertainty:
    uncertainty_horizon_input_electricity = 0.0691/2        # fraction, maximum uncertainty added/subtracted (half of uncertainty added and half subtracted from mean)    # +-3.455%
    uncertainty_horizon_demand_electricity = 0.0384 / 2     # fraction, maximum uncertainty added/subtracted (half of uncertainty added and half subtracted from mean) # +-1.92%
    uncertainty_horizon_demand_heat= 0.0895 / 2             # fraction, maximum uncertainty added/subtracted (half of uncertainty added and half subtracted from mean)          # +-4.475%
else:
    uncertainty_horizon_input_electricity = 0
    uncertainty_horizon_demand_electricity = 0
    uncertainty_horizon_demand_heat= 0

# Degradation (start at 1.0 = no degradation)
electrolyser_degradation = 1.0
metalhydride_degradation = 1.0
fuelcell_degradation = 1.0

# Start code
total_hours = num_days * hours_per_day
start_day = start_date.timetuple().tm_yday

# Setup season start indices
# Read and scale input data using vectorized operations
start_index = (start_day - 1) * hours_per_day
first_half = df_ipp.iloc[:start_index]
second_half = df_ipp.iloc[start_index:-11]
df_shifted = pd.concat([second_half, first_half], ignore_index=True)
available_energy_MH = initial_energy_MH_year

electricity_input_n = pd.to_numeric(df_shifted.iloc[:total_hours, 1], errors='coerce').values
ambient_temp = pd.to_numeric(df_shifted.iloc[:total_hours, 2], errors='coerce').values
space_heat_demand_n = pd.to_numeric(df_shifted.iloc[:total_hours, 3], errors='coerce').values
electricity_demand_n = pd.to_numeric(df_shifted.iloc[:total_hours, 4], errors='coerce').values
domestic_hot_water_demand_n = pd.to_numeric(df_shifted.iloc[:total_hours, 5], errors='coerce').values

# Scale inputs
electricity_input_total = electricity_input_n * yearly_PV_supply
space_heat_demand = space_heat_demand_n * yearly_space_heat_demand
electricity_demand = electricity_demand_n * yearly_electricty_demand
domestic_hot_water_demand = domestic_hot_water_demand_n * yearly_domestic_hot_water

ambient_temp_K = ambient_temp + 273.15
electrolyser_temp_min_K = electrolyser_temp_min + 273.15
electrolyser_temp_max_K = electrolyser_temp_max + 273.15
fuelcell_temp_min_K = fuelcell_temp_min + 273.15
fuelcell_temp_max_K = fuelcell_temp_max + 273.15
temp_abs_K = temp_abs + 273.15
temp_des_K = temp_des + 273.15
```

```
132
133 #efficiency electrolyser
134 electrolyser_efficiency_MPC_noSOS2 = 0.70 #average efficiency over input
135 x_data = np.array([0.1, 0.2, 0.3, 0.4, 0.5, 0.6, 0.7, 0.8, 0.9, 1.0])
136 y_data = np.array([0.73,  0.74,  0.75, 0.74,  0.73,  0.72,  0.70,  0.67,  0.63,  0.60 ])
137 coeffs = np.polyfit(x_data, y_data, 3)
138 a, b, c, d = coeffs
139
140 def electrolyser_efficiency_curve(setpoint):
141     x = max(0.1, min(1.0, setpoint))
142     return a*x**3 + b*x**2 + c*x + d
143
144 #efficiency fuelcell
145 fuelcell_efficiency_MPC_noSOS2 = 0.54 # Average efficiency over input
146 def fuelcell_efficiency_curve(setpoint):
147     if setpoint <= 0.1:
148         return 0.56
149     elif setpoint < 0.2:
150         return 0.3*setpoint + 0.53
151     elif setpoint <= 1.0:
152         return -0.125*setpoint + 0.615
153     else:
154         return 0.0
155
156 # SOS2 breakpoint definitions for efficiency approximations
157 breakpoint_electrolyser = [0.1, 0.3, 0.65, 1.0]
158 electrolyser_efficiency_MPC = [electrolyser_efficiency_curve(breakpoint_electrolyser[0]),
      electrolyser_efficiency_curve(breakpoint_electrolyser[1]), electrolyser_efficiency_curve(
      breakpoint_electrolyser[2]), electrolyser_efficiency_curve(breakpoint_electrolyser[3])]
159 factor_electrolyser = [breakpoint_electrolyser[i]*electrolyser_efficiency_MPC[i] for i in range(len(
      breakpoint_electrolyser))]
160
161 breakpoint_fuelcell = [0.1, 0.2, 1.0]
162 fuelcell_efficiency_MPC = [fuelcell_efficiency_curve(breakpoint_fuelcell[0]),
      fuelcell_efficiency_curve(breakpoint_fuelcell[1]), fuelcell_efficiency_curve(breakpoint_fuelcell
      [2])]
163 factor_fuelcell = [breakpoint_fuelcell[i]/fuelcell_efficiency_MPC[i] for i in range(len(
      breakpoint_fuelcell))]
164
165 def compute_startup_factor(startup_remaining, startup_total, dt=seconds_per_hour):
166     if startup_remaining < dt:
167         ramp_avg = (((startup_total - startup_remaining) / startup_total) + 1) / 2
168         total_avg = (ramp_avg * startup_remaining + 1 * (dt - startup_remaining)) / dt
169         return total_avg
170     else:
171         f_start = (startup_total - startup_remaining) / startup_total
172         f_end = (startup_total - startup_remaining + dt) / startup_total
173         return (f_start + f_end) / 2
174
175 # MPC function with minimum setpoint constraints and both-off possibility
176 def mpc_step(current_hour, battery_energy, hydrogen_storage, degradation_elec, degradation_fc,
177              prev_setpoint_electrolyser, prev_setpoint_fuelcell, horizon=horizon_hour,
                     uncertainty_horizon_demand_electricity=uncertainty_horizon_demand_electricity,
                     uncertainty_horizon_input_electricity=uncertainty_horizon_input_electricity,
178              uncertainty_horizon_demand_heat = uncertainty_horizon_demand_heat,
                     lambda_setpoint_change=lambda_setpoint_change, lambda_on_off_electrolyser=
                     lambda_on_off_electrolyser, lambda_on_off_fuelcell=lambda_on_off_fuelcell):
179     m = Model()
180     T = min(horizon, len(electricity_input_total) - current_hour)
181
182     # Generate uncertainty for forecast: current hour deterministic (0), future hours get random
          noise
183     indices = np.arange(current_hour, min(current_hour + T, len(electricity_input_total)))
184     if len(indices) > 1:
185         uncertainty_input = np.concatenate(([0],electricity_input_total[indices[1:]] * np.random.
              uniform(-uncertainty_horizon_input_electricity, uncertainty_horizon_input_electricity,
              len(indices) - 1)))
186         uncertainty_demand = np.concatenate(([0],electricity_demand[indices[1:]] * np.random.uniform
              (-uncertainty_horizon_demand_electricity, uncertainty_horizon_demand_electricity, len(
              indices) - 1)))
187         uncertainty_heat = np.concatenate(([0],space_heat_demand[indices[1:]] * np.random.uniform(-
              uncertainty_horizon_demand_heat, uncertainty_horizon_demand_heat, len(indices) - 1)))
188         uncertainty_domestic_hot_water = np.concatenate(([0],domestic_hot_water_demand[indices[1:]]
              * np.random.uniform(-uncertainty_horizon_demand_heat, uncertainty_horizon_demand_heat,
              len(indices) - 1)))
189     else:
```

```
        uncertainty_input = uncertainty_demand = uncertainty_heat = uncertainty_domestic_hot_water =
            np.array([0])

    E_in = np.clip(electricity_input_total[indices] + uncertainty_input, 0, None)
    E_dem = np.clip(electricity_demand[indices] + uncertainty_demand, 0, None)
    H_dem = np.clip(space_heat_demand[indices] + uncertainty_heat, 0, None)
    DHW_dem = np.clip(domestic_hot_water_demand[indices] + uncertainty_domestic_hot_water, 0, None)
    net_energy = E_in - E_dem - H_dem - DHW_dem

    # Start Constraints:
    # Decision variables: continuous setpoints (fractions in [0.1,1])
    setpoint_electrolyser = m.addVars(T, lb=0, ub=1, name="setpoint_electrolyser")
    setpoint_fuelcell = m.addVars(T, lb=0, ub=1, name="setpoint_fuelcell")

    # Single binary variable for switching (1 selects electrolyser; 0 selects fuel cell)
    y = m.addVars(T, vtype=GRB.BINARY, name="y")
    for t in range(T):
        m.addConstr(setpoint_electrolyser[t] <= y[t])
        m.addConstr(setpoint_fuelcell[t] <= 1 - y[t])
    electrolyser_active = m.addVars(T, vtype=GRB.BINARY, name="electrolyser_active")
    fuelcell_active = m.addVars(T, vtype=GRB.BINARY, name="fuelcell_active")
    for t in range(T):
        # Link the additional binaries to the switching decision:
        m.addConstr(electrolyser_active[t] <= y[t])
        m.addConstr(fuelcell_active[t] <= 1 - y[t])
        # Force the setpoint to be zero if the unit is not active:
        m.addConstr(setpoint_electrolyser[t] <= electrolyser_active[t])
        m.addConstr(setpoint_fuelcell[t] <= fuelcell_active[t])

    # Define minimum operating fractions (if the unit is on, its setpoint must be at least this
        value)
    min_electrolyser_setpoint = electrolyser_min_power / electrolyser_max_power
    min_fuelcell_setpoint = fuelcell_min_power_output / fuelcell_max_power_output
    for t in range(T):
        m.addConstr(setpoint_electrolyser[t] >= min_electrolyser_setpoint * electrolyser_active[t])
        m.addConstr(setpoint_fuelcell[t] >= min_fuelcell_setpoint * fuelcell_active[t])

    # Battery and hydrogen dynamics
    battery = m.addVars(T+1, lb=min_energy_battery, ub=max_storage_capacity_battery, name="battery")
    m.addConstr(battery[0] == battery_energy)
    hydrogen = m.addVars(T+1, lb=min_storage_capacity_MH, ub=max_storage_capacity_MH *
        metalhydride_degradation, name="hydrogen")
    hydrogen_storage = min(hydrogen_storage, max_storage_capacity_MH * metalhydride_degradation)
    if hydrogen_storage >= max_storage_capacity_MH * metalhydride_degradation -
        electrolyser_min_power*1 :
        for t in range(T):
            m.addConstr(electrolyser_active[t] == 0)
            m.addConstr(setpoint_electrolyser[t] == 0)
    m.addConstr(hydrogen[0] == hydrogen_storage)
    if hydrogen_storage <= min_storage_capacity_MH + fuelcell_min_power_output*1:
        for t in range(T):
            m.addConstr(fuelcell_active[t] == 0)
            m.addConstr(setpoint_fuelcell[t] == 0)

    # Start objective function MPC:
    # Grid variables (kW)
    if grid_capacity_limit:
        grid_export = m.addVars(T, lb=0, ub= maximum_grid_capacity, name="grid_export")
        grid_input = m.addVars(T, lb=0, ub= maximum_grid_capacity, name="grid_input")
        grid_usage = m.addVar(lb=0, ub= maximum_grid_capacity, name="z")
        for t in range(T):
            m.addConstr(grid_export[t] <= grid_usage)
            m.addConstr(grid_input[t] <= grid_usage)
    else:
        grid_export = m.addVars(T, lb=0, name="grid_export")
        grid_input = m.addVars(T, lb=0, name="grid_input")
        grid_usage = m.addVar(lb=0, name="z")
        for t in range(T):
            m.addConstr(grid_export[t] <= grid_usage)
            m.addConstr(grid_input[t] <= grid_usage)
    obj =  lambda_grid * grid_usage

    # On/off transition binaries for every step including t=0
    epsilon = 1e-2
    u_elec = m.addVars(T, vtype=GRB.BINARY, name="u_elec")
    u_fc   = m.addVars(T, vtype=GRB.BINARY, name="u_fc")
```

```
    # Link initial transition (prev -> t=0)
    prev_active_elec = 1 if prev_setpoint_electrolyser > epsilon else 0
    prev_active_fc   = 1 if prev_setpoint_fuelcell   > epsilon else 0
    # transition at t=0
    m.addConstr(u_elec[0] >= electrolyser_active[0] - prev_active_elec)
    m.addConstr(u_elec[0] >= prev_active_elec - electrolyser_active[0])
    m.addConstr(u_fc[0]   >= fuelcell_active[0]    - prev_active_fc)
    m.addConstr(u_fc[0]   >= prev_active_fc    - fuelcell_active[0])
    # transitions for t>0
    for t in range(1, T):
        m.addConstr(u_elec[t] >= electrolyser_active[t]   - electrolyser_active[t-1])
        m.addConstr(u_elec[t] >= electrolyser_active[t-1] - electrolyser_active[t])
        m.addConstr(u_fc[t]   >= fuelcell_active[t]      - fuelcell_active[t-1])
        m.addConstr(u_fc[t]   >= fuelcell_active[t-1]    - fuelcell_active[t])

    obj += lambda_on_off_electrolyser * sum(u_elec[t] for t in range(1, T))
    obj += lambda_on_off_fuelcell    * sum(u_fc[t]   for t in range(1, T))

    # Setpoint change cost variables
    delta0_elec = m.addVar(lb=0, name="delta0_electrolyser")
    delta0_fc   = m.addVar(lb=0, name="delta0_fuelcell")
    m.addConstr(delta0_elec >= setpoint_electrolyser[0] - prev_setpoint_electrolyser)
    m.addConstr(delta0_elec >= prev_setpoint_electrolyser - setpoint_electrolyser[0])
    m.addConstr(delta0_fc   >= setpoint_fuelcell[0]    - prev_setpoint_fuelcell)
    m.addConstr(delta0_fc   >= prev_setpoint_fuelcell    - setpoint_fuelcell[0])

    delta_electrolyser = m.addVars(T-1, lb=0, name="delta_electrolyser")
    delta_fuelcell    = m.addVars(T-1, lb=0, name="delta_fuelcell")
    for t in range(1, T):
        m.addConstr(delta_electrolyser[t-1] >= setpoint_electrolyser[t] - setpoint_electrolyser[t
            -1])
        m.addConstr(delta_electrolyser[t-1] >= setpoint_electrolyser[t-1] - setpoint_electrolyser[t
            ])
        m.addConstr(delta_fuelcell[t-1]    >= setpoint_fuelcell[t]    - setpoint_fuelcell[t-1])
        m.addConstr(delta_fuelcell[t-1]    >= setpoint_fuelcell[t-1] - setpoint_fuelcell[t])

    obj += lambda_setpoint_change * (delta0_elec + delta0_fc + sum(delta_electrolyser.values()) +
        sum(delta_fuelcell.values()))

    # SOS2 approximations for the efficiency functions in hydrogen dynamics
    efficiency_electrolyser_term = {}
    efficiency_fuelcell_term = {}

    if use_efficiency_curve_MPC:
        for t in range(T):
            # Electrolyser efficiency curve MPC formulation
            lambda_electrolyser = m.addVars(len(breakpoint_electrolyser), lb=0, name="
                lambda_electrolyser_%d" % t)
            m.addConstr(sum(lambda_electrolyser[i] for i in range(len(breakpoint_electrolyser))) ==
                electrolyser_active[t])
            m.addConstr(setpoint_electrolyser[t] == sum(breakpoint_electrolyser[i] *
                lambda_electrolyser[i]
                                                    for i in range(len(breakpoint_electrolyser)))
                                                        )
            efficiency_electrolyser_term[t] = m.addVar(name="efficiency_electrolyser_term_%d" % t)
            m.addConstr(efficiency_electrolyser_term[t] == sum(factor_electrolyser[i] *
                lambda_electrolyser[i]
                                                           for i in range(len(
                                                               breakpoint_electrolyser))))
            m.addSOS(GRB.SOS_TYPE2, [lambda_electrolyser[i] for i in range(len(
                breakpoint_electrolyser))])

            # Fuel Cell efficiency curve MPC formulation
            lambda_fc = m.addVars(len(breakpoint_fuelcell), lb=0, name="lambda_fc_%d" % t)
            m.addConstr(sum(lambda_fc[i] for i in range(len(breakpoint_fuelcell))) ==
                fuelcell_active[t])
            m.addConstr(setpoint_fuelcell[t] == sum(breakpoint_fuelcell[i] * lambda_fc[i]
                                                   for i in range(len(breakpoint_fuelcell))))
            efficiency_fuelcell_term[t] = m.addVar(name="␣efficiency_fuelcell_term_%d" % t)
            m.addConstr( efficiency_fuelcell_term[t] == sum(factor_fuelcell[i] * lambda_fc[i]
                                                for i in range(len(breakpoint_fuelcell))))
            m.addSOS(GRB.SOS_TYPE2, [lambda_fc[i] for i in range(len(breakpoint_fuelcell))])

            # Dynamics constraints for battery and hydrogen with SOS2
            m.addConstr(battery[t+1] == battery[t] + net_energy[t] + grid_input[t] - grid_export[t]
                        - setpoint_electrolyser[t]*electrolyser_max_power + setpoint_fuelcell[t]*
```

```
                            fuelcell_max_power_output)
            m.addConstr(hydrogen[t+1] == hydrogen[t] + electrolyser_max_power * degradation_elec *
                efficiency_electrolyser_term[t]
                        - fuelcell_max_power_output/degradation_fc * efficiency_fuelcell_term[t])
            m.addConstr(hydrogen[t] >= fuelcell_min_power_output * setpoint_fuelcell[t])

    # Not using efficiency curve approximation, but just using a constant value for the efficiencies
         of electrolyser and fuelcell
    else:
        for t in range(T):
            # Dynamics constraints for battery and hydrogen without SOS2
            m.addConstr(battery[t+1] == battery[t] + net_energy[t] + grid_input[t] - grid_export[t]
                        - setpoint_electrolyser[t]*electrolyser_max_power + setpoint_fuelcell[t]*
                            fuelcell_max_power_output)
            m.addConstr(hydrogen[t+1] == hydrogen[t] + setpoint_electrolyser[t]*
                electrolyser_max_power*degradation_elec*electrolyser_efficiency_MPC_noSOS2
                        - setpoint_fuelcell[t]*fuelcell_max_power_output/(degradation_fc*
                            fuelcell_efficiency_MPC_noSOS2))
            m.addConstr(hydrogen[t] >= fuelcell_min_power_output * setpoint_fuelcell[t])

    m.setObjective(obj, GRB.MINIMIZE)
    m.Params.OutputFlag = 0
    m.optimize()
    if m.status != GRB.OPTIMAL:
        print("Warning: MPC optimization did not find an optimal solution.")
        if m.status == GRB.INFEASIBLE:
            m.computeIIS()
            m.write("model.ilp")
        return

    setpoint_electrolyser_0 = setpoint_electrolyser[0].X
    setpoint_fuelcell_0 = setpoint_fuelcell[0].X
    grid_export_0 = grid_export[0].X
    grid_input_0 = grid_input[0].X
    battery_next = battery[1].X
    hydrogen_next = hydrogen[1].X
    grid_usage_val = grid_usage.X

    return setpoint_electrolyser_0, setpoint_fuelcell_0, grid_export_0, grid_input_0, grid_usage_val
        , battery_next, hydrogen_next

# Initialize states
battery_energy = initial_energy_battery
hydrogen_storage_log = [available_energy_MH]
battery_history = []
grid_export_history = []
grid_input_history = []
net_energy_history = []
electrolyser_setpoint_history = []
fuelcell_setpoint_history = []
electrolyser_energy_usage = []
fuelcell_electrical_output = []
fuelcell_h2_input_history = []
electrolyser_heat_history = []
absorption_heat_history = []
fuelcell_heat_history = []
exergy_heat_history = []
effective_heat_demand_history = []
met_by_exergy_history = []
required_H2_history = []
battery_charge_log = []
battery_discharge_log = []
potential_H2_history = []
exergy_des_required_history = []
max_battery_C_charge_required_history = []
max_battery_C_discharge_required_history = []
electrolyser_temp_K_history = []
fuelcell_temp_K_history = []
used_exergy_for_space_heating_history = []
used_exergy_for_dhw_history = []
usable_heat_fuelcell_history = []
fuelcell_exergy_history = []
fuelcell_exery_minus_des_exergy_history = []
electrolyser_exergy_history = []
absorption_exergy_history = []
heat_required_des_history = []
```

```
electrolyser_efficiency_history = []
fuelcell_efficiency_history = []
planned_fuelcell_power_history = []
planned_electrolyser_power_history = []

# Startup dynamics flags and counters
electrolyser_active = False
electrolyser_startup_remaining = electrolyser_startup
fuelcell_active = False
fuelcell_startup_remaining = fuelcell_startup

global_hour = 0

while global_hour < total_hours:

    prev_setpoint_electrolyser = electrolyser_setpoint_history[-1] if electrolyser_setpoint_history else 0.0
    prev_setpoint_fuelcell = fuelcell_setpoint_history[-1] if fuelcell_setpoint_history else 0.0

    # Solve MPC
    setpoint_electrolyser, setpoint_fuelcell, grid_export, grid_input, battery_next_mpc, hydrogen_next_mpc, grid_usage_val = mpc_step(
        current_hour=global_hour,
        battery_energy=battery_energy,
        hydrogen_storage=hydrogen_storage_log[-1],
        degradation_elec=electrolyser_degradation,
        degradation_fc=fuelcell_degradation,
        prev_setpoint_electrolyser=prev_setpoint_electrolyser,
        prev_setpoint_fuelcell=prev_setpoint_fuelcell,
        horizon=horizon_hour,
        uncertainty_horizon_input_electricity=uncertainty_horizon_input_electricity,
        uncertainty_horizon_demand_electricity=uncertainty_horizon_demand_electricity,
        uncertainty_horizon_demand_heat=uncertainty_horizon_demand_heat,
        lambda_setpoint_change=lambda_setpoint_change,
        lambda_on_off_electrolyser=lambda_on_off_electrolyser,
        lambda_on_off_fuelcell=lambda_on_off_fuelcell
    )
    # MPC outputs
    planned_electrolyser_power = setpoint_electrolyser * electrolyser_max_power
    planned_fuelcell_power = setpoint_fuelcell * fuelcell_max_power_output

    planned_fuelcell_power_history.append(planned_fuelcell_power)
    planned_electrolyser_power_history.append(planned_electrolyser_power)

    # Electrolyser startup dynamics:
    if startup:
        if planned_electrolyser_power > 0:
            if not electrolyser_active:
                electrolyser_startup_factor = compute_startup_factor(electrolyser_startup_remaining, electrolyser_startup, dt=seconds_per_hour)
                applied_electrolyser_power = planned_electrolyser_power * electrolyser_startup_factor
                electrolyser_startup_remaining -= seconds_per_hour
                if electrolyser_startup_remaining <= 0:
                    electrolyser_active = True
                    electrolyser_startup_remaining = 0
                else:
                    print(f"Electrolyser in startup, factor: {electrolyser_startup_factor:.2f}, remaining: {electrolyser_startup_remaining} s")
            else:
                applied_electrolyser_power = planned_electrolyser_power
        else:
            electrolyser_active = False
            electrolyser_startup_remaining = electrolyser_startup
            applied_electrolyser_power = 0

        # Fuel cell startup dynamics:
        if planned_fuelcell_power > 0:
            if not fuelcell_active:
                fuelcell_startup_factor = compute_startup_factor(fuelcell_startup_remaining, fuelcell_startup, dt=seconds_per_hour)
                applied_fuelcell_power = planned_fuelcell_power * fuelcell_startup_factor
                fuelcell_startup_remaining -= seconds_per_hour
                if fuelcell_startup_remaining <= 0:
                    fuelcell_active = True
                    fuelcell_startup_remaining = 0
```

```
                else:
                    print(f"Fuel cell in startup, factor: {fuelcell_startup_factor:.2f}, remaining:
                        {fuelcell_startup_remaining} s")
            else:
                applied_fuelcell_power = planned_fuelcell_power
        else:
            fuelcell_active = False
            fuelcell_startup_remaining = fuelcell_startup
            applied_fuelcell_power = 0
    else:
        applied_electrolyser_power = planned_electrolyser_power
        applied_fuelcell_power = planned_fuelcell_power

    # Electrolyser setpoint and efficiency
    setpoint_electrolyser = applied_electrolyser_power / electrolyser_max_power if
        electrolyser_max_power > 0 else 0
    electrolyser_efficiency = electrolyser_efficiency_curve(setpoint_electrolyser)
    potential_H2 = applied_electrolyser_power * electrolyser_efficiency * electrolyser_degradation
    electrolyser_output = potential_H2

    # Check hydrogen storage capacity
    current_H2_storage = hydrogen_storage_log[-1]
    if current_H2_storage + potential_H2 > max_storage_capacity_MH * metalhydride_degradation:
        allowable_H2 = max_storage_capacity_MH * metalhydride_degradation - current_H2_storage
        if allowable_H2 > 0 and electrolyser_efficiency > 0:
            applied_electrolyser_power = min(allowable_H2 / (electrolyser_efficiency *
                electrolyser_degradation), applied_electrolyser_power)
            potential_H2 = allowable_H2
        else:
            applied_electrolyser_power = 0
            potential_H2 = 0
        print("Warning: Hydrogen storage capacity reached")
    potential_H2_history.append(potential_H2)

    # Fuel cell setpoint and efficiency
    setpoint_fuelcell = applied_fuelcell_power / fuelcell_max_power_output if
        fuelcell_max_power_output > 0 else 0
    fuelcell_efficiency = fuelcell_efficiency_curve(setpoint_fuelcell)
    required_H2 = applied_fuelcell_power / (fuelcell_efficiency * fuelcell_degradation) if
        fuelcell_efficiency > 0 else 0
    available_H2 = current_H2_storage + potential_H2
    actual_H2_used = min(required_H2, available_H2)
    actual_fuelcell_output = actual_H2_used * fuelcell_efficiency * fuelcell_degradation
    hydrogen_new = current_H2_storage + potential_H2 - actual_H2_used
    hydrogen_new = max(min(hydrogen_new, max_storage_capacity_MH * metalhydride_degradation),
        min_storage_capacity_MH)
    hydrogen_storage_log.append(hydrogen_new)
    required_H2_history.append(required_H2)
    fuelcell_efficiency_history.append(fuelcell_efficiency)
    electrolyser_efficiency_history.append(electrolyser_efficiency)

    # Temperatures of electrolyser and fuelcell at selected setpoint
    electrolyser_temp_K = setpoint_electrolyser*(electrolyser_temp_max_K - electrolyser_temp_min_K)
        + electrolyser_temp_min_K
    fuelcell_temp_K = setpoint_fuelcell*(fuelcell_temp_max_K - fuelcell_temp_min_K) +
        fuelcell_temp_min_K

    electrolyser_temp_K_history.append(electrolyser_temp_K)
    fuelcell_temp_K_history.append(fuelcell_temp_K)

    # Fuel cell exergy heat calculation for desorption process
    if actual_H2_used > 0:
        effective_fuelcell_efficiency = actual_fuelcell_output / actual_H2_used
    else:
        effective_fuelcell_efficiency = 0
    #heat for desorption process is always required, even if exergy heat = False
    exergy_des_factor =  max(0, 1 - ambient_temp_K[global_hour] / temp_des_K)
    exergy_fuelcell_factor =  max(0, 1 - ambient_temp_K[global_hour] / fuelcell_temp_K)
    # Total heat required for desorption
    Q_use_des = deltaH_des / LHV_H2_mol * actual_H2_used
    # Exergy required to drive desorption
    exergy_des_required = Q_use_des * exergy_des_factor

    # Usable heat and its exergy content
    usable_heat_fraction_fuelcell = max(1 - fuelcell_unreacted_hydrogen -
        effective_fuelcell_efficiency, 0)
```

```
    usable_heat_fuelcell = actual_H2_used * usable_heat_fraction_fuelcell * fuelcell_usable_heat
    usable_exergy_fuelcell = usable_heat_fuelcell * exergy_fuelcell_factor

    # Remaining exergy after meeting desorption demand
    fuelcell_exergy_minus_des_exergy = max(usable_exergy_fuelcell - exergy_des_required, 0)
    if fuelcell_exergy_minus_des_exergy == 0 and actual_H2_used > 0:
        print(f"[hour {global_hour}] Warning: Fuel cell exergy fully used for desorption. No surplus exergy available.")

    electrolyser_heat = applied_electrolyser_power * (1 - electrolyser_efficiency) * electrolyser_useful_waste_heat * (1 - electrolyser_preheat_deionized_water)
    absorption_heat = (deltaH_abs / LHV_H2_mol) * electrolyser_output

    # Compute exergy based on Carnot efficiency factors
    current_ambient = ambient_temp_K[global_hour]
    carnot_electrolyser = max(0, 1 - current_ambient / electrolyser_temp_K)
    carnot_abs = max(0, 1 - current_ambient / temp_abs_K)
    carnot_fuelcell = max(0, 1 - current_ambient / fuelcell_temp_K)

    exergy_electrolyser = electrolyser_heat * carnot_electrolyser
    exergy_abs = absorption_heat * carnot_abs
    hourly_exergy = (exergy_electrolyser + exergy_abs + fuelcell_exergy_minus_des_exergy) # is in thermal kW

    electrolyser_heat_history.append(electrolyser_heat)
    electrolyser_exergy_history.append(exergy_electrolyser)
    absorption_heat_history.append(absorption_heat)
    absorption_exergy_history.append(exergy_abs)
    usable_heat_fuelcell_history.append(usable_heat_fuelcell)
    fuelcell_exergy_history.append(usable_exergy_fuelcell)
    fuelcell_exery_minus_des_exergy_history.append(fuelcell_exergy_minus_des_exergy)
    exergy_des_required_history.append(exergy_des_required)
    exergy_heat_history.append(hourly_exergy)
    heat_required_des_history.append(Q_use_des)

    # Calculate effective heat demand after exergy recovery
    if use_exergy_heat:
        # hourly_exergy is in kWh_heat
        # Convert the available exergy to its electric equivalent for space heating
        hourly_exergy_space_heat_demand_electric = hourly_exergy / COP_space_heating

        if hourly_exergy_space_heat_demand_electric >= space_heat_demand[global_hour]:
            # Full space heating demand is met
            met_by_exergy_space_heat_demand = space_heat_demand[global_hour]
            used_exergy_for_space_heating = met_by_exergy_space_heat_demand * COP_space_heating
            remaining_exergy_heat = hourly_exergy - used_exergy_for_space_heating
            effective_space_heating = 0

            # Now use any remaining exergy heat for DHW
            met_by_exergy_dhw_electric = remaining_exergy_heat / COP_dhw
            if met_by_exergy_dhw_electric >= domestic_hot_water_demand[global_hour]:
                met_by_exergy_dhw = domestic_hot_water_demand[global_hour]
                used_exergy_for_dhw = met_by_exergy_dhw * COP_dhw
                effective_dhw = 0
            else:
                met_by_exergy_dhw = met_by_exergy_dhw_electric
                used_exergy_for_dhw = met_by_exergy_dhw * COP_dhw
                effective_dhw = domestic_hot_water_demand[global_hour] - met_by_exergy_dhw

            met_by_exergy = met_by_exergy_space_heat_demand + met_by_exergy_dhw
            effective_heat = effective_dhw  # space heating is fully met

        else:
            # Not enough exergy heat to fully cover the space heating electric demand
            met_by_exergy_space_heat_demand = hourly_exergy_space_heat_demand_electric
            used_exergy_for_space_heating = met_by_exergy_space_heat_demand * COP_space_heating
            used_exergy_for_dhw = 0  # No exergy left for DHW
            effective_space_heating = space_heat_demand[global_hour] - met_by_exergy_space_heat_demand
            effective_dhw = domestic_hot_water_demand[global_hour]
            effective_heat = effective_space_heating + effective_dhw
            met_by_exergy = met_by_exergy_space_heat_demand
    else:
        # No exergy heat is used, all demand must be met by other means
        met_by_exergy_heat_demand = 0
        used_exergy_for_space_heating = 0
```

```
        used_exergy_for_dhw = 0
        met_by_exergy_dhw = 0
        met_by_exergy = 0
        effective_heating = space_heat_demand[global_hour]
        effective_dhw = domestic_hot_water_demand[global_hour]
        effective_heat = effective_heating + effective_dhw

    # Compute net energy available using effective heat demand
    met_by_exergy_history.append(met_by_exergy)
    effective_heat_demand_history.append(effective_heat)
    net_energy_effective = electricity_input_total[global_hour] - electricity_demand[global_hour] -
        effective_heat
    net_energy_history.append(net_energy_effective)
    used_exergy_for_space_heating_history.append(used_exergy_for_space_heating)
    used_exergy_for_dhw_history.append(used_exergy_for_dhw)

    delta_energy = (electricity_input_total[global_hour] - electricity_demand[global_hour] -
        effective_heat
                    - applied_electrolyser_power + actual_fuelcell_output + (grid_input -
                        grid_export))

    # Apply battery charge/discharge limits based on the computed delta.
    if delta_energy >= 0:
        available_storage = max_storage_capacity_battery - battery_energy
        allowed_charge = C_charge_battery * max_storage_capacity_battery
        battery_change = min(delta_energy, available_storage, allowed_charge)
        # Log the charge amount and record max charge requirement.
        battery_charge_log.append(battery_change)
        max_battery_C_charge_required = max([electricity_input_total[global_hour] +
            applied_fuelcell_power + grid_input]) / max_storage_capacity_battery
        max_battery_C_charge_required_history.append(max_battery_C_charge_required)
    else:
        allowed_discharge = C_discharge_battery * max_storage_capacity_battery
        # Limit the discharge such that it does not exceed allowed discharge.
        battery_change = max(delta_energy, -allowed_discharge)
        # Log the discharge amount and record max discharge requirement.
        battery_discharge_log.append(battery_change)
        max_battery_C_discharge_required = max([applied_electrolyser_power + grid_export +
            domestic_hot_water_demand[global_hour] + space_heat_demand[global_hour]]) /
            max_storage_capacity_battery
        max_battery_C_discharge_required_history.append(max_battery_C_discharge_required)

    # Update the battery energy once with the computed change.
    battery_energy += battery_change
    # Ensure the battery stays within its minimum and maximum limits.
    battery_energy = max(min(battery_energy, max_storage_capacity_battery), min_energy_battery)

    battery_history.append(battery_energy)
    grid_export_history.append(grid_export)
    grid_input_history.append(grid_input)
    fuelcell_electrical_output.append(actual_fuelcell_output)
    fuelcell_h2_input_history.append(actual_H2_used)
    electrolyser_setpoint_history.append(setpoint_electrolyser)
    fuelcell_setpoint_history.append(setpoint_fuelcell)
    electrolyser_energy_usage.append(applied_electrolyser_power)

    if degradation:
        if applied_electrolyser_power > 0:
            electrolyser_degradation -= electrolyser_degradation_rate
            metalhydride_degradation -= metalhydride_degradation_rate*(applied_electrolyser_power/
                max_storage_capacity_MH) #degradatie gaat niet hierover de max, anders zou
                degradatie steeds erger worden, nu is degradatie constant aangenomen
        if applied_fuelcell_power > 0:
            fuelcell_degradation -= fuelcell_degradation_rate
            metalhydride_degradation -= metalhydride_degradation_rate*(actual_H2_used/
                max_storage_capacity_MH) #degradatie gaat niet hierover de max, anders zou
                degradatie steeds erger worden, nu is degradatie constant aangenomen

    global_hour += 1

# Outputs
total_electrolyser_energy_used = sum(electrolyser_energy_usage)
electrolyser_energy_output = [p * electrolyser_efficiency_curve(p / electrolyser_max_power) for p in
     electrolyser_energy_usage]
total_electrolyser_energy_output = sum(electrolyser_energy_output)
total_fuelcell_input = sum(fuelcell_h2_input_history)
```

```
total_fuelcell_electrical_output = sum(fuelcell_electrical_output)
total_unused_hydrogen = sum(fuelcell_h2_input_history) * fuelcell_unreacted_hydrogen
total_operational_hours_electrolyser = sum(1 for x in electrolyser_energy_output if x != 0)
total_operational_hours_fuelcell = sum(1 for x in fuelcell_electrical_output if x != 0)

total_electrolyser_heat = sum(electrolyser_heat_history)
total_absorption_heat = sum(absorption_heat_history)
total_fuelcell_heat = sum(fuelcell_heat_history)
total_exergy_heat = sum(exergy_heat_history)
total_effective_heat_demand = sum(effective_heat_demand_history)

system_size = (max_storage_capacity_MH - 2000) /8300 + 1
net_energy_history = np.array(net_energy_history)
positive_values = np.where(net_energy_history > 0, net_energy_history, 0)
area_positive = np.trapz(positive_values)
negative_values = np.where(net_energy_history < 0, net_energy_history, 0)
area_negative = np.trapz(negative_values)
total_combined_heat = sum(absorption_heat_history) + sum(electrolyser_heat_history) + sum(
    usable_heat_fuelcell_history)
excess_grid_export = sum(max(0, grid_export - 40) for grid_export in grid_export_history)

#prints
print(f"Total␣electrolyser␣energy␣used:␣{total_electrolyser_energy_used:.2f}␣kWh")
print(f"Total␣electrolyser␣energy␣output:␣{total_electrolyser_energy_output:.2f}␣kWh")
print(f"Total␣fuel␣cell␣hydrogen␣input:␣{total_fuelcell_input:.2f}␣kWh")
print(f"Total␣fuel␣cell␣electrical:␣{total_fuelcell_electrical_output:.2f}␣kWh")
print(f"Total␣electrolyser␣operational␣hours:␣{total_operational_hours_electrolyser:.2f}␣hours")
print(f"Total␣fuel␣cell␣operational␣hours:␣{total_operational_hours_fuelcell:.2f}␣hours")
print(f"Total␣unreacted␣hydrogen:␣{total_unused_hydrogen:.2f}␣kWh")
print(f"Final␣battery␣energy:␣{battery_energy:.2f}␣kWh")
print(f"Final␣hydrogen␣storage:␣{hydrogen_storage_log[-1]:.2f}␣kWh")
print(f"Total␣net␣energy␣(effective,␣nominal):␣{sum(net_energy_history):.2f}␣kWh")
print()
print(f"Total␣usable␣heat␣produced:␣{total_combined_heat:.2f}␣kWh")
print(f"Total␣exergy␣heat␣produced:␣{total_exergy_heat:.2f}␣kWh")
print(f"Total␣exergy␣heat␣reused␣for␣heating:␣{sum(used_exergy_for_space_heating_history):.2f}␣kWh")
print(f"Total␣exergy␣heat␣reused␣for␣domestic␣hot␣water:␣{sum(used_exergy_for_dhw_history):.2f}␣kWh"
    )
print(f"Total␣exergy␣heat␣reused:␣{sum(used_exergy_for_space_heating_history)+sum(
    used_exergy_for_dhw_history):.2f}␣kWh")

print()
print(f"Total␣energy␣sent␣back␣to␣the␣grid:␣{sum(grid_export_history):.2f}␣kWh")
print(f"Max␣energy␣sent␣back␣to␣grid␣in␣hour:␣{max(grid_export_history):.2f}␣kW")
print(f"Total␣energy␣taken␣from␣the␣grid:␣{sum(grid_input_history):.2f}␣kWh")
print(f"Max␣energy␣taken␣from␣the␣grid␣in␣hour:␣{max(grid_input_history):.2f}␣kW")
print(f"Total␣energy␣that␣exceeded␣the␣grid␣capacity:␣{excess_grid_export:.2f}␣kWh")
print(f"Max␣flow␣input/output␣metal␣hydride␣storage:␣{max(max(required_H2_history),␣max(
    potential_H2_history))*3600/120000:.2f}␣kg␣per␣hour")
print()
print(f"System␣size:␣{(system_size):.2f}␣measured␣in␣20␣foot␣containers")
print()
if degradation:
    print(f"Electrolyser␣degradation:␣{electrolyser_degradation:.6f}")
    print(f"Metalhydride␣degradation:␣{metalhydride_degradation:.6f}")
    print(f"Fuel␣cell␣degradation:␣{fuelcell_degradation:.6f}")

#plots
fontsize_labels = 14
fontsize_title = 16
fontsize_legend = 13
fontsize_ticks = 15

# Daily plots
plt.figure(figsize=(10, 6))
plt.plot(electrolyser_energy_usage, label='Electrolyser␣power␣input', marker='o', color='blue')
plt.plot(fuelcell_electrical_output, label='Fuel␣cell␣power␣output', marker='x', color='red')
plt.xlabel('Hour', fontsize=fontsize_labels)
plt.ylabel('Power␣(kW)', fontsize=fontsize_labels)
plt.title('Electrolyser␣Input␣&␣Fuel␣Cell␣Output␣Power', fontsize=fontsize_title)
plt.grid(True)
plt.legend(fontsize=fontsize_legend)
plt.xticks(fontsize=fontsize_ticks)
plt.yticks(fontsize=fontsize_ticks)
plt.tight_layout()
plt.show()
```

```
742
743 plt.figure(figsize=(10,6))
744 hours = range(len(hydrogen_storage_log))
745 plt.plot(hours, hydrogen_storage_log, marker='o', linestyle='-', color='purple')
746 plt.xlabel("Hour", fontsize=fontsize_labels)
747 plt.ylabel("Hydrogen␣storage␣(kWh)", fontsize=fontsize_labels)
748 plt.title("Hydrogen␣Storage␣per␣Hour", fontsize=fontsize_title)
749 plt.grid(True)
750 plt.xticks(fontsize=fontsize_ticks)
751 plt.yticks(fontsize=fontsize_ticks)
752 plt.show()
753
754 # Results per day
755 daily_electricity_input = [sum(electricity_input_total[i*hours_per_day:(i+1)*hours_per_day]) for i
      in range(num_days)]
756 daily_electricity_demand = [sum(electricity_demand[i*hours_per_day:(i+1)*hours_per_day]) for i in
      range(num_days)]
757 daily_effective_heat_demand = [sum(effective_heat_demand_history[i*hours_per_day:(i+1)*hours_per_day
      ]) for i in range(num_days)]
758 daily_net_energy = [sum(net_energy_history[i*hours_per_day:(i+1)*hours_per_day]) for i in range(
      num_days)]
759 dates = list(rrule(DAILY, dtstart=start_date, count=num_days))
760
761 plt.figure(figsize=(12, 6))
762 plt.plot(dates, daily_electricity_input, label="Daily␣electricity␣supply␣PV␣panels", marker='o')
763 plt.plot(dates, [-x for x in daily_electricity_demand], label="Daily␣electricity␣demand", marker='x'
      )
764 plt.plot(dates, [-x for x in daily_effective_heat_demand], label="Daily␣heat␣demand␣(space␣heating␣
      and␣DHW)", marker='s')
765 plt.plot(dates, daily_net_energy, label="Daily␣net␣energy", linestyle="--", color="black", marker='d
      ')
766 plt.xlabel("Date", fontsize=fontsize_labels)
767 plt.ylabel("Energy␣(kWh)", fontsize=fontsize_labels)
768 plt.title("Daily␣Energy␣Balance", fontsize=fontsize_title)
769 plt.legend(fontsize=fontsize_legend)
770 plt.grid(True)
771 plt.xticks(fontsize=fontsize_ticks)
772 plt.yticks(fontsize=fontsize_ticks)
773 plt.gca().xaxis.set_major_formatter(mdates.DateFormatter("%b"))
774 plt.gca().xaxis.set_major_locator(mdates.MonthLocator())
775 plt.show()
776
777 electrolyser_energy_output = [p * electrolyser_efficiency_curve(p / electrolyser_max_power) for p in
       electrolyser_energy_usage]
778 daily_electrolyser_energy_usage = [sum(electrolyser_energy_usage[i*hours_per_day:(i+1)*hours_per_day
      ])/hours_per_day for i in range(num_days)]
779 daily_fuelcell_output = [sum(fuelcell_electrical_output[i*hours_per_day:(i+1)*hours_per_day])/
      hours_per_day for i in range(num_days)]
780
781 plt.figure(figsize=(10, 6))
782 plt.plot(dates, daily_electrolyser_energy_usage, label='Daily␣Average␣Electrolyser␣input', marker='o
      ', color='blue')
783 plt.plot(dates, daily_fuelcell_output, label='Daily␣Average␣Fuel␣Cell␣Output', marker='x', color='
      red')
784 plt.xlabel("Date", fontsize=fontsize_labels)
785 plt.ylabel("Average␣Hourly␣Output␣(kWh)", fontsize=fontsize_labels)
786 plt.title("Daily␣Average␣Electrolyser␣Input␣&␣Fuel␣Cell␣Output␣Power", fontsize=fontsize_title)
787 plt.legend(fontsize=fontsize_legend)
788 plt.grid(True)
789 plt.xticks(fontsize=fontsize_ticks)
790 plt.yticks(fontsize=fontsize_ticks)
791 plt.gca().xaxis.set_major_formatter(mdates.DateFormatter("%b"))
792 plt.gca().xaxis.set_major_locator(mdates.MonthLocator())
793 plt.show()
794
795 daily_hydrogen_storage = [hydrogen_storage_log[(i+1)*hours_per_day - 1] for i in range(num_days)]
796
797 plt.figure(figsize=(10,6))
798 plt.plot(dates, daily_hydrogen_storage, marker='o', linestyle='-', color='purple')
799 plt.xlabel("Date", fontsize=fontsize_labels)
800 plt.ylabel("Hydrogen␣Storage␣(kWh)", fontsize=fontsize_labels)
801 plt.title("Daily␣Hydrogen␣Storage␣Level", fontsize=fontsize_title)
802 plt.grid(True)
803 plt.xticks(fontsize=fontsize_ticks)
804 plt.yticks(fontsize=fontsize_ticks)
805 plt.gca().xaxis.set_major_formatter(mdates.DateFormatter("%b"))
```

```
plt.gca().xaxis.set_major_locator(mdates.MonthLocator())
plt.show()

daily_grid_export = [sum(grid_export_history[i*hours_per_day:(i+1)*hours_per_day]) for i in range(num_days)]
daily_grid_input = [sum(grid_input_history[i*hours_per_day:(i+1)*hours_per_day]) for i in range(num_days)]

plt.figure(figsize=(10,6))
plt.plot(dates, daily_grid_export, label="Daily Electricity exported ", marker='o', color='green')
plt.plot(dates, daily_grid_input, label="Daily Electricity imported", marker='x', color='orange')
plt.xlabel("Date", fontsize=fontsize_labels)
plt.ylabel("Daily grid usage (kWh)", fontsize=fontsize_labels)
plt.title("Daily Electricity Imported to and Exported from the Grid", fontsize=fontsize_title)
plt.legend(fontsize=fontsize_legend)
plt.grid(True)
plt.xticks(fontsize=fontsize_ticks)
plt.yticks(fontsize=fontsize_ticks)
plt.gca().xaxis.set_major_formatter(mdates.DateFormatter("%b"))
plt.gca().xaxis.set_major_locator(mdates.MonthLocator())
plt.show()

dates_hourly = pd.date_range(start=start_date, periods=len(electrolyser_energy_usage), freq='h')
plt.figure(figsize=(10, 6))
plt.plot(dates_hourly, electrolyser_energy_usage, label='Electrolyser power input', marker='o', color='blue')
plt.plot(dates_hourly, fuelcell_electrical_output, label='Fuel cell power output', marker='x', color='red')
plt.xlabel('Month', fontsize=fontsize_labels)
plt.ylabel('Power (kW)', fontsize=fontsize_labels)
plt.title('Electrolyser Input & Fuel Cell Output Power', fontsize=fontsize_title)
plt.grid(True)
plt.legend(fontsize=fontsize_legend)
plt.xticks(fontsize=fontsize_ticks)
plt.yticks(fontsize=fontsize_ticks)
plt.gca().xaxis.set_major_formatter(mdates.DateFormatter("%b"))
plt.gca().xaxis.set_major_locator(mdates.MonthLocator())
plt.tight_layout()
plt.show()

plt.figure(figsize=(10, 6))
plt.plot(dates_hourly, grid_export_history, label="Electricity exported", marker='o', color='green')
plt.plot(dates_hourly, grid_input_history, label="Electricity imported", marker='x', color='orange')
plt.xlabel("Month", fontsize=fontsize_labels)
plt.ylabel("Grid usage (kW)", fontsize=fontsize_labels)
plt.title("Electricity Imported to and Exported from the Grid per Hour", fontsize=fontsize_title)
plt.legend(fontsize=fontsize_legend)
plt.grid(True)
plt.xticks(fontsize=fontsize_ticks)
plt.yticks(fontsize=fontsize_ticks)
plt.gca().xaxis.set_major_formatter(mdates.DateFormatter("%b"))
plt.gca().xaxis.set_major_locator(mdates.MonthLocator())
plt.tight_layout()
plt.show()

plt.figure(figsize=(10, 6))
plt.plot(dates_hourly, battery_history, marker='o', linestyle='-', color='blue', markersize=1)
plt.axhline(y=max_storage_capacity_battery, color='r', linestyle='--', label='Max battery capacity')
plt.xlabel("Month", fontsize=fontsize_labels)
plt.ylabel("Battery level (kWh)", fontsize=fontsize_labels)
plt.title("Battery Level over Time", fontsize=fontsize_title)
plt.grid(True)
plt.legend(fontsize=fontsize_legend)
plt.xticks(fontsize=fontsize_ticks)
plt.yticks(fontsize=fontsize_ticks)
plt.gca().xaxis.set_major_formatter(mdates.DateFormatter("%b"))
plt.gca().xaxis.set_major_locator(mdates.MonthLocator())
plt.tight_layout()
plt.show()
```